SURFACE MODIFICATION OF LAYERED ZIRCONIUM PHOSPHATES: A NOVEL PATHWAY TO MULTIFUNCTIONAL NANOMATERIALS

A Dissertation

by

BRIAN MATTHEW MOSBY

Submitted to the Office of Graduate and Professional Studies of
Texas A&M University
in partial fulfillment of the requirements for the degree of

DOCTOR OF PHILOSOPHY

Chair of Committee,	Abraham Clearfield
Committee Members,	James Batteas
	Janet Bluemel
	Hong Liang
Head of Department,	David H. Russell

May 2014

Major Subject: Chemistry

ABSTRACT

The surface functionalization of inorganic nanoparticles for improved and novel applications is the topic of this dissertation; specifically the surface modification of inorganic layered materials. In this case the goal is to exclusively modify the surface or exterior layers of the material, while leaving the internal layers and structure unchanged. This allows for organic derivatives of layered materials in which the interlayer chemistry is not lost to achieve organic functionalization. The addition of organic character along with the retention of the original interlayer character produces a material with dual functionality and opens the window for many unique compounds and applications.

The surface reactivity of α- zirconium phosphate nanoplatelets was investigated with a variety of coupling agents. Initially, covalent attachment of molecules to the exterior surface of the nanoparticles was attempted with silanes and epoxides. Subsequently, the ion exchange character of the surface phosphate groups was used to deposit metal ions on the surface. The metal ion layer was then coordinated with phosphonic acid ligands to produce surface functionalized ZrP. In all cases the exclusive functionalization of the surface and covalent attachment of the reactive groups to the inorganic layer was confirmed using a combination of techniques including X-ray powder diffraction, XPS, electron microprobe, Solid State NMR, FTIR, and TGA. The viability of producing nanoparticles with both a controlled interior and exterior by combining the intercalation chemistry of ZrP with the newly developed surface chemistry was then investigated.

Characterization of the resulting materials indicated that functionalization of intercalated ZrP was successful and an efficient procedure for the design of multifunctional nanoparticles. The control of the interlayer and surface allows for nanoparticles to be designed for particular applications. Polymer nanocomposites and a photo-induced electron transfer system were prepared using the multifunctional nanoparticles as test cases.

DEDICATION

This dissertation is dedicated to all those who were unable to attain the level of education they desired due to the circumstances of life. It is through the sacrifices they made and the wisdom they imparted that I was able to achieve all that I have. Especially to my grandmother, Lillia Mae, and my father, John.

ACKNOWLEDGEMENTS

There are many people who have contributed to my development throughout the years. I am very appreciative of all that I received and endeavor to be a good steward.

First of all I would like to thank my family for their continued support and encouragement during the course of my education. My parents have always expected academic success from me and it is those high standards that have made me challenge myself and continue to grow intellectually. I would also like to acknowledge my brother and sister who challenged me to succeed academically through friendly competition.

I would like to offer my thanks to Prof. Danny Hubbard for the guidance he provided throughout my undergraduate and graduate career. Upon entering Grambling State University I had no intention of attending graduate school and obtaining a doctoral degree. My initial exposure to chemical research was gained through an opportunity offered by Dr. Hubbard. Through researching in his laboratory I found that I enjoyed chemical research and decided to pursue chemistry as a career as opposed to a professional degree after graduation. Additionally, through serving as a tutor for Dr. Hubbard's general chemistry course I found that I enjoy teaching. All the conversations and lectures were certainly beneficial and are appreciated along with the relationship we have developed.

Additionally, I would like to thank all those who have taught me chemistry. Initially, Coach Boltz in high school followed by the faculty at Grambling State University. Prof. Danny Hubbard, Prof. Connie Walton, Prof. Pia Albuquerque, Prof. Frank Ohene, Prof. Allen Miles, Prof. Bobby Burkes, and Prof. Tony Perry. It was through your teaching during lectures, training during laboratories, and interaction outside the classroom that I became the chemist that I am today.

Certainly I must acknowledge my chemistry classmates from GSU. We began as classmates but became the closest of friends. Your support has been invaluable not only academically but personally as well. I am proud of the success we all have achieved and I wish you all much more in the future. Also, those who came before us at GSU and gave use useful insights on the chemistry program. Thanks for the advice, encouragement, and for being good examples of success.

There were several programs I participated in that were crucial in my development as a chemist and taught me much about the nature of research I would like to thank the Tulane University LS-AMP Summer Research Program, the North Carolina State University Chemistry REU and the Dartmouth College Nanomaterials REU. Specifically I would like to thank professors Bradley Taylor, James Martin, and David Glueck. It is through the work in their laboratories that I gained an appreciation for inorganic and materials chemistry. A special thanks to the graduate and postdoctoral researchers that

directly supervised me during these research programs, Robert Wilcox and Marites Guino-o.

I would like to thank all the members of the Clearfield research group that I have worked with the past five years, the TAMU chapter of NOBCChE, and my peers in the chemistry doctoral program at TAMU for all the support through the years. I wish you all continued success.

I would like to thank my graduate committee, Prof. James Batteas, Prof. Janet Bluemel, and Prof. Hong Liang. The expertise they possess in their respective fields was valuable in helping me think about my research from different viewpoints leading to a much more comprehensive investigation.

Finally, I would like to thank Prof. Abraham Clearfield for his contribution to my graduate education. Whether through a course, meeting, or a conversation in the laboratory he was always teaching and passing on his experience from the many years he has done chemistry. I thank him for allowing me to be a part of his research group and giving me the liberty I needed to engage in original research. I thoroughly enjoyed the project and hope it will add a substantial component to the field of zirconium phosphate and inorganic layered materials.

NOMENCLATURE

AFM	Atomic Force Microscopy
BPBPA	Biphenylbisphosphonic acid
BQ	1,2-benzoquinone
CP	Cross Polarization
CTAB	Cetyltriethylammonium bromide
FTIR	Fourier Transform Infrared Spectroscopy
HDT	Hydrothermal
MAS	Magic Angle Spinning
NMR	Nuclear Magnetic Resonance
ODPA	Octadecylphosphonic acid
OTS	Octadecytrichlorosilane
PEG	Polyethylene glycol
PS	Polystyrene
Ref	Reflux
SAMs	Self Assembled Monolayers
SEM	Scanning Electron Microscopy
SS	Solid state
TBA	Tetrabutylammonium
TEM	Transmission Electron Microscopy
TGA	Thermogravimmetric Analysis

UV	Ultraviolet
WDS	Wavelength Dispersive Spectroscopy
XPS	X-ray Photoelectron Spectroscopy
XRD	X-ray Diffraction
XRPD	X-ray Powder Diffraction
ZrP	Zirconium Phosphate

TABLE OF CONTENTS

Page

LIST OF FIGURES

Page

LIST OF TABLES

Page

CHAPTER I

INTRODUCTION*

1.1 Inorganic Layered Materials

There are a variety of inorganic layered materials that exist such as clays, metal phosphates and phosphonates, metal chalcogenides, transition metal oxyhalides, titanates, and layered double hydroxides among others. [1-10] A defining feature of this category of materials is the strong covalent interactions of the atoms within an individual layer and somewhat weaker Van der Waals interactions by which the layers interact with each other. [11] Inorganic layered materials can further be divided into categories based on the charge of the layers. Layers can be uncharged, cationic, or anionic; in which case uncharged layers can be conductors or insulators and cationic and anionic layers interact well with anions and cations respectively.[11] Additionally it has become accepted to categorize these materials based on the thickness of the individual layers in which case

---

* Part of this chapter is reprinted with permission from "Self-Assembled Monolayers Based Upon a Zirconium Phosphate Platform" by Díaz, A., Mosby, B.M., Bakhmutov ,V.I., Martí, A., Batteas, J. and Clearfield, A. *Chemistry of Materials*, **2013**, 25 (5), 723-728, copyright 2013 by American Chemical Society; "Surface Modification of Zirconium Phosphate Nanoplatelets for the Design of Polymer Fillers" by Mosby, B.M., Díaz, A., Bakhmutov ,V.I., and Clearfield, A. *ACS Applied Materials and Interfaces*, **2014**, 6 (1), 585-592, copyright 2013 by American Chemical Society; and "Designable Architectures on Nanoparticle Surfaces: Zirconium Phosphate Nanoplatelets as a Platform for Tetravalent Metal and Phosphonic Acid Assemblies" by Mosby, B.M., Goloby, M., Díaz, A., Bakhmutov ,V.I., and Clearfield, A., *Langmuir*, **2014**, 30 (9), 2513-2521, copyright 2014 by American Chemical Society.

class I materials are made up of atomic monolayers, class II materials possess layers that have a thickness of a few atoms, and class III materials possess layers with a thickness of many atoms.[12] The charge of the individual layers and the atomic thickness greatly affect the applicability of these materials. In addition the particle size, shape, and degree of crystallinity can also be used to tune the applicability.

1.1.1 Metal (IV) Phosphates

Metal phosphates make up one of the largest families of inorganic layered materials and have been synthesized with chemicals from groups 4,5,14, and 15.[2] Tetravalent metal phosphates exist mainly in two phases the α and γ.[2, 13] The primary difference between the two structures is the phosphate groups, as seen in **Figure 1**. The γ type structure contains two types of phosphates, both PO_4 and H_2PO_4 groups.[13]

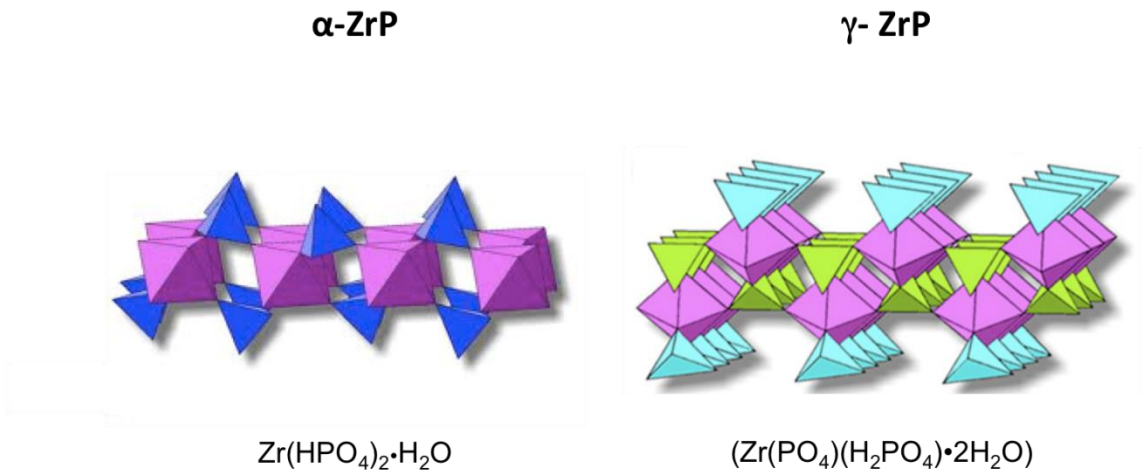

Figure 1. Structure of α and γ ZrP displaying the structural differences within the layers and arrangement of phosphates in the compounds. Taken from reference 13 and http://www.chm.unipg.it/chimino/1/fig/3phosphates.html**.**

The PO_4 tetrahedra are present in the core of the layer and bound to four different metal ions. The H_2PO_4 groups bond only to two metal ions and leave two OH groups pointing away from the layer either in the interlayer or the surface. Two water molecules reside in the interlayer that engage in hydrogen bonding with the hydroxyl groups of the phosphates. On the other hand the α type structure has only one type of phosphate, PO_4. These phosphates bond to three different metal ions and the remaining hydroxyl group points in the interlayer or the surface. The metal ions in this case are slightly above and below the plane. Tetravalent metal phosphates with α type structures make up one of the largest groups within the family. These type of compounds have been synthesized from all M(IV) ions in group 4 and 14 except for carbon.[2] Although the structure remains the same, variation of the tetravalent metal used can lead to slight changes in the bond

distances and can also change certain properties of the materials such as rate of hydrolysis or thermal stability.

1.2 α-ZrP

1.2.1 Structure

Of primary interest in this case is α- zirconium phosphate. *α*-zirconium hydrogen phosphate ($Zr(O_3POH)_2 \cdot H_2O$, ZrP) has been extensively studied since reported by Clearfield in 1964, the structure of the layers and surface can be seen in **Figure 2**.[14] Single crystal X-ray diffraction data of the α phase showed that the Zr atoms lie in a plane, slightly below and above the layer, and are connected to each other by phosphate groups. Three of the oxygen atoms of each phosphate group are bonded to a different Zr atom and the remaining hydroxyl group points away from the layer, either in the interlayer region or on the surface.[15] The arrangement of the layers forms a zeolitic cavity where a water molecule resides; this cavity has been utilized for intercalation chemistry, the reversible incorporation of guest molecules into the interlayer. The distance between two layers is 7.6 Å and is calculated by the distance from the center of an atom in one layer to the same atom in the next layer. The thickness of the layers is 6.3 Å, leaving a free space of 1.3 Å. A view down the c-axis shows the structure of the surface of the layered material. The phosphates with surface hydroxyl groups form a

triangle and are approximately 5.3 Å apart. It should be noted that phosphates are not perfectly level with each other and do not form a plane on the surface.

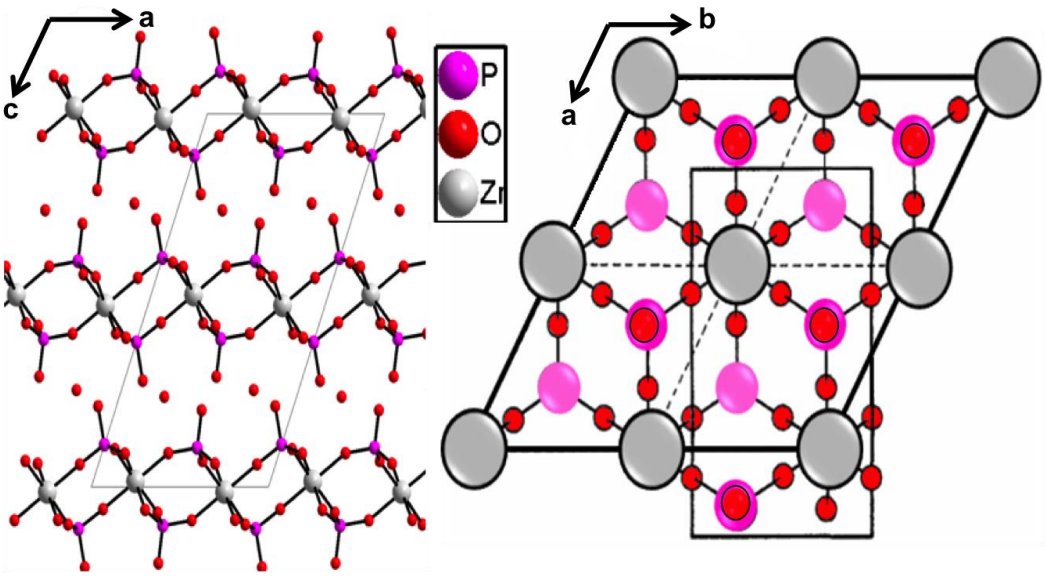

Figure 2. Structure of ZrP viewed down two different axes, focusing on the interlayer and surface structure.

1.2.2 Intercalation

Intercalation in ZrP proceeds by three main mechanisms, ion exchange, acid base, and/or electron transfer, **Figure 3**.[16] The most common of these are the ion exchange and acid base mechanisms. For the ion exchange process cations displace the acidic protons of the hydroxy phosphate groups in the interlayer region of ZrP, forming a new phase.

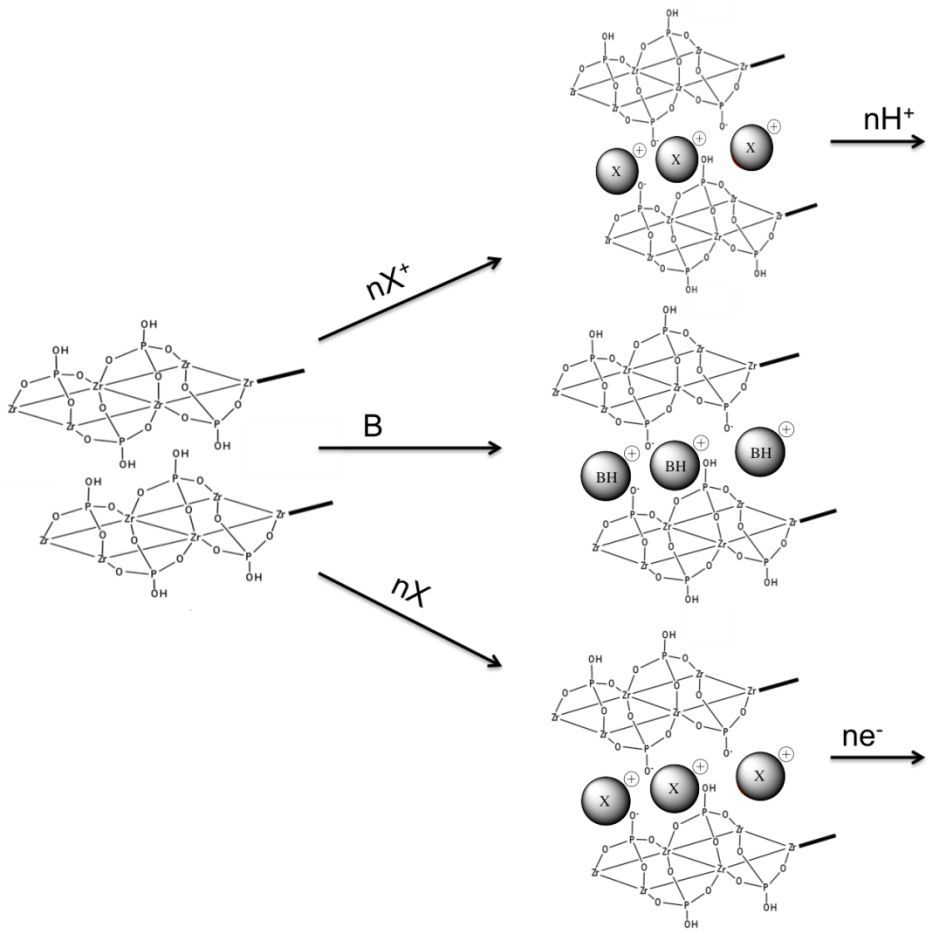

Figure 3. Intercalation mechanisms for ZrP; ion exchange (top), acid base (middle), and redox (bottom).

On the other hand, the intercalation via an acid base reaction takes place when a Brønsted base is protonated by the acidic protons of the hydroxy phosphate groups, forming an ionic pair between the deprotonated phosphate and the protonated base. The intercalation reactions proceed from the edges of the particle and move toward the interior, in many cases a phase boundary is formed and there exist both an exchanged and non exchanged phase simultaneously.[17] For example, in the case of the Na^+ phase of

ZrP multiple steps occur before the fully exchanged phase is formed.[18, 19] Initially Na^+ enters the edge of the particles producing a new phase with an interlayer spacing of 11.8 Å that coexists with the 7.6 Å phase. The spacing of the entire material is then increased to 11.8 Å by continuing the exchange, this is the half exchanged phase with an increase in hydration, $ZrHNa(PO_4)_2 \bullet 5H_2O$. Further Na^+ exchange leads to the fully exchanged trihydrate phase of composition $Zr(NaPO_4)_2 \bullet 3H_2O$ and a 9.9Å interlayer spacing. Water loss yields a new phase with composition $Zr(NaPO_4)_2$, with an interlayer spacing of 8.42 Å, forming the most stable conformation of the layers around the sodium ions. This type of ion exchange proceeds smoothly for a number of monovalent and divalent cations including Li^+, Na^+, Ag^+, Tl^+, Cu^+, and Ca^{2+}.[20] It was found that larger cations such as Cs^+, NH_4^+, Rb^+, and Ba^{2+} did not form fully exchanged phases of ZrP at acidic pH.[20-24] The largest entrance to the interlayer region of α-ZrP is 2.61 Å, therefore ions above this size cannot enter the interlayer by direct ion exchange.[25] Further investigation showed

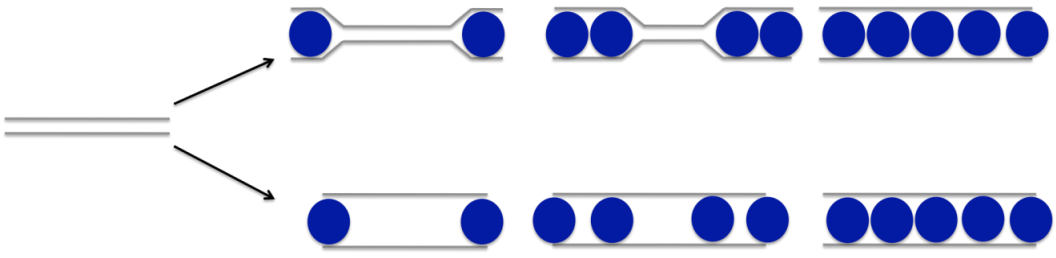

Figure 4. Intercalation of ZrP in the case of high (top) and low (bottom) intercalation energy barriers. Modified from reference 29.

that although these ions were not able to enter the interlayer at low pH, they were able to displace exclusively the surface protons of ZrP by ion exchange.[26] The ion-exchange capacity of ZrP has made ZrP very useful for a number of applications. In theory any positively charged species can be intercalated into ZrP whether a metal ion or a coordination complex. In cases of some of the larger species it is common to use Θ-ZrP, a hydrated phase of α-ZrP, in which the interlayer distance is larger due to the increased hydration.[27, 28] The increase in the interlayer distance effectively decreases the intercalation energy and allows for molecules to enter the interlayer more readily, including some large molecules that typically would not be able to enter the interlayer region.[29] **Figure 4** displays intercalation in the case of high and lower energy barriers. Additionally, a number of swelled phases of ZrP can be prepared using sodium ions or alcohols in order to spread the layers to foster the intercalation of large molecules.[18, 30, 31]

Intercalation via an acid base reaction takes place when a Brønsted base is protonated by the acidic protons of the hydroxy phosphate groups, forming an ionic pair between the deprotonated phosphate and the protonated base. This type of intercalation is most common with amines but also possible with other molecules such as amides, pyridine, quinoline, ammonium salts, and dimethyl sulfoxide in the case of ZrP.[32-37] Titrations reveal that in the fully intercalated amine phase each amino group interacts with one phosphate however, there are many phases produced as the interlayer becomes saturated due to different packing of the amines within the interlayer, as displayed in **Figure 5**.[38, 39] To elucidate the structure of the amine intercalated phases the titration and powder

X-ray diffraction data was combined with NMR studies.[39, 40] Ultimately it was found that at the maximal loading levels several alkylamines were found to have nearly identical ^{31}P NMR spectra suggesting an identical intercalation process and resulting material.[40] The shift of the phosphorus signal from ZrP to the intercalated compounds was used to determine the interaction of the amines with the interlayer. It was observed that deprotonation of the interlayer phosphate resulted in a chemical shift change of ~10 ppm, whereas formation of a donor or acceptor hydrogen bond resulted in shifts of ~3 ppm and ~-2 ppm respectively.[40] It was found that the initial conformation of the amine is flat, parallel to the layers. As the loading increases the nitrogen atoms begin to interact with the deprotonated phosphates thus becoming oriented perpendicular to the layer. This is also shown by the change in interlayer spacing as a function of amine uptake. Initially the tail part of the alkyl chain folds and prefers the parallel orientation but once the loading is further increased the chains become completely perpendicular to the layer. The increase in loading is attributed to the formation of bilayers of amine within the layers, as both sides of the interlayer region will be reacting with amines. This has been confirmed by experiments with ethylenediamine in which the fully loaded phase contains 1 mole of amine per phosphate and the interlayer distance is 11.1 Å, much lower than the species that form bilayers.[38]

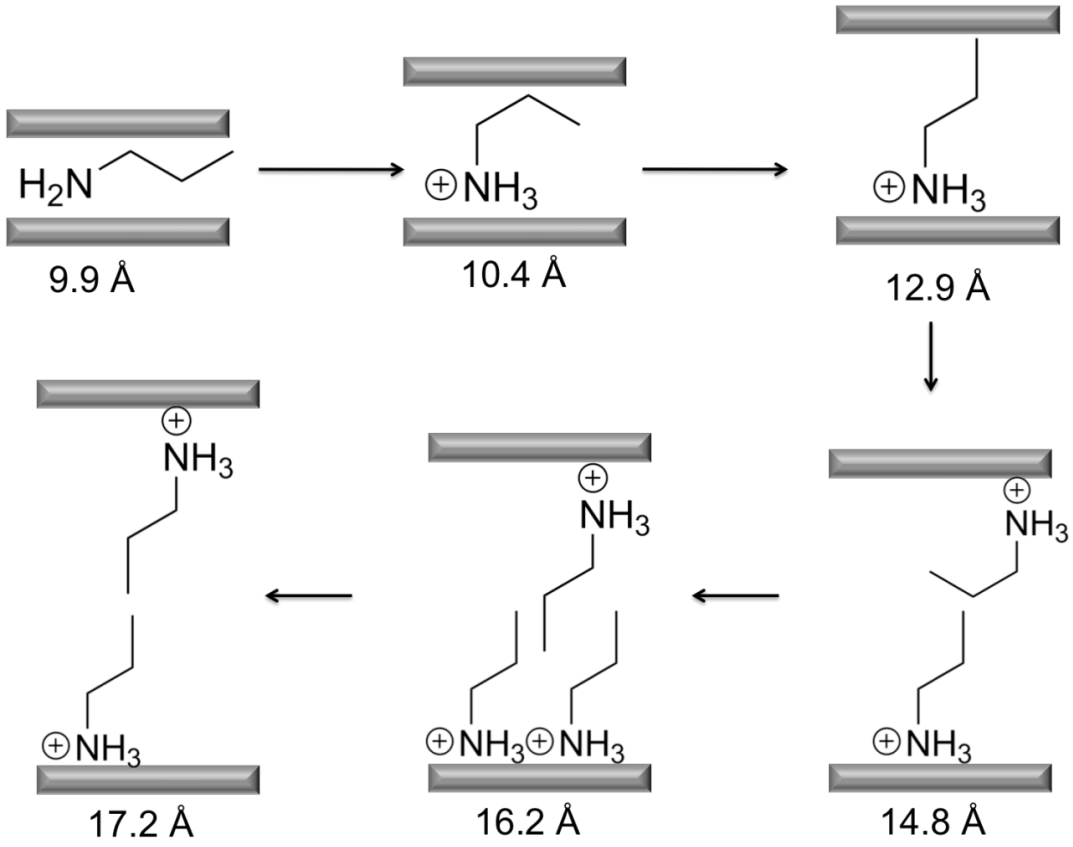

Figure 5. Conformations of propylamine within the interlayer of ZrP as the intercalation reaction proceeds. Modified from reference 39.

The redox based intercalation method is not so common and has only been observed in a few cases.[16, 41] Such reactions typically take place in polar solvents; the host material is reduced by the potential guest molecule and the solvent is often protonated as a result. [41] Additionally pi-pi interactions are typically formed among the intercalated molecules to give further stability.[16] Colón and coworkers were able to demonstrate that the direct intercalation of ferrocene into Θ-ZrP yielded a ferrocenium intercalated phase.[42] In this case the oxidation of the ferrocene was confirmed by diffuse reflectance UV-visible spectroscopy, Mössbauer, and cyclic voltammetry.[42]

In addition to the intercalation mechanisms presented it was also found that molecules such as alkanols, glycols, and polymers that are not charged or bases could be intercalated.[31, 43-45] Although they can be intercalated it should be noted that in order to achieve the encapsulation of these molecules the layers must be pre-swelled. This suggests that there is not a large driving force for these molecules to enter the interlayer, this is verified by Costantino's observation that there was no uptake when ZrP was treated with alkonols and glycols directly.[31] Spreading of the layers lowers the intercalation energy barrier and allows molecules with weaker interactions to enter the interlayer region. The polymers lay flat within the interlayer and are thought to be stabilized by hydrogen bonding interactions between the interlayer phosphates and the polymer.[43] In the case of alkanols and glycols the intercalated molecule is thought to displace the interlayer water molecule and engage in hydrogen bonding with its alcohol

functionality and the interlayer phosphates. [31] It should be noted that in both cases the intercalation is stabilized by hydrogen bonding.

1.2.3 Exfoliation

Exfoliation is the process in which the layers of a layered material are swollen to the point where they lose their attraction for each other and individual nanosheets are formed in solution.[46, 47] In the case of ZrP, exfoliation is usually achieved using tetrabutylammonium hydroxide, however alkylamines can be used for a milder

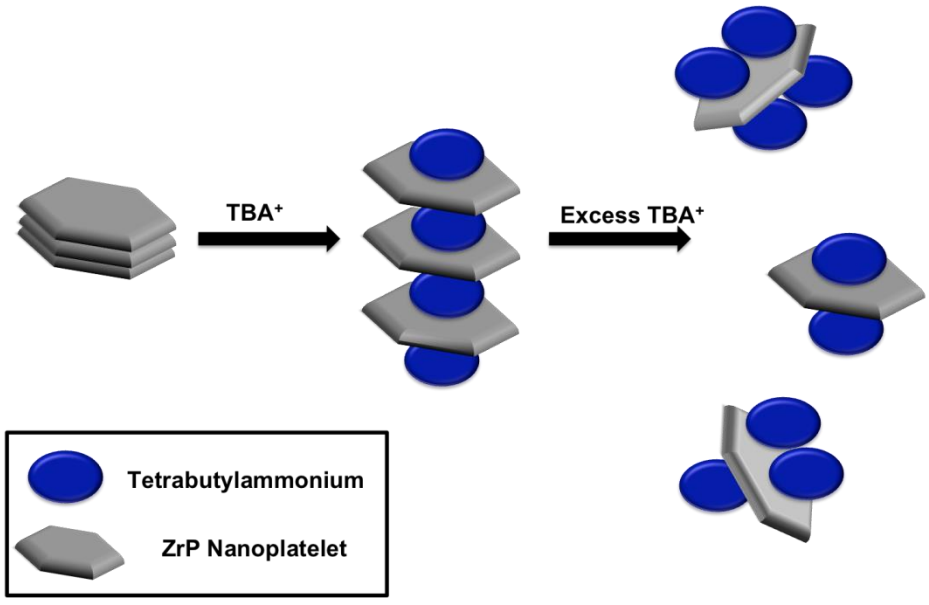

Figure 6. Exfoliation of ZrP nanoparticles into individual nanosheets through treatment with tetrabutylammonium hydroxide. Modified from reference 52.

exfoliation process.[48-52] The process of intercalation of tetrabutyammonium followed by exfoliation can be seen in **Figure 6**. In some cases the produced colloidal dispersion of ZrP is used as a precursor for intercalation of large molecules, such as proteins, that cannot be intercalated directly in ZrP.[53, 54] Although exfoliated particles can be used as a precursor for intercalation, when the new compound is formed the order and stacking of the particles will not be as fine as it was in the original material. The successful exfoliation can be observed in TEM, where individual nanosheets with a thickness below 1 nm are seen. Also upon successful exfoliation the particles should no longer display an X-ray diffraction pattern as all order has been destroyed.[48] Exfoliated ZrP has been utilized as a building block for layer-by-layer assemblies and also for a number of applications such as polymer fillers. [48, 52, 55]

1.2.4 Organic Derivatives

The introduction of organic functionality into ZrP was thought to be ideal as a means of producing hybrid materials with diverse applicability. Alberti and Costantino found that organic derivatives of ZrP could be achieved by reaction of zirconium fluoro complexes with phosphonic acids or phosphoric acid esters.[56] Initial investigations were carried out using benzene phosphonic acid and hydroxymethane phosphonic acid. The interlayer spacing of the precipitates suggested a layered compound in which double layers of phosphonic acids formed; in these organic derivatives the interlayer and surface of the compound contain the R group, thus incorporating the organic directly into the

structure.[56] Eventually Clearfield and co-workers were able to solve the structure of zirconium phenyl phosphonate using powder X-ray diffraction data, as seen in **Figure 7**.[57] The inorganic layers of the phenylphosphonate are identical to that of ZrP, confirming the hypothesis of Alberti and coworkers.

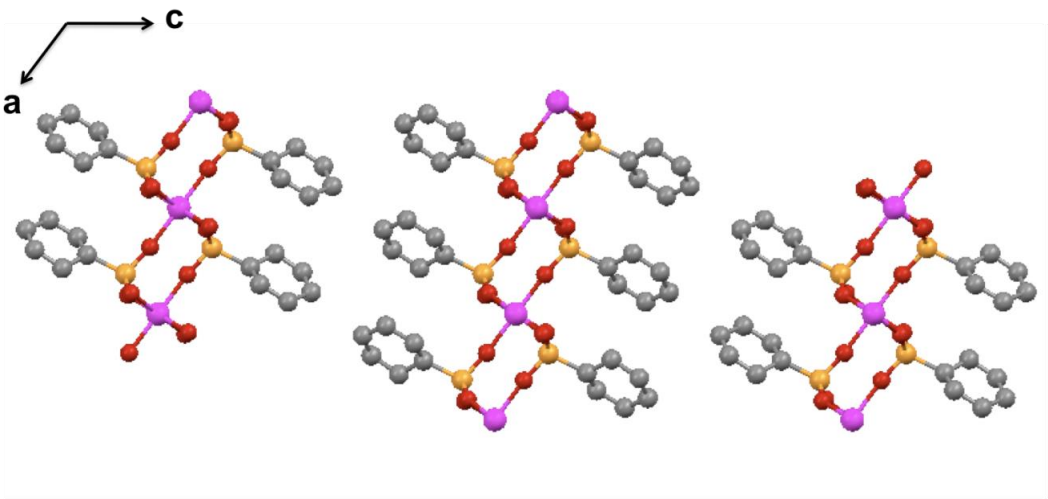

Figure 7. Crystal structure of Zirconium phenylphosphonate viewed down the b axis.

It was noticed however that the phenyl groups are tilted at a 30° angle to form the most stable conformation of the product. In the case of other organic derivatives synthesized using this method it is assumed that they have identical structures and that the variability in the interlayer spacing is caused by the preferred orientation of the organic within the interlayer. Organic derivatives have been synthesized with organophosphates containing alkyl, aryl, carboxyl, crown ether, amino, and a variety of other functionalities. [10] As the

inorganic layers of ZrP and the organic derivatives were found to be identical it was thought that substitutions could be made with the interlayer ligands producing hybrid materials with multiple functionalities. Originally, a mixed zirconium phosphate-phosphite system was synthesized by mixing phosphorous and phosphoric acid in the initial synthesis.[58] This approach was then applied to phosphate phosphonate systems, an idealized structure can be seen in **Figure 8**.[59]

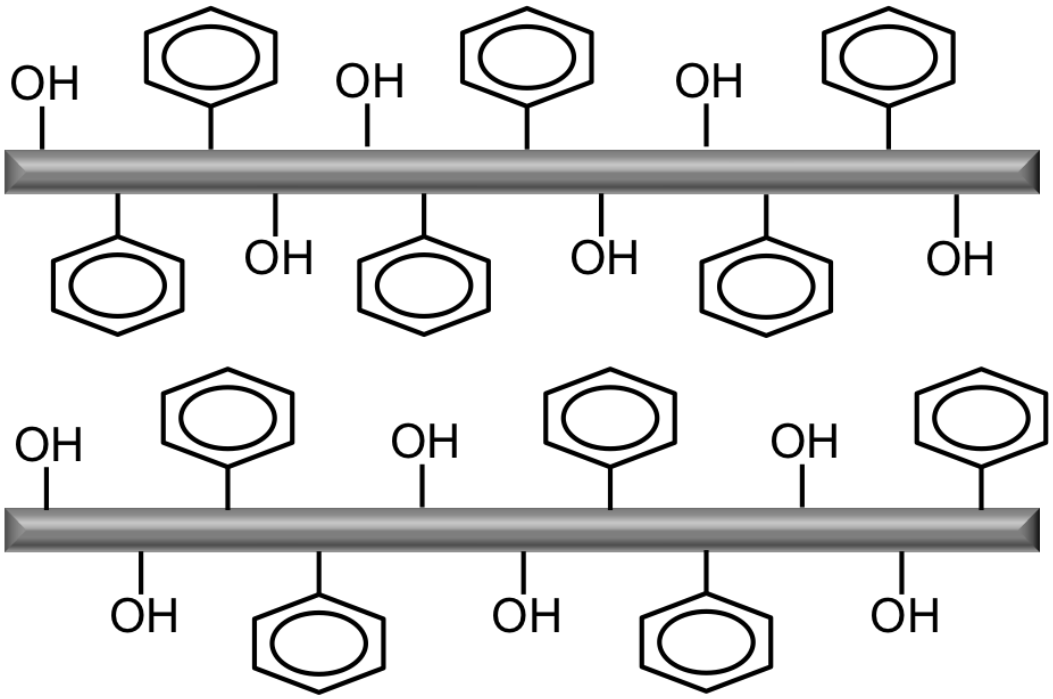

Figure 8. Schematic representation of zirconium phenyl phosphonate phosphate.

The added organic interlayer functionality made the resulting materials useful for the intercalation of organic molecules within the interlayer of ZrP. [59] Investigation then

began to shift to a new type of mixed derivative, known as staged materials.[60, 61] In this case the organic phosphonate and phosphate did not alternate sites as in other models but formed their own layers, **Figure 9**. The first three reflections in the powder x-ray diffraction pattern are that of the staged material and it's individual components. For example, the phenylphosphonate-phosphate staged material synthesized by Clearfield and co-workers the signals are for d-spacings of 22.5 Å, 14.8 Å, and 7.6 Å correspond to the sum of the phenylphosphnate and phosphate layer, the phenylphosphonate layer, and the phosphate layer respectively. [61]

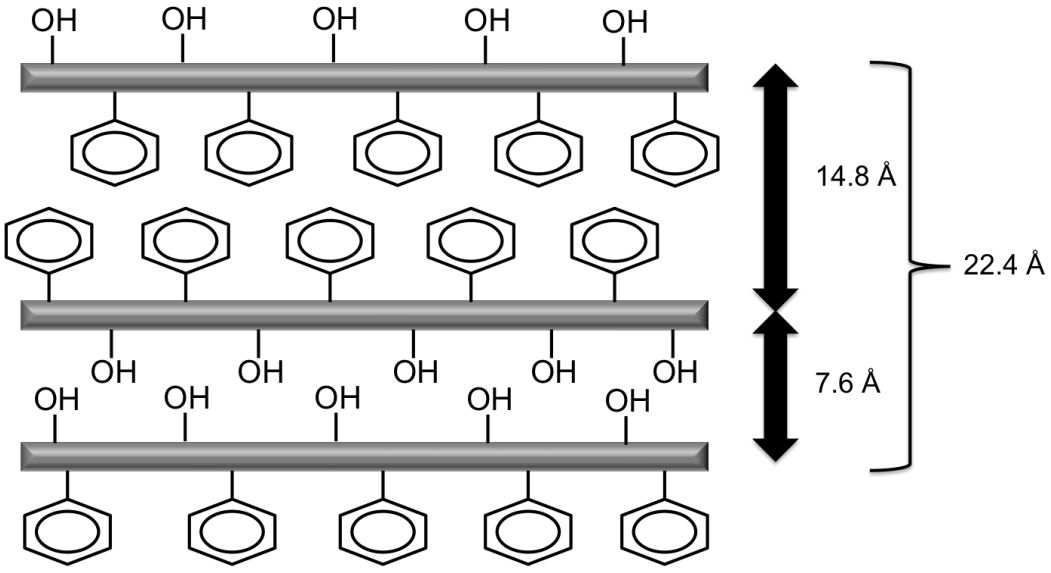

Figure 9. Schematic representation of a staged material in which the mixed derivatives form layers with common functionalities.

The use of bisphosphonic acid led to pillared materials with the α type structure.[62, 63] In this case the phosphonic acids of the ligand each bond to a different layer. The layers are cross-linked and connected by covalent interactions as opposed to van der waals interactions in other cases. Mixed derivatives were then synthesized along with pillars as a method to introduce porosity into the particles, **Figure 10**. [64, 65] These types of materials have found usefulness in many applications, of recent interest is nuclear waste remediation in which the porous materials can be used to separate lanthanides from actinides.[66]

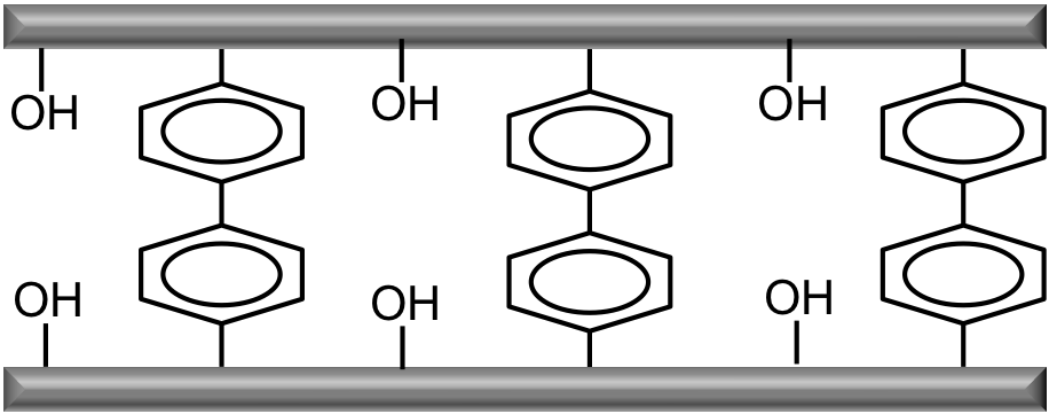

Figure 10. Idealized structure of a pillared mixed derivative of zirconium biphenylphosphonate phosphate.

1.2.5 Post-Synthetic Modification

Eventually it was found that organic derivatives could be achieved post synthetically. Yamanaka and Clearfield reported the bonding of ethylene oxide with γ and α ZrP respectively by esterification of the P-OH groups.[35,67] In Yamanaka's case the uptake of the epoxide was covalent and he was able to observe phosphate ester stretching in the FTIR and recover the phosphate ester through a procedure involving solubilizing the Zr with HF and adding barium to precipitate the phosphate ester.[35] In the experiments with α-ZrP it was found that in some cases there was uptake of epoxide without a corresponding increase in interlayer distance.[67] This suggests that the exterior surface was esterified or absorbed the epoxide selectively. The attachment of epoxides was recently used by Pica and coworkers, who reported the complete modification of α-ZrP using 1,2-epoxydodecane as the coupling agent and exfoliated α-ZrP as the precursor in a tetrahydrofuran suspension.[68] The exfoliation of ZrP allowed all phosphates to be accessible, addition of the long alkyl chain epoxide then imparted organic and hydrophobic functionality to the particles. Upon drying the layers were able to reform and the resulting material was found to be useful at uptaking polymers in the interlayer region. Additionally it was shown that in the case of poorly crystallized ZrP particles that functionalization could be achieved through an anionic exchange of the phosphate groups of ZrP with phosphonic acids. [69]

A number of attempts to add organic functionality to ZrP were also carried out using silanes.[70-73] Early use of the silanes to modify the structure of α-ZrP was directed towards obtaining porous pillared products.[70, 71] The silanes utilized were either triethoxy- or methoxyaminopropyl silanes where the amino group allowed direct intercalation of the silane between the layers. In this case there is a direct competition between the grafting on the surface and the intercalation of the silane through an acid-base reaction between the amino group and the phosphate on the layers. Extensive NMR studies showed that hydrolysis of the ethoxy groups to hydroxyl groups occurred, accompanied by polymerization of the silane. Roziere et al also attempted pre-polymerizing the silane into octa(3 aminopropylsilasquioxane) before incorporation into the ZrP but neither effort produced a porous product.[70] Clearfield and co-workers later demonstrated that a porous product could be achieved (~200 m^2/g) if the α-ZrP is first exfoliated and then allowed to encapsulate the added silane.[72] Similar results were obtained by Takei et al. who spread the layers of α-ZrP apart by intercalating octylamine and then added 1,2-bis(dimethyl-chlorosilyl)ethane, dichloromethylvinylsilane, and dichlorodi-methylsilane in toluene.[73] The product contained both silanes and undisplaced octylamine.

In recent efforts it was found that octadecylisocyanate could be used to modify *α*-ZrP, forming a hydrophobic monolayer on the surface of the platelets.[74] The isocyanate group not only reacts with the surface, but also with the edges of the platelets. When the

modified ZrP was exfoliated it produced a mixture of Janus and Gemini nanoplatelets that were used as stabilizers in Pickering emulsions.[74]

Additionally, it is also common for ZrP intercalated with functional amines to be referred to as organic derivatives. As discussed earlier the amino groups interact with the phosphates strongly. Kumar and co-workers intercalated butylamine hydrochloride to foster favorable interactions with aromatic electron donor and acceptor molecules within the layers and in solution. [75-77] In other cases alkylamines have been used to impart hydrophobic character to ZrP that would subsequently be used for polymer nanocomposites or other applications.[78, 79]

1.2.6 Layer-by-Layer

Eventually, the ZrP and other similar materials were synthesized on platforms in a layer-by-layer fashion. There is a large literature on layer-by-layer assemblies of tetravalent metals with phosphonic acids, over the years a variety of different methodologies have been developed including self-assembly and Langmuir-Blodgett based techniques.[80-83] It was shown that reactive surfaces could be functionalized in a fashion where the PO_3^{2-} groups are on the surface. These groups can then be reacted with tetravalent metals followed by phosphonates to build multilayer films. Mallouk and coworkers utilized gold and silicon surfaces as their platform of choice, by bonding a thiol or silane with a phosphate group at the distal end to the platform, a metal layer could be added by

absorption to the free phosphates.[84, 85] This metal layer could then be built upon by addition of another layer of phosphonic or a bisphosphonic acid to build multilayer films. Soon after, Katz developed a method based on Mallouk's work that produced multilayers of polar order.[71, 86, 87] In Katz's approach a gold substrate was reacted with a bifunctional alkane in which one side was a thiol and the other a hydroxyl group. The hydroxyl group is then phosphorylated using phosphoryl chloride and Zr^{4+} ions are absorbed to the surface. Additional layers can be made and the initial procedure repeated by reacting the Zr^{4+} ions on the surface with a hydroxyl terminated phosphonic acid. Talham later claimed that previous work using such methods resulted in materials that did not possess close packing of the template layer, which is necessary to form inorganic monolayers with a high level of order.[82, 88] Talham in turn proposed the use of a close packed organic template formed with Langmuir- Blodgett techniques as the substrate of choice. A Si wafer treated with octadecyltrichlorosilane (OTS) was the initial platform to which a Langmuir-Blodgett layer of octadecylphosphonic acid (ODPA) was added. The C_{18} chain is known to pack extremely well due to Van der Waals interactions of the long alkyl chains. This highly packed and organized OTS layer then interacts with the C_{18} of the ODPA stacking vertically leaving the phosphonate on the surface to react, Zr^{+4} is then absorbed to the phosphonic acid in a self-assembly step. Utilizing this combination of Langmuir-Blodgett and self-assembly, highly ordered assemblies are formed. Similar chemistry is applicable and has been achieved with a number of different phosphonic acids and metal ions.[89-94]

1.3 Surface Modification

Self-assembled monolayers (SAMs) have attracted much attention over the past three decades due to the simplicity of synthesis and broad range of applicability. Sagiv originally found that reaction of trichlorosilanes with the hydroxyl terminated surface of SiO_2 led to addition of a monolayer which greatly altered the properties of the material.[95] The smooth faces of silicon based platforms with Si-H and Si-OH bonds made them the initial platforms of choice but subsequently SAMs have extended to a large number of platforms including gold and metal oxides, **Figure 11**.[96, 97] SAMs are of interest due to the ability of the monolayer to alter the properties of the material.

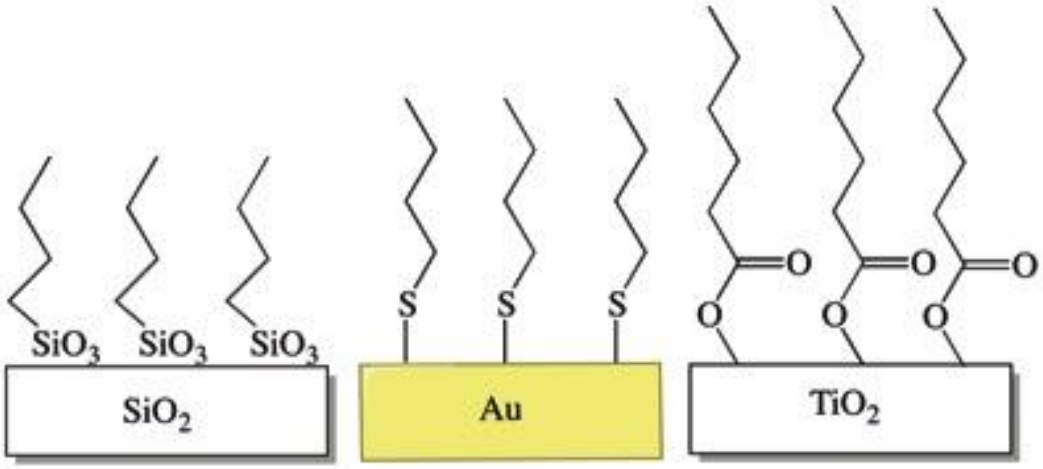

Figure 11. Typical SAMs observed on a variety of different platforms or nanoparticle surfaces.

By carefully choosing the substrate and composition of the monolayer SAMs have found applicability in a large number of fields such as chemical sensors, biosensors, cell adhesion, microelectronics, and thin film technology.[98, 99] The principles of SAMs were soon applied to nanoparticles in which case surface modification is used to build monolayers. As is the case with SAMs, modification of nanoparticles can alter the properties of the material and dictate how they interact with their environment. Modification of inorganic nanoparticles can be achieved in a number of ways including absorption or covalent attachment of coupling agents such as silanes to the surface, grafting polymers directly to the nanoparticle surface, and ligand exchange techniques in which the capping agent of the nanoparticle is exchanged for some other functional linker.[100] In such cases the aim of the functionalization is highly dependent on the desired application of the materials. One area of particular interest is the synthesis of organic-inorganic composite materials in which case the inorganic particles are dispersed in an organic matrix.[100] Another area of much interest has been biological applications in which case molecules are attached to the surface that improves the biological activity of the nanoparticles. Previous studies have indicated that foreign particles are regularly removed from the bloodstream and that particle recognition by the cells is largely based on physicochemical factors.[101] Among other things it was demonstrated that hydrophilic particles remain in the blood stream much longer than hydrophobic particles, which are removed quickly.[101] As a result one of the most common ligands used for biological activity is polyethylene glycol (PEG); addition of PEG to a molecule is commonly referred to as PEGylation. PEG is highly soluble in

both polar and apolar solvents, inert, biocompatible, and effectively repels other molecules by steric effects; the resulting PEGylated material therefore displays less non-specific binding and an increase in circulation within the bloodstream.[102] Additionally, nanoparticles can be functionalized through bioconjugation in which case biological molecules such as proteins, peptides, antibodies, enzymes, DNA, and fluorescent dyes can be attached to the surface of nanoparticles in order to initiate specific interactions with biological systems.[102] Bioconjugation can be achieved through similar chemistry as traditional surface modification in most cases, taking advantage of ligands, specific functional groups, and electrostatic interactions. Functionalization through non-covalent receptor interactions, such as the biotin-avidin couple, is somewhat unique to bioconjugation as opposed to traditional surface functionalization.[102]

The previously mentioned surface modification of nanoparticles plays an integral part in the synthesis of multifunctional nanoparticles, **Figure 12**. In such systems surface modification is used to impart functionality to an already functional nanoparticle or base material. Magnetic iron oxides are one of the most popular nanoparticle cores for such systems; in this case surface modification adds new functionality to an already magnetic particle, making it multifunctional.[103] Additionally, it should be noted that in some cases the core nanoparticle is coupled with other nanoparticles instead of functional ligands. Several examples display various combinations of quantum dots, metal nanoparticles, and magnetic particles with each other to produce core shell and heterodimer particles.[104-107]

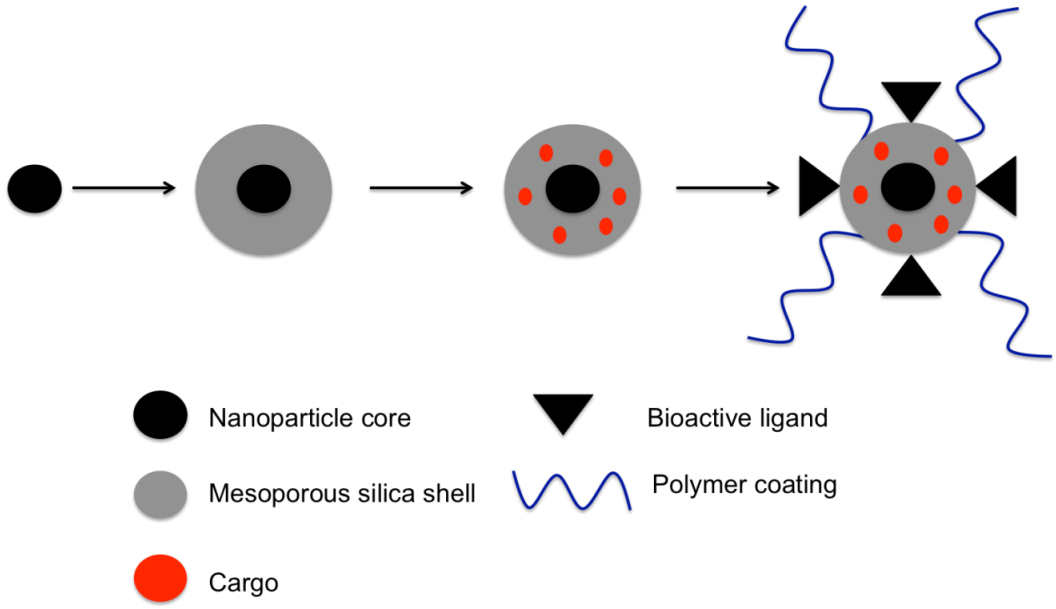

Figure 12. Schematic displaying the synthesis of multifunctional nanoparticles using the core shell approach. Modified from references 110 and 111.

Different combinations of functionalities allow the multifunctional nanoparticles to be tailored for specific applications. Among some of the more notable applications include live cell imaging, biosensing, and drug delivery.[108-113] A common method employed for the synthesis of these particles is the use of core shell systems. Hyeong and co-workers successfully synthesized multifunctional nanoparticles by combination of magnetic iron oxide, fluorescent dyes, and silica spheres.[114] The iron oxide nanoparticles were treated with cetyltriethylammniumbromide (CTAB) to produce hydrophilic nanoparticles. Mesoporus silica spheres were then formed around the CTAB surface layer to form a

core shell compound. To add fluorescent functionality for cellular imaging, dyes were conjugated with 3-aminopropyltriethoxysilane and bonded to the interior pores of the silica spheres. The resulting fluorescent and magnetic particles were used for in vivo multimodal imaging, as they are applicable with both fluorescence and magnetic resonance imaging. Additionally, the hydrophobic core can be used to load hydrophobic molecules such as doxorubicin, an anticancer agent, in which case the particles can also be used for drug delivery applications.

1.4 Scope of Study

The crystal structure of ZrP reveals that phosphate groups exist within the layer and on the surface of ZrP. Previous research clearly indicates that the P-OH groups of α-ZrP are indeed reactive. Although the intercalation chemistry of the interlayer region has been heavily investigated, ZrP also has an interesting and unique surface chemistry, which has been largely ignored. The flat surface of ZrP would be an ideal platform for reactivity, as it is expected that the disorder of alkyl modifiers that results from the nanoscopic curvature of silica surfaces will not persist in the case of ZrP.[115] Although some surface chemistry has been done with other metal phosphates, the materials used were not crystalline and the structures are not known with great certainty, as is ZrP.[116, 117] It is our aim therefore to investigate the surface functionalization of ZrP with a variety of reactive groups including epoxides, silanes, metal ions, and phosphonic acids. The successful

modification of the surface will be investigated in each case in addition to the coordination of the modifier to the surface.

An understanding of the surface chemistry of ZrP will lead to the ability to produce multifunctional nanoparticles based on ZrP. In this case the functionality can be added to ZrP through intercalation and additionally functionality through surface reactions. Manipulation of both the interlayer and surface of ZrP could lead to development of new classes of materials with tunable properties and could also greatly improve the applicability of all the current ZrP based systems. Surface functionalization allows control of how the particles interact with the environment therefore it is advantageous to functionalize the surface in order to improve the applicability of all current ZrP systems. ZrP has been investigated for uses in numerous applications such as catalysis, ion exchange, and nanocomposites.[25, 55, 118-120] More recently ZrP has been used for the encapsulation of hormones, such as insulin, and as drug delivery vehicles for cancer therapy.[121-123] In the case of the insulin ZrP particles, it was found that at lower loading levels some insulin reacted with the surface and caused an agglomeration of the particles.[121] Surface functionalization with a mucoadhesive polymer could block the surface sites, avoiding the agglomeration issue. In addition, surface functionalization with a mucoadhesive polymer is expected to improve the retention time of the insulin-loaded nanoparticles in the intestine, giving a better release and absorption of the hormone over time. Likewise, functionalization of ZrP loaded with anticancer drugs with

polymers, peptides, and other biological molecules could greatly increase the retention time of the drug and also selectively target cancer cells.

The viability of using ZrP for the synthesis of multifunctional nanomaterials will be discussed in this dissertation. Chapter II includes the experimental details of all compounds used and synthesized. Chapter III gives a thorough characterization of all ZrP starting materials of various size and crystallinity. Chapter IV discusses the covalent attachment of reactive molecules like silanes and epoxides to the surface. Chapter V investigates how the size of the particle affects the surface reaction. The investigation of a surface ion exchange and subsequent ligand functionalization as a means to surface modification of ZrP is discussed in Chapter VI. In Chapter VII the synthesis of multifunctional nanoparticles based on ZrP is investigated, and in Chapter VIII the applicability of such systems and other systems resulting from the newly developed surface chemistry is investigated. Lastly, in Chapter IX an overview of the presented work is given along with an outlook of some of the future work to be completed.

CHAPTER II

EXPERIMENTAL PROCEDURES[*]

2.1 Introduction

This chapter is intended to give an overview of the synthetic methods and parameters for the characterization techniques that will be discussed in subsequent chapters. Initially, the purity of all starting materials will be addressed (Section 2.2), followed by the synthesis of nanoparticles (Section 2.3), ligands (Section 2.4), and coordination complexes (Section 2.5). Next general techniques regarding ZrP such as intercalation (Section 2.6) and exfoliation (Section 2.7) are discussed. The methods for functionalizing ZrP with epoxides (Section 2.8), metal ions (Section 2.9), and phosphonic acids (Section 2.10) are then discussed. Finally, the chapter concludes with a detailed listing of the instruments used for characterization (Section 2.11).

---

[*] Part of this chapter is reprinted with permission from "Self-Assembled Monolayers Based Upon a Zirconium Phosphate Platform" by Díaz, A., Mosby, B.M., Bakhmutov ,V.I., Martí, A., Batteas, J. and Clearfield, A. *Chemistry of Materials*, **2013**, 25 (5), 723-728, copyright 2013 by American Chemical Society; "Surface Modification of Zirconium Phosphate Nanoplatelets for the Design of Polymer Fillers" by Mosby, B.M., Díaz, A., Bakhmutov ,V.I., and Clearfield, A. *ACS Applied Materials and Interfaces*, **2014**, 6 (1), 585-592, copyright 2013 by American Chemical Society; and "Designable Architectures on Nanoparticle Surfaces: Zirconium Phosphate Nanoplatelets as a Platform for Tetravalent Metal and Phosphonic Acid Assemblies" by Mosby, B.M., Goloby, M., Díaz, A., Bakhmutov ,V.I., and Clearfield, A., *Langmuir*, **2014**, 30 (9), 2513-2521, copyright 2014 by American Chemical Society.

2.2 Materials

Zirconyl chloride octahydrate (98% ,$ZrOCl_2 \bullet 8H_2O$), calcium nitrate tetrahydrate (99%, $Ca(NO)_3 \bullet H_2O$), polystyrene (MW ~ 192,000), titanium isopropoxide (97%, $Ti[OCH(CH_3)_2]_4$, glycidol (96%, $C_3H_6O_2$), 1,2-epoxydodecane (90%, $C_{12}H_{24}O$), poly (ethylene glycol) diglycidyl ether (MW~526), 1-bromo-3-chloropropane ($Cl(CH_2)_3Br$), 2-(4-fluorophenyl)-oxirane (95%, C_6H_7FO), sodium azide (NaN_3), Dowex 50WX8-400 hydrogen form, copper bromide (CuBr), tetraethylene glycol (99%, $C_8H_{18}O_5$), phosphoryl chloride ($POCl_3$), cyclohexylamine (99%, $C_6H_{11}NH_2$), poly(ethylene glycol) methyl ether (MW~2000), sodium L-ascorbate (98%, $C_6H_7NaO_6$), octylamine ($C_8H_{19}N$), iron(iii) acetylacetonate (97%, $Fe(C_5H_7O_2)_3$), iron(iii) nitrate nonahydrate ($Fe(NO_3)_3 \bullet 9 H_2O$) , triethylamine ($C_6H_{15}N$), triisopropyl phosphite (95%,$C_9H_{21}O_3P$), rhodamine 6G ($C_{28}H_{31}NO_3Cl$), cesium chloride (99.9%, CsCl), tris(2,2'-bipridyl)dichlororuthenium(II) hexahydrate ($C_{30}H_{24}Cl_2N_6Ru$) were purchased from Sigma-Aldrich; 1,10-phenanthroline iron(ii) sulfate complex ($[Fe(C_{12}H_8N_2)_3]SO_4$), hydrobromic acid (48%), epichlorhydrin (C_3H_5ClO), tetrabutylammonium hydroxide solution (~1M), copper(ii) sulfate pentahydrate ($CuSO_4 \bullet 5H_2O$), ferric sulfate ($Fe_2(SO_4)_3$), ferrous chloride ($FeCl_2 \bullet 4 H_2O$) were purchased from Fluka; 1,10 phenanthroline monohydrate (ACS, $C_{12}H_8N \bullet H_2O$), 1,10 phenanthroline anhydrous(ACS, $C_{12}H_8N$), cyclohexene oxide (98%, $C_6H_{10}O$), hafnium dichloride oxide octahydrate (98%, $HfOCl_2 \bullet 8 H_2O$), 1- octanol (99%, $C_8H_{18}O$), propargyl alcohol (99%, C_3H_4O), trimethylsilylazide (94%, $C_3H_9N_3Si$), n-octadecylphosphonic acid (97%, $C_{18}H_{39}O_3P$), chromium hexacarbonyl (99%, $Cr(CO)_6$),

Tungsten hexacarbonyl (99%, $W(CO)_6$), tetra-n-butylammonium hydrogen sulfate (97%, $C_{16}H_{37}NO_4S$), 1,2-epoxy-9-decene (96%, $C_{10}H_{18}O$), 1,2-epoxyoctadecane (90%, $C_{18}H_{36}O$), tin chloride hydrate (98%, $SnCl_4 \bullet xH_2O$), styrene oxide (98+%, C_8H_8O), zinc chloride (98+%, $ZnCl_2$) were purchased from Alfa Aesar; ammonium hydroxide solution (~ 1M, NH_4OH), phosphoric acid (85%, H_3PO_4) were purchased from EMD Chemicals; phosphorus acid (H_3PO_3), iodine (I_2), chromium oxide (CrO_3), manganous sulfate ($Mn(SO_4)_2$) , manganese dioxide (MnO_2), chromium chloride ($CrCl_3$), cuprous chloride (CuCl), cupric sulfate ($CuSO_4$), barium hydroxide octahydrate ($Ba(OH)_2 \bullet 8 H_2O$), barium chloride dihydrate (99.9%, $BaCl_2 \bullet 2 H_2O$) were purchased from Fischer; sodium carbonate anhydrous (Na_2CO_3) was purchased from Mallinckrodt chemicals; hydrochloric acid (32%,HCl) was purchased from Macron chemicals; ammonium chloride(NH_4Cl) was purchased from Spectrum chemicals; Zirconyl chloride octahydrate (99% ,$ZrOCl_2 \bullet 8H_2O$) was purchased from Inframat Advanced Materials; copper chloride dihydrate (97%, $CuCl_2 \bullet 2 H_2O$) was purchased from J.T. Baker Chemicals; potassium nitrate (99%, KNO_3) was purchased from EM Science; sodium hypochlorite solution (8.25%,NaClO) was obtained commercially through the use of Clorox bleach.

2.3 Nanoparticle Synthesis

2.3.1 Synthesis of α-ZrP

α-ZrP was synthesized using both the reflux and hydrothermal methods described by Sun.[48] In a typical reflux procedure 10g of $ZrOCl_2 \bullet 8H_2O$ was added to 100 mL of H_3PO_4 of a given concentration and refluxed at 100°C for 24 hours. In the hydrothermal procedure 4 grams of $ZrOCl_2 \bullet 8\ H_2O$ was added to a Teflon lined reaction vessel followed by addition of 40 mL of H_3PO_4 of a given concentration and reacted at 200°C for 24 hours. In both cases the products were washed with deionized water several times to remove all excess phosphoric acid and then dried in an oven at 65°C overnight to yield a white powder after grinding with a motar and pestle.

2.3.2 Synthesis of θ-ZrP

θ-ZrP was prepared using the method of Kijima to yield highly crystalline particles.[27] A 0.05M solution of $ZrOCl_2 \bullet 8\ H_2O$ was prepared by dissolving 3.22 g of $ZrOCl_2 \bullet 8H_2O$ in 200 mL of deionized water, this solution was added dropwise to 200 mL of 6M H_3PO_4 at 94°C. The mixture was refluxed at 94°C for 48 hours. Upon completion of the reaction the solution was rinsed with deionized water and centrifuged several times. The product was then allowed to remain in solution to prevent dehydration.

2.3.3 Synthesis of Iron Oxide (Fe_3O_4) Nanoparticles

6 nm iron oxide nanoparticles were prepared by the hydrothermal method of Tian.[124] 0.177g (0.5 mmol) of iron(iii) acetylacetonate was dissolved in a 16 mL of a 1:3 mixture of octylamine and octanol and allowed to shake overnight. The resulting solution was added to a Teflon lined reaction vessel and heated at 240°C for 2 hours. The product was washed with ethanol and dried.

2.4 Ligand Synthesis

2.4.1 Synthesis of Polyethylene Glycol Phosphate

The procedure to phosphorylate polyethylene glycol was adapted from Ortiz-Avilia and Clearfield.[67] 10 grams (5 mmol) of polyethylene glycol methyl ether was dissolved in 50 mL of chloroform. 466 μL of phosphoryl chloride in 60 mL of chloroform was added dropwise to the PEG solution while stirring at room temperature. After 1 hour of stirring the solution was placed in an ice bath and 20 mL of water was added to produce the acid form of the phosphate. The solution was then rotovapped to ~ 100 mL total volume and 5 grams (excess) of barium hydroxide was added to neutralize the acid formed. Dry ice was then added slowly to precipitate the reaction biproducts , which were then filtered off. The filtrate was concentrated to 50 mL by rotary evaporation and diluted by addition of 400 mL of ethanol. The resulting solution was kept in the freezer overnight to

precipitate any residual impurities. Additional precipitates were then filtered off and the solution was concentrated to 100 mL. 300 mL of acetone was added to the concentrated solution dropwise while stirring to precipitate the product, which was filtered and dried in a desiccator.

2.4.2 Synthesis of Dicyclohexyl Ammonium Prop-2-ynyl Phosphate

Synthesis of an alkyne phosphate was adapted from Sharpless and co-workers.[125] 30 mL of propargyl alcohol was mixed with 7.5 mL of triethylamine. 1.23g of crystalline phosphorous acid was then added while stirring. 5.7 grams of iodine was added over 5 minutes, after addition was complete the reaction was allowed to stir for 10 additional minutes. This solution was poured into a second solution consisting of 400 mL of acetone and 15 mL of cyclohexylamine and allowed to stir for 2 hours to produce the compound as the cyclohexyl ammonium salt. The precipitate was filtered, recrystalized from ethanol, and dried in a desiccator.

2.4.3 Synthesis of 3-Azidopropyl Phosphonic Acid

3- azidopropyl phosphonic acid was prepared based on the methods of Garrell and coworkers.[126] Initially 3-bromopropyl phosphonic acid diethyl ester was synthesized by reacting a 1 to 1 mixture of dibromopropane and triethyl phosphite at 160°C for 3 hours with a distillation apparatus. The product was converted to 3-azidopropyl phosphonic

acid ester by reaction with an excess of sodium azide in dry acetone under a nitrogen atmosphere . The ester was treated with an excess of bromotrimethyl silane in acetonitrile for 24 hours, after which the solution was rotovapped and a 40 mL 9:1 solution of methanol to water was added and allowed to stir for an additional 24 hours. The product was concentrated to yield 3-azido propyl phosphonic acid.

2.4.4 Synthesis of Biphenylbisphosphonic Acid

Biphenylbisphosphonic acid (BPBPA) was synthesized by a modified Arbuzov reaction as previously reported .[127] In summary, 4,4-dibromobiphenyl (20 mmol) was added to a three-neck- round bottom flask equipped with a reflux condenser, addition funnel, and N_2 along with 50 mL of 1,3- diisopropylbenzene. The mixture was heated at 185°C followed by addition of nickel bromide as a catalyst. After a N_2 purge 10 mL of triethyl phosphite was added dropwise over the course of 6 hours. After the completion of the triethylphosphite addition the mixture was refluxed for 24 hours then allowed to cool. The cool solution was distilled to remove solvent and unreacted phosphite compounds. The solid product was recrystallized using a mixture of petroleum ether and dichloromethane. The esterified biiphenyl product was hydrolyzed by a reflux in HCl to produce biphenyl bisphosphonic acid.

2.4.5 Synthesis of 1,10-Phenanthroline 5,6 Epoxide

1,10-phenanthroline 5,6 epoxide was prepared according to the method of Sullivan and Hamilton.[128, 129] 0.901 grams (5 mmol) of 1,10-phenanthroline and 0,2 equivalents of tetrabutylammonium hydrogen sulfate (0.339 grams) was dissolved in 100 mL of chloroform. 250 mL of bleach adjusted to pH ~ 8.5 by addition of ~ 3 mL of HCl was added to the mixture and stirred rapidly so that the aqueous and organic phases would mix. The reaction was monitored by NMR and was found to be complete in 20 to 30 minutes. After this time the stirring was stopped allowing the layers to separate, the organic phase was isolated and washed several times with cold deionozed water. The organic phase was then treated with anhydrous sodium carbonate and concentrated using rotary evaporation. The product was recrystalized with a 5:1 mixture of chloroform and hexanes to yield crystals.

2.4.6 Synthesis of Polyethylene Glycol Bis (Hydrogen Phosphate)

Synthesis of PEG bisphosphate from diglycidyl polyethylene glycol was based on the synthesis of Holubka.[130] In a typical experiment 10 mL of PEG diglycidyl ether was mixed with 20 mL of dimethoxy ethane. 3.7 mL of phosphoric acid was added and the mixture was reacted at 75°C for 2 hours. The solution was concentrated using rotary evaporation to yield the product as a gel.

2.5 Synthesis of Coordination Complexes

The syntheses of 1,10-phenanthroline 5,6-epoxide derivatives of group VI carbonyls were adapted from Stiddard's group VI metal tetracarbonyl bipy syntheses and Marti's rhenium carbonyl chloride derivative with the same ligand.[131, 132] In a typical experiment 0.1 grams of $M(CO)_6$ and a slight excess of of 1,10-phenanthroline 5,6-epoxide were added to the desired solvent. The solution was allowed to reflux for two hours. Upon cooling the product precipitated. The product was then filtered and washed with diethyl ether. This reaction was carried out with both Cr and W, in the case of Cr toluene was used as a solvent and xylene was used for the W analogue.

2.6 Intercalation Procedure

Intercalations were carried out by mixing a solution of θ-ZrP with a solution of the molecule or ion to be encapsulated within the interlayer of ZrP. In a typical procedure a solution containing 0.500 grams of ZrP in water was added to a solution containing a stoichiometric amount of the desired intercalant in an appropriate solvent. The solution was allowed to stir at room temperature for 3 days. Upon completion of the reaction the products were centrifuged and washed several times. Powder X-ray diffraction was used to determine the interlayer spacing of the new intercalated phases; TGA and electron microprobe were used to determine the composition of the materials.

2.7 Exfoliation Procedure

Exfoliation is carried out by treating ZrP with an equimolar amount of amine source. In a typical procedure 0.5 grams (1.66 mol) of ZrP is dispersed in 25 mL of water. The ZrP solution is then sonicated until well dispersed. A solution of 0.1 M tetrabutylammonium hydroxide is prepared and placed in an ice bath along with the ZrP solution before the reaction begins. 16.6 mL (1.66 mol) of the 0.1 M TBA is added dropwise to the ZrP solution while stirring, upon completion of the addition the stirring is allowed to continue for ten minutes. After the stirring the mixture is sonicated to yield exfoliated ZrP.

2.8 Epoxide Surface Modification Procedure

2.8.1 Neat Epoxide Microwave Method

100 mg of α-ZrP was placed in a 15 mL microwave reaction vessel. 1 mL of pure epoxide was then added followed by sonication of the vessel. The vessel was sealed and heated at 70 °C for 1 hour while stirring. In all cases the reaction products were washed multiple times with hexanes and ethanol, filtered, and dried in an oven at 65 °C.

2.8.2 Stoichiometric Microwave Method

100 mg of α-ZrP was placed in a 15 mL microwave reaction vessel followed by addition of ~ 8 mL of hexanes. A stoichiometric amount (5:1) of epoxide was then added followed by sonication of the vessel. The vessel was sealed and heated at 70 °C for 1 hour while stirring. In all cases the reaction products were washed multiple times with hexanes and ethanol, filtered, and dried in an oven at 65 °C.

2.8.3 Reflux Method

100 milligrams of ZrP is placed in 50 mL round bottom flask to which 30 mL of hexanes is added. A stoichiometric amount of epoxide (5:1) is then added and the solution is refluxed at ~ 70°C overnight. The product is rinsed and filtered with hexanes and ethanol and dried in an oven at 65°C . An identical reaction can be carried out using toluene and a temperature of 111°C or at room temperature without refluxing.

2.9 M(IV) Surface Modification

100 mg of α-ZrP was dispersed in ~50 mL of solvent. A stoichiometric amount of M(IV) salt was dissolved , added to the ZrP dispersion, and allowed to stir for 30 minutes. Set ratios of 10:1, 5:1, and 1:1, Zr: M(IV) were used in all cases. The product was washed

thoroughly with an appropriate solvent and recovered by filtration to ensure that all uncoordinated metal ions were removed.

2.10 Attachment of Phosphate Ligands to M(IV) Surface

M(IV) modified ZrP was dispersed in ethanol, the phosphate ligand was dispersed in an appropriate solvent, added to the M(IV) ZrP solution(1:1 M(IV): Phosphate ligand) and allowed to stir overnight to ensure complete reaction. The product was rinsed with hexanes and ethanol, filtered, and dried in an oven at 65°C.

2.11 Characterization

XRPD experiments were performed from 2 to 40° (2θ-angle) using a Bruker-AXS D8 short arm diffractometer equipped with a multi-wire lynx eye detector using Cu (Kα , λ = 1.542 Å) and operated at a potential of 40 kV and a current of 40 mA. Thermogravimetry experiments were carried out on a TGA Q500 TA Instrument. Samples were heated from room temperature to 800°C at a heating rate of 5 °C per minute under a mixture of air and N2 (9:1). FTIR spectra were acquired using a Shimadzu IRAffinity-1 Fourier Transform Infrared Spectrophotometer. Measurements were taken from 600 to 4000 cm^{-1} at a resolution of 4.0 cm^{-1} and 32 scans were averaged. XPS measurements were obtained with a Kratos Axis ULTRA X-ray photoelectron spectrometer equipped with a 165 mm hemispherical electron energy

analyzer. The incident radiation X-ray excitation was from a monochromatic Al anode with a 10 mA current. The analysis chamber was maintained at a steady base pressure of 10-9 Torr during sample analysis. Survey scans of up to 1100 eV were carried out at an analyzer pass energy of 160 eV with 1.0 eV steps and a dwell time of 300 ms. Multiplexed high resolution scans of the Zr(3d), C(1s), Sn(3d), and O(1s) regions were taken at a pass energy of 40 eV with 0.1 eV steps and a dwell time of 60 ms. The survey and high resolution spectra were obtained with averages of 5 and 10 scans, respectively. The C(1s) peak at 284.8 eV was set as a reference for all XPS peak positions to compensate for energy shifts due to the spectrometer work function. Quantitative compositional analyses were carried out on a four spectrometer Cameca SX50 electron microprobe at an accelerating voltage of 15 kV at a beam current of 20 nA. All quantitative work employed wavelength-dispersive spectrometers (WDS). Analyses were carried out after standardization using very well characterized compounds or pure elements. Pressed powder micro pellets were prepared by pressing a few milligrams of powder between the highly polished surfaces (0.25 μm) of hardened steel dies, and transferring the pellets onto double-sided conductive carbon tape. The pellets were carbon coated before analysis to make them electrically conductive. Analyses of pressed powder pellets were carried out with a 20 μm diameter beam while the stage was being moved 20 μm every two seconds, repeated over a ten spot traverse. This ensured representative sampling and minimized possible thermal damage to the samples. The $^{31}P\{^{1}H\}$, $^{13}C\{^{1}H\}$, and $^{119}Sn\{^{1}H\}$ MAS NMR experiments were performed with a Bruker Avance-400 spectrometer (400 MHz for ^{1}H nuclei) using a 7-mm MAS probe

head at a spinning rate of 6 kHz. Standard one pulse (direct nuclear excitation) and/or CP pulse sequences were applied in these experiments at relaxation delays necessary for a quantitative analysis of the spectra. The contact times of 2 and 6 ms were adjusted for ^{13}C and ^{31}P nuclei in the CP experiments. The external standards used for ^{13}C, ^{31}P, and ^{119}Sn NMR experiments were $SiMe_4$, H_3PO_4, and $SnMe_4$ solution, respectively. The transmission electron micrographs (TEM) of the samples were acquired using a JEOL 2010 transmission electron microscope at an acceleration voltage of 200 kV. Samples were prepared using copper grids from Ted Pella. The scanning electron microscopy images of the samples were acquired using the JOEL JSM- 7500 F FE-SEM. UV-visible measurements were obtained using a Shimadzu UV-1601PC spectrophotometer. Elemental analysis for C, H, N, Cl, and F were conducted by Atlantic Microlab.

CHAPTER III

CHARACTERIZATION OF ZIRCONIUM PHOSPHATE STARTING MATERIALS[*]

3.1 Introduction

It is widely known that depending on the synthetic conditions, ZrP can be made in a variety of particle sizes and with various degrees of crystallinity.[48] Although the lateral particle size has been considered, the thickness of the particles has not been systematically investigated. It is often assumed that the thickness of ZrP is a tenth of the lateral particle size, however this is not true in most cases.[133] Also, it is well understood that the crystallinity of ZrP affects the ease of the intercalation and exfoliation processes.[29] This suggests that altering synthetic conditions produces ZrP materials that are somewhat different, however a thorough characterization of each individual material has not been reported in the literature. In most cases the highly crystalline form or single crystals of ZrP are cited in regards to the characterization, but these results differ greatly from the nanoparticles. In this chapter the characterization of ZrP materials of different particle sizes will be carried out using powder X-ray diffraction, FTIR, NMR, and TGA.

---

[*] Part of this chapter is reprinted with permission from "Surface Modification of Zirconium Phosphate Nanoplatelets for the Design of Polymer Fillers" by Mosby, B.M., Díaz, A., Bakhmutov ,V.I., and Clearfield, A. *ACS Applied Materials and Interfaces*, **2014**, 6 (1), 585-592, copyright 2013 by American Chemical Society.

3.2 Reflux ZrP

3.2.1 Powder X-Ray Diffraction

3M, 6M, 9M, and 12 M ZrP were synthesized according to the reflux method of Sun and coworkers.[48] Powder X-Ray diffraction of all samples reveals the characteristic pattern of α-ZrP indicating that it was successfully synthesized, **Figure 13**. It is well known that the width of a peak in powder X-ray diffraction pattern is directly related to the crystallinity of the material, in which more crystalline materials will exhibit narrower peaks.[14] In the case of ZrP as prepared by the reflux method, it can clearly be observed that the 3M sample has the broadest peaks and the trend continues as an increase in phosphoric acid concentration leads to progressively narrower peaks. In the case of the 9M and 12M samples the diffraction patterns are nearly identical, this suggests that the crystallinity of the materials is very similar and not significantly different. The 12M sample displays a more intense 002 peak, however this does not necessarily mean the sample is more crystalline as preferred orientation and other factors can artificially increase the intensity. Crystalline ZrP also has dominant reflections at 2 theta values of *ca.* 20, 25, and 34, that appear as doublets. These doublets can be observed clearly in all the samples except the 3M. As the crystallinity increases these features become more dominant, in the case of the 3M sample reflections appear at these positions but are not doublets due to the broad nature of the peaks. In addition, at higher 2 theta values all of the reflections tend to become less intense and in the case of less crystalline samples

some of the signals are unobservable. Based on the analysis of the X-ray diffraction patterns it can be said that in regards to samples prepared by the reflux method, 3M samples posses low crystallinity, 6M have a moderate crystallinity, and 9M-12M posses high crystallinity.

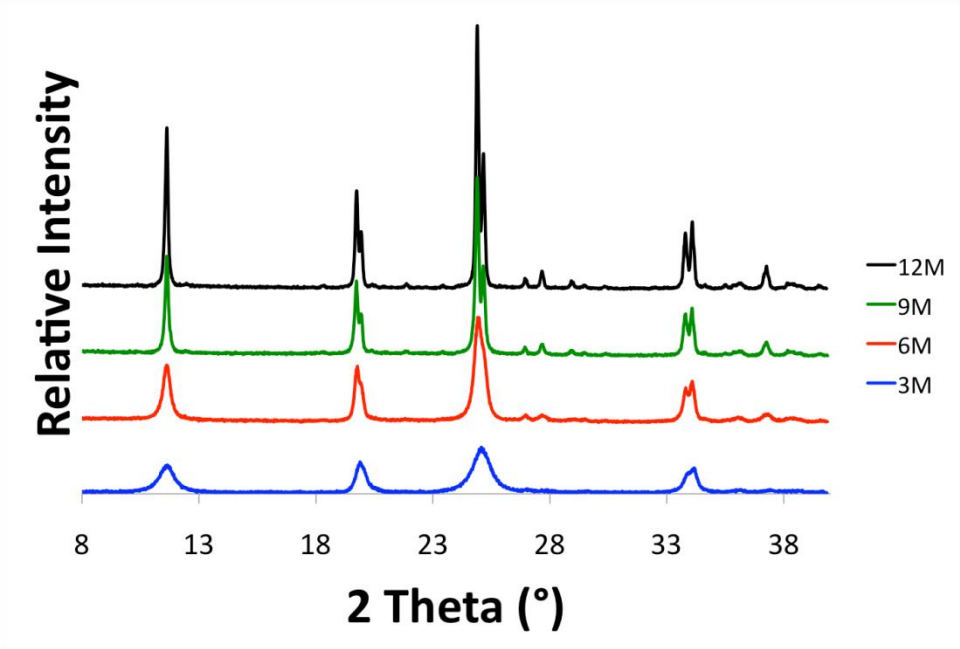

Figure 13. Powder X-ray diffraction patterns of ZrP prepared by the reflux method with phosphoric acid of various concentrations.

3.2.2 FTIR

The infrared spectra of the reflux ZrP materials were acquired and found to be largely identical to what was cited in the literature by Horsley, in which he found the spectra to

be comprised mainly of stretches due to the phosphate groups and the lattice water, **Figure 14**.[134] In summary the stretches at 3590 cm^{-1}, 3510 cm^{-1}, 3150 cm^{-1}, and 1618 cm^{-1} are all from the stretching and bending of the lattice water, the large range of stretching frequencies is seen due to the two crystallographically different phosphates in ZrP hydrogen bonding to different extents with the interlayer water molecule. The shoulder observed at 3280 cm^{-1} and the peaks at 2300 cm^{-1} and 2100 cm^{-1} are (very weak) due to the P-OH groups within the structure and their hydrogen bonding interactions. All other bands ranging from 1250 cm^{-1} to 980 cm^{-1} are thought to be associated with the orthophosphate in some way. FTIR is based solely on the chemical composition and stretches of bonds, therefore the crystallinity of the samples should not significantly affect the spectra. However, a slight shift was observed in the phosphate stretch of the less crystalline samples when compared to the highly crystalline samples. Overall, the FTIR confirms the successful synthesis of ZrP.

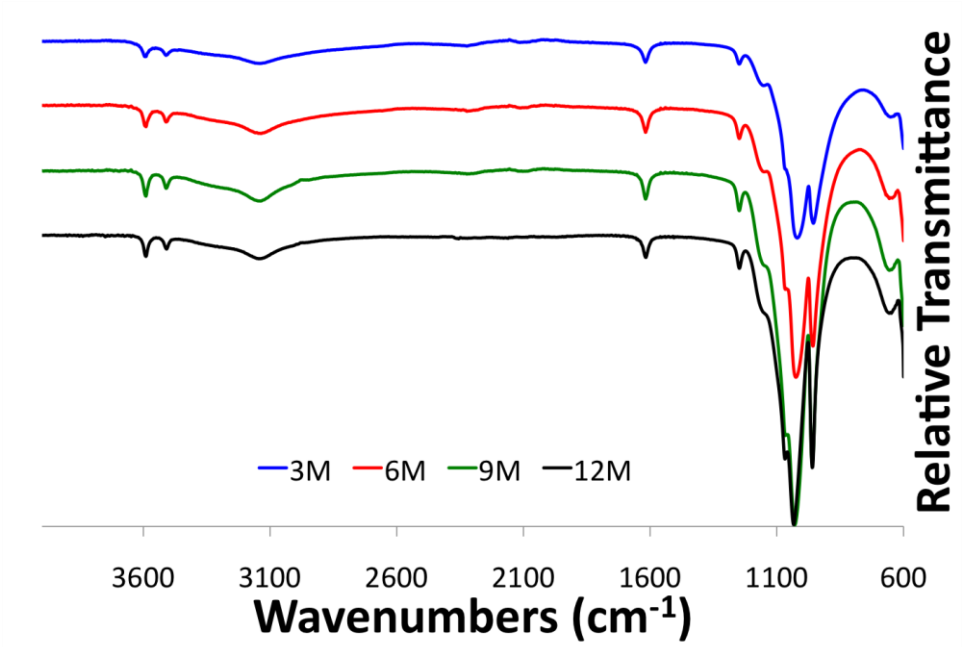

Figure 14. FTIR spectra of ZrP prepared by the reflux method with phosphoric acid of various concentrations.

3.2.3 TGA

In general the TGA of ZrP is said to consist of two major weight loss events, the first in which the water molecule is removed from the interlayer region and the ZrP is dehydrated, and the second in which the interlayer phosphates are condensed producing P-O-P bonds and thus zirconium pyrophosphate.[135] The synthetic method used in preparing ZrP is known to influence the thermal behavior, however both the heating rate and the crystallinity of the particles affect the thermogram as well.[136-138] The dehydration begins from the exterior of the nanoparticles therefore it is expected that less crystalline materials will be dehydrated more rapidly than their more crystalline counterparts.[138] In

addition, materials of lesser crystallinity may contain higher amounts of water absorbed to the surface of the nanoparticles.

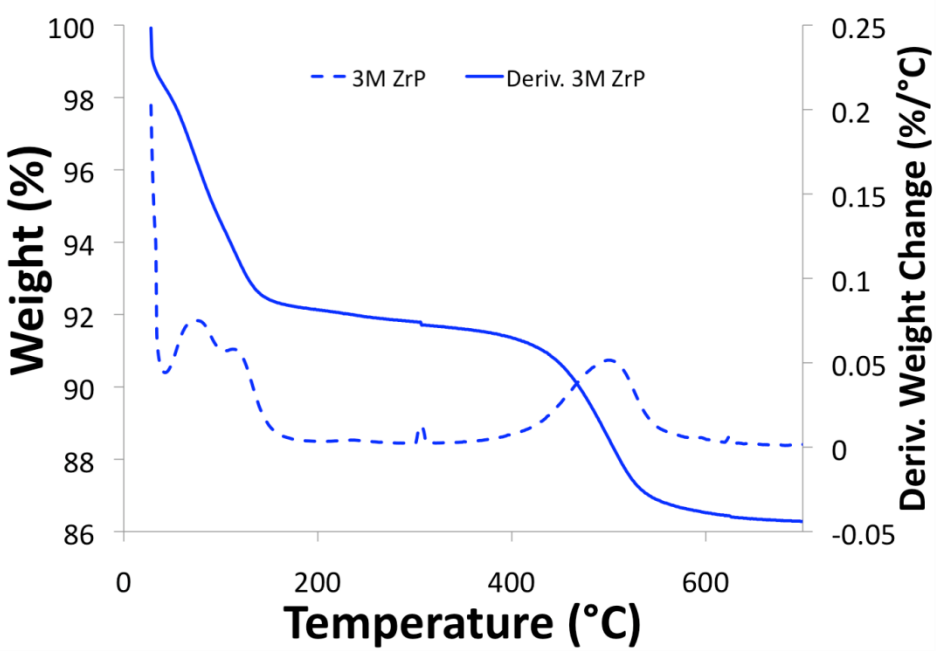

Figure 15. TGA thermogram of 3M reflux ZrP.

The TGA thermogramm of the 3M sample is displayed in **Figure 15.** The total weight loss for 3M ZrP was observed to be 13.57%. Typically weight losses below 100°C are attributed to surface water but this does not hold true for particles of lower crystallinity. The initial rapid weight loss below 35°C is attributed to water that is absorbed to the nanoparticle surface and accounts for 1.3% of the total weight loss. The derivative of the weight loss displays two overlapping weight loss events occurring from 75°C to 145°C.

The first event (4.3%) is the water near the edges of the ZrP particles that is less stabilized and lost more easily relative to the water that is in the inner part of the particles, which accounts for the second event (2.8%). The condensation occurs in the expected range for this material and is shown to begin at 449°C.

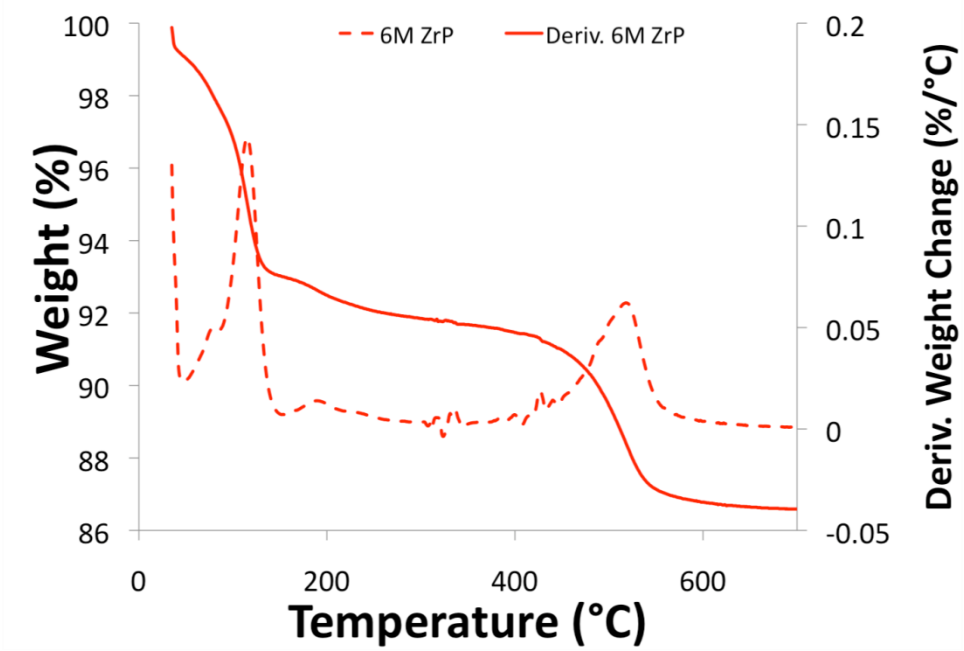

Figure 16. TGA thermogram of 6M reflux ZrP.

The 6M particles have a similar total weight loss of 13.45%, **Figure 16**. Although the total weight loss is close to that of 3M ZrP, the increase in crystallinity of the particles changes the individual events. In this case the surface water is observed to make up 0.95% of the total weight and the dehydration takes place in three steps as opposed to the

two seen for the 3M particles. In addition to the new weight loss event, the intensity of the original signals has changed. In the 3M samples the loosely held water was the dominant weight loss in the dehydration process, but for the 6M sample the loosely held water only accounts for 1.5% whereas the bulk of the water makes up 4.6% of the total weight loss and is lost from 100°C to 130°C .The new weight loss event occurs from 175°C to 225°C and accounts for 1.1% of the weight. This weight loss is the water at the very inner part of the particles, at times this water can be lost at higher temperatures especially at slower heating rates. The condensation starts at a slightly higher temperature of 471°C and accounts for 5.3% of the total weight.

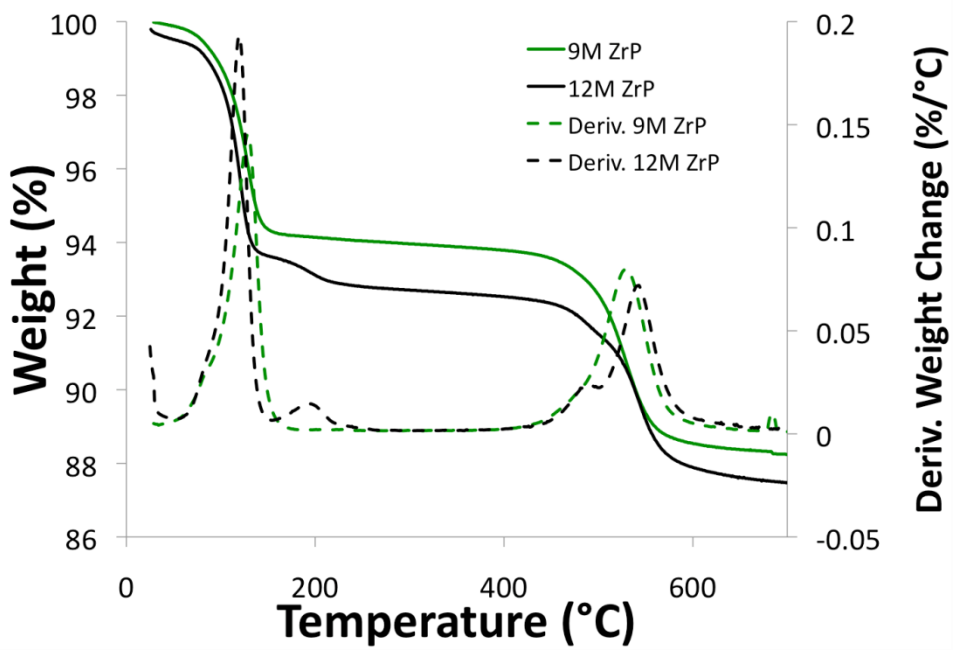

Figure 17. TGA thermograms of 9M and 12M reflux ZrP.

The thermal decomposition of the 9M and 12M particles are very similar therefore they will be presented together, **Figure 17**. The total weight losses of the 9M and 12M samples are 11.8% and 12.1% respectively. Both particles exhibit a very small amount of surface hydration with contributions below 1% of the total weight loss. The 9M sample displays what could be a slight shoulder indicative of some loosely held water coming off before the main dehydration occurs but it is not significant enough to ascribe any values to. The dehydration of the interlayer occurs from 120°C to 150°C in both cases and the condensation begins roughly at 500°C.

3.2.4 NMR

Solid state NMR experiments have been conducted on ZrP in the past.[39, 40, 139] ^{31}P spectra provide useful information on the environment of the phosphates within ZrP. Although there are two crystographically different phosphates in the crystal structure, only a single resonance exists in the spectra. This resonance is generally cited as -19 ppm although there appears to be some variation in the literature as other values such as -18.7 ppm have been reported as well.[139, 140]

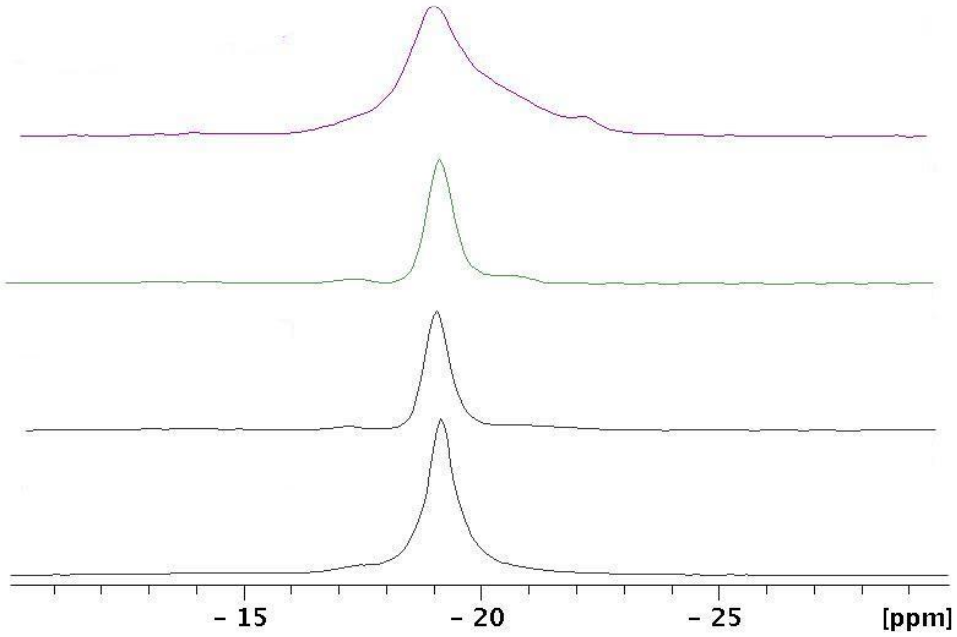

Figure 18. NMR of ZrP samples prepared by the reflux method, 3M, 6M, 9M, and 12M, from top to bottom.

The ^{31}P spectra of the reflux particles are presented in **Figure 18.** Upon investigation of the ^{31}P spectra it can be seen that the ZrP synthesized by reflux methods contain more than one peak as is commonly reported. The peak that corresponds to the P-OH groups is the dominant peak in the spectra, it appears that the peak moves closer to -19 ppm as the crystallinity of the material increases. The 3M sample displays a unique signal at ~- 21 ppm. Based on literature reports this peak is representative of anhydrous ZrP.[40] It is highly possible that during the drying of the particles overnight at 65°C that less crystalline materials can be slightly dehydrated, based on the weight loss events observed in TGA it is possible for water to be lost at this temperature. Even highly crystalline ZrP can be completely dehydrated at prolonged heating at 110°C, the

threshold appears to be lower for the less crystalline particles.[138] This dehydration peak does not appear in any other materials and only accounts for a small percentage of the total phosphorus in the 3M ZrP. A slight signal at -17.1 ppm can also be observed in all samples prepared by the reflux method regardless of crystallinity. Although the literature nearly always assigns the ^{31}P spectra of α-ZrP as a single peak close examination of published spectra shows a slight shoulder on the left of the dominant peak, which is usually not mentioned or assigned.[40, 139-143] This small peak is prevalent in materials that are less crystalline and prepared through reflux methods. It is possible that during washing of the material that the expected 2:1 P:Zr ratio is reduced by hydrolysis of the phosphates and leaves a small percentage of phosphate in a different environment from the bulk, especially on the edges of the particles.[144]

3.3 Dried Θ-ZrP (3MT)

The Θ phase of ZrP is synthesized by slightly modifying the traditional reflux method used to make α-ZrP.[27] As Θ-ZrP is a hydrated phase of α-ZrP, it is synthesized in an excess of water and an excess of phosphoric acid. In addition, a zirconyl chloride solution is added drop wise to hot phosphoric acid in the synthesis. These synthetic conditions lead to a more uniform particle size distribution compared to particles produced by the traditional reflux method. For this cause, Θ-ZrP can be dehydrated to yield α-ZrP particles that are thinner and possess a more consistent particle size. The

acid concentration used to prepare Θ-ZrP is 3M therefore particles will be designated as 3MT.

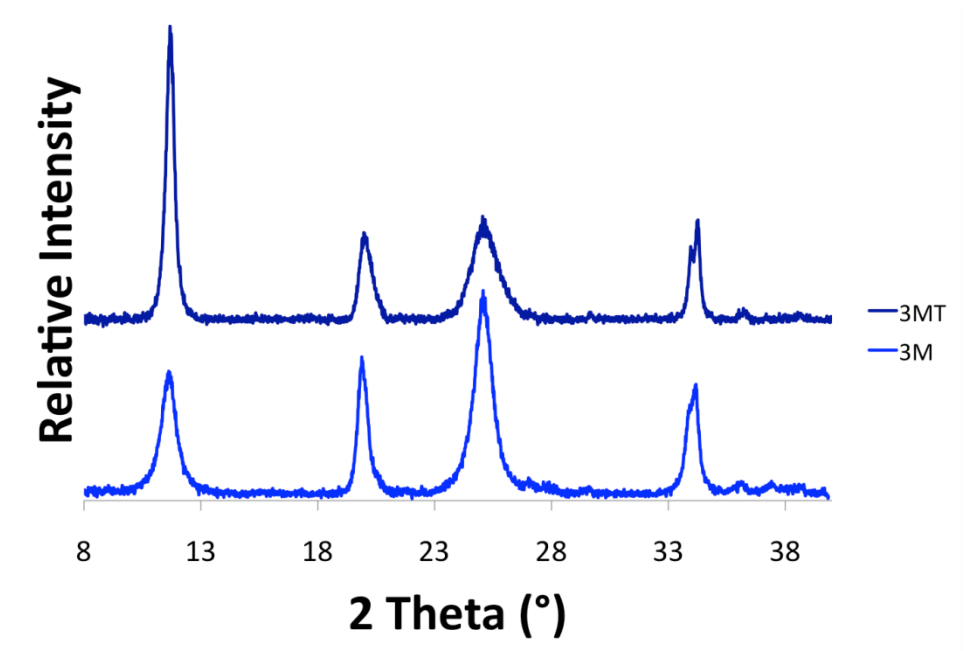

Figure 19. XRPD patterns of 3M and 3MT ZrP.

Powder X-Ray diffraction shows 3MT to be slightly more crystalline than the traditional 3M particles, **Figure 19**, however, this added crystallinity is not very significant and it is expected that the two particles will behave very similarly. As discussed earlier there is no reason to expect a noticeable difference in the IR spectra of 3MT but TGA shows a slightly different pattern for the interlayer water losses, **Figure 20**. From 55°C to 190°C the interlayer water of 3MT is lost in three distinct steps. The first of the three weight

loss events is the most dominant and each successive event decreases in intensity. The first event occurs at 55°C to 75°C and accounts for ~3% of the total weight, the second from 110°C to 140°C makes up 2% and finally the material is completely dehydrated from 170°C to 190°C with a weight loss of 1%. The condensation occurs at 480°C and the total weight loss of the material is 12.83%. Although the total weight loss is lower than 3M, the content of surface water is a third of samples prepared by traditional reflux. It should also be noted that the drying of the Θ-ZrP will affect the TGA weight loss. Some samples that are dried for longer periods of times display a one step dehydration followed by a very small water loss at higher temperatures.

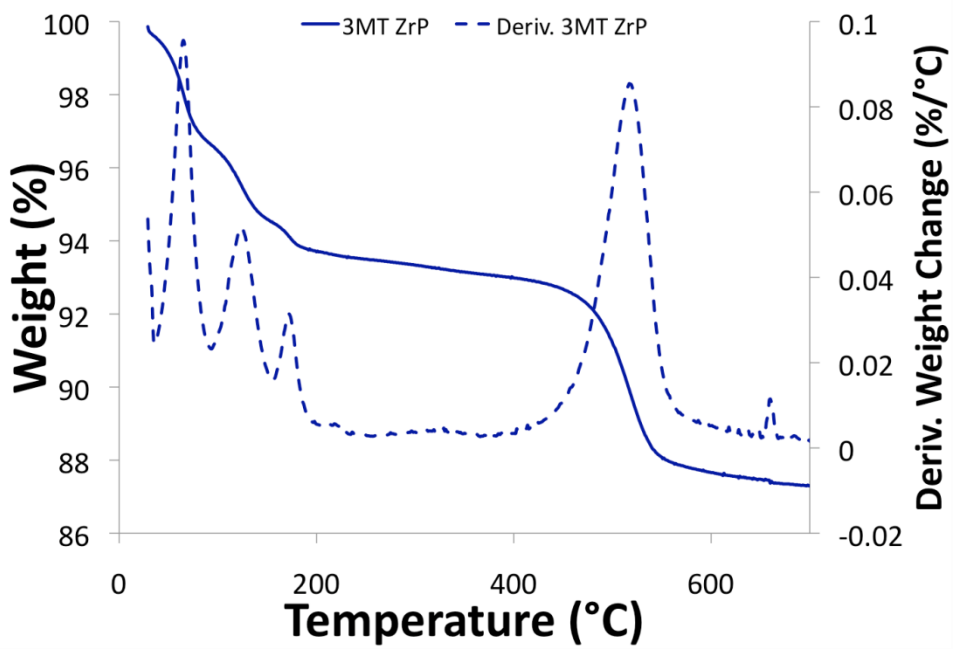

Figure 20. TGA thermogram of 3MT ZrP.

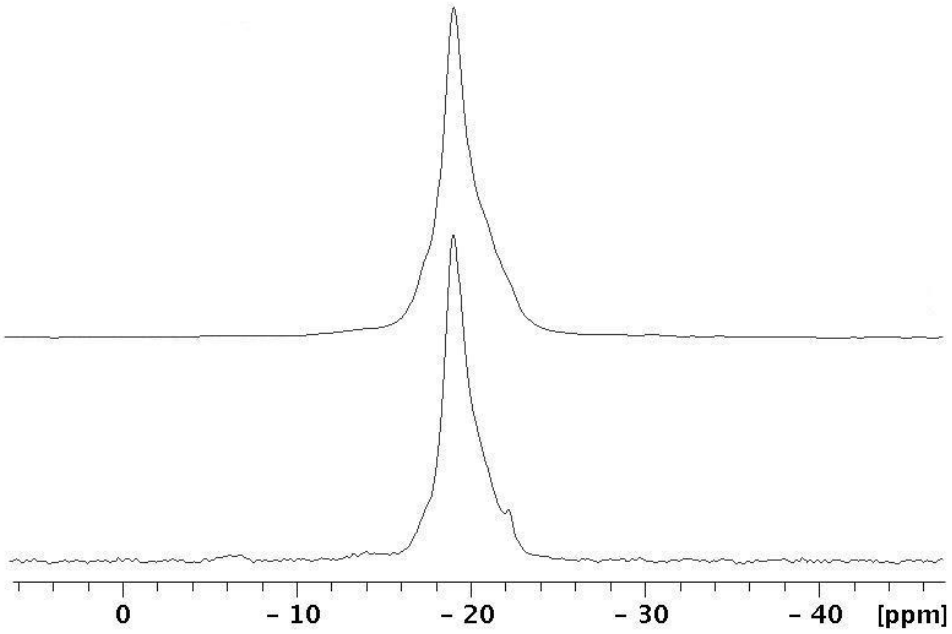

Figure 21. NMR spectra of 3MT (top) and 3M Reflux (bottom) ZrP.

The ^{31}P NMR of 3MT displays three resonances as 3M does and is nearly identical in nature regarding the ratios and intensities of the signals, **Figure 21**.

3.4 Hydrothermal (HDT) ZrP

3.4.1 Powder X-Ray Diffraction

The powder X-Ray diffraction of hydrothermal ZrP samples is displayed in **Figure 22**. It should be noted that due to the synthetic conditions of the hydrothermal method that these particles are generally referred to as highly crystalline. It can be seen that all the

samples exhibit the expected pattern for ZrP. As seen in the reflux case, the highly crystalline samples have narrower peaks. In the case of the hydrothermal samples, the 3M is clearly the least crystalline as it possess the broadest reflections, however the reflections of 6M, 9M, and 12M are very similar and judging strictly from the XRPD it can be said that they are all highly crystalline samples and no distinction can be made other than this.

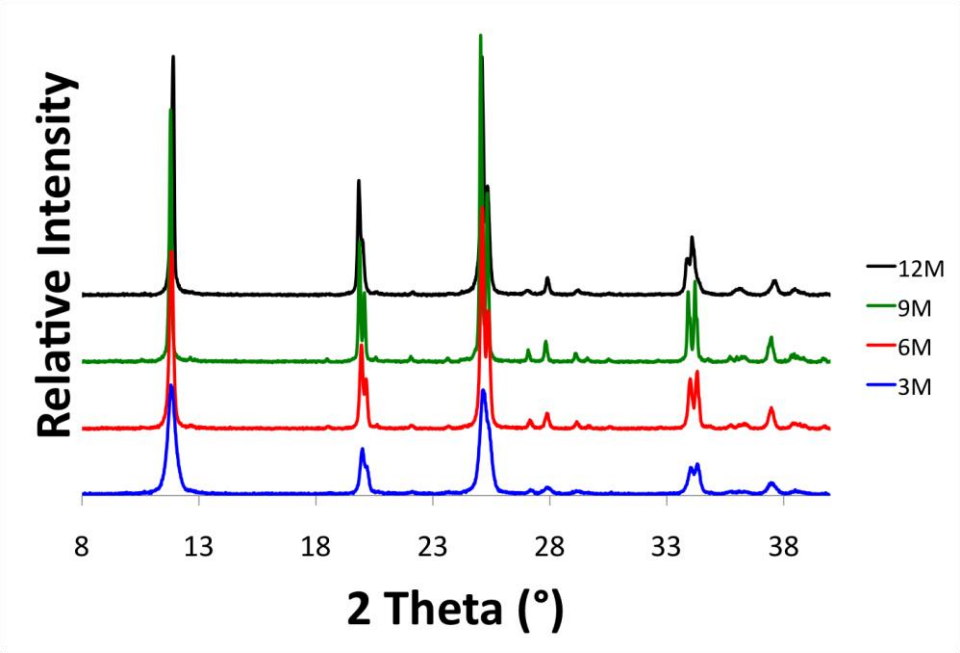

Figure 22. Powder X-ray diffraction patterns of ZrP prepared hydrothermally with phosphoric acid of various concentrations.

Even in the case of the lesser crystalline 3M sample, doublets can be observed at the reflections at 2 theta values of *ca.* 20, 25, and 34. This was not the case in the reflux

samples therefore it can be said with certainty that the hydrothermal samples are more crystalline than those prepared by the reflux method. In the hydrothermal case it can also be seen that there are a number of reflections at higher 2 theta values that are not present in the reflux samples, also supporting the fact that the hydrothermal samples are more crystalline. In addition to the crystallinity effects on XRPD it can also be noted that particle size has an effect on the reflections obtained. Smaller particles tend to give broader reflections whereas larger particles give better diffraction. All the trends observed thus far correlate the particle size very well with the observed diffraction data.

3.4.2 FTIR

The FTIR spectra of the hydrothermally synthesized ZrP can be seen in **Figure 23**. As discussed earlier no significant changes are expected in the FTIR even with the increased crystallinity. It is noted however that in the case of the hydrothermal samples that the signal around 1170 cm^{-1} appears to be more well defined than in the lesser crystalline samples. This signal is a result of the phosphate group in ZrP. It is likely that as some reflux particles are hydrolyzed by washing, that this signal could be diminished whereas in the hydrothermal case the hydrolysis is not as likely therefore yielding a more intense signal in this region.

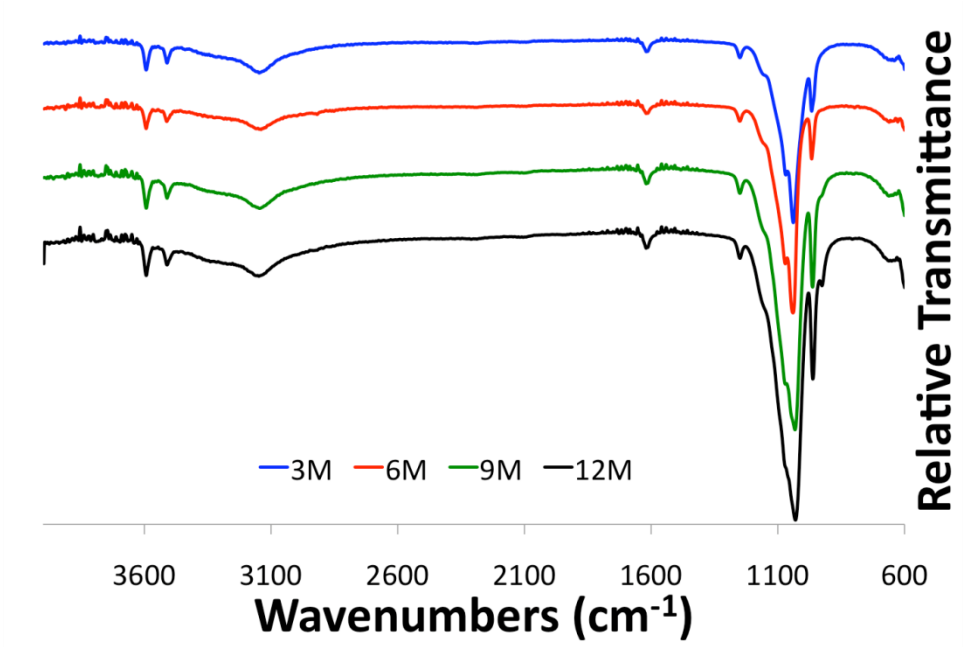

Figure 23. FTIR spectra of ZrP prepared hydrothermally with phosphoric acid of various concentrations.

3.4.3 TGA

TGA data of ZrP synthesized hydrothermally confirms that there is a distinct difference between the dehydration and condensation of ZrP that is synthesized using different methods and phosphoric acid concentrations. 3M HDT ZrP displays a total weight loss of 13.51%, **Figure 24**. The initial weight loss below 40°C is due to the small extent of surface water, which makes up 1.2% of the total weight loss. Although hydrothermal samples are more crystalline, the three-step dehydration observed in some of the reflux samples can be seen in the 3M HDT case. The dehydration takes place between 80°C and 205°C in three overlapping processes identified in the derivative of the weight loss.

These three processes are thought to be the loosely held water on the exterior of the particles, the standard water loss, and the water that is in the inner part of the layer; the losses are 1.6%, 3.9% and 1.9% respectively. The condensation to the pyrophosphate begins at 475°C and attributes 4.6% to the total weight loss of 13.51%.

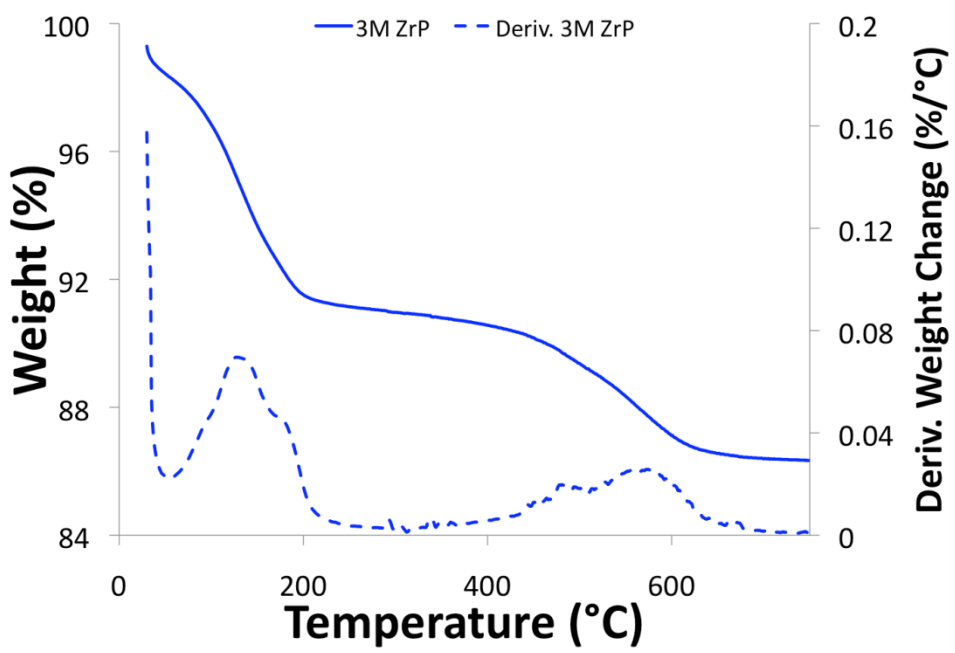

Figure 24. TGA thermogram of 3M hydrothermal ZrP.

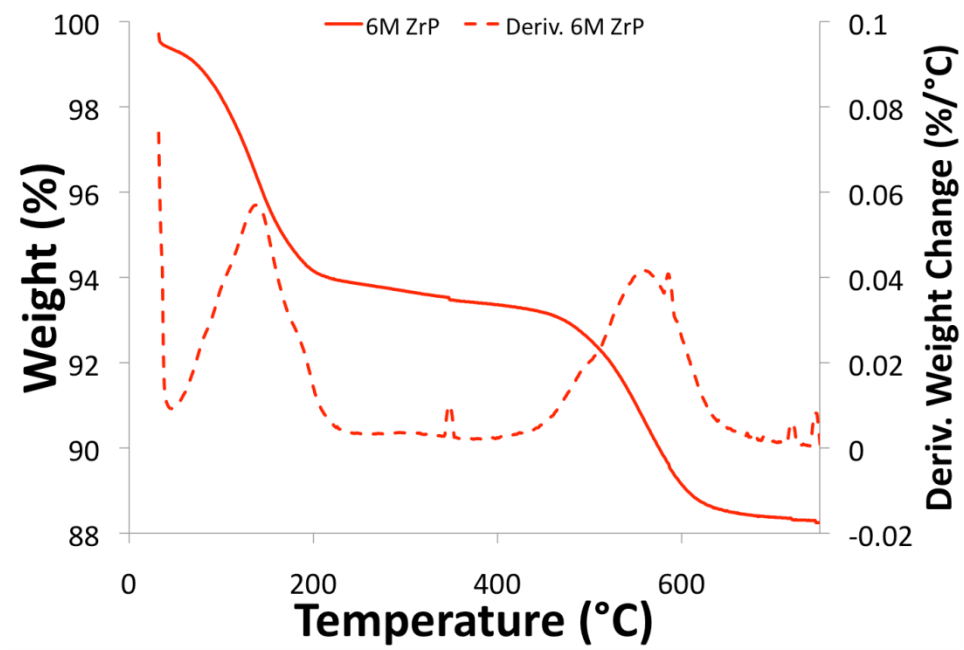

Figure 25. TGA thermogram of 6M hydrothermal ZrP.

The 6M material exhibits a very similar pattern to the 3M sample, **Figure 25**, however the amount of surface water is decreased to 0.53%. The derivative for the dehydration displays a very broad peak that is likely due to the three water loss processes but it cannot be resolved in this case. The total water loss for all dehydration processes is 5.5%. In addition to the typical dehydration losses there appears to be an additional high temperature water loss from 345°C to 350°C in which a small portion of water deep inside the interior of the layer, within the middle of the nanoparticle is dehydrated (0.45%). The condensation begins at 500°C with a weight loss of 5.2% and the total weight loss of the material is 11.8%.

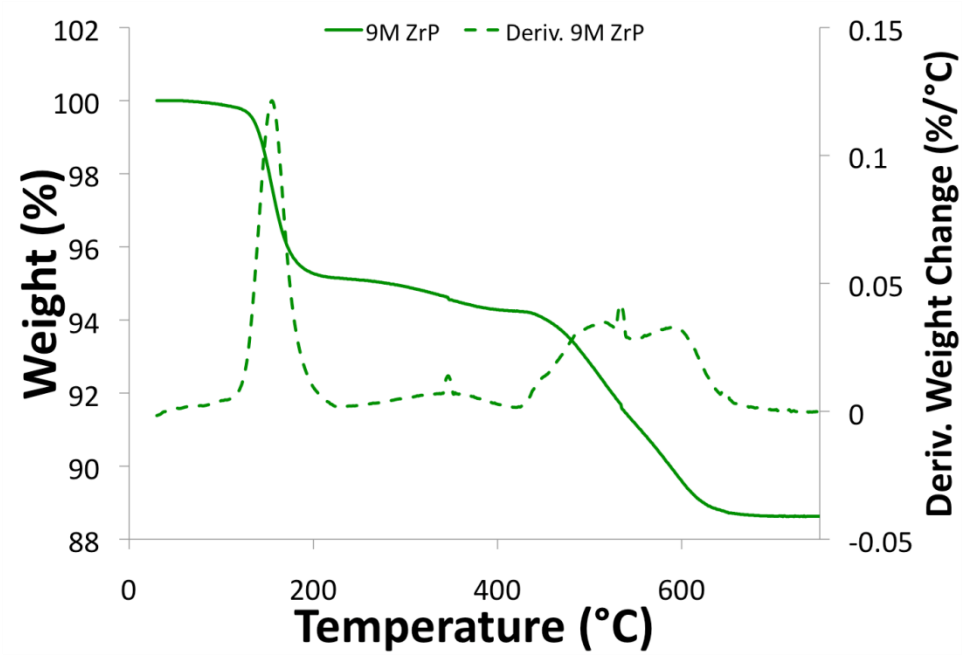

Figure 26. TGA thermogram of 9M hydrothermal ZrP.

The TGA of 9M HDT ZrP shows no surface water and a predominantly one step process for the dehydration with a weight loss of 4.87%, **Figure 26.** At this crystallinity even the water that is more loosely held is lost at a temperature comparable to the tightly held water in less crystalline samples. As a result the tightly held water loss is elevated to higher temperatures as seen in the 6M HDT case. For the 9M HDT sample the high temperature water loss is observed at 315°C and accounts for 1% of the total weight loss. Unlike other samples the condensation appears to occur in two steps, the first from 460°C to 540°C and the second from 575°C to 630°C. It is likely that this two step

process may in fact involve some additional dehydration of interlayer water mixed with the condensation, however it is not possible to distinguish the two. The total weight loss for the 9M HDT sample is 11.35%.

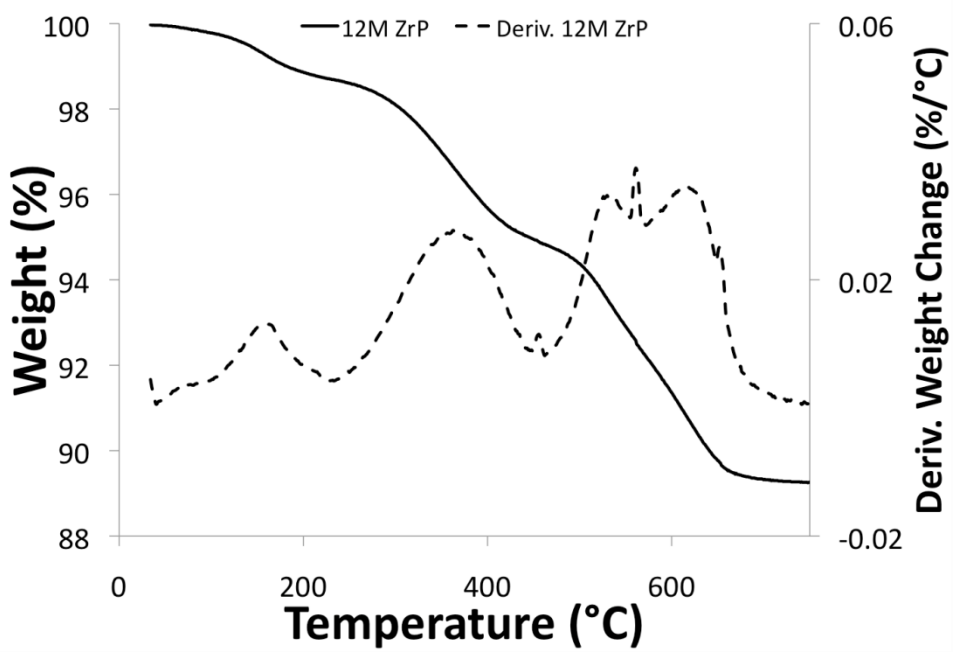

Figure 27. TGA thermogram of 12M hydrothermal ZrP.

The TGA thermogram of 12M HDT ZrP displays a total weight loss of 10.75% and is able to confirm that it is of a higher crystallinity than all other samples, **Figure 27**. As with the 9M HDT ZrP there is no surface water present however the dehydration pattern is much different when compared to of the other materials. The first water loss begins at 115°C and accounts for only 1.3% of the total weight loss, the dominant dehydration

step occurs from 300°C to 410°C and accounts for 3.9% of the total weight loss. In this case the bulk of the water is held very tightly due to the large particle size and high crystallinity of the sample. The condensation is also seen to occur in two steps, however the temperatures at which they occur (500°C to 530°C and 600°C to 660°C) are higher than the 9M HDT ZrP. It should be noted that the total weight loss is below 12%, which is the value nearly always attributed to a ZrP TGA.

3.4.4 NMR

Figure 28 displays the ^{31}P spectra of the hydrothermally synthesized ZrP samples. The spectra obtained are much more in line with what is cited within the literature. In all cases the spectra are largely identical and the dominant signal of the orthophosphate is observed at -19 ppm. The dehydration observed in the reflux case is not evident here nor is the small peak to the left of the shoulder from hydrolysis. As these particles are more crystalline than the reflux case it is much more difficult for dehydration or hydrolysis to occur.

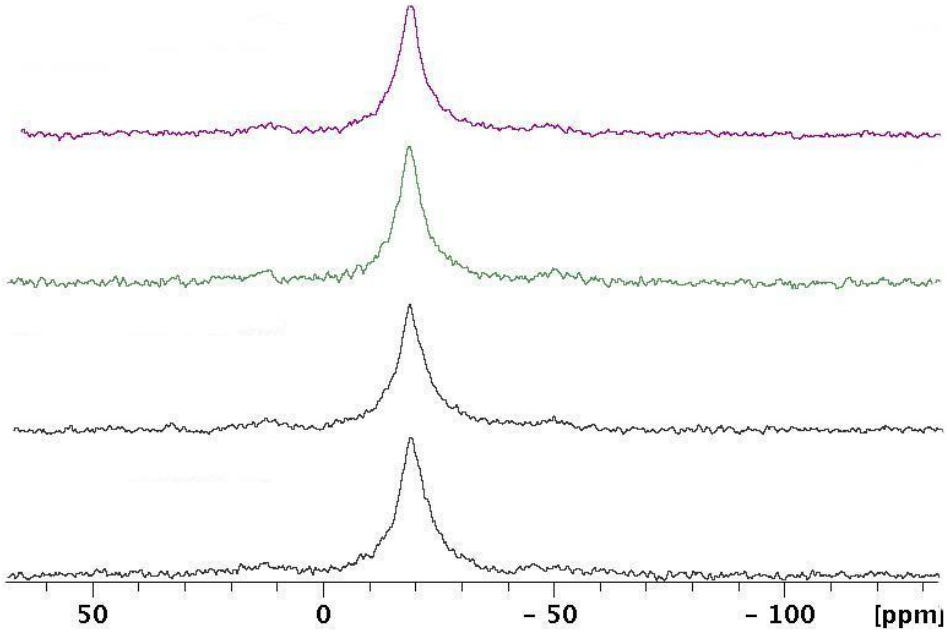

Figure 28. NMR of hydrothermal ZrP; 3M, 6M, 9M, and 12M, from top to bottom.

3.5 Aspect Ratio

Additionally electron microscopy can be used to determine the average particle size and thickness of the synthesized ZrP. Sun et al originally reported particle size ranges for ZrP synthesized by reflux, hydrothermal, and HF methods with varying concentrations of phosphoric acid.[48] Sun's values encompass a wide range of particle sizes and do not comment on the median or average size within the given range. It should be noted that there is some overlap in the sizes he reports, however based on the characterization presented thus far all the materials seem to differ in other areas. Although Sun discusses the lateral particle size, he does not consider the thickness of the particles, therefore his

discussion of the aspect ratio is somewhat incomplete. SEM images displaying the particles synthesized by the reflux method can be seen in **Figure 29** along with images displaying the thickness of the particles in **Figure 30**. Additionally, TEM images of 3MT ZrP can be seen in **Figure 31**. Lastly, SEM images of hydrothermally synthesized ZrP are seen in **Figure 32** and the images displaying the particle thickness in **Figure 33**. For comparison a summary of the particle size, thickness, and aspect ratio can be seen in **Table 1**.

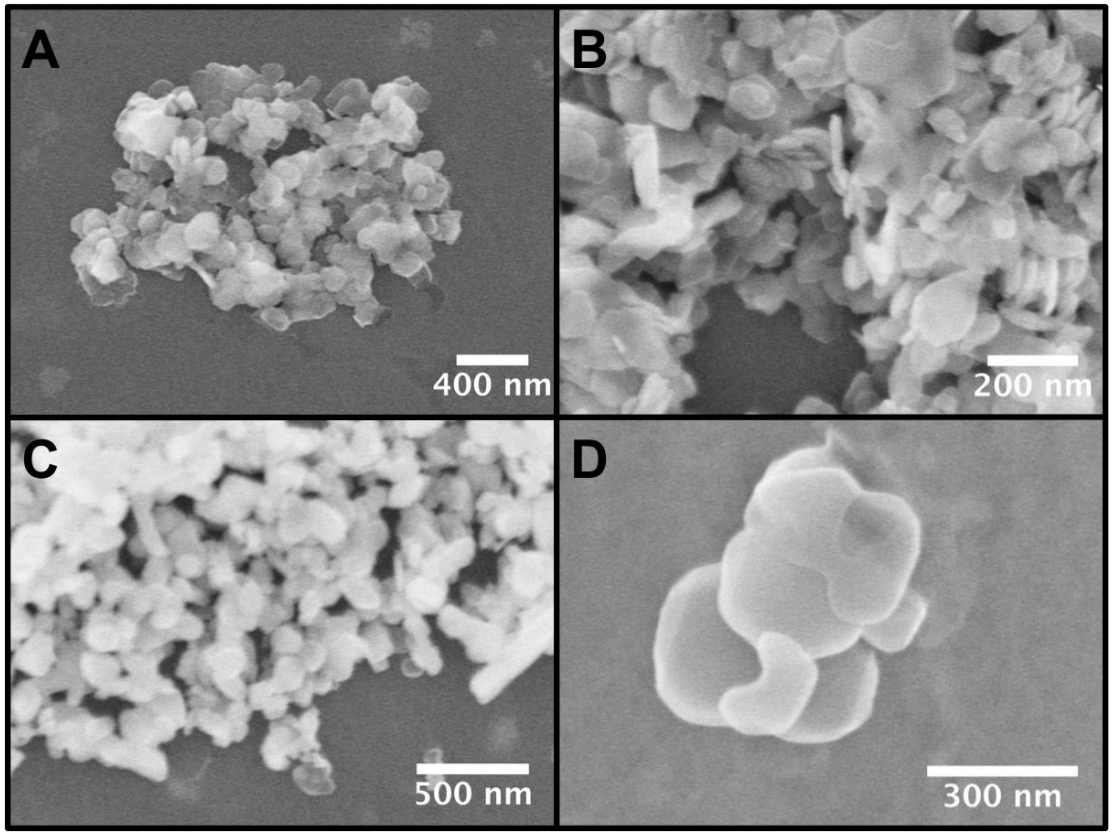

Figure 29. SEM images of ZrP synthesized by the reflux method. (A) 3M, (B) 6M, (C) 9M, (D) 12M.

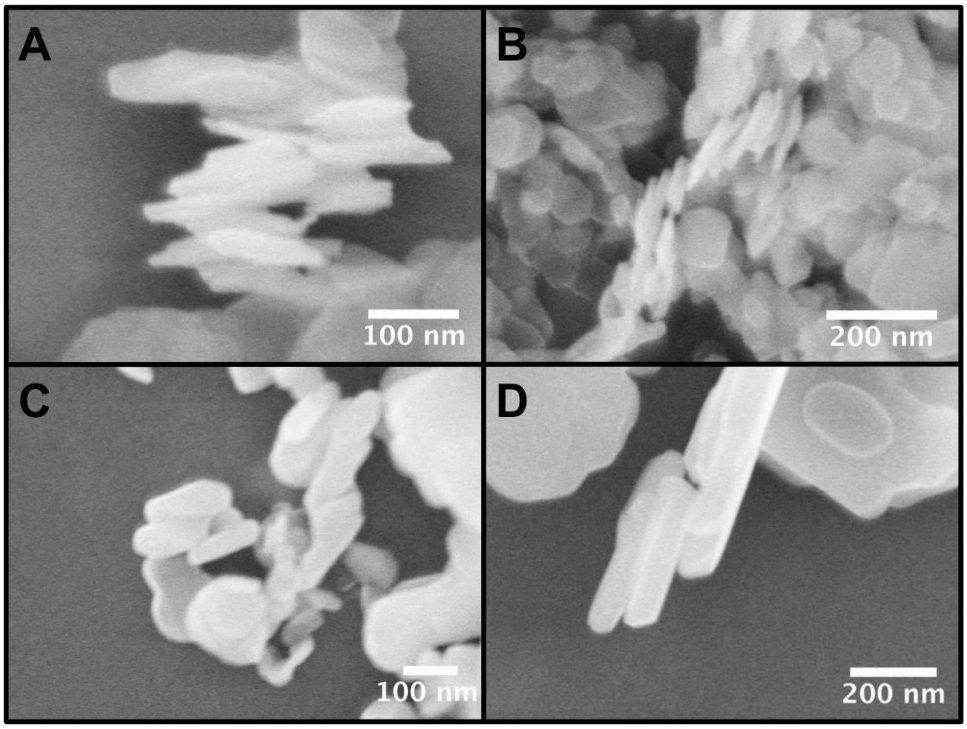

Figure 30. SEM images of reflux ZrP displaying the thickness of the nanoparticles. (A) 3M, (B) 6M, (C) 9M, (D) 12M.

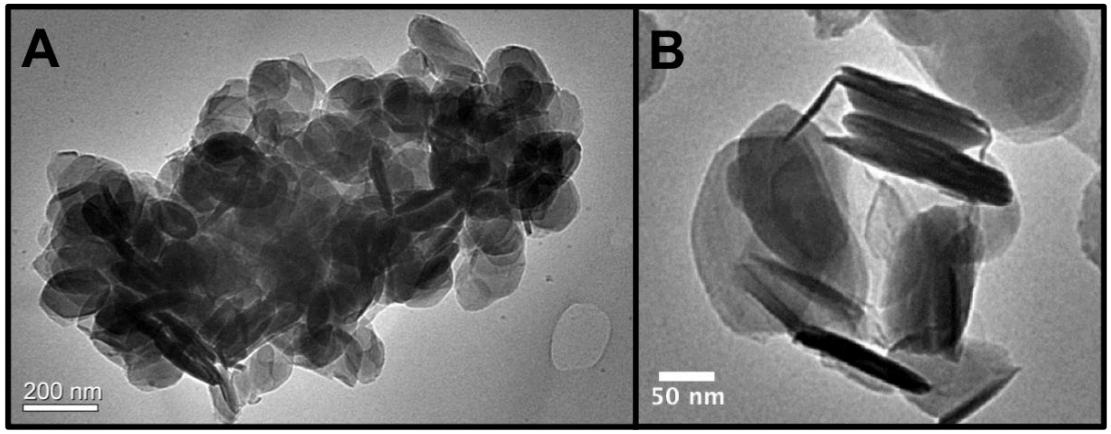

Figure 31. TEM of 3MT ZrP displaying the average particle size (A), and thickness (B) of the nanoparticles.

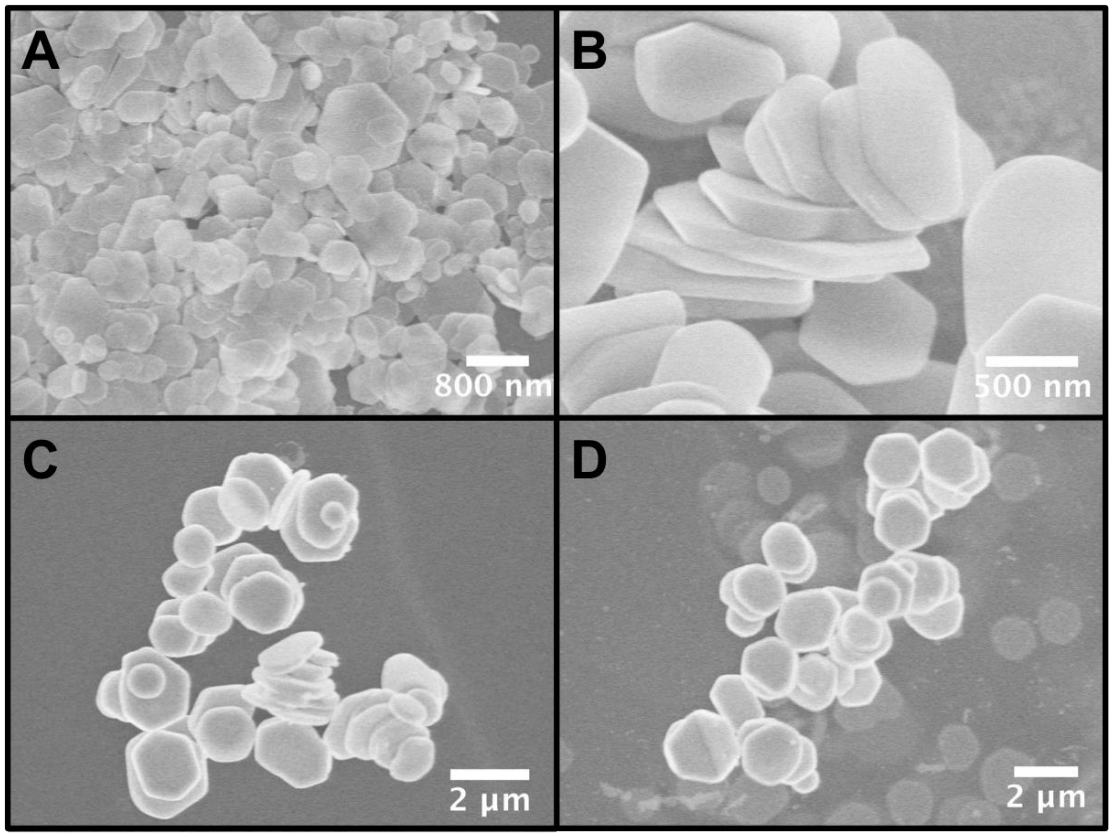

Figure 32. SEM images of hydrothermal ZrP synthesized with (A) 3M, (B) 6M, (C) 9M, and (D) 12M phosphoric acid.

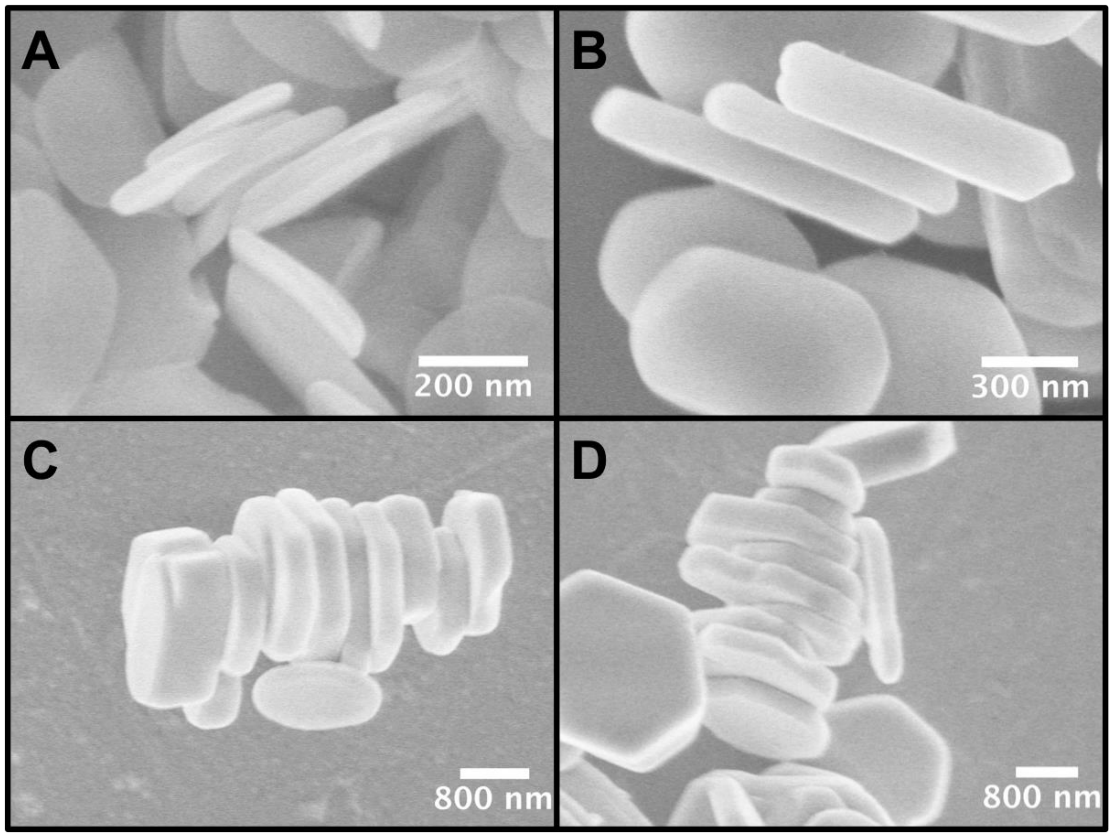

Figure 33. SEM images of hydrothermal ZrP displaying the thickness of the nanoparticles. (A) 3M, (B) 6M, (C) 9M, (D) 12M.

Table 1. Summary of the particle sizes, thicknesses, and aspect ratio of all ZrP synthesized.

Sample	Reported Range (nm)	Particle Size (nm)	Thickness (nm)	Aspect Ratio
3MT	--	120	10	12
3M Reflux	50- 100	135	10	14
6M Reflux	100-200	130	20	7
9M Reflux	100-200	170	40	4
12M Reflux	150-300	275	80	3
3M HDT	300-500	550	40	14
6M HDT	600-800	850	125	7
9M HDT	800-1000	1400	295	5
12M HDT	1000-1200	1600	310	5

In regards to the particles prepared by the reflux method, the 3M and 6M particles are thought to have roughly the same particle size, even though the average is slightly higher for the 3M case. The difference between the two samples is primarily in the thickness of the particles where the 6M samples doubles in thickness relative to the 3M. This trend continues throughout the reflux samples, as 9M samples are twice as thick as 6M, and 12M twice as thick as 9M. While the thickness changes drastically among all the samples, the lateral particle growth does not differ much from 3M to 9M. This suggests that in the reflux synthetic method the primary growth of the particles is not in the lateral direction but down the c axis of ZrP. All the average particle sizes found in this study fall within the expected range proposed by Sun except for the 3M case. 3M is said to be 50 nm – 100 nm, however in our case the average particle size was found to be 135 nm. It was found that the 3MT ZrP is only slightly smaller than particles prepared by the traditional 3M reflux method. It can however be noted that the particle size distribution is much narrower than all other cases. The excess of phosphoric acid leads to a more uniform size. It may be ideal to extend this approach to the other phosphoric acid concentrations to produce a narrower particle size range. These particles have also been characterized by AFM, the thickness observed in electron microscopy agrees well with the AFM experiments.[145, 146]

The hydrothermal method does not always produce a single particle size and it is likely that there will be extremes in which some particles will be much larger or smaller than others. Although extremes exist there is indeed an average particles size that the bulk of

the particles will possess. It is observed in all cases that the particles appear to be larger than Sun originally reported.[48] This could likely be a factor of how the reaction was conducted. Sun synthesized ZrP on a 4-gram scale, which required 40 mL of H_3PO_4 and a Teflon lined pressure vessel with a large volume. In our case, the reaction was done on a 1 gram scale with 10 mL of H_3PO_4 , and a pressure vessel with a total volume of 15 mL. Due to the difference in volume of the Teflon lined pressure vessel and phosphoric acid, it is probable that the synthesis carried out in the smaller vessel produced higher pressure and therefore yielded particles larger than those originally reported.

As the particle sizes and thicknesses have now been documented, the aspect ratio can be calculated by dividing the lateral particle size by the thickness. The average particle size, thickness, and aspect ratio are listed in **Table 1** for comparison. The aspect ratio of ZrP appears to decrease with an increase in phosphoric acid concentration. It should be noted however that the relationship is not solely due to the acid concentration but more so the phosphoric acid to zirconium ratio. As the concentration of phosphoric acid increases, the excess of phosphoric acid is increased as well. In both the reflux and hydrothermal cases 3M, 6M, 9M, and 12M phosphoric acid produce a ratio H_3PO_4:Zr of 10:1, 20:1, 30:1, and 40:1 respectively. This relationship explains why the aspect ratios are similar for both methods when identical phosphoric acid concentration is used. The aspect ratio decreases as the particles grow laterally; the lateral growth is more rapid than growth in the c direction. Once a highly crystalline sample is obtained the aspect ratio appears to stabilize at 5 for the hydrothermal case and around 3 for the reflux.. It is

known that after a certain point, continued refluxing of ZrP no longer causes an increase in particle size. Although there is a slight increase in lateral particle size and thickness between the 9M and 12M samples, it is clear that they are both approaching the point to which particle growth no longer occurs.

The 3MT particles have a H_3PO_4:Zr ratio of 120:1, the highest of all samples. Although the molarity of the acid is identical to the 3M reflux ZrP, the ratio is 12 times higher. Typically the aspect ratio decreases as the H_3PO_4:Zr ratio increases, however in this case the aspect ratio remains relatively high. The particle growth must therefore be a function of both the acid concentration and the H_3PO_4:Zr ratio. High concentrations of acid typically allow the particles to dissolve relatively easily and thus recrystallize and grow in size. On the contrary, low concentrations of acid do not facilitate crystal growth as well. Further investigation is needed in this area to gain further control of the particle sizes produced when synthesizing ZrP.

3.6 Conclusion

It has been shown that the synthetic methods used to make ZrP play a large part in the nature of the produced materials. Although generalizations are common when dealing with ZrP, it is more appropriate to take the synthetic method, crystallinity, and particle size of the materials into consideration when characterizing ZrP based materials. Powder X-ray diffraction was able to confirm that increasing the phosphoric acid concentration

in the synthesis effectively increases the crystallinity of the particles and that the hydrothermal particles are more crystalline than those prepared by reflux. FTIR was able to confirm the successful synthesis of ZrP but is not useful in the discussion of crystallinity or particle size. It was found that the dehydration and thus the thermal behavior of ZrP is highly dependent on the crystallinity of the ZrP particles. NMR was utilized to determine the homogeneity of the phosphorous environments, which correlates directly with the crystallinity of the samples. Essentially less crystalline samples are more prone to dehydration and hydrolysis, which produces distinctions among the phosphorous atoms. In addition, the average particle sizes and thicknesses were catalogued for the first time. The behavior and composition of the synthesized samples is essential to understand if they will be used as starting materials for subsequent reactions such as surface functionalization.

CHAPTER IV

COVALENT ATTACHMENT OF REACTIVE LIGANDS TO THE SURFACE OF ZIRCONIUM PHOSPHATE NANOPLATELETS[*]

4.1 Introduction

It has been previously shown that organic functionality could be added to ZrP by two predominant methods, exfoliation of ZrP and subsequent reaction with a reactive organic species or by replacing phosphoric acid with a phosphonate or phosphate ester in the synthesis of the material. Although both methods are effective, the ion exchange chemistry of the interlayer is sacrificed to acquire the organic derivative, as the particles are delaminated or the phosphate functionality is replaced with phosphonic acids. In the latter case a non-exchangeable alkyl or aromatic group replaces the exchangeable proton of the phosphate group. The interlayer of ZrP is one of its most appealing features; therefore it is our aim to determine if it is possible to selectively functionalize the surface of ZrP while leaving the interlayer region unaffected. In this case the surface would be esterified while the interlayer retains P-OH groups, which can undergo further ion

[*] Part of this chapter is reprinted with permission from "Self-Assembled Monolayers Based Upon a Zirconium Phosphate Platform" by Díaz, A., Mosby, B.M., Bakhmutov ,V.I., Martí, A., Batteas, J. and Clearfield, A. *Chemistry of Materials,* **2013**, 25 (5), 723-728, copyright 2013 by American Chemical Society; and "Surface Modification of Zirconium Phosphate Nanoplatelets for the Design of Polymer Fillers" by Mosby, B.M., Díaz, A., Bakhmutov ,V.I., and Clearfield, A. *ACS Applied Materials and Interfaces,* **2014**, 6 (1), 585-592, copyright 2013 by American Chemical Society.

exchange and intercalation reactions. It has been shown in several studies that functional groups such as silanes and epoxides can react with ZrP.[35, 67, 68, 70, 72, 73, 147, 148] Our aim is to utilize these known reactive groups to determine if it is possible to selectively functionalize the surface of ZrP.

4.2 Surface Modification with Silanes

The initial reactive group of choice for the functionalization of ZrP was silanes; ZrP nanoparticles were reacted with octadecyltrichlorosilane by reflux in toluene. **Figure 34** shows the X-ray diffraction pattern for the pristine α-ZrP and the surface modified material. Both materials show the characteristic diffraction peak at 7.6 Å for the 002 planes of α-ZrP and the XRPD shows no significant difference between the two materials. The identical XRPD patterns eliminate the possibility of the intercalation of OTS into α-ZrP; such an interaction would cause diffraction peaks at lower angles. Electron microscope images of the modified particles show that the morphology of the nanoparticles is not altered in any way due to the surface modification reaction, **Figure 35**. It can therefore be concluded that the surface modification reaction does not alter the nanocrystal morphology in any significant way.

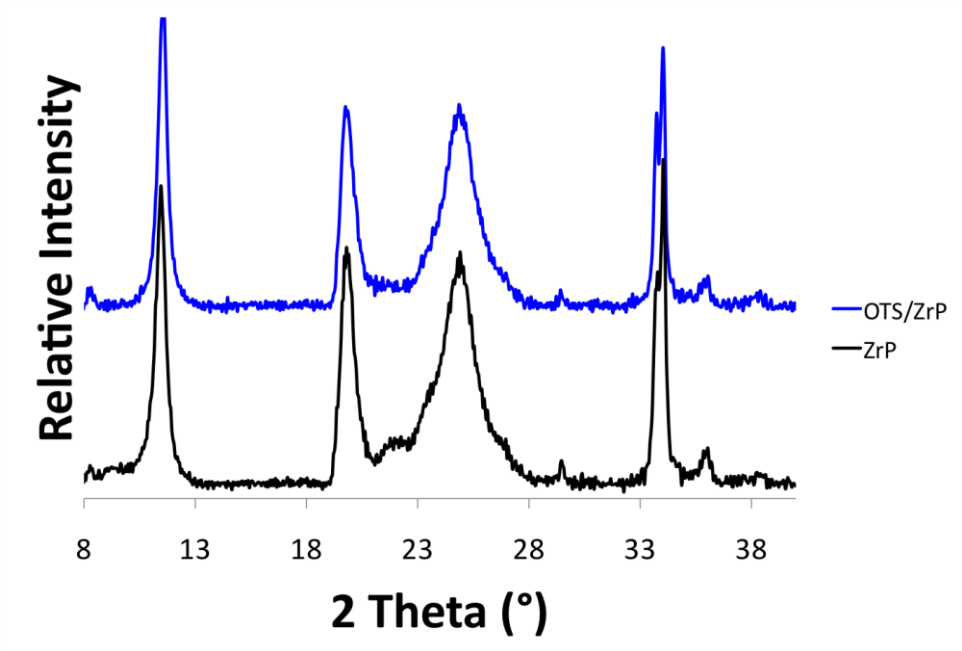

Figure 34. XRPD of OTS modified ZrP and the ZrP starting material.

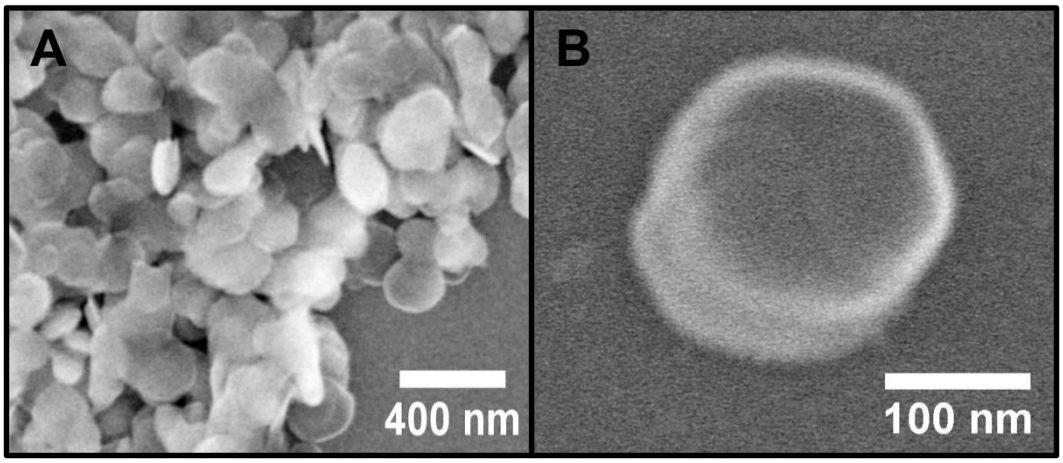

Figure 35. SEM images of OTS/ZrP.

Additionally, AFM can be used to observe differences between the pristine and modified particles. **Figure 36** shows AFM images of pristine and modified ZrP. It can be seen that the morphology of the nanoparticles is similar, as observed by AFM. In addition, a slight

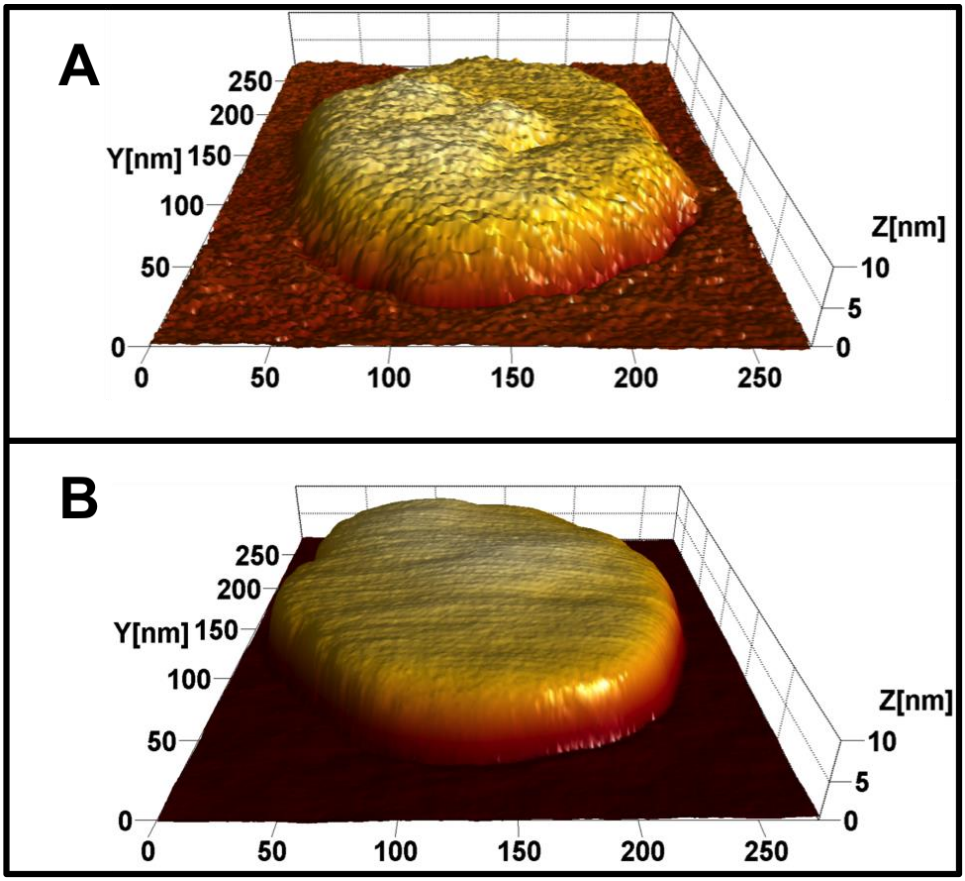

Figure 36. AFM images of (A) ZrP and (B) OTS/ZrP.

increase in the thickness of the modified sample can be observed, which can be attributed to the successful modification of the surface with OTS. The friction images of

the nanoparticles also show a contrast in which the unmodified sample with a hydrophilic surface and the modified samples with a hydrophobic surface interact differently with the polar SiO_2 tip. The images of the pristine ZrP have more distinct features due to the favorable interactions between the tip and the surface whereas the hydrophobic surface is somewhat repulsive to the tip and therefore the image does not possess well-defined features.

Additional support for the surface functionalization of the nanoparticles can be found through FTIR, **Figure 37**. The FTIR spectrum of OTS/α-ZrP shows the strong characteristic bands associated with the antisymmetric and symmetric stretching of the C-H, between 2900 cm^{-1} and 3000 cm^{-1} and bending at ca. 1450 cm^{-1}. The presence of alkyl chains is a direct result of OTS therefore modification is supported. Additionally, the bands that correspond to the splitting of the crystallization water in α-ZrP remain in the spectrum of the surface modified material. This confirms the XRPD results showing that there was no intercalation or displacement of the intercalated water molecule.

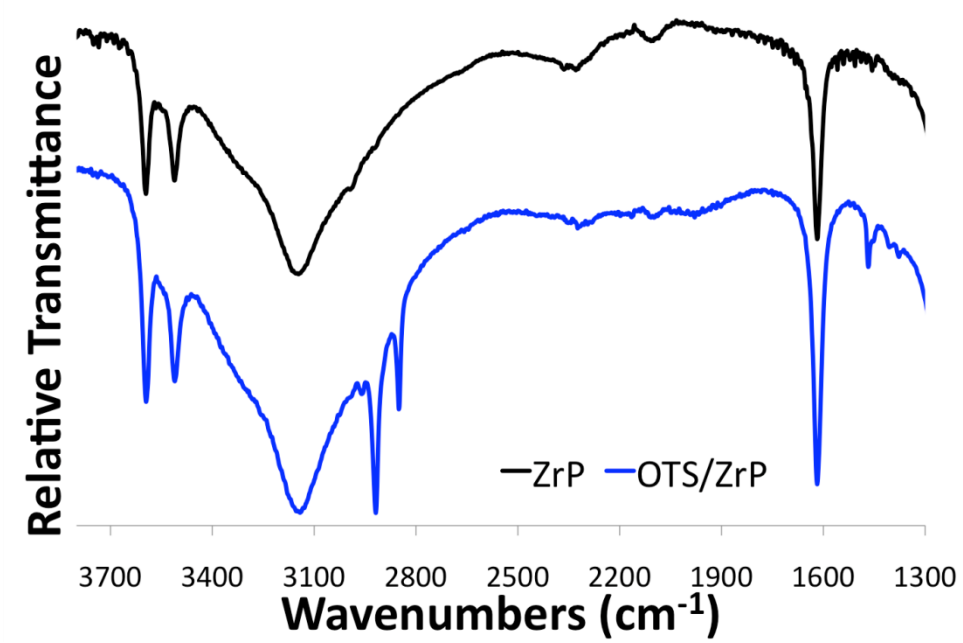

Figure 37. FTIR spectra of ZrP and OTS/ZrP.

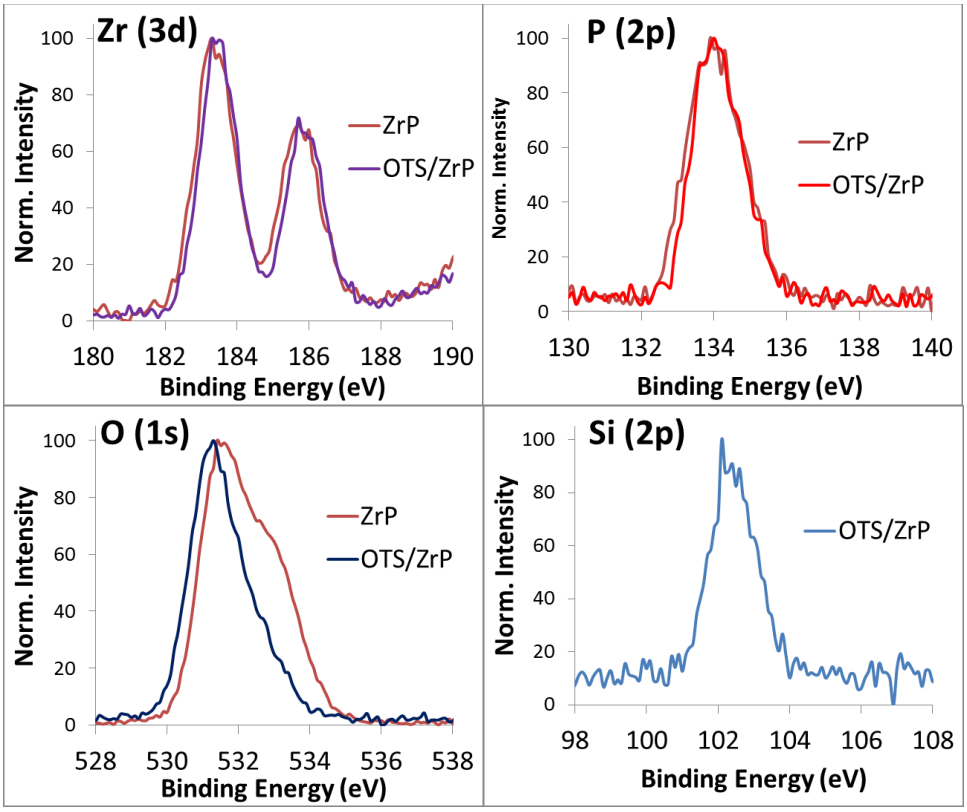

Figure 38. XPS spectra of ZrP and OTS/ZrP.

The presence of the silane on the surface of the nanoparticles was also confirmed by XPS. In this case signals were obtained for all expected elements including Zr, P, O, and Si, **Figure 38**. It can be observed that the modification does not have any substantial effect on the XPS signals, however a disappearance of the high energy shoulder in the O 1s spectrum is observed after modification. This shoulder is representative of the oxygen atoms of the P-OH groups; modification with a silane adds new O atoms to the surface and therefore limits the P-OH groups to the interlayer of the particles. Considering the penetration depth of the technique most of the oxygen atoms analyzed

are from the silane rather than the phosphates of the nanoparticle. The signal for Si is unique of the modified sample and reveals that the silanes are in fact on the surface of the nanoparticles. It should be noted that the broadness of the signal indicates that there is likely more than one Si environment within the sample, therefore the bonding of the silane is not homogenous throughout the sample.

The TGA of OTS/α-ZrP shows an increase in weight loss compared to the pristine α-ZrP, **Figure 39**. The weight loss for α-ZrP is of ca. 12%, where two water molecules are vaporized per mol of α-ZrP. The first weight loss comes from the intercalated water molecules, at ca. 120 °C, and the second from the condensation of the phosphate at ca. 540 °C, producing ZrP_2O_7 as the final pyrolysis product. The TGA for the OTS/α-ZrP shows a 16.6% weight loss, where two new weight losses, in addition to the typical weight losses for α-ZrP, can be appreciated. The first weight loss for the OTS/α-ZrP material is of ca. 2% at 78 °C and is attributed to the intercalation of ethanol within the aliphatic chains on the surface modified nanoplatelets during the cleaning procedure. The second weight loss takes place at 135 °C, with a ca. 3% of weight loss, corresponding to the vaporization of the intercalated water molecule. It is important to note the shift of this specific weight loss, by 15 °C, consistent with the encapsulation of the nanoplatelets by the aliphatic groups making it harder for the water molecules to escape from the interlayer region.

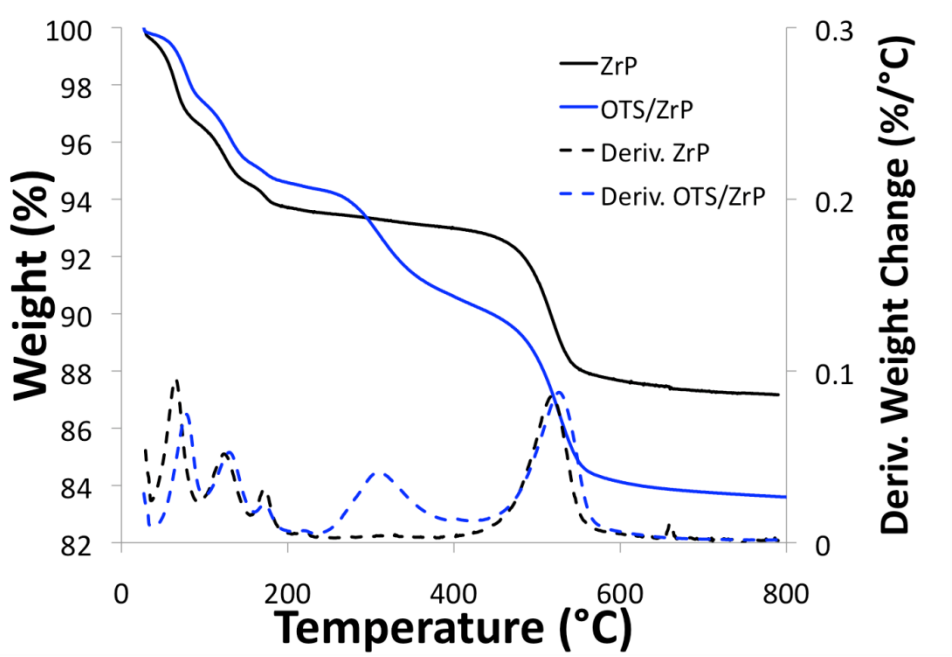

Figure 39. TGA thermogramm of ZrP and OTS/ZrP.

The third weight loss takes place at 300 °C with a weight loss of ca. 5% due to the thermo-decomposition of the aliphatic chain on the surface of ZrP. The final weight loss takes place at 525 °C and is mainly attributed to the condensation of the phosphate groups of ZrP.

It has now been confirmed that OTS has been successfully attached to the surface of ZrP. SSNMR experiments will now be conducted to gain additional insight on the bonding of the silane with the surface phosphate groups, **Figure 40**. **Figure 40 A** shows the single pulse magic-angle spinning (MAS) solid-state ^{1}H NMR spectrum (top) recorded for the sample at a spinning rate of 14 kHz, where the three broad resonances

are centered at 8.2, 6.5 and 1-2 ppm and accompanied by intense sidebands. The spectrum illustrates strong proton-proton dipolar interactions typical for relatively rigid solids. The low-field lines at 8.2 and 6.5 ppm can be well assigned to HPO_4^- and H-bonded water, respectively.[68, 142] A superposition of the broad line centered at 1-2 ppm and sharp resonances with δ of 1.5, 1.3 and 0.87 ppm can be attributed to alkyl protons of the organic ligand with less mobility (these alkyl groups are located closer to the ZrPsurface) and protons of more mobile alkyl groups remote from the surface. In accord with this assignment, the broad component is accompanied by intense sidebands while the sharp lines show sidebands with very low intensity (Figure 40A). Moreover, the wide and narrow components are well observed in the partially relaxed ^{1}H MAS NMR spectrum recorded by the inversion-recovery experiments performed at delay time of 0.45 s (Figure 40A, bottom).

Based on the TGA and the particle dimensions the O-Si-Alk:P-OH ratio for a ZrP nanoplatelet completely modified is ca. 1:3.4 on the surface. However, the integration of the ^{1}H signals leads to ratio O-Si-Alk:P-OH ratio of 1:26 for the whole particle. Nevertheless, taking in account an average particle thickness of 8 nm there should be an average of ca. 10 nanosheets of ZrP per nanoplatelet, resulting in a O-Si-Alk:P-OH ratio of ca. 1 to 2.6 on the surface of ZrP in fair agreement with that calculated by TGA. Finally a very weak and sharp resonance at 4 ppm obviously belongs to residual ethanol, as confirmed by TGA.

The room-temperature inversion-recovery experiments performed for the ZrP sample spinning at 14 kHz have shown spin lattice relaxation of all the protons as a non-exponential process. At the same time, the relaxation curves are well described with a stretched exponential:[149]

$$I = I_0(1-2e^{-(\tau/T_1)^{\beta}})$$ (Equation 1)

where the β parameter takes the values between 0.72 and 0.62. Such a relaxation is often observed in solids when ^{1}H relaxation is not dominated by spin diffusion to paramagnetic centers.[150] Under these conditions, the different ^{1}H resonances show different T_1 times. For the sharp ^{1}H resonances the T_1 times are determined as 0.62-0.64 s versus 1.0 and 0.79 s obtained for P-OH and water signals, respectively. It is remarkable that similar T_1 values have been reported for a water resonance in crystalline zirconium phosphates[149, 150] where the ^{1}H T_1 data have been discussed in terms of motional modulation of interproton dipole-dipole interactions due to H_2O 180°-flips, for example.

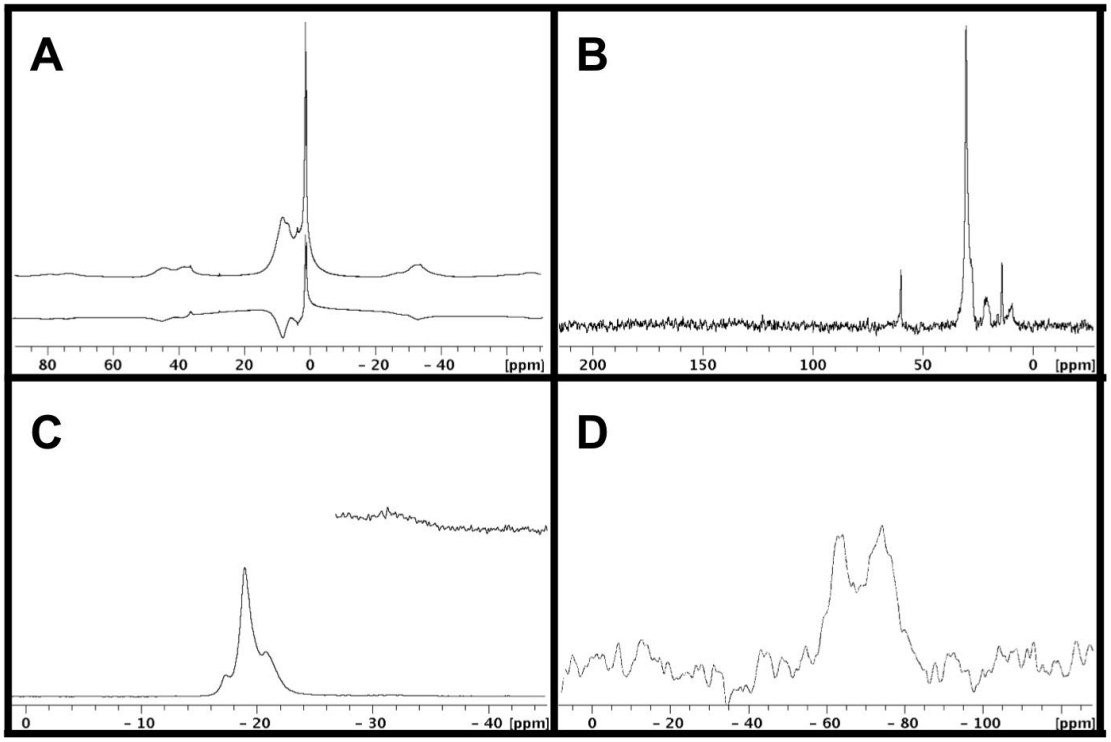

Figure 40. (A)The single pulse ^{1}H NMR spectrum (top) and the partially relaxed ^{1}H MAS NMR spectrum (bottom, delay time between 1800 and 900 pulses is 0.45 s) recorded for the ZrP sample spinning at a rate of 14 kHz. (B) The $^{13}C\{^{1}H\}$ CP MAS NMR spectrum of the ZrP sample recorded at a spinning rate of 10 kHz. (C) The $^{31}P\{^{1}H\}$ MAS NMR spectrum of the ZrP sample recorded at a spinning rate of 8 kHz (top). The same spectrum scaled with a coefficient of 4 (bottom). (D) The $^{29}Si\{^{1}H\}$ CP MAS NMR spectrum recorded for the ZrP sample at a spinning rate of 10 kHz.

The Si-O-Alk groups in the ZrP sample shows the resonances at 30.3, 28.1, 27.5, 20.9, 15.9 and 9.9 ppm in the $^{13}C\{^{1}H\}$ CP MAS NMR spectrum recorded at a spinning rate of 10 kHz **Figure 40 B**. The lines are broadened as it is generally observed in amorphous solids.[150] At the same time, the two sharp lines with values of 60.1 ppm and 14.3 ppm can be attributed to CH_3CH_2OH in accordance with the ^{1}H MAS NMR spectrum and TGA results.

The ^{31}P MAS NMR experiments, performed for the ZrP sample spinning at various rates with the single-pulse proton-decoupled and cross-polarization pulse sequences have provided reliable signal assignments. **Figure 40 C** shows the $^{31}P\{^{1}H\}$ MAS NMR spectrum where intense lines at -17.3, -19.0 and -20.8 ppm can be well attributed to the moieties HPO_4^- in $Zr(HPO_4)_2$ layers.[142, 151, 152] A ratio for these moieties with different phosphorus environments is calculated after a deconvolution procedure as 1/5.1/1.9, respectively. In addition, the $^{31}P\{^{1}H\}$ MAS NMR spectrum exhibits a low-intense line centered at -31.2 ppm. This resonance can be well assigned to PO_4^- groups.[68, 153] Since the HPO_4^- / PO_4^- ratio is determined by integration as ~30 to 1, the resonance at -31.2 ppm can be attributed to O_3P-O-Si-Alk situated at the surface of the ZrP nanoplatelet.[153]

The $^{29}Si\{^{1}H\}$, CP MAS NMR spectrum recorded at a spinning rate of 10 kHz is shown in **Figure 40 D**. It should be noted that in spite of using cross-polarization, the experiment required a significant number of scans; in some sense this correlates with a low content of organic ligand on the surface of ZrP. The $^{29}Si\{^{1}H\}$ CP MAS NMR spectrum exhibits two resonances with similar integral intensities that are detected at -64.1 and -74.1 ppm. These signals are assigned to O-P-(O_3Si-Alk) and O-P-(O_2(HO)Si-Alk) groups, respectively because the intensity of the high-field resonance decreases strongly in the $^{29}Si\{^{1}H\}$ MAS NMR spectrum with direct excitation of ^{29}Si nuclei. The presence of two different types of Si suggests that the silane is not bonding in a uniform fashion, as suggested by XPS data. Based on the crystal structure of ZrP it is not likely that the silane can bond in a three-fold coordination. As a result the silane must either

bond to two surface phosphates or one, the remaining bonds are likely siloxane bonds. The low intensity of the ^{31}P signal for P-O-Si agrees well with the hypothesis of predominantly siloxane bonds. It is likely that after the silane bonds to the surface (probably through a single P-O-Si bond) the free Si-OH groups that are not coordinated form siloxane bonds with neighboring silanes which have a similar bonding scheme. The result would be two distinct types of Si environments.

4.3 Surface Modification with Epoxides

Although modification with silanes was successful the multiple possible bonding configurations limits the uptake of modifier and also makes it difficult to determine the bonding motif. In addition, for a fundamental understanding of surface reactivity a simpler group should be used. In this case epoxides were selected as they are expected to bond to the surface phosphates in a one to one fashion. Additionally, the epoxides are completely organic and therefore the materials can be characterized to a fuller extent and the exact composition can be determined. After the completion of the surface modification reaction the nanocrystal morphology of the products were investigated to determine the effect of the modification on the crystallinity and morphology of the particles. The XRPD pattern of both α-ZrP and epoxide modified ZrP samples are provided in **Figure 41**. The first peak in the α-ZrP pattern shows a d-spacing of 7.6 Å. This spacing corresponds to the interlayer distance between the 002 planes of α-ZrP. It is expected that if the surface of our materials has been successfully modified that this

distance should remain unchanged, an increase in this spacing would indicate that the modifier reacted with the interlayer region or intercalated within the layers, which in this case is unwanted. Examination of **Figure 41** shows that all the XRPD patterns display a d-spacing of 7.6 Å, from this we can conclude that there is no unwanted interaction of

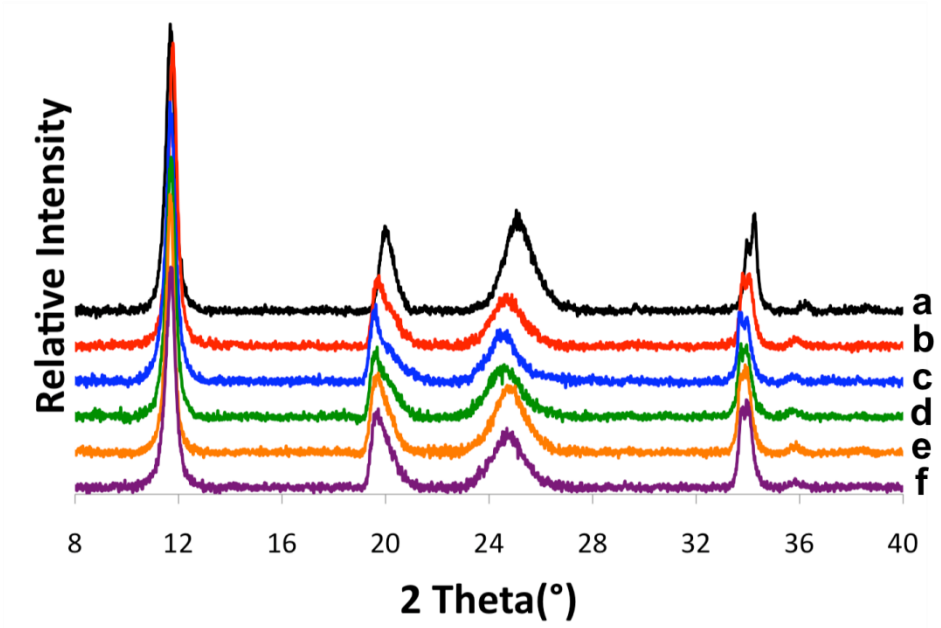

Figure 41. XRPD patterns of ZrP and modified samples showing that the modification does not affect the interlayer spacing. a) α-ZrP, b) 1,2-epoxyoctadecane/ZrP, c) 1,2-epoxydodecane/ZrP, d) 1,2-epoxy-9-decene/ZrP, e) styrene oxide/ZrP, and f) fluorophenyl oxirane/ZrP

the epoxide with the interlayer, therefore if there is modification it must be exclusively on the surface of the nanoplatelets. Although the 002 peak is in the same position it can

be observed from the pattern that the subsequent peaks are shifted to lower 2 theta values when compared to pristine ZrP. The shift observed is indicative of dehydration of ZrP, several studies have shown that upon dehydration the hydrogen bonding with the interlayer water is lost and a new hydrogen bonding interaction is formed with other phosphate groups producing a more rigid structure.[154, 155] The fact that the 002 peaks are identical while the subsequent peaks are shifted suggests that the particles are only partially dehydrated; this is likely a result of the extended reflux and the ease of dehydration for less crystalline ZrP particles. It is well known that the thermal behavior of ZrP is contingent upon the crystallinity of the material, where less crystalline samples lose the interlayer water more readily than samples of higher crystallinity.[136-138] In previous investigations it was found that crystalline ZrP can be completely dehydrated by prolonged heating at 110°C.[138] In addition, the continued reflux of ZrP in phosphoric acid has also been shown to yield dehydrated phases of ZrP.[154] As the surface modification was conducted at 111°C in this case, and the particles are of low crystallinity, the observed dehydration is reasonable. TEM further confirms that the particle shape and crystallinity are not affected by the surface reaction, **Figure 42.** The average particle size of the functionalized particles is 120 nm, which is in the expected range for particles prepared by reflux methods with 3M H_3PO_4 according to Sun et al.[48] The thickness of the particles can also be observed by electron microscopy, **Figure 42 B**, the average thickness is *ca.* 8.5 nm, which agrees well with previous studies.[123, 146]

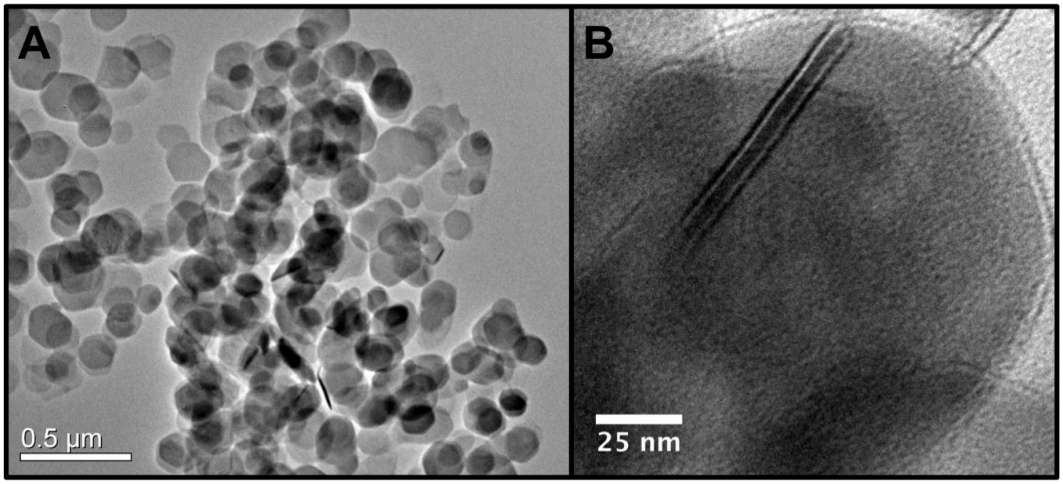

Figure 42. TEM images of 1,2 epoxyoctadecane/ZrP displaying (A) the retention of nanocrystal morphology and (B) the thickness of the particles.

The surface modification products were then analyzed by FTIR to determine if any organic material was present, suggesting the successful bonding of epoxide to the ZrP surface. The infrared spectra of the epoxide modified ZrP shows a mixture of vibration modes for the epoxide and the ZrP, where the ZrP dominates the spectrum due to the high concentration of ZrP layers relative to the modifiers on the top and bottom surfaces, **Figure 43**. The expected region for C-H stretching between 2850 cm^{-1} and 3000 cm^{-1} can be seen for all ZrP modified with alkyl epoxides, stretches can also be observed between 1350 cm^{-1} and 1480 cm^{-1} due to C-H bending. Aryl epoxides display stretches at 690 cm^{-1}, 710 cm^{-1}, and 1500 cm^{-1} for the arene functionality. Although these stretches indicate that the modifier and ZrP have interacted to some extent they do not confirm that covalent attachment has occurred. A number of other phenomena such as

physisorption could produce similar signals, however if this were the case the signals would be expected to be more dominant.

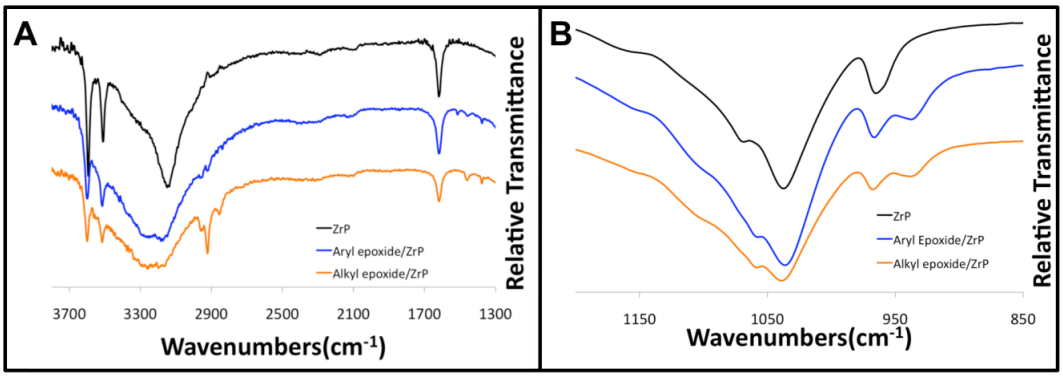

Figure 43. FTIR spectra of epoxide modified ZrP displaying (A) the stretches of the modifier and (B) formation of a phosphate ester through modification.

In all cases a signal is present at 910 cm^{-1} for the phosphate ester, **Figure 43 B**, this signal therefore confirms the covalent attachment of the epoxide to the phosphate groups of ZrP and the formation of P-O-C bonds within the material. The presence of this stretch in conjunction with the XRPD data suggests that any functionalization that occurred is exclusively on the surface of the nanoparticles.

In addition, the stretches for the lattice water are still present confirming that there is no interaction of the modifier with the interlayer region or intercalation. Upon successful intercalation of a molecule in the interlayer region of ZrP the stretches for the water in

the zeolitic cavities no longer exist due to the exchange of the interlayer water with the intercalated molecule. Although the water stretch is present it is slightly deformed. This is due to the partial dehydration of the surface modified product, as discussed earlier (vide infra). This result also confirms that the attachment of the epoxide occurs on the exterior surface of the particles and supports exclusive esterification of the ZrP surface.

It has been established that FTIR can be used to identify the degree of disorder of aliphatic chains film on nanoparticle surfaces.[115] It has been reported that crystalline microenvironments are formed when long alkyl chain lengths greater than six carbon atoms are assembled on oxidized surfaces.[156] Disordered systems (liquid-like) show a CH_2 asymmetric stretching band near 2924 cm^{-1}, while with more ordered monolayers the band appears closer to 2917 cm^{-1}, indicating a more crystalline state. In our case the assymetric stretching appears at ~ 2924 cm^{-1} for the C_{12} alkyl chain and at 2922 cm^{-1} for the C_{10} and C_{18} chains. It was expected that the C_{18} chain would be more ordered than the shorter chains , the fact that the C_{10} shows identical ordering as the C_{18} is likely due to pi interactions of the terminal alkene functionality of the C_{10} chains. Therfore in all cases the aliphatic chains are not assembling in a fully closed pack manner. This is likely due to the large distance between the surface phosphate groups and the fact that the surface phosphates may not all be on a perfrectly level plane.

To quantify the amount of modifier on the surface of the ZrP nanoparticles thermogravimetric analysis (TGA) was used. Upon heating the total weight loss

exhibited by α-ZrP of this size is ~12%, with two major weight losses wherein the sample is completely dehydrated and the phosphate groups condense to yield zirconium pyrophosphate as the end product.[135] The weight loss of modified samples occurs in three events as is seen for similar organically modified ZrP materials.[68, 74, 146] All surface and interlayer water and residual solvent is expected to be lost below 150 °C. The next weight loss occurring anywhere from 200 °C to 350 °C is expected to be the loss of the organic modifier. Lastly, the condensation of the monohydrogenphosphate to the pyrophosphate occurs roughly between 450 °C and 600 °C. Typical thermograms can be seen in **Figure 44**. It should be noted that in all cases the weight loss that corresponds to the epoxide modifier takes place in two steps as observed by the derivative curve in the TGA, **Figure 44 B and D** . The first step occurs between 200°C and 240°C and the second ranging from 280°C to 350°C. The second step is the dominant weight loss in the process and seems to increase with the size of the aliphatic chain of the epoxide. The first weight loss remains roughly the same size in all cases.

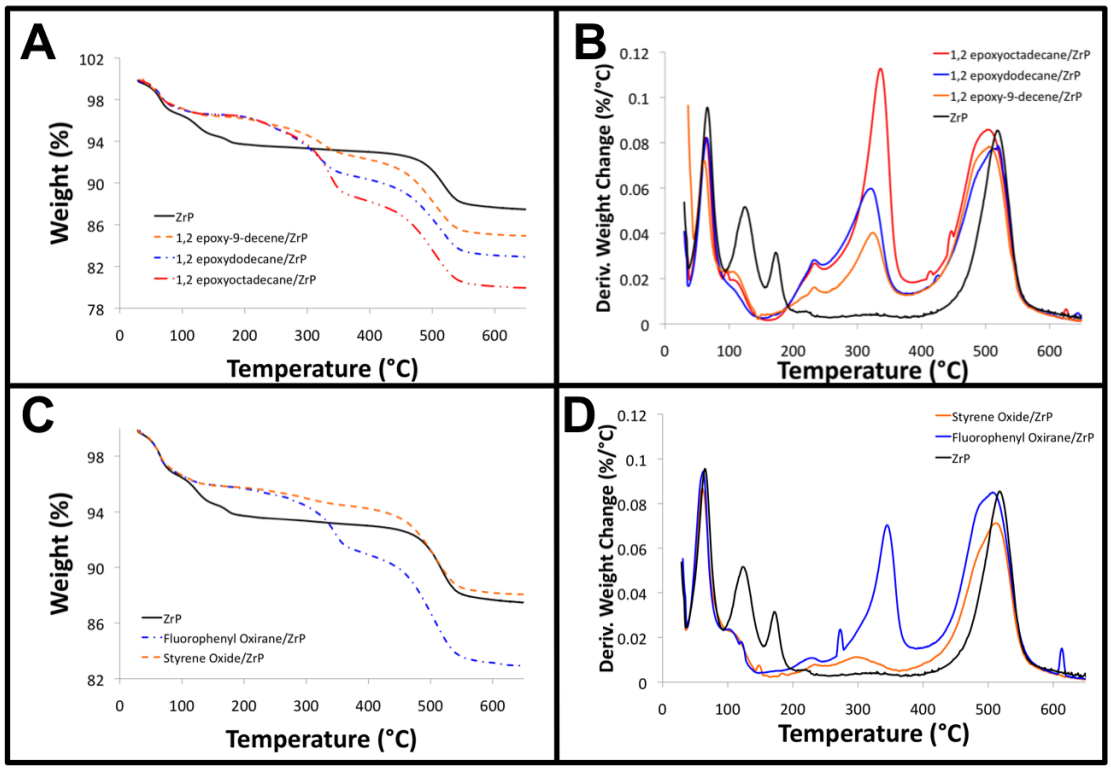

Figure 44. TGA thermograms of (A) alkyl and (C) aryl epoxide modified ZrP along with the derivatives of the alkyl (B) and aryl (D) modified compounds.

It can therefore be hypothesized that the initial weight loss could be the epoxide covalently attached to the ZrP whereas the latter is simply the decomposition of the alkyl chain or aromatic group. This suggests that the P-O-C bond is not very thermally stable which is somewhat unexpected. Pica suggests that the epoxide can bond to the phosphates of ZrP in two possible conformations; in this case the bonding is not equal and the ratio of the major conformation to the minor in the product is ~ 3.[68] It is more likely that the two processes are representative of the different bonding conformations of the epoxide to the ZrP surface. The percent weight losses obtained are all within the

expected range. Using the TGA results, formulas and molecular weights of the surface modified samples can be obtained; this information is presented in **Table 2**.

Table 2. Summary of TGA data along with estimated percent coverage (assuming 11 layers) and proposed formulas for epoxide modified ZrP.

Modifier	Total TGA Weight Loss (%)	Percent Coverage (%)	Calculated Formula
fluorophenyl oxirane	17.24	87.3	$Zr(H_{0.831}PO_4)_2(Mod)_{0.169}\cdot 0.7\ H_2O$
styrene oxide	14.65	67.6	$Zr(H_{0.873}PO_4)_2(Mod)_{0.127}\cdot 0.6\ H_2O$
1,2-epoxy-9-decene	15.22	62.2	$Zr(H_{0.882}PO_4)_2(Mod)_{0.118}\cdot 0.5\ H_2O$
1,2-epoxydodecane	17.15	72.5	$Zr(H_{0.860}PO_4)_2(Mod)_{0.140}\cdot 0.6\ H_2O$
1,2-epoxyoctadecane	20.18	69.4	$Zr(H_{0.861}PO_4)_2(Mod)_{0.139}\cdot 0.6\ H_2O$

The extent of modification is somewhat similar in all cases and can be seen to range from ~0.12 to 0.17 moles of modifier per mole of Zr. It can be noted that in the case of the pure aliphatic chains that the amount of modifier bonded to the surface is nearly identical, this suggests that the packing is somewhat similar and did not cause an increase in uptake. The fluorination of the styrene ring appears to increase the uptake as opposed to a styrene ring alone; this could possibly be due to the electron withdrawing effects of the fluorine atom. The electron-withdrawing group would decrease the

electron density within the aromatic ring and could possible make the epoxide ring more susceptible to nucleophillic attack by the phosphate groups. The proposed partial dehydration of the modified particles is also confirmed by TGA. The samples exhibit between 0.5 and 0.7 moles of water showing that they are 30% -50% dehydrated.

It has now been confirmed that the epoxide groups have been successfully attached to the ZrP surface. A theoretical mass contribution can be calculated for a sample in which all surface phosphates have been successfully modified by taking into account the nanoparticle thickness, number of reactive surface sites, and the one to one interaction of epoxide rings with surface phosphate groups. A proportion of the mass contribution observed in the TGA with the theoretical value yields an estimate of the surface coverage. The simplest approximation is as follows. Initially, the number of inorganic layers present in the nanoparticle is calculated by dividing the thickness of the particle by the interlayer distance. In our case the nanoparticles were found to be *ca.* 8.5 nm and the interlayer distance of ZrP is 7.6Å (0.76 nm), therefore we estimate about 11 layers per nanoparticle. A mass contribution of the layers can be obtained by multiplying the number of layers by the molecular weight of ZrP. To estimate the contribution of the organic modifier the molecular weight of the epoxide is multiplied by two as only the top and bottom layers will be modified. A ratio of the mass contributions of the organic modifier to ZrP yields an estimate for the percent weight loss, corresponding to the epoxide, which should be observed in the TGA of a surface modified material if all sites are covered.

The percent coverage estimates are collected in **Table 2** along with the TGA data and calculated formulas. All estimates range from 62% to 87% and the moles of epoxide are all within the same general vicinity. This suggests that sterics do not play a major role in the bonding of the epoxides, which is reasonable as each surface phosphate group is 5.28 Å apart.[34]

To further investigate the bonding within the surface modified particles both ^{31}P and ^{13}C SSNMR experiments were carried out. All epoxide reactions proceed through bonding of the surface phosphate groups with the epoxide rings therefore the ^{31}P-NMR spectra should be similar for materials with the similar surface coverage regardless of which epoxide is used. In the case of 1,2 epoxyoctadecane/ZrP the ^{31}P spectrum reveals four signals of which two can be assigned to ZrP, **Figure 45**. The signal at ca. -19 ppm is assigned to the orthophosphate of ZrP, as phosphates exist throughout all the layers this is the dominant signal in the spectra. The weak resonance at -17.1 ppm is also characteristic of ZrP as some phosphates are in a slightly different environment due to hydrolysis near the edges of the particles in the reflux case.[144] The remaining signals are observed at -21.4 and -22.4 ppm. The signal at -21 ppm can be assigned to the dehydrated phase of ZrP and is in good agreement with the XRD, FTIR, and TGA data, which suggests a lower level of hydration than pristine ZrP.[40] It is likely that during the extended reflux some of the interlayer water that was held loosely escaped the interlayer. The second signal can be assigned to the phosphorus atom that has been esterified and is involved in modification through a P-O-C linkage, as previously reported by Pica et al.[68]

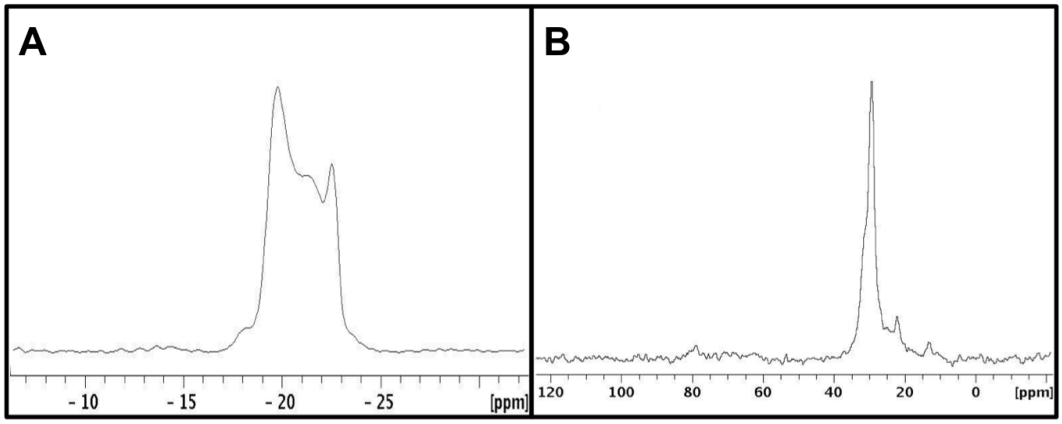

Figure 45. MAS Solid State NMR of 1,2 epoxyoctadecane/ZrP, (A) $^{31}P\{^{1}H\}$ (B) ^{13}C CP.

In addition to the observation of successful modification in the ^{31}P NMR, bonding of the alkyl chains to the surface of the samples agrees well with the CP/MAS ^{13}C-NMR spectrum of 1,2 epoxyoctadecane/ZrP. In the case of the C_{18} alkyl chain, for each bond to the surface only 2 distinct carbons appear; there should be a P-O-C linkage to the surface and also the C-OH that occurs as a result of the ring opening of the epoxide. The signals for the alkyl carbons are observed from 10.4 ppm to 30.4 ppm and additional signals pertaining to the ring opening of the epoxide are present at 63 ppm, 69.9 ppm, and 77.8 ppm. These resonances can be assigned to carbon environments that are a direct result of covalent attachment of epoxide to the ZrP surface. Previous reports suggest that epoxides can adopt two bonding formations, one in which a secondary alcohol is formed,

which is the dominant product, and the other in which a primary alcohol is formed.[68] In the former case signals at ~62 ppm are assigned to the P-O-C linkage and signals at ~ 71 ppm are assigned to the carbon atom of the secondary alcohol. In the latter case it is thought that the P-O-C linkage is seen at the same place as the previous case but the carbon atom of the primary alcohol is thought to be observed at ~ 80 ppm. There are some slight shifts in the values from the surface modified samples as opposed to those reported for the fully functionalized derivative but they are indeed indicative of the same carbon environments. It should also be noted that the signals of the three membered ring of the starting organic material are absent in the spectra, this confirms that all organic matter present is covalently attached to the ZrP platform.

In regards to the surface modification the ^{31}P spectra of the modified samples is of most importance. All epoxide reactions proceed through bonding of the surface phosphate groups with the epoxide rings therefore the ^{31}P-NMR spectra should be similar for materials with the similar surface coverage regardless of which epoxide is used. As was observed for the case of 1,2-epoxyoctadecane/ZrP, ZrP modified with other alkyl and aryl epoxides also display 4 resonances, **Figure 46**. Although the resonances appear at the same place it can be seen that the intensities vary somewhat between the samples, this is a direct correlation of the differences in uptake of the epoxides as shown in **Table 2**.

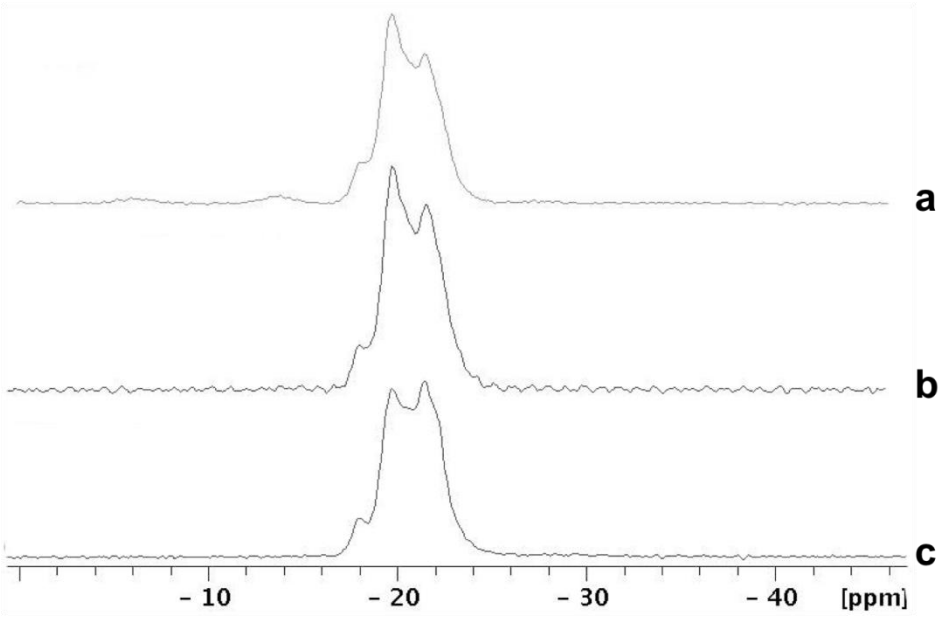

Figure 46. ^{31}P NMR data of epoxide modified ZrP, (a) 2,4 fluorophenyl oxirane/ZrP (b) 1,2 epoxy-9- decene /ZrP (c) 1,2 epoxydodecane/ZrP.

As expected our results greatly differ from those obtained by Pica et al.[68] In our synthesis we focus on exclusively functionalizing the surface whereas Pica attempted to functionalize all P-OH groups homogenously throughout the material. In regards to the ^{31}P spectra Pica was able to identify three distinct signals at -22.6 ppm, -24.7 ppm, and -19 ppm that corresponded to the two different epoxide bonding conformations and the free P-OH groups respectively. The epoxide bonding conformations made up 99.5% of the integral whereas free P-OH made up 0.5%. Integration in our material leads to 19% epoxide bonding conformations and 81% that corresponded to the base ZrP structure, in good agreement with our surface coverage estimation. The ^{13}C spectra are largely identical however the signals indicative of ring opening of the epoxide are much less

intense in our spectra due to the fact that we are functionalizing only the surface P-OH groups. The fact that unmodified phosphates dominate our ^{31}P spectra while the presence of the reactive epoxide can be confirmed by CP/MAS ^{13}C-NMR, greatly supports the exclusive functionalization of the nanoplatelet surface.

4.4 Surface Modification with Epoxides via Microwave Irradiation

The second procedure for modifying the surface of ZrP with epoxides is based on the work of Levitt, in which he found epoxides to fully react with γ-ZrP more effectively with no solvent.[147] In this case an excess of neat epoxide is reacted directly with α-ZrP by microwave irradiation; herein the microwave synthesized epoxide modified products will be discussed. As the particles were reacted in neat epoxide it was necessary to increase the crystallinity and thus the particle size to attempt to avoid intercalation of the epoxides within the interlayer. The X-ray powder diffraction pattern of both α-ZrP and epoxide modified ZrP samples are provided in **Figure 47** The first peak in the α-ZrP pattern shows a d-spacing of 7.6 Å as in the reflux case suggesting that there was no interaction of the epoxide with the interlayer of ZrP. Examination of **Figure 47** shows that all the X-ray diffraction patterns are identical to each other and to ZrP. Contrary to the reflux case there is no shifting of the higher angle peaks as in the reflux case. This is likely as the reaction time (1 hour) and temperature (70°C) were much lower in the microwave synthetic method compared to the reflux (12 hours and 111°C) and the particles used are now more crystalline.

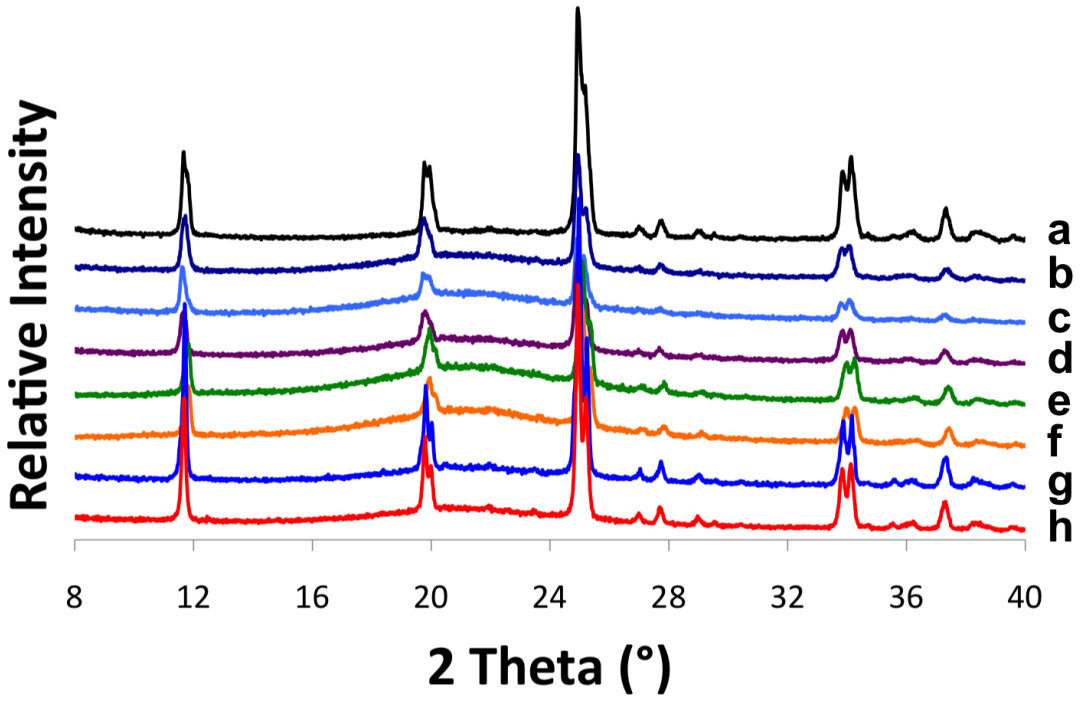

Figure 47. X-ray powder diffraction of ZrP and modified samples showing that the modification does not affect the interlayer spacing. (a) ZrP, (b) fluorophenyl oxirane/ZrP, (c) epichlorohydrin/ZrP, (d) glycidol/ZrP, (e) cyclohexene oxide/ZrP, (f) 1,2-epoxy-9-decene/ZrP, (g) 1,2-epoxydodecane/ZrP, and (h) 1,2-epoxyoctadecane/ZrP.

Based on the data presented it can be concluded that there is no unwanted interaction with the interlayer, therefore if there is modification it must be exclusively on the surface of the nanoplatelets. Transmission electron microscopy further confirms that the particle shape and crystallinity are not affected by the surface reaction, **Figure 48**. The hexagonal shape of the particles can still be observed after surface modification. The average particle size of the functionalized particles is 175 nm, the thickness of the

particles is observed to be 45 nm by electron microscopy, which corresponds to about 59 layers.

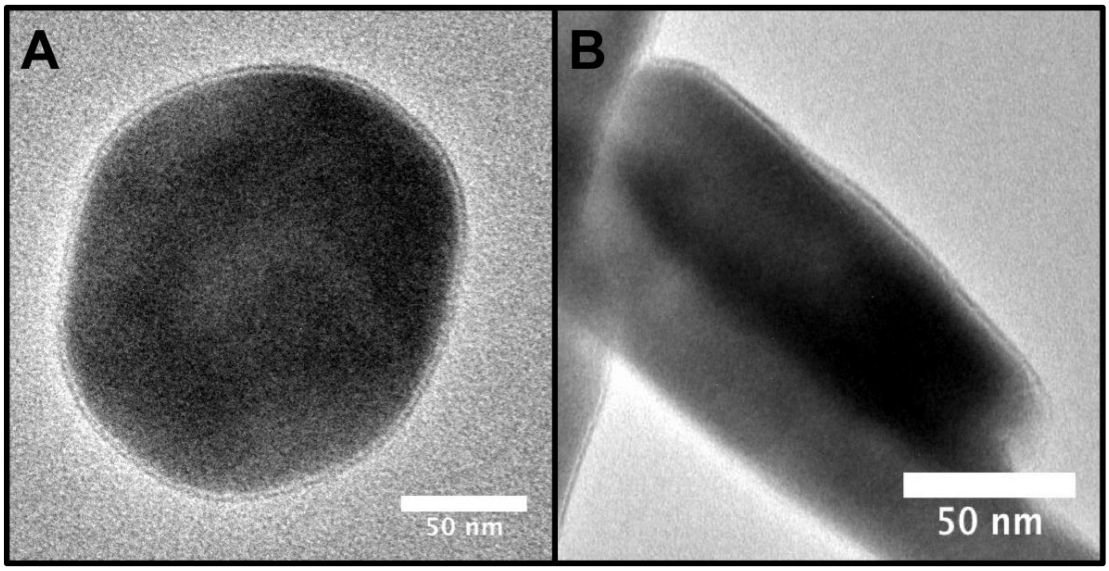

Figure 48. TEM images of 1,2 eoxyoctadecane/ZrP displaying (A) the retention of the nanocrystal morphology after modification and (B) the thickness of the particles.

The microwave surface modification products were then analyzed by FTIR to determine if any of the epoxide modifiers were successfully bonded to the surface. Similarly to the reflux samples the alkyl and aryl stretches can be observed in all cases. The expected region for C-H stretching between 2850 cm^{-1} and 3000 cm^{-1} can be seen for all epoxide modified ZrP except fluorophenyl oxirane which has no CH_2 groups. In the case of longer alkyl modifiers like 1,2-epoxydodecane and octadecane, three of the symmetric

and antisymmetric CH_2 and CH_3 stretches were observed. Modification can also be observed between 1350 cm^{-1} and 1480 cm^{-1} due to C-H bending and in the case of fluorophenyl oxirane at 1500 cm^{-1} for the arene functionality. In contrast to the samples prepared by the reflux method, the formation of a phosphate ester was not observed. It should be noted that the inorganic contribution has increased due to the change of thickness therefore the absence of the signal may simply be a result of a decreased percentage of phosphate esters formed.

Smaller molecular weight epoxides such as epichlorohydrin and glycidol were not expected to exhibit significant stretching due to the small amount of alkyl groups in the molecules. **Figure 49** shows the stretching in the alkyl region of fluorophenyl oxirane, epichlorohydrin and glycidol to be very broad in this region when compared to the other modified samples. The presence of these stretches suggests there is a substantial amount of alkyl groups in the samples that are absorbing over a range of frequencies; therefore we conclude that polymerization has occurred as is common with epoxides.

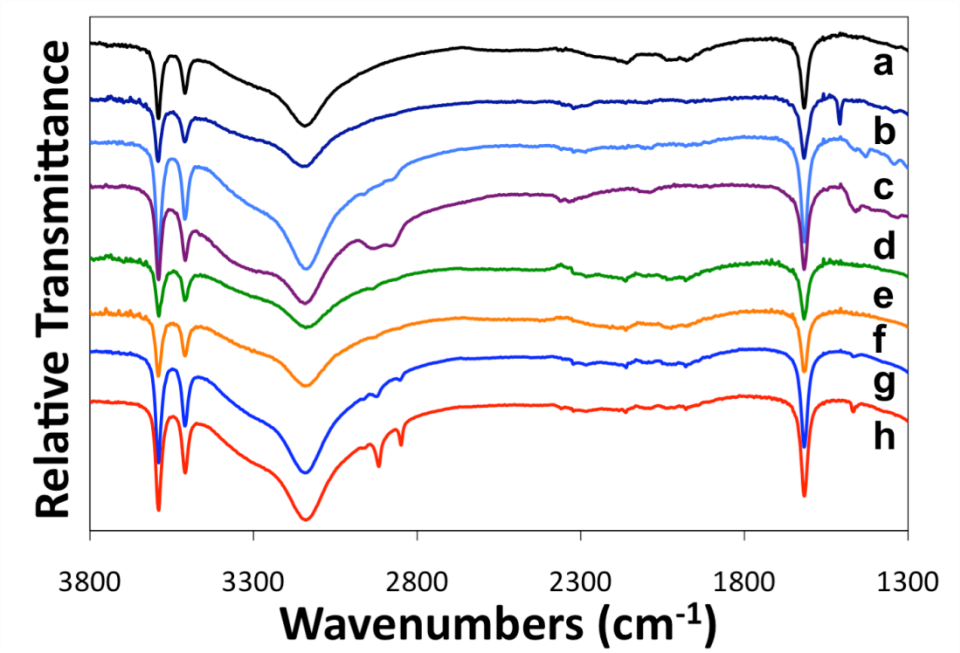

Figure 49. FTIR spectra of epoxide modified ZrP focusing on the region where stretches due to modification appear. a) α-ZrP, b) fluorophenyl oxirane/ZrP, c) epichlorohydrin/ZrP, d) glycidol/ZrP, e) cyclohexene oxide/ZrP, f) 1,2-epoxy-9-decene/ZrP, g) 1,2-epoxydodecane/ZrP, and h) 1,2-epoxyoctadecane/ZrP.

Typical thermograms of the microwae modified samples can be seen in **Figure 50**. The weight loss pattern is identical to that of the reflux samples and other modified materials however in the case of the smaller epoxides (epichlorohydrin, glycidol, and fluorophenyl oxirane) the weight losses obtained are much larger than what is expected for full coverage of the surface. The large weight losses observed in TGA for these smaller epoxides also supports the polymerization of the epoxides on the surface of the ZrP nanoparticles. Examination of the derivative for the non-polymerized sample shows very similar behavior compared to the reflux case however the two step process is not as

evident. It appears that the second step occurs over a much broader range of temperatures suggesting more thermal stability. The polymerized samples also display more thermal stability; it can be observed that the loss of intercalated water is elevated to higher temperatures due to the polymerization on the surface. In addition, the decomposition of organic begins at a much higher temperature when compared to other non-polymerized samples. Using the TGA and elemental analysis data formulas and molecular weights of the modified samples were proposed, this information is presented in **Table 3**. A similar trend can be seen between the uptake of epoxide in these samples and the reflux. The long alkyl chains once again have very similar uptakes but the others show no clear trend. Also no dehydration is evident based upon the proposed formulas agreeing well with the XRPD patterns that are nearly identical to ZrP.

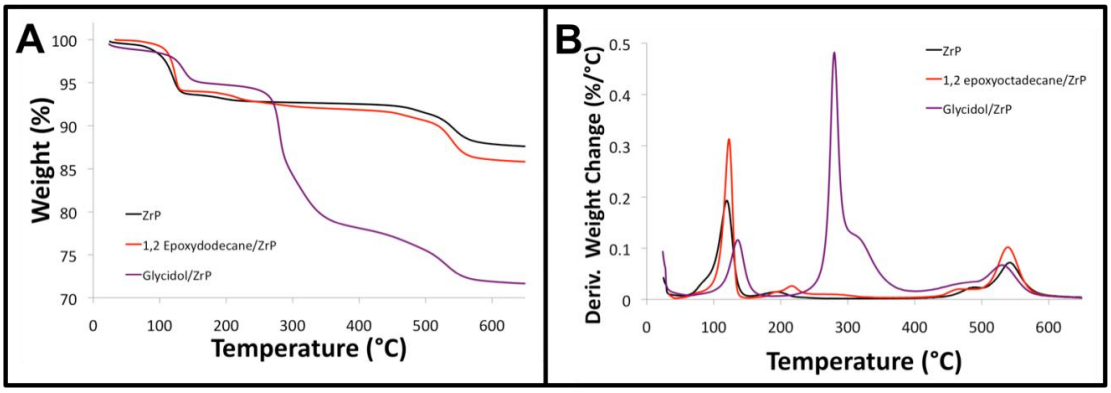

Figure 50. (A) TGA and (B) derivative of weight loss of ZrP alongside a typical surface modified and polymerized sample.

The percent coverage estimates can be seen in **Table 3** along with the TGA and elemental analysis data. In the case of the polymerized samples values over 100% were obtained and it cannot be said definitively how much of the modifier is actually covalently attached to the surface phosphate groups. In regards to the longer alkyl chains, the C_{10} has a slightly higher percent coverage than C_{12}. This is likely a result of the rigidity of the terminal carbons on the alkene functionality in the C_{10} epoxide providing less steric hindrance to other surface phosphates, allowing more epoxide to bond. The C_{18} also shows a slightly higher coverage than both the C_{10} and C_{12}, this is in good accordance with the fact that longer alkyl chains have increased Van der Waals interactions thus making packing more effective while shorter chains have more disorder and limit the extent of modification.[96, 157] Ultimately the coverage of the surface is similar for the akyl epoxides as was observed in the reflux case. The cyclohexene oxide is a smaller more compact molecule and as a result is able to effectively functionalize more sites. It is possible that the long aliphatic chains of the alkyl epoxides could block reactive surface sites depending on which orientation they adopt upon bonding whereas an epoxide that is compact and cannot interfere with neighboring phosphate would have a higher coverage.

Table 3. Summary of TGA and elemental analysis data along with estimated percent coverage (assuming fifty nine layers) and proposed formulas for epoxide modified ZrP samples.

Modifier	Total TGA Weight Loss (%)	Actual Weight % C/H/X	Percent Coverage	Proposed Formula
epichlorohydrin	23.59	5.4/1.8/5.0	*	$Zr(H_{0.975}PO_4)_2(Mod)_{0.40}\bullet H_2O$
glycidol	27.84	9.4/2.5/--	*	$Zr(H_{0.953}PO_4)_2(Mod)_{0.52}\bullet H_2O$
fluorophenyl oxirane	21.36	5.7/1.6/1.21	*	$Zr(H_{0.986}PO_4)_2(Mod)_{0.17}\bullet H_2O$
cyclohexene oxide	13.17	1.0/1.4/--	97.8	$Zr(H_{0.97}PO_4)_2(Mod)_{0.034}\bullet H_2O$
1,2-epoxy-9-decene	13.31	1.2/1.4/--	69.1	$Zr(H_{0.98}PO_4)_2(Mod)_{0.024}\bullet H_2O$
1,2-epoxydodecane	13.07	1.2/1.5/--	63.6	$Zr(H_{0.999}PO_4)_2(Mod)_{0.022}\bullet H_2O$
1,2-epoxyoctadecane	14.53	2.0/1.6/--	74.8	$Zr(H_{0.95}PO_4)_2(Mod)_{0.026}\bullet H_2O$

The observed surface polymerization is the first of its kind for α-ZrP, although surface initiated polymerization does exist for a variety of materials including carbon nanotubes and silica nanoparticles.[158-160] In the case of carbon nanotubes the polymerization is often a multi-step procedure in which a functional group is anchored to the surface and reacted to introduce an initiator, followed by a polymerization reaction.[159] In our compounds it is believed that the α-ZrP particles act as acid catalysts in the epoxide polymerization reaction. Belbachir et al conducted many experiments in which an acid-exchanged montmorillonite clay was used as a heterogeneous acid catalyst for the cationic polymerization of epoxides.[161-163] There was no bonding between the clay and epoxide so he was able to polymerize various epoxides and separate the clay from the polymers at the end of the reaction. Although separation is not possible in our case due to the covalent attachment of the epoxides to the surface, the acidic mechanism is expected to be very similar.

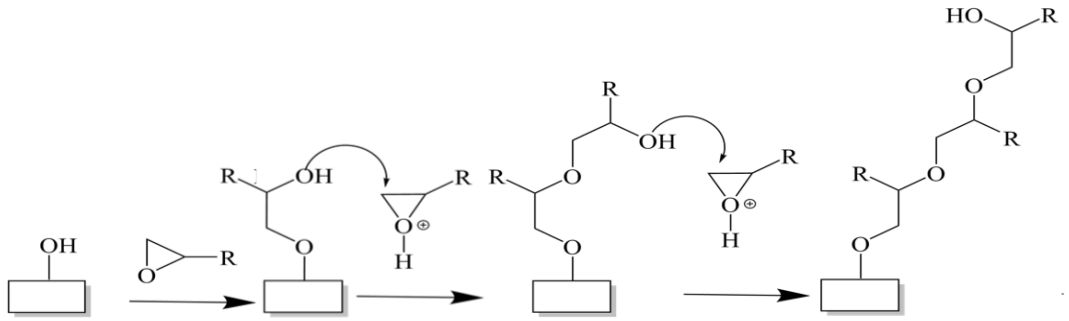

Figure 51. Schematic displaying the polymerization of epoxides on the surface of ZrP, the initial surface modification is shown followed by two polymerization steps. Note: Both the top and bottom surfaces of ZrP are modified and after each ring opening reaction a proton is released, causing the protonation of the oxygen of an epoxide.

It is believed that α-ZrP surface polymerization of epoxides initially proceeds by the bonding of the epoxide to α-ZrP by nucleophillic attack of the surface P-OH groups to a carbon of the epoxide ring, producing a hydroxyl group from the ring opening.[68] This reaction releases a proton, which can be used to protonate the oxygen of an epoxide ring, which in turn is attacked by the hydroxyl group formed from the ring opening, **Figure 51**. Several studies agree that the dominant product for the ring opening reaction is the attack of the α carbon of the epoxide ring and formation of a secondary alcohol.[68, 161, 164, 165] For each epoxide that undergoes ring opening an additional hydroxyl group becomes available therefore the polymerization reaction proceeds smoothly even in the presence

of excess epoxide. It is reasonable that a hydroxyl group can polymerize with epoxides in the presence of acid, this occurs regularly in the cationic polymerization of glycidol, an epoxide with a hydroxyl functional group.[166-169]

Mechanistically all epoxides should be able to polymerize but sterics prevent some epoxides from doing so. Bulky epoxides can block the hydroxyl group formed from the ring opening and the long chain alkyl epoxides are likely to be able to block the hydroxyl group due to disorder or close packing of the alkyl chains. It is worth noting that other experiments have shown that in the presence of solvent the polymerization is greatly limited if not stopped altogether (**Table 4**), the solvent disperses the epoxides and therefore limits direct exposure to ZrP and other epoxide molecules. In addition, when solvent is used a stoichiometric amount of epoxide can be added to the reaction, which also prevents the polymerization. The polymerization presented here is a one-pot synthetic procedure and as a result is not as well controlled as other multi-step methods. Using the surface chemistry of ZrP it may be possible to use a multi step procedure to conduct more controllable polymerizations as is used in other work.

Table 4. Summary of TGA data along with estimated percent coverages (assuming fifty nine layers) and proposed formulas for epoxide modified ZrP samples prepared in solvent.

Modifier	Total TGA Weight Loss (%)	Actual Weight % C/H/X	Percent Coverage	Proposed Formula
epichlorohydrin	12.42	0.37/1.32/0.46	75.3	$Zr(H_{0.975}PO_4)_2(Mod)_{0.026}\bullet H_2O$
glycidol	14.42	1.74/1.52/--	230.3*	$Zr(H_{0.953}PO_4)_2(Mod)_{0.08}\bullet H_2O$
fluorophenyl oxirane	15.96	3.49/1.48/0.58	270.8*	$Zr(H_{0.986}PO_4)_2(Mod)_{0.096}\bullet H_2O$
cyclohexene oxide	12.51	0.77/1.3/--	66.1	$Zr(H_{0.97}PO_4)_2(Mod)_{0.023}\bullet H_2O$
1,2-epoxy-9-decene	12.74	1.06/1.39/--	63.9	$Zr(H_{0.98}PO_4)_2(Mod)_{0.022}\bullet H_2O$
1,2-epoxydodecane	12.62	0.97/1.38/--	48.7	$Zr(H_{0.999}PO_4)_2(Mod)_{0.017}\bullet H_2O$
1,2-epoxyoctadecane	13.31	1.52/1.41/--	52.6	$Zr(H_{0.95}PO_4)_2(Mod)_{0.018}H_2O$

*Polymerization still occured in these samples but was limited when compared to reaction with neat epoxide.

The structural features of the modified ZrP have been additionally characterized by solid state MAS NMR experiments. Experiments were conducted using the samples modified with 1,2-epoxydodecane and 1,2-epoxyoctadecane, noted here as 1,2-epoxydodecane/ZrP and 1,2-epoxyoctadecane/ZrP. The α-ZrP matrix of modified samples 1,2-epoxydodecane/ZrP and 1,2-epoxyoctadecane/ZrP are characterized by the $^{31}P\{^1H\}$ MAS NMR spectra in **Figure 52**. As seen, the spectra of both samples are similar and show a strong resonance at -19.1 and a weak resonance at -17.1 ppm. Deconvolution using Lorentz line shape leads to a ratio of 33 to 1. We therefore see that our modified samples have identical ^{31}P spectra to α-ZrP, the signals for dehydration and

the modification are not present in this case. As estimated earlier, we believe these particles to have around 59 layers and estimate a percent coverage of 60 to 75 percent; therefore out of the 59 layers only the equivalent of one complete layer is modified. It is reasonable that at this ratio the surface P-OH groups are insignificant and cannot be observed due to the abundance of interlayer P-OH groups, therefore the spectra of the modified samples is identical to that of α-ZrP.

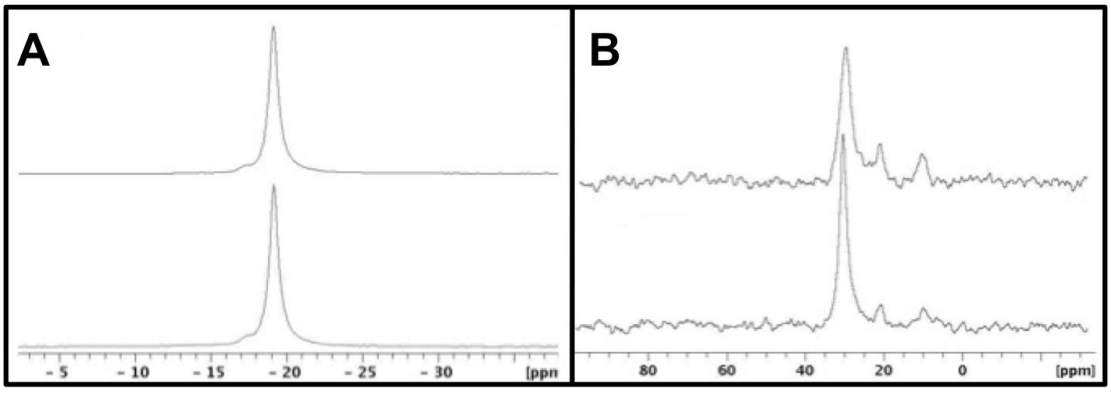

Figure 52. MAS Solid State NMR of 1,2-epoxydodecane/ZrP and 1,2-epoxyoctadecane/ZrP. (A) $^{31}P\{^{1}H\}$ of 1,2-epoxydodecane/ZrP (top) and 1,2-epoxyoctadecane/ZrP (bottom) and (B)^{13}C CP of 1,2-epoxydodecane/ZrP (top) and 1,2-epoxyoctadecane/ZrP (bottom).

Although the ^{31}P spectra shows no evidence of successful modification, chemical bonding of the alkyl chains to the surface of the samples agrees well with the ^{13}C CP MAS NMR spectra of 1,2-epoxydodecane/ZrP and 1,2-epoxyoctadecane/ZrP in **Figure 52,** where the resonances between 30.4 ppm and 10.4 ppm correspond to carbons of the

alkyl chains. In comparing the 1,2-epoxydodecane/ZrP and 1,2-epoxyoctadecane/ZrP it can be seen that the resonance at ~30 ppm greatly increases due to the longer chain length of the modifier, this is in agreement with the assignment of this peak to the alkyl chain. (It should be noted that cross polarization $\{^{1}H\}^{13}C$ generally does not produce actual signal intensities in the ^{13}C CP MAS NMR spectra. Therefore, the above comparison is valid if mobility of the alkyl chains in the two materials is very similar.) It should be emphasized that the signals of the three membered rings of the starting organic materials are absent in the spectra, this confirms that all organic modifier present is covalently attached to the ZrP platform. Additionally, it can be observed that signals corresponding to the ring opening of the epoxide are absent from the spectra. It is likely that the absence of the signal is also due to the small amount of surface phosphates as was the case for the ^{31}P NMR.

The microwave samples show a contrast to the fully functionalized samples prepared by Pica and also the surface functionalized samples prepared by the reflux method. The data clearly suggests that the organic is present on the surface of the sample rather than the interlayer, however it is difficult to say whether covalent attachment has occurred due to the large size of the ZrP sample used in the microwave case.

4.5 Conclusion

In conclusion, it has been shown that it is possible to selectively functionalize the surface of zirconium phosphate nanoparticles with silanes and epoxides to synthesize inorganic-organic hybrid materials using microwave synthetic or traditional reflux methods. This functionalization leads to new organic derivatives of ZrP in which the top and bottom layers are modified while the interlayer structure remains unchanged. This is the first known report of a functionalized inorganic layered material in which the interlayer is unaffected and is still available to perform intercalation or ion exchange chemistry. In the case of silanes it was found that the bonding to the surface phosphates was very minimal, likely due to geometric constraints. Bonding was found to be more substantial in the case of epoxides, where each surface phosphate is thought to interact with an epoxide ring. The polymerization of epoxides from the ZrP surface was also introduced. The discovery of polymerization of epoxides in the case of smaller molecules calls into question whether the larger epoxides are polymerizing as well rather than bonding to the surface in the neat microwave case. In addition, it appears that the uptake of modifier is largely related to the size of the particles, this will be discussed in further detail in the next chapter.

CHAPTER V

EFFECT OF PARTICLE SIZE ON SURFACE MODIFICATION

5.1 Introduction

The investigation of the surface functionalization of ZrP with epoxides was able to confirm the covalent attachment of the epoxides to the nanoparticle surface, Chapter IV. When using the reflux method and small particles, the covalent attachment of the epoxide to the ZrP surface was clearly observed, however when the microwave method and more crystalline particles were used, the covalent attachment could not be confirmed definitively. Smaller particles have a higher external surface area than larger particles and also a smaller contribution of interlayer phosphates compared to thicker particles, therefore it is expected that functionalization will become less apparent as the thickness of the particles is increased. **Figure 53** displays a schematic of modified particles of various thicknesses. It can clearly be observed that the increase in the number of inorganic layers will make the mass contribution of the modification less significant and also considering that each layer introduces more phosphate, will decrease the percentage of phosphates available to be modified. In this section identical reflux and microwave reactions (70°C) will be carried out with ZrP of low (3M), medium (6M), and high crystallinity (12M). The materials will be characterized and the effects of the particle size on the functionalization will be discussed.

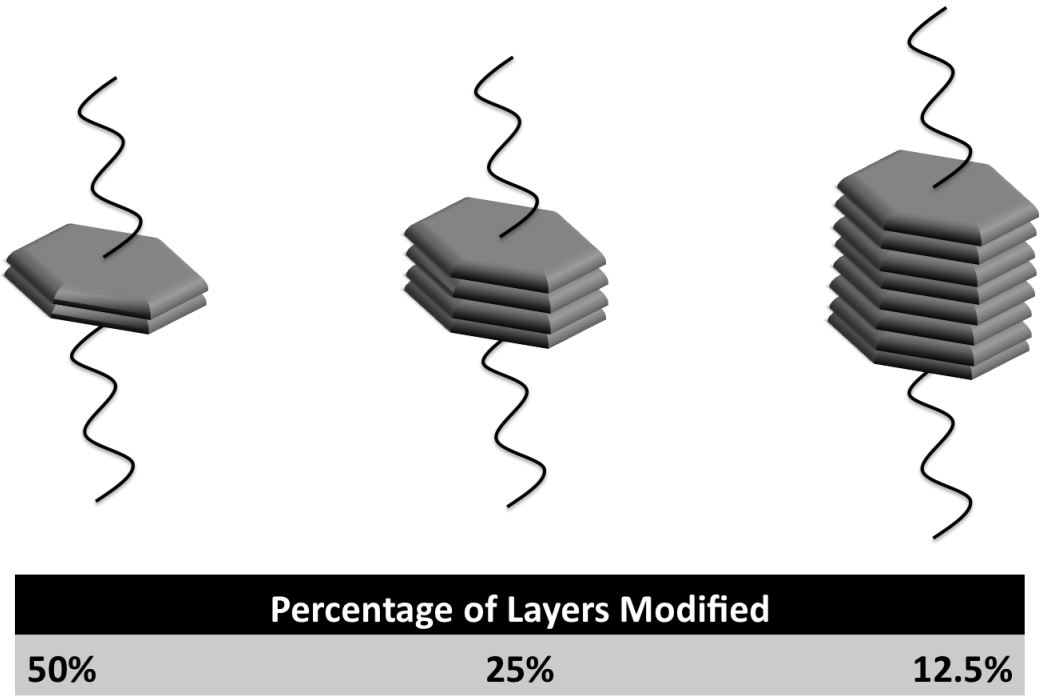

Figure 53. Representation of modified ZrP of various thicknesses and the corresponding percentage of layers modified.

5.2 Surface Modification of Reflux ZrP

The previous chapter has confirmed that using the reflux method no intercalation of the epoxide occurs with the interlayer region, even with particles of low crystallinity. In this case particles of equal or greater crystallinity were used therefore intercalation is not expected. In addition, 1,2-epoxyoctadecane is very hydrophobic and therefore has no driving force to interact with the hydrophilic interlayer of ZrP. FTIR will be used to screen the samples and determine if the organic modifier is present in the product,

however TGA and NMR will be used to quantify the uptake of organic modifier and confirm the bonding with surface phosphates.

The infrared spectra of the modified samples (**Figure 54**) agree well with those discussed in the previous chapter as expected**.** In this case we are seeking the effects of the particle size on the spectra. It is expected that as the ZrP becomes more crystalline both the particle size and thickness will increase. As a result there will be a smaller percentage of sites that can be esterified, therefore leading to a smaller contribution of organic in the sample and a corresponding decrease in the signals associated with the modification. The initial area of interest is that of the alkyl stretching of the 1,2-epoxyoctadecane. The stretching due to the alkyl chain can be observed in the low, medium, and high crystallinity cases suggesting that modification successfully occurred in all samples. It can be noted however that the intensity of the stretching is substantially lower in the medium and high crystallinity cases as compared to the low crystallinity sample. This is reasonable as the low crystallinity particles are expected to be *ca.*11 layers whereas the highly crystalline material is estimated to be *ca.* 50 layers or more.

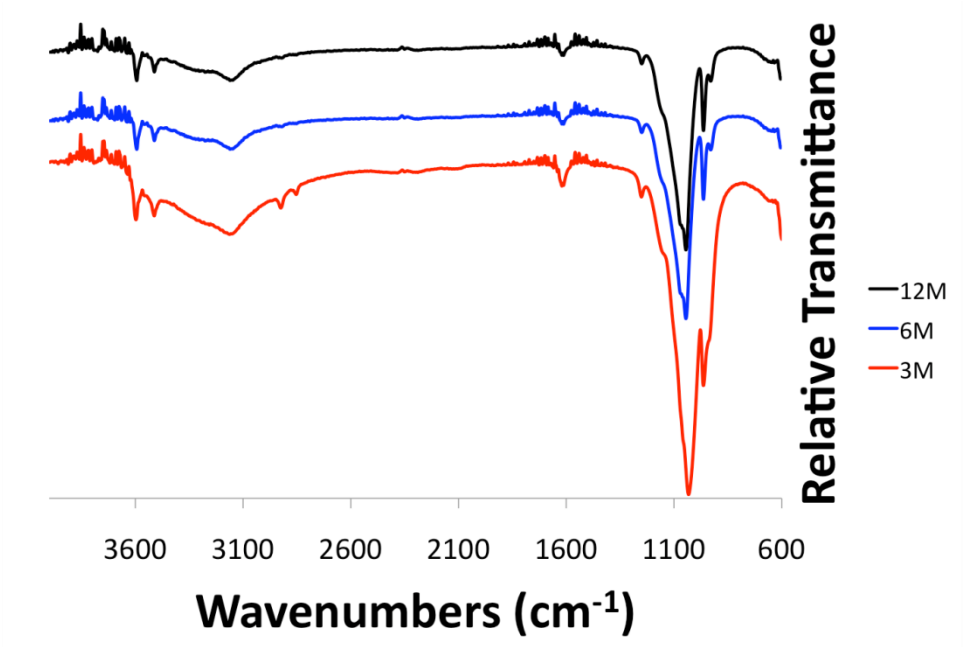

Figure 54. FTIR spectra of 1,2-epoxyoctadecane/ZrP synthesized with reflux ZrP of low, medium, and high crystallinity.

The 6M and 12M samples appear to display similar stretching due to modification in both the alky region and phosphate ester region. Further investigation of the phosphate ester region shows that in all cases the signal corresponding to ester formation can be observed. This suggests that in the reflux case that there are still a significant amount of phosphates on the surface relative to those in the interlayer.

As the particle size increases the particles become thicker, therefore larger particles are expected to have a large contribution of inorganic layers and a small contribution of organic modifier. The TGA thermograms of the three modified samples follow this trend, as the highest weight loss is observed for the 3M particles and the lowest for the

12M, as seen in **Figure 55.** It should be noted that in this case hexanes is used as the solvent, it appears that the lower reaction temperature causes a decrease in the amount of epoxide that is bonded to the surface. The 3M sample uptakes 0.06 moles of epoxide in this case as opposed to ~ 0.14 moles when toluene is used as the solvent An overlay of the derivative of the weight loss can be seen in **Figure 55 B**. As with all modified samples there are four main weight loss regions corresponding to surface water, interlayer water, the modifier, and the condensation of the phosphates to pyrophosphate. Initially, it can be seen that the amount of surface water differs in all the samples. The particles with lower crystallinity (3M-6M) both display water absorbed to the surface whereas the more crystalline particles do not exhibit this weight loss. Secondly, the interlayer water molecule is different in the samples as well. There are two peaks in the second derivative, which correspond to the interlayer water molecule. The first can be said to be the water that is held loosely by the particles, mostly on the edges whereas the second is the water that is deeper within the core of the particles, as discussed in Chapter III. The trend is observed that the more crystalline the particles become the less significant is the first peak and the more dominant the second becomes. This is reasonable as more crystalline particles should have a stronger attraction between the layers and thus hold the water molecule more efficiently. The derivative of the water loss also shows that the dehydration behavior of the low and medium crystalline samples to be very similar.

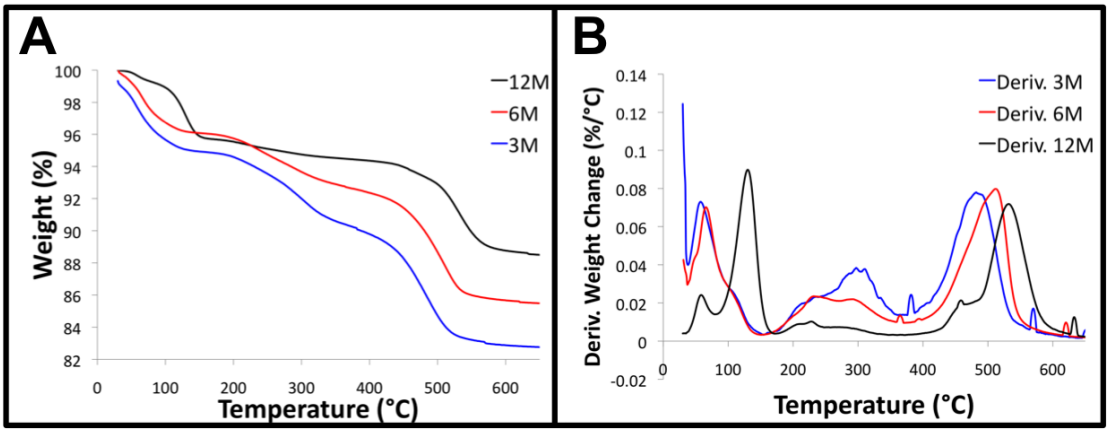

Figure 55. (A)TGA and (B) derivative of weight loss of 1,2-epoxyoctadecane/ZrP synthesized with reflux ZrP of low, medium, and high crystallinity.

As in the case of the toluene reflux, the derivative corresponding to the modifier exists in two steps, however it appears that the first and not the second peak is the dominant process in all cases except the 3M. The inversion of intensity of the two derivative processes suggests that the bonding of the epoxide to the surface differs somewhat amongst different particle sizes, however it still cannot be said with certainty what the two steps represent. Lastly, it can be noted that the peak corresponding to the condensation is shifted in all cases, however this is a function of the crystallinity of the particles and not the modification.

TGA has successfully confirmed that the organic contribution of all the samples is different and therefore modification has occurred to different extents in all the samples. NMR will be utilized to probe the overall effect of the modification on the environment of the phosphorus and carbon atoms in the materials. Based on previous experiments it

is expected that in the case of successful modification by reflux that four signals will be observed in the ^{31}P NMR, the two original signals observed corresponding to ZrP and two additional signals at -21.4 and -22.4 ppm corresponding to the dehydration of ZrP and the formation of a phosphate ester. All four of these signals are observed in the 3M, 6M, and 12M materials, **Figure 56**. Although less epoxide exist in these samples compared to the neat reaction or toluene reflux, the signal for the modification can still be observed in the ^{31}P spectra. **Table 5** displays the percentage of phosphorus atoms that make up each environment based on integration. It can clearly be observed that as the particles become more crystalline that the peak at -19 ppm becomes more dominant and all other signals decrease in intensity. In the 12M case the signals corresponding to ZrP make up 90% of the phosphorus environment whereas modification only accounts for 10% of the phosphorus in the compound. This corroborates with the TGA data that suggest that the uptake of epoxide on the surface decreases as the particles increase in size.

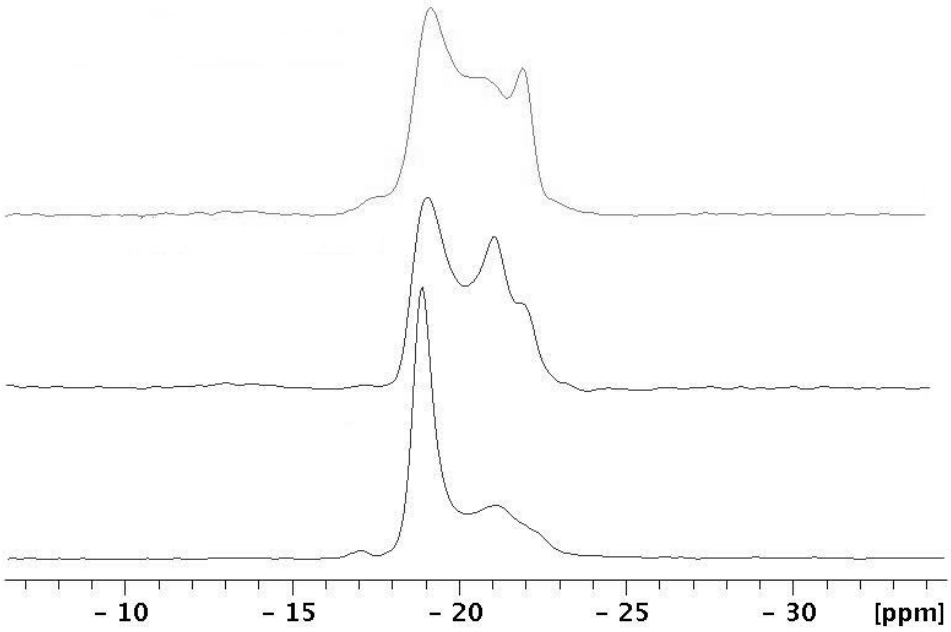

Figure 56. ^{31}P NMR of 1,2-epoxyoctadecane/ZrP synthesized with reflux ZrP of low (top), medium (middle), and high (bottom) crystallinity.

Table 5. Intergration values of the four signals present in the ^{31}P NMR of 1,2-epoxyoctadecane/ZrP.

	Signal 1	Signal 2	Signal 3	Signal 4
3M	1.5%	47%	33%	19.1%
6M	0.8%	51%	35%	13.3%
12M	1.3%	66%	23%	9.6%

In addition to the observation of successful modification in the ^{31}P NMR, ^{13}C NMR also supports covalent attachment of the epoxide to ZrP, **Figure 57**. Once again, the alky chains are seen from 10.4 to 31.4 ppm. These signals can be observed clearly in all the samples regardless of the particle size as a long aliphatic chain was used to modify the surface. The signals indicative of the P-O-C linkages are also present but the intensity decreases as the particles become more crystalline. Also there is some variability in regards to the dominant peak in the spectra. In some cases it is at ~29 whereas in others it is at ~31. The relationship seems to be that the less crystalline particles tend to have the dominant signal at 29 ppm whereas the more crystalline display the dominant signal at 31 ppm, **Figure 57 B**. These signals are assigned to the carbon atoms in the aliphatic chain therefore it is likely that the difference in signal intensity could be a function of mobility of the chains and thus directly related to the amount of epoxide covalently attached to the surface of the nanoparticles and the

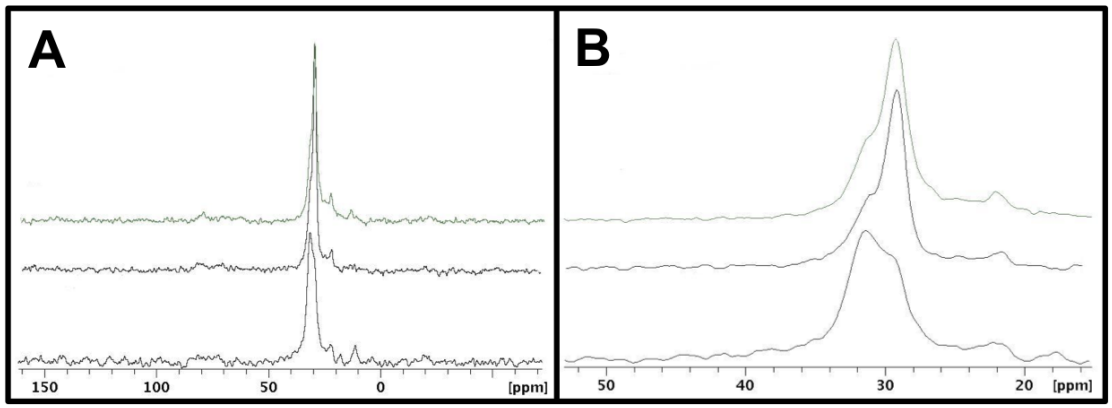

Figure 57. ^{13}C NMR of 1,2-epoxyoctadecane/ZrP synthesized with reflux ZrP of low (top), medium (middle), and high (bottom) crystallinity displaying the (A) complete spectra and (B) focusing on the alkyl resonances.

bonding conformation of the epoxide. It should be noted however that ^{13}C NMR cannot be used to confirm bonding with the ZrP surface. The spectra only indicate that the organic modifier is present in the sample and that the rings of the epoxide are open. As was the case for the microwave samples, it is possible that this could occur without bonding. The ^{13}C NMR spectra are therefore complementary to the ^{31}P and will not be discussed further, as the aim of this section is to quantify the impact of thickness on bond formation.

5.3 Surface Modification of Hydrothermal ZrP

The infrared spectrum of the hydrothermal surface modified particles was analyzed next. The spectra displays signals for the aliphatic chains of the 1,2-epoxyoctadecane in the cases of the low and medium crystalline samples, however in the case of highly

crystalline sample the stretching is not present, **Figure 58**. This suggests that as the particles approaches micron size, the large contribution of hundreds of inorganic layers makes the organic modification insignificant. There are 18 carbon atoms attached to the surface for each successful modification, even at this number no stretching is observed therefore it is not likely that the phosphate ester will be present as only one bond is formed per alkyl chain. The spectra do not display the phosphate ester stretch but this does not necessarily mean that no bonds are formed; as discussed earlier the inorganic contribution is too high to observe the functionalization.

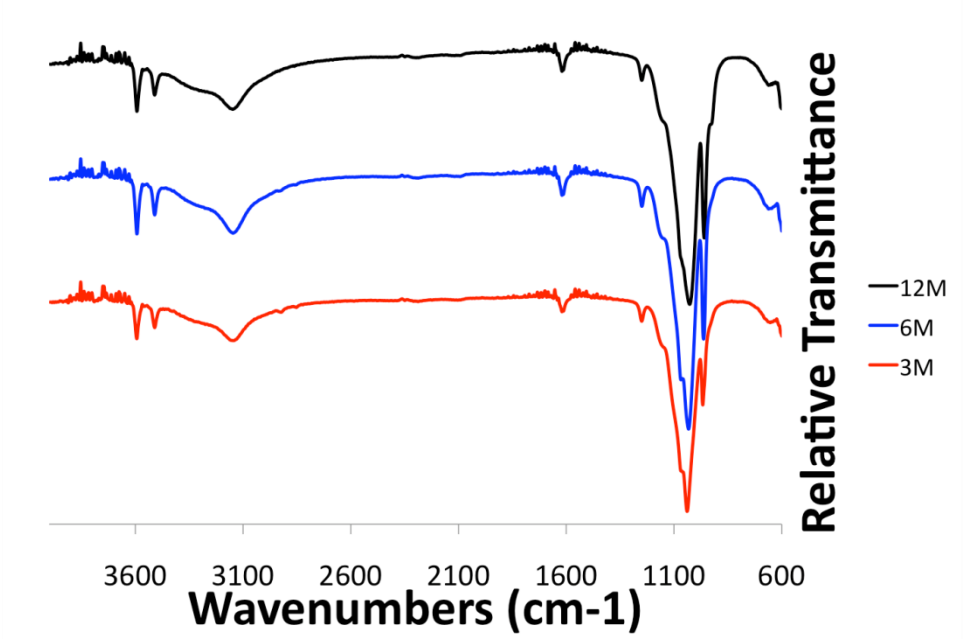

Figure 58. FTIR spectra of 1,2-epoxyoctadecane/ZrP synthesized with hydrothermal ZrP of low, medium, and high crystallinity.

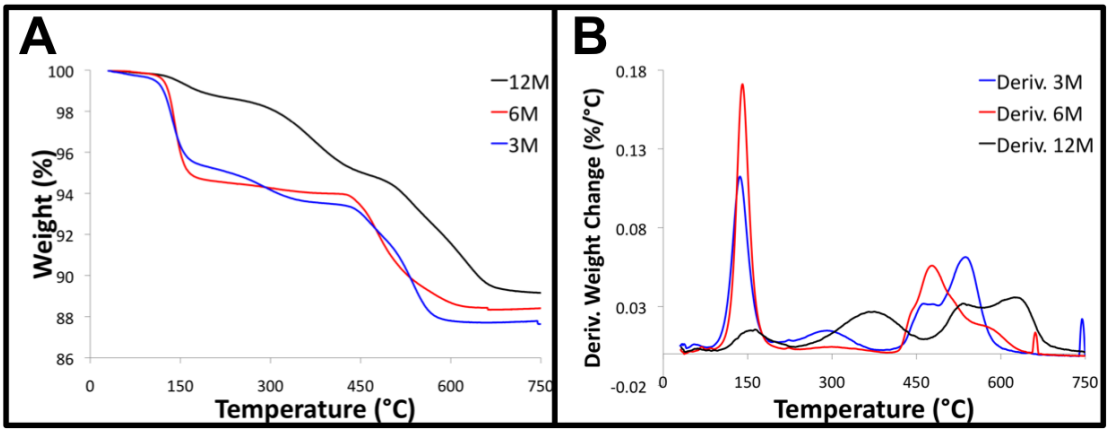

Figure 59. (A)TGA and (B) derivative of weight loss of 1,2-epoxyoctadecane/ZrP synthesized with hydrothermal ZrP of low, medium, and high crystallinity.

The TGA of the modified hydrothermal particles can be seen in **Figure 59.** Interpreting the TGA of the modified hydrothermal particles is not as clear as in the case of reflux materials. As discussed in Chapter III, the water loss is delayed until much higher temperatures in the hydrothermal case. As a result, the weight loss for the organic modifier is embedded within the water loss and not able to be identified distinctly. It can be said however that the total weight losses observed for the samples does follow the expected trend with the least crystalline sample having the highest weight loss and the most crystalline having the least. In addition it can be observed that compared to the starting material an increase in total weight loss is observed after functionalization. Even in this case the total increase cannot be accounted solely to the modifier as the level of hydration could have possibly changed.

To further investigate the bonding within the hydrothermal particles ^{31}P NMR was utilized. Contrary to the reflux case, all spectra displayed only a single resonance at -19 ppm, **Figure 60**. This resonance is indicative of the orthophosphate of ZrP as discussed earlier. Bonding to the ZrP surface in the case of thicker particles cannot be verified by traditional techniques. This is not surprising, as even in the case of modified 12M reflux particles the modification accounted for only 10% of the total integral. The hydrothermal particles percentage of surface phosphates is only a fraction of that of the reflux case and the percentage of modified phosphates is negligible.

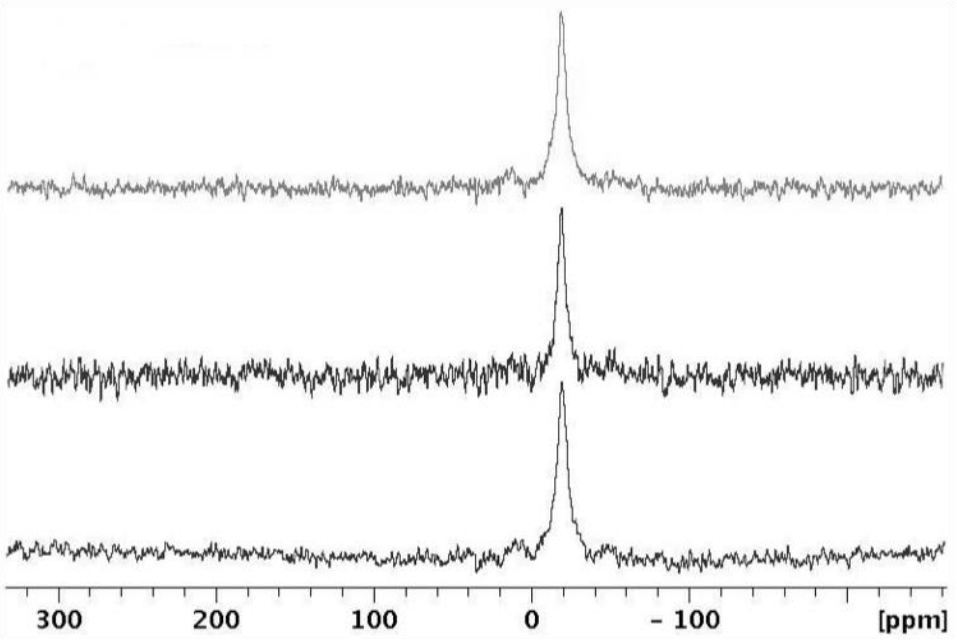

Figure 60. ^{31} P NMR of 1,2-epoxyoctadecane/ZrP synthesized with hydrothermal ZrP of low (top), medium (middle), and high (bottom) crystallinity.

5.4 Neat Microwave Surface Modification of Reflux ZrP

FTIR of the microwave-modified products can be seen in **Figure 61**. Overall, the amount of organic present in these samples is substantially higher than in the reflux case. The alkyl stretching signal can clearly be seen in all three samples, additionally in the 3M and 6M case three of the symmetric and antisymmetric CH_2 stretches can be observed as opposed to only two in the reflux. Interestingly, although there is a large

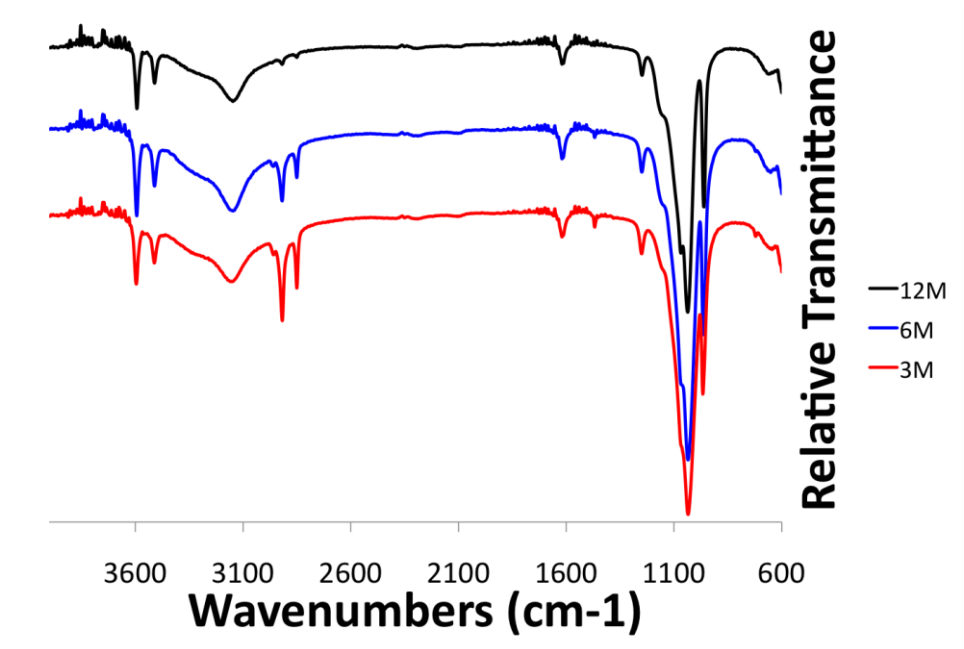

Figure 61. FTIR spectra of 1,2-epoxyoctadecane/ZrP synthesized by the neat microwave method using reflux ZrP of low, medium, and high crystallinity.

amount of organic modifier in the samples the stretch for P-OR bond formation is not present in any case. This suggests that the organic modifier is not covalently attached to the surface. As these reactions were carried out in excess of epoxide it is likely that the epoxide simply polymerized around the ZrP nanoparticle and adsorbed to the surface.

The TGA theromgrams displayed the same trend as in the case of the reflux experiments when the neat microwave synthetic method was used, **Figure 62**. Although the trend is identical the amount of epoxide determined by TGA is much higher as discussed in the previous chapter. In this case the moles of epoxide present are nearly double what was reported in the case of the reflux method. This confirms that it cannot all be bonded to the surface, as the percent coverage estimates were nearly 70% in the reflux cases. Examination of the derivative of the 3M sample reveals a very broad weight loss. In this case it is likely that the epoxide weight loss consist of more than two steps. This would support possible polymerization on the surface of the nanoparticles.

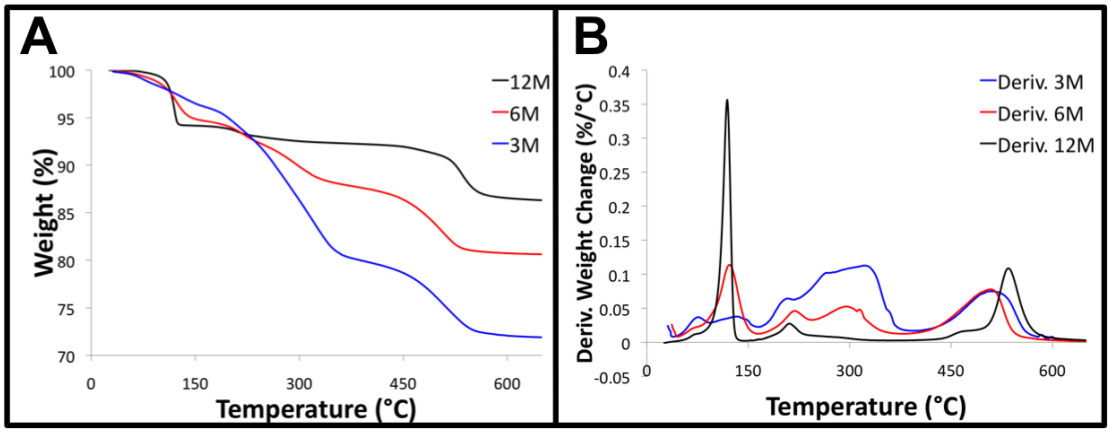

Figure 62. (A)TGA and (B) derivative of weight loss of 1,2-epoxyoctadecane/ZrP synthesized by the neat microwave method using reflux ZrP of low, medium, and high crystallinity.

^{31}P NMR of all samples were largely identical, displaying a dominant resonance at -19 ppm and the small shoulders on either or both sides regardless of particle size, **Figure 63**. It was originally hypothesized that the 12M reflux particles modified by the neat microwave method did not display a signal in the NMR due to their thickness and the percentage of phosphates on the surface. The current results suggest that this hypothesis is not true as even the thinnest particles, 3M, do not display a resonance corresponding to phosphate ester formation. In addition, it was shown in the reflux case that successful modification could be evidenced by a ^{31}P NMR signal in the case of 3M, 6M, and 12M particles. It is therefore concluded that in the case of the neat microwave method bond formation does not occur at all or only in limited quantity. These results appear to be contrary to those found by Levitt, who suggested that neat reaction of ZrP with epoxide yielded a more complete reaction.[147] In his case IR stretches at 1150 cm-^{1} and 1130 cm^{-1}

were used to verify the bonding. The reactions were however carried out with γ -ZrP and under different synthetic conditions. It is likely that the coupling of microwave irradiation with the excess of epoxide could lead to the polymerization.

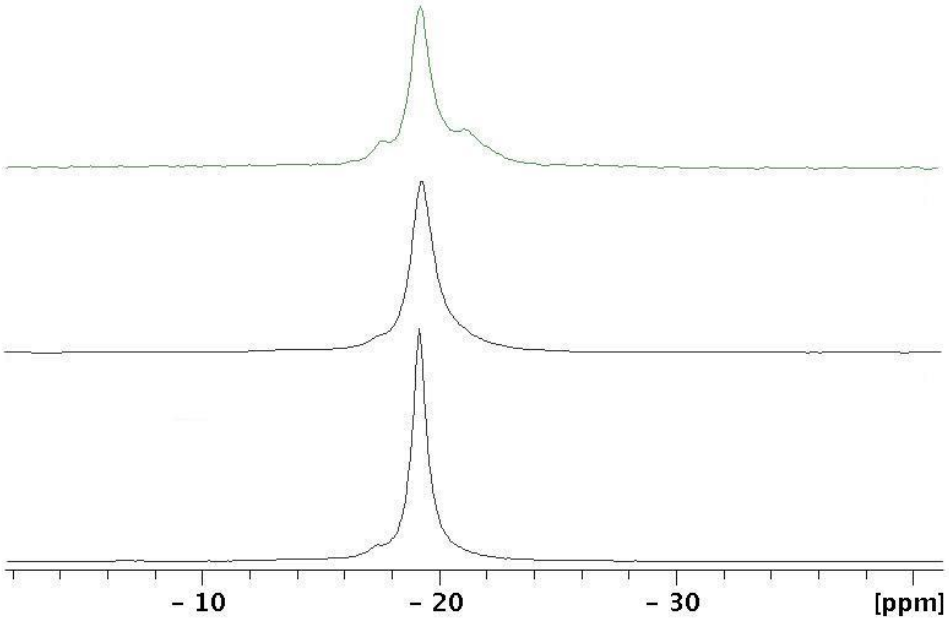

Figure 63. ^{31} P NMR of 1,2-epoxyoctadecane/ZrP synthesized by the neat microwave method using reflux ZrP of low (top), medium (middle), and high (bottom) crystallinity.

Levitt carried out reactions at room temperature and used a special vessel to avoid polymerization. Yamanaka on the other hand, recovered the phosphate ester salt of the esterified ZrP product to confirm bond formation.[35] In the case of γ -ZrP it is known that the reaction proceeds initially by absorbing into the interlayer; as the interlayer of α-ZrP

is not available and excess epoxide exists at the surface, the reaction is likely forced to proceed through another route.

5.5 Stoichiometric Microwave Surface Modification of Reflux ZrP

To investigate whether the microwave or the excess epoxide is the source of polymerization, microwave experiments were carried out using a stoichiometric amount of epoxide. The FTIR spectra of the samples modified using the stoichiometric microwave method do not differ largely from those of the reflux case, **Figure 64**. The alkyl stretching is observed in the expected region, it is noted that the intensity of the stretching is very low compared to the neat microwave case. This suggests that the polymerization has been limited by the use of solvent and addition of only a stoichiometric amount of epoxide. The stretching for the phosphate ester is not present in this case. Again, this suggests no bonding or a very low level. In this case it is likely that the reaction time should be increased in order to ascertain whether the reaction is plausible in the microwave.

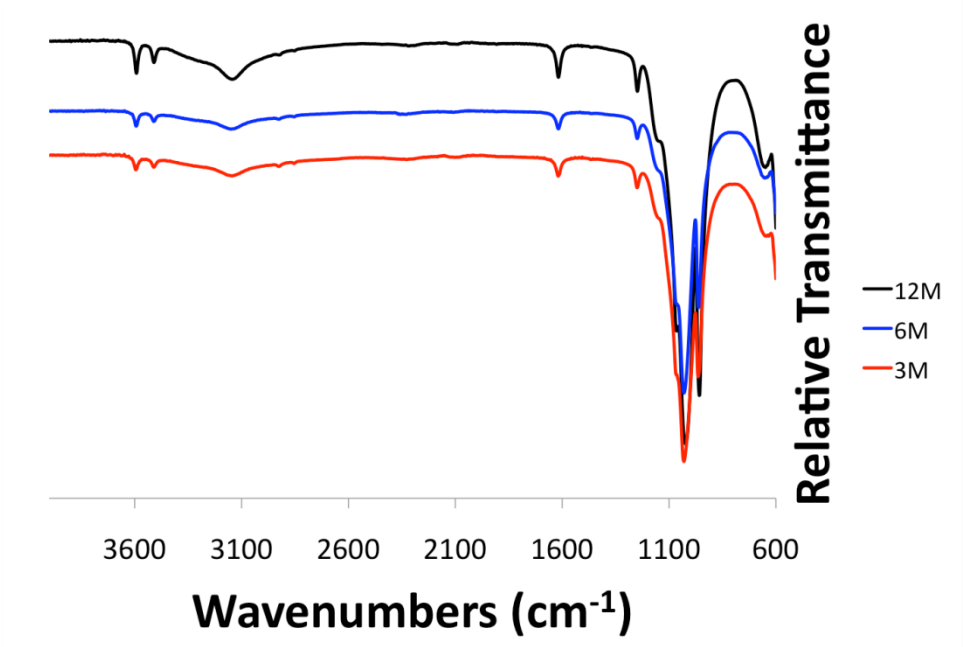

Figure 64. FTIR spectra of 1,2-epoxyoctadecane/ZrP synthesized by the stoichiometric microwave method using reflux ZrP of low, medium, and high crystallinity.

TGA of the modified samples revealed that generally the uptake of epoxide in the stoichiometric microwave case was lower than all other methods previously discussed, **Figure 65**. Even in comparison with the reflux samples, this method produces only a third of the uptake. The data therefore suggests that the polymerization that occurred in the neat case is eliminated due to the presence of solvent and small amount of epoxide. As with all other experiments, the observed trend that the less crystalline materials uptake the most epoxide still holds true. It is also observed that the derivative of the weight losses still exists as a two-step process. In this case both steps appear to contribute nearly equally to the observed weight loss. It is likely that the short time

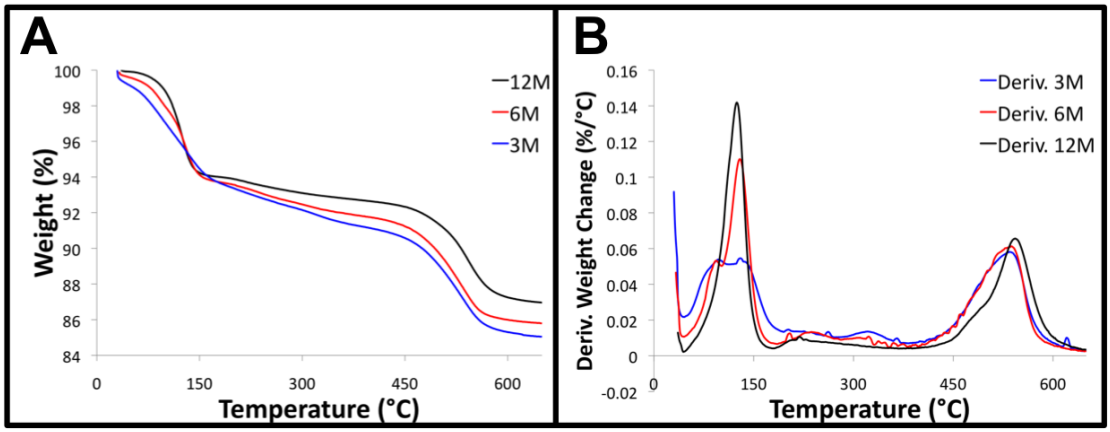

Figure 65. (A)TGA and (B) derivative of weight loss of 1,2-epoxyoctadecane/ZrP synthesized by the stoichiometric microwave method using reflux ZrP of low, medium, and high crystallinity.

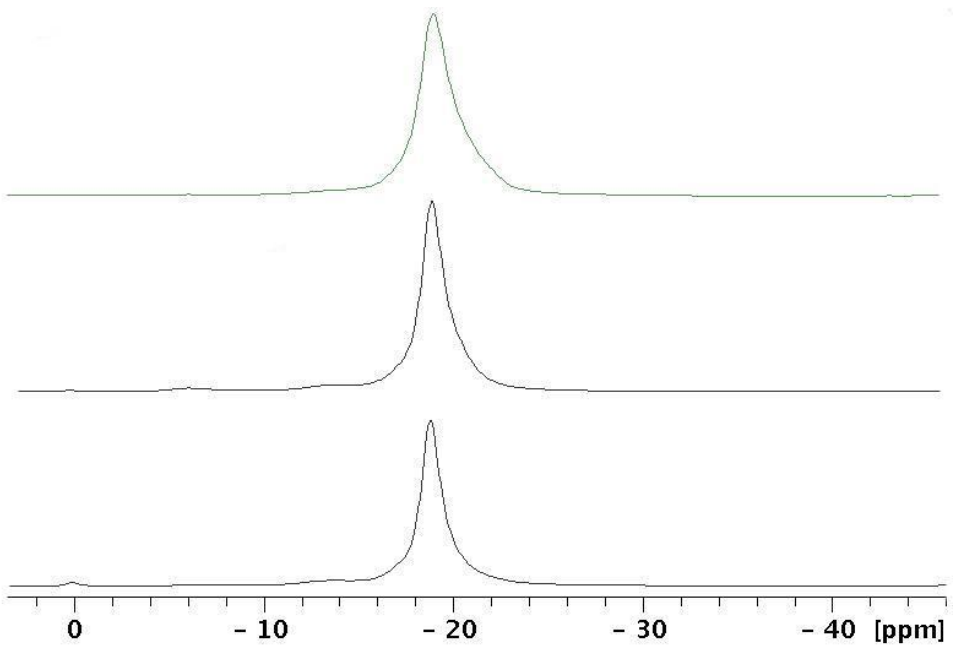

Figure 66. ^{31} P NMR of 1,2-epoxyoctadecane/ZrP synthesized by the stoichiometric microwave method using reflux ZrP of low (top), medium (middle), and high (bottom) crystallinity.

frame of the reaction severely limits the uptake. The reaction may however be successful if a longer reaction time were used.

The NMR spectra of these samples as with the other microwave case display a single resonance at -19 ppm, **Figure 66**. This data does in fact suggest that bonding does not occur in the samples, however it should be taken into account that in this case the amount of organic present in the samples is extremely low. The resulting surface coverages are not substantial at all and an extended reaction time is needed before it can be said definitively that the microwave method is not useful.

5.6 Conclusion

Several important conclusions can be drawn from this investigation. First of all, it can be said that bonding of epoxides to the surface of ZrP is possible with a variety of particle sizes. The thickness of the particles lowers the percentage of phosphates on the surface and available for bonding but the bonding can still be monitored up to a certain extent. In the case of hydrothermal samples it is likely that bonding has occurred as identical reactions were conducted, as with the reflux particles but due to the large size of the particles the bonding cannot be confirmed by any traditional techniques. It is however possible that the bonding could be verified by exfoliating the ZrP and recovering exclusively the modified layers. The modified layers could then be analyzed FTIR to see if the phosphate ester is present. In the case of microwave samples it appears that

bonding does not occur in any case. This is likely a factor of many things. The reaction time may not be long enough, if this is the case the epoxide will readily reacted with itself and polymerize before it can bond with the ZrP surface. Also, the microwave irradiation may have some effect on the ring opening of the epoxide in which case polymerization would also occur.

CHAPTER VI

ZIRCONIUM PHOSPHATE AS A PLATFORM FOR TETRAVALENT METAL AND PHOSPHONIC ACID ASSEMBLIES[*]

6.1 Introduction

A new functionalization method will now be investigated using the ion exchange chemistry of ZrP. The phosphate groups of ZrP contain exchangeable protons, therefore, if an ion of a large size is used, it is to be expected to exclusively exchange the surface protons. If such an approach is taken with transition metals, it is expected that the metal ion layer can be functionalized using ligands. This approach will now be investigated with tetravalent metals and phosphonic acids.

6.2 Sn(IV) on the ZrP Surface

For the initial investigation, highly crystalline 12M reflux ZrP particles were used in order to avoid intercalation of the metal ion into the interlayer region. Titration of ZrP can yield information such as the exchange capacity, surface area, and thickness of the

[*] Part of this chapter is reprinted with permission from "Designable Architectures on Nanoparticle Surfaces: Zirconium Phosphate Nanoplatelets as a Platform for Tetravalent Metal and Phosphonic Acid Assemblies" by Mosby, B.M., Goloby, M., Díaz, A., Bakhmutov, V.I., and Clearfield, A., *Langmuir*, **2014**, 30 (9), 2513-2521, copyright 2014 by American Chemical Society.

nanoparticles. The synthesized ZrP nanoparticles were titrated with 0.01 M NH_4Cl. The NH_4^+ ion cannot enter the interlayer region and exchanges only the surface protons of the nanoplatelets, therefore the pH of the solution should decrease as protons are liberated from the surface due to formation of HCl, and begin to rise once the surface has been fully exchanged with NH_4^+. Using the volume of NH_4^+ solution added at the minimum pH, the moles of protons liberated and therefore the moles of phosphate groups on the surface were calculated. It was found that the ammonium surface exchanged material had a Zr to NH_4^+ ratio of 135 to 1. Since each ammonium group displaces a single surface proton, this is the proper ratio for an ion that interacts with the surface phosphates in a 1 to 1 fashion. These ratios were employed during our experiments along with 10:1, 8:1, 5:1, and 2:1 Zr:Sn ratios which are thought to be a large excess of Sn in regards to the surface. If the deposition of the ions on the surface proceeds by ion exchange, analysis of the Zr:Sn(IV) ratio of the products can be used to estimate the coordination of the metal ion on the surface.

First the presence of the tetravalent metal, Sn, on the surface of α-ZrP was examined by several techniques. Initially, powder x-ray diffraction can reveal whether there has been any intercalation of the Sn ion into ZrP or if there are any structural changes in the material. The interlayer spacing of 7.6 Å is the distance between two layers, incorporation of an ion between the layers would increase this distance and the resulting change in spacing would be observed in the powder x-ray diffraction pattern. **Figure 67** shows the XRPD of α-ZrP along with the Sn modified ZrP (Sn/ZrP) samples. It can be

seen that the patterns are identical to that of α-ZrP suggesting that the α-ZrP structure is intact and there have been no interlayer changes.

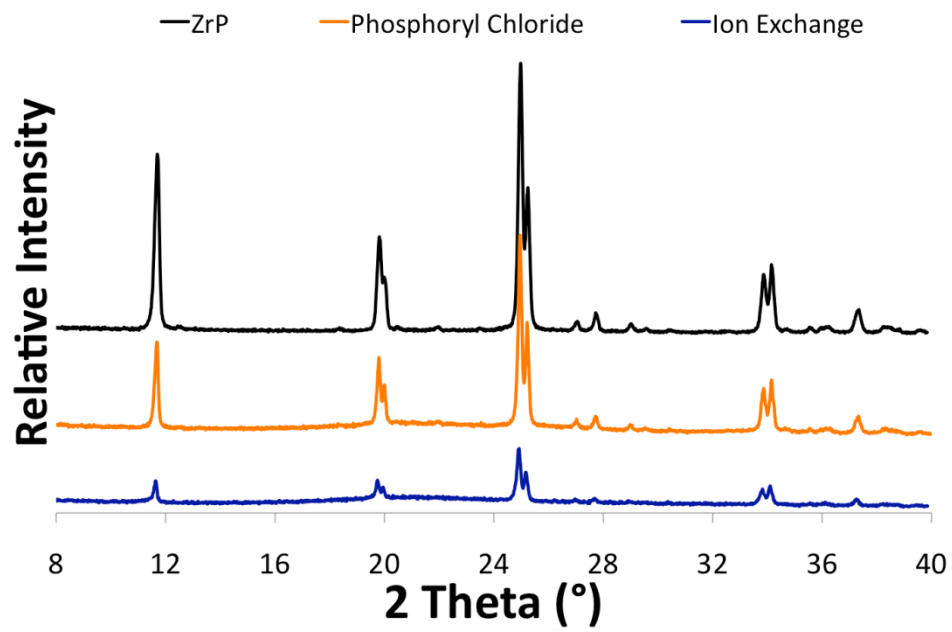

Figure 67. XRPD of ZrP and Sn/ZrP prepared by the ion exchange and phosphoryl chloride methods.

To investigate the presence of Sn in the material XPS spectra were obtained; initially the Zr, P, and O spectra were investigated **Figure 68**. Observation of the spectra revealed the characteristic peaks for Zr, P, O, and Sn, confirming the presence of all expected elements. Both the 5/2 and 3/2 signals for the Sn(3d) electrons are observed at 486 and 493 eV, respectively, **Figure 69**. Previous XPS studies of ZrP intercalation compounds have shown that the interaction of an intercalated molecule with the interlayer phosphate

groups effectively decreases the positive charge of both the Zr and P atoms, lowering their binding energies as compared to pristine ZrP.[170] The XPS spectra of the ZrP and Sn(IV) modified materials are fairly similar, however a slight shift in the binding energies of Zr, P, and O was observed in the phosphoryl chloride modified samples relative to ZrP and the ion exchange material. The shift can be attributed to the new oxygen and phosphorus atoms that are added to the surface through coordination of phosphoryl chloride. Excluding the phosphoryl chloride, the Zr, P, and O are in relatively the same environment after the deposition of metal ions on the surface.

The XPS spectra appear to be identical in all cases regardless of the amount of Sn on the surface. Although variation of the amount of Sn on the surface leads to variation in the intensity of the Sn and Zr signals, this is only a factor of the penetration depth of XPS and no change or shifting of the signal occurs. Examination of the Sn 3d XPS spectra in **Figure 69** confirms that more Sn is being deposited on the material as the amount of Sn used in the reaction is increased. XPS is a surface technique therefore it cannot be used to determine the atomic makeup of the compound. Comparing the Sn signals for the ion exchange and phosphoryl chloride methods reveals that overall the amount of Sn is the same when equal ratios are used. It can be noted however that the intensity of the phosphoryl chloride signals are not in the expected order based on the reaction stoichiometry. This may be a result of the homogeneity within the sample or a structural effect.

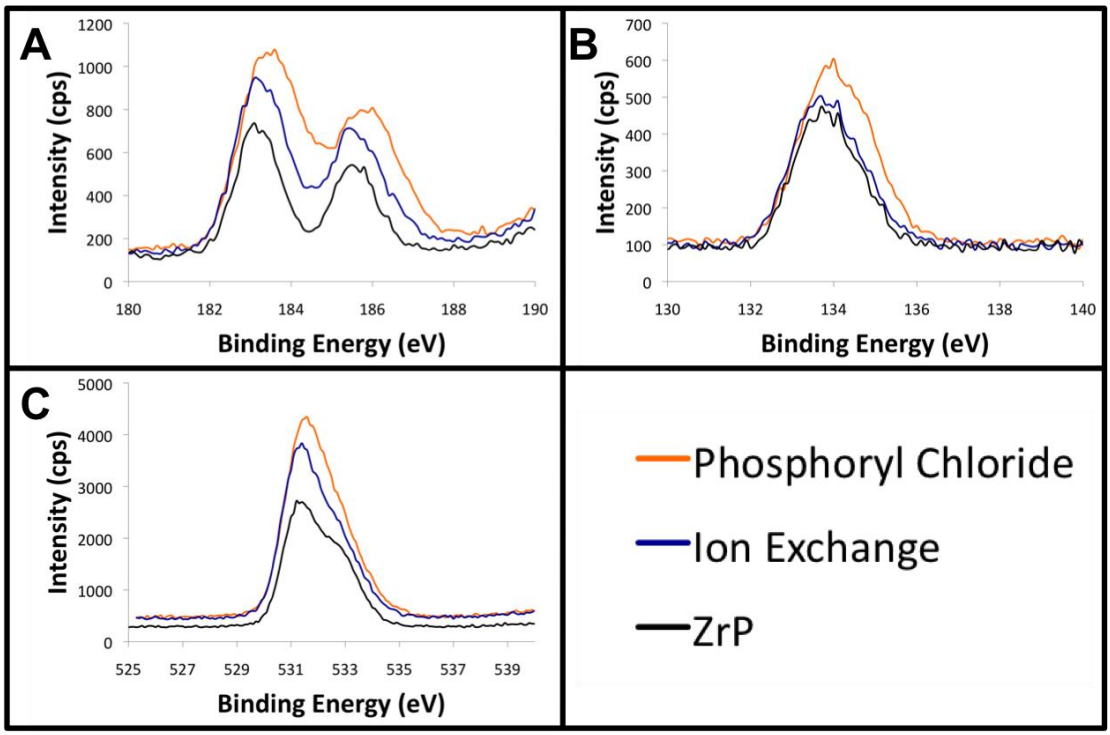

Figure 68. (A) Zr, (B) P, and (C) O XPS spectra of Sn/ZrP prepared using the phosphoryl chloride and ion exchange methods.

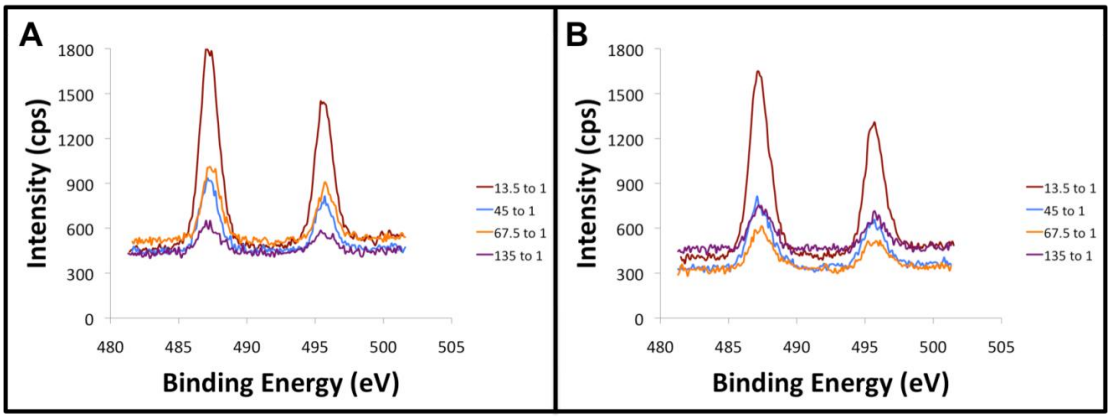

Figure 69. Sn 3d XPS spectra of Sn/ZP prepared by the (A) ion exchange and (B) phosphoryl chloride method.

To quantify the amount of Sn in the samples and to investigate the homogeneity of the synthesized materials electron microprobe analysis was utilized. **Figure 70** shows the Zr:Sn ratio used in the reaction compared to that found in the product. It can be seen that in all cases Sn has been deposited on the nanoparticles. Changing the Zr:Sn ratio leads to a fluctuation in the amount of Sn relative to Zr. An interesting result is found in that the amount of Sn on the surface exceeds the expected amount for saturation of the surface in all cases. This suggests that after all surface sites have been exchanged with Sn the metal ion continues to agglomerate on the surface of ZrP, producing Sn layers of variable thickness on the surface. It was thought that the phosphoryl chloride method would avoid the buildup of excess Sn; the multiple oxygen atoms of each surface PO_3^{2-} group were expected to better stabilize the valency of the Sn ion due to their proximity to each other. This stabilization would then reduce the chance that Sn would interact unfavorably with the surface and agglomerate as in the ion exchange case. The metal ratios observed for these materials are very similar if not identical to those observed in the ion exchange case. This suggests that in both cases, ion exchange and phosphoryl chloride, the Sn ions can agglomerate on the surface of the ZrP nanoplatelets.

Using microprobe analysis the homogeneity of the samples can also be investigated, **Figure 71**. In viewing the samples and analyzing with WDS, there appeared to be three different regions that exist in the samples; Sn poor areas, Sn rich areas, and the bulk, which is the evenly distributed Sn on the surface of ZrP.

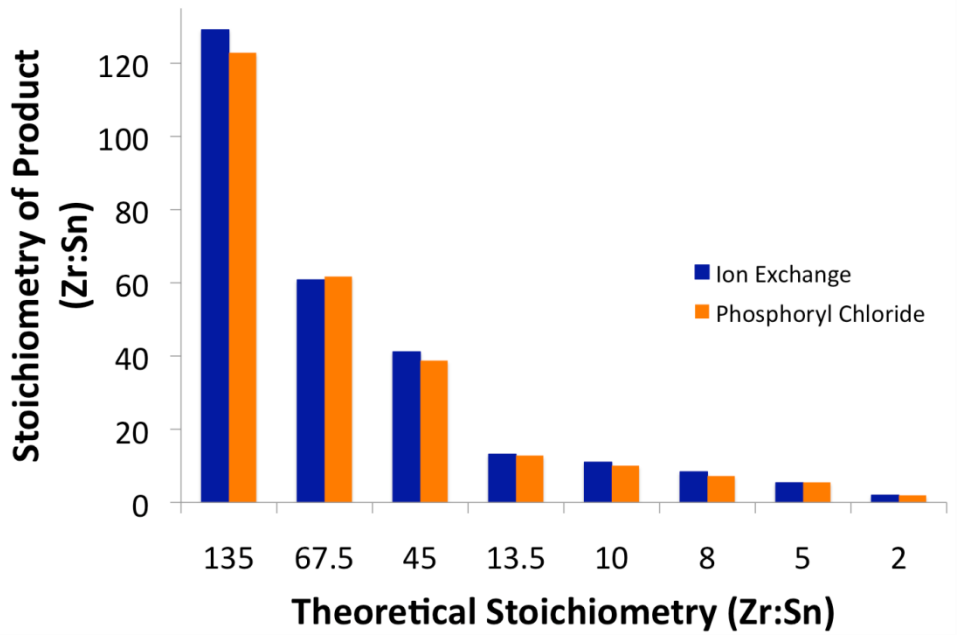

Figure 70. Graph comparing the Zr:Sn ratio used in the synthesis with that found in the product.

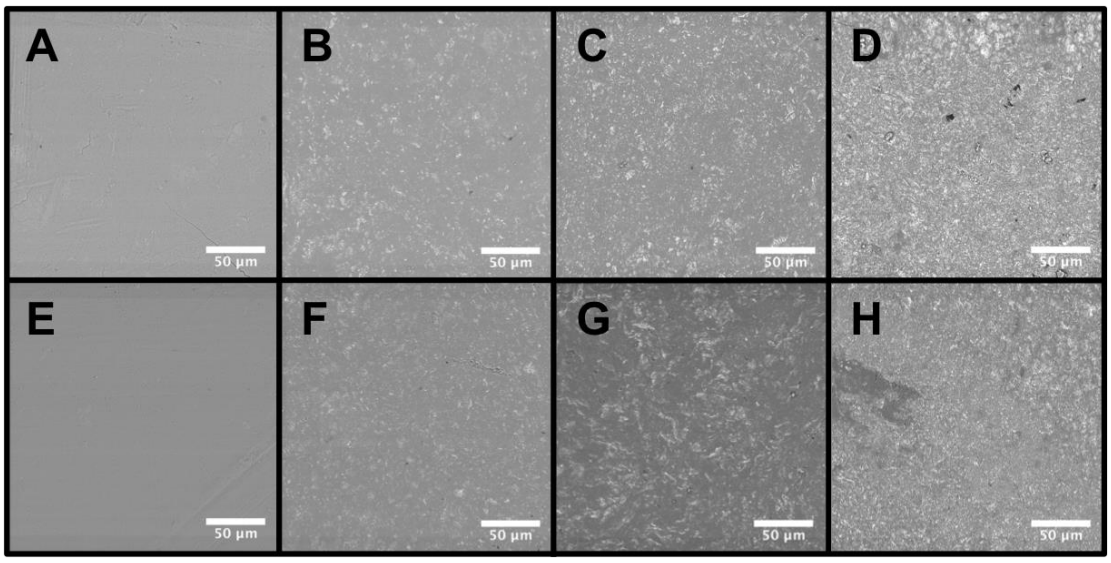

Figure 71. Microprobe images displaying the homogeneity of Sn/ZrP synthesized with the ion exchange (A-D) and phosphoryl chloride method (E-H). Zr:Sn ratios are (A/E) 135:1, (B/F) 10:1, (C/G) 5:1, and (D/H) 2:1.

The Sn rich areas appear as bright spots on the images whereas the areas void of Sn appear darker. The sample with a Zr:Sn ratio of 135:1 was found to be completely homogeneous. Based on the thickness of the particles and the surface area obtained by the titration data we expect that this ratio should give a monolayer of Sn on the surface. A variety of other ratios were investigated ranging from 135:1 to 2:1 Zr:Sn and it was found that the material remained largely homogeneous until a ratio of 10:1 was used. As the amount of Sn is increased, its distribution throughout the surface becomes more irregular and regions where Sn is void and exists in abundance could be found. It can be observed that some of the phosphoryl chloride samples have a higher Sn content than the ion exchange materials synthesized with identical amounts of Sn. This result is due to the fact that the phosphoryl chloride samples are slightly less homogeneous than the ion exchange samples. When acquiring the data, some areas with higher Sn content were used, artificially raising the content for the phosphoryl chloride samples. In all cases it seems that Sn can be deposited on the surface of ZrP nanoplatelets at all ratios. The method of deposition and the stoichiometry can be used to prepare a uniform surface and a homogeneous material. It is worth noting that both XPS and microprobe analysis showed exclusively Zr, P, O, and Sn in the samples. This data suggests that the Sn on the surface must exist as an oxide, hydroxide, or mixture of both to achieve charge balance of the Sn(IV) ion.

Once the presence of Sn on the surface was confirmed the coordination of phosphonic acids to the deposited metal ions was investigated. The ODPA modified ZrP using both

the traditional ion exchange method and $POCl_3$ surface activation was examined by XRPD, FTIR, and TGA to confirm the presence of the phosphonic acid ligand. The X-ray diffraction pattern of the ODPA modified ZrP samples are identical to α-ZrP and Sn Modified ZrP confirming no unwanted interaction of our modifier with the interlayer region. Examination of the FTIR spectra in **Figure 72** shows a mixture of vibration modes for both species, ZrP and ODPA. The intensity of the ODPA stretches are lower than ZrP due to a larger contribution of the many layers of ZrP compared to only 2 functionalized surfaces per nanoparticle. Successful surface modification is supported by the presence of the alkyl stretching and bending bands seen between 2850 -3000 cm^{-1} and 1350-1470 cm^{-1}, respectively. Comparing the ion exchange method with the phosphoryl chloride method it can be seen that there is not a large difference in the intensity of the alkyl region for the materials with Zr:Sn ratios below 13.5:1 . This suggests that at low Sn concentration both materials have similar amounts of ligands on the surface and that the phosphoryl chloride does not significantly increase the uptake of ligand. Initially, it was believed that the ion exchange method would coordinate one Sn ion per multiple surface phosphates whereas the $POCl_3$ method would introduce one PO_3^{2-} group per surface phosphate, thus increasing the amount of metal and the amount of ODPA that can be coordinated.

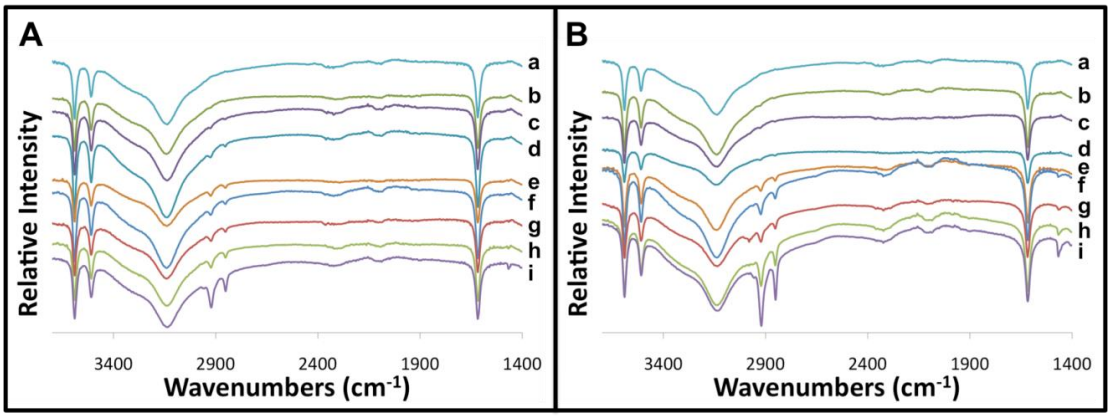

Figure 72. FTIR of ODPA modified Sn/ZrP synthesized by the (A) ion exchange and (B) phosphoryl chloride method. (a) ZrP, (b) 135:1, (c) 67.5:1, (d) 45:1, (e) 13.5:1, (f) 10:1, (g) 8:1, (h) 5:1, and (i) 2:1.

It appears that at higher concentrations of Sn the amount of ligand bonded using the phosphoryl chloride method exceeds that of the ion exchange material. It is possible that although the amount of Sn in each material is the same its orientation is different, causing the apparent difference in ligand uptake. As expected the intensity of the alkyl stretches increases as more Sn and ODPA are added. The alkyl stretching for samples with Zr:Sn ratios of 135: are barely visible in the IR spectra whereas those samples with a large excess of Sn produce more dominant stretches. Additionally it can be observed that at higher Sn concentrations the alkyl stretching seems to be more dominant in the phosphoryl chloride method; this also supports the hypothesis of different Sn ion structures between the two methods.

TGA was used to determine the extent of modification within the samples, **Figure 73**. A sample of unaltered ZrP displays a weight loss of ~12% when analyzed by TGA. The

compound is dehydrated in the first weight loss event and then condensed to zirconium pyrophosphate as the final product at ~ 450° C.[171] In the case of the ODPA modified

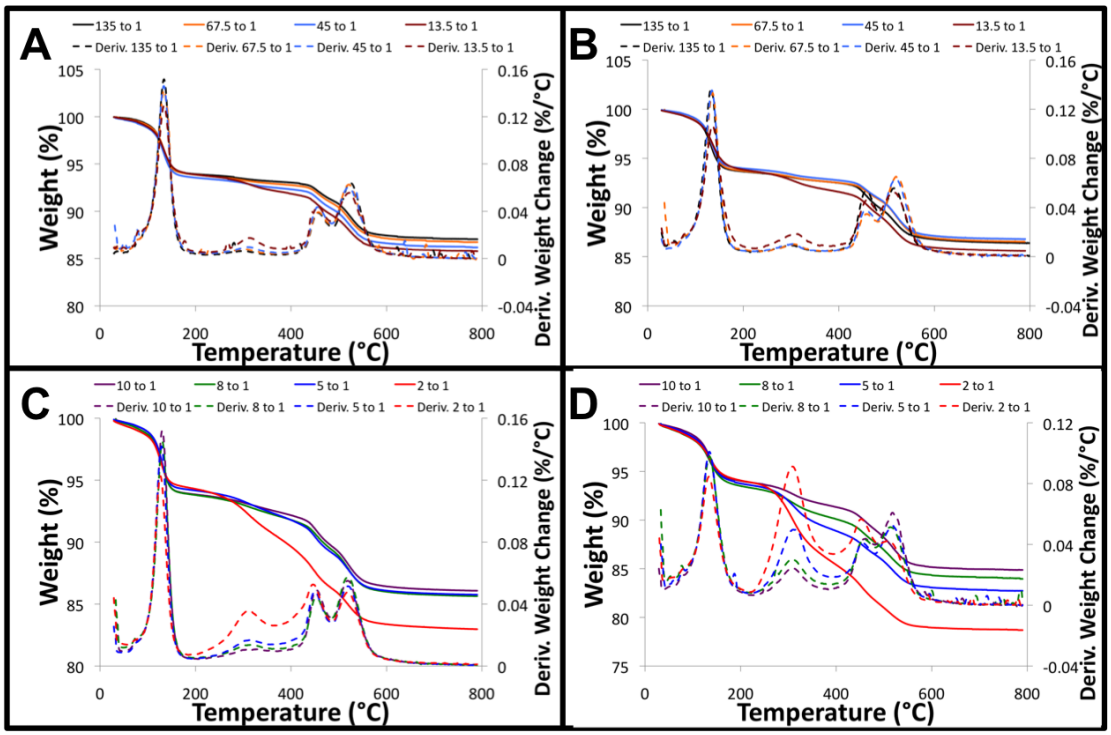

Figure 73. TGA of ODPA modified Sn/ZrP prepared by the (A-B) ion exchange and (C-D) phosphoryl chloride methods.

sample three main weight losses exist, the first from 70°C to 150°C is attributed to residual solvent and intercalated water, secondly from 270°C to 355°C as a result of the decomposition of ODPA, and from 480°C to 570°C for the condensation to the pyrophosphate. Close examination of the first derivative shows that the initial weight loss peak has a shoulder on it. This suggests a mixture of events is occurring, in this case

it can be said to be the residual solvent and water coming off at approximately the same temperature. Also, the first processes due to solvent and water loss has been shifted to slightly higher temperatures compared to pristine ZrP, this is believed to be a result of the modification. In addition it should be noted that the intensity of the water loss derivative peak decreases as the amount of Sn is increased. The addition of Sn on the surface adds additional mass to the product that does not undergo thermal degradation. The amount of water in ZrP remains constant in all cases while the mass of the compounds increases as Sn is added therefore, the total weight percent of interlayer water decreases. Along the same lines it is expected that as metal ions are added to the surface the total weight loss in TGA will decrease, this however is normally not the case as an increase in surface hydration is observed due to the metal ions. It is worth noting that the derivative peak for the condensation exists as two separate peaks whose intensities vary based on the extent of modification. These two peaks are believed to be a result of the surface phosphate groups from the ODPA, which are expected to condense before the phosphate group contained within the ZrP in the interlayer region and also contributions from water. The dehydration process begins from the outside edges of the particle and moves to the interior. This process is accompanied by a decrease in interlayer spacing, therefore some of the interlayer water can become trapped in the inner most part of the particles, delaying the weight loss until higher temperatures.[138]

The total weight loss for the ion exchange ODPA modified and the phosphoryl chloride ODPA modified are very similar. It appears that the phosphoryl chloride material has slightly more ligand but the difference may not be significant at lower Sn concentrations. A more definitive difference can be seen only with higher concentrations of Sn , in the case of 2:1 Zr:Sn the weight loss due to modification is 3.89% for the ion exchange method and 8.23% for the phosphoryl chloride method. The drastic difference in ligand uptake suggests some type of structural difference of the Sn layers within the two materials. If the Sn ions were a monolayer the functionalization would be identical in all cases. The difference in height of the Sn layers adds additional spots for functionalization. In addition, if the structures differ more area may be available to be functionalized as well. The formulas calculated from TGA and microprobe can be viewed in **Table 6** for comparison. Based on the TGA, IR, microprobe, and XPS results we conclude that it is possible to deposit Sn on the surface of ZrP and coordinate phosphonic acid ligands to the Sn surfaces to functionalize ZrP nanoplatelets.

Table 6. Calculated Formulas for ODPA modified Sn/ZrP prepared with ion exchange and phosphoryl chloride methods at various ratios.

Ratio	Ion Exchange	Phosphoryl Chloride
Zr:Sn	Calculated Formula	Calculated Formula
135:1	$Zr(H_{0.99}PO_4)_2Sn_{0.01}(ODPA)_{0.002}\bullet H_2O$	$Zr(H_{0.99}PO_4)_2Sn_{0.01}(ODPA)_{0.012}\bullet H_2O$
67.5:1	$Zr(H_{0.99}PO_4)_2Sn_{0.02}(ODPA)_{0.002}\bullet H_2O$	$Zr(H_{0.99}PO_4)_2Sn_{0.02}(ODPA)_{0.012}\bullet H_2O$
45:1	$Zr(H_{0.99}PO_4)_2Sn_{0.02}(ODPA)_{0.005}\bullet H_2O$	$Zr(H_{0.99}PO_4)_2Sn_{0.03}(ODPA)_{0.011}\bullet H_2O$
13.5:1	$Zr(H_{0.99}PO_4)_2Sn_{0.08}(ODPA)_{0.006}\bullet H_2O$	$Zr(H_{0.99}PO_4)_2Sn_{0.08}(ODPA)_{0.024}\bullet H_2O$
10:1	$Zr(H_{0.99}PO_4)_2Sn_{0.09}(ODPA)_{0.02}\bullet H_2O$	$Zr(H_{0.99}PO_4)_2Sn_{0.10}(ODPA)_{0.033}\bullet H_2O$
8:1	$Zr(H_{0.99}PO_4)_2Sn_{0.12}(ODPA)_{0.025}\bullet H_2O$	$Zr(H_{0.99}PO_4)_2Sn_{0.14}(ODPA)_{0.040}\bullet 1.1\ H_2O$
5:1	$Zr(H_{0.99}PO_4)_2Sn_{0.19}(ODPA)_{0.03}\bullet H_2O$	$Zr(H_{0.99}PO_4)_2Sn_{0.18}(ODPA)_{0.059}\bullet 1.1\ H_2O$
2:1	$Zr(H_{0.99}PO_4)_2Sn_{0.50}ODPA)_{0.079}\bullet 1.1\ H_2O$	$Zr(H_{0.99}PO_4)_2Sn_{0.51}(ODPA)_{0.134}\bullet 1.2\ H_2O$

Solid state NMR experiments were conducted on the functionalized samples to gain further information on the Sn, P, and C atoms in the materials. ^{31}P and ^{119}Sn experiments were conducted on SnZrP of different concentrations. In all cases it was found that the ^{31}P spectra were identical to ZrP, with a dominant peak at -19 ppm. There does not seem to be any indication of the interaction of Sn with phosphorus in the NMR spectra. Based on the thickness of the nanoparticles used they are expected to have *ca.* 59 layers. The Sn ions only interact with the surface phosphates of 2 layers, in comparison to the other layers this interaction is weak and it is reasonable that it does

not appear in the spectra. ^{119}Sn NMR did not display any signal at lower concentrations of Sn. In the 45:1 sample a weak signal can be seen at -350 ppm and in the 2:1 sample a resonance is observed at -493 ppm along with two side bands. It can be noted that the resonances vary by over 100 ppm but this may not be very significant due to the large chemical shift range of Sn. In both cases it can be concluded that the Sn present is four coordinate, six coordinate Sn typically displays resonances between -600 and – 850 ppm, as can be seen for SnO_2 and several Sn phosphates.[172] Addition of the ligand to the material did not significantly alter the spectra.

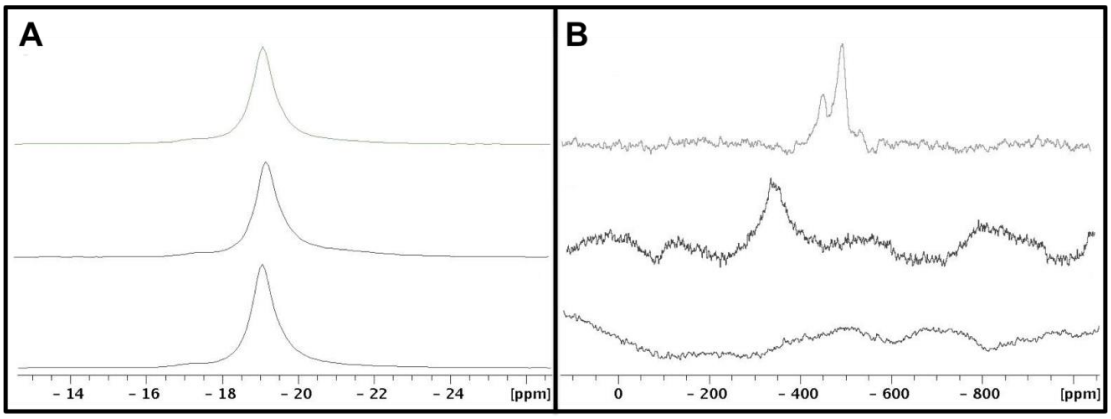

Figure 74. (A) ^{31}P and (B) ^{119}Sn NMR spectra of ion exchange Sn/ZrP synthesized with Zr:M ratios of 2:1(top), 45:1 (middle), and 135:1(bottom).

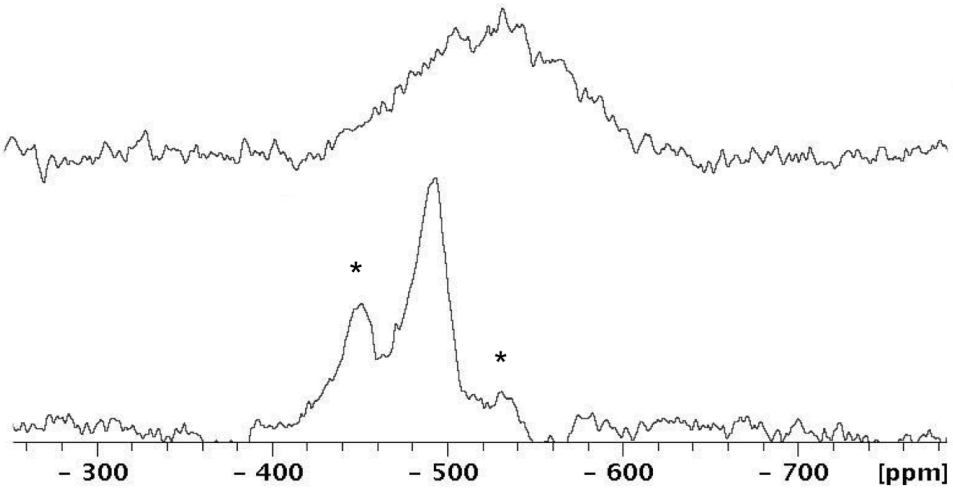

Figure 75. ^{119} Sn NMR spectra of ODPA modified Sn/ZrP (top) and Sn/ZrP (bottom) synthesized using a 2:1 Zr:Sn ratio. * denotes spinning sidebands

The ^{31}P spectra remained unchanged, the phosphonic acid that was coordinated to the Sn is not observed even though the phosphorus atom is in a slightly different environment due to covalent attachment to a carbon atom. The many phosphate groups of ZrP still dominate the spectra and make it difficult to observe the functionalization by ^{31}P NMR. The ^{119}Sn spectra of both the pre and post functionlized 2:1 ion exchange material can be seen in **Figure 74**. The ^{119}Sn spectrum of the functionalized sample displays a broad resonance with a center at -523 ppm. This resonance is only shifted slightly from the -439 ppm observed from the non-functionalized material and still well within the range of four coordinate Sn, **Figure 75**. The ^{13}C NMR spectrum displays two signals, one at -28.1 ppm and another at -20.7 ppm. These resonances are similar to those of other C18

functionalized ZrP using both epoxides and silanes.[146] The resonances can be assigned to the alkyl chains of the ODPA.

6.3 Monolayers of M(IV) on the Surface of ZrP

Although the Sn(IV) method was successful in depositing metal ions on the surface of ZrP, there are many problems with the resulting materials. First of all, the Sn(IV) does not exist as a monolayer on the surface; although theoretically this can be controlled with stoichiometry, it suggests that the deposition process is not by ion-exchange. The experiments were carried out in water with Sn(IV); the agglomeration of Sn on the nanoparticle surface is likely a factor of the solvent and the behavior of Sn(IV) in aqueous solution. Secondly, the particles used were very large and therefore miniscule amounts of Sn(IV) were needed to saturate the surface. Although not intrinsically a problem, for a thorough investigation it would be ideal for a smaller particle that to be used. In addition, although the phosphoryl chloride method seems to be successful, it is unclear exactly what is occurring on the surface; each phosphate group deposited by the phosphoryl chloride could be absorbing either one or three metal ions. With the agglomeration of metals on the surface it is not possible to determine which is the case. Additionally, the phosphoryl chloride may change the structure and thus add another variable, which is not favorable for an initial investigation.

A new methodology was adapted in order to address all the previous concerns. As the agglomeration is attributed to the behavior of Sn(IV) in aqueous solution, the solvent was switched to ethanol. Additionally, other metal ions that are thought to be more stable in aqueous solution and more compatible with ZrP, such as Hf(IV) were investigated. The estimated Zr:Sn(IV) ratio of 135:1 is very large and therefore undesirable for study. To reduce the ratio thinner nanoparticles were used. In this case 3MT ZrP was used, as these particles are expected to have *ca.* 11 layers, ratios of 10:1, 5:1, and 1:1 Zr to M(IV) were used to investigate the surface ion-exchange. The aim is to focus exclusively on the surface ion exchange initially; therefore the phosphoryl chloride method will be discarded until more is understood about the ion exchange process with the surface. Results obtained using the new approach will now be discussed.

The presence of the tetravalent metal ions on the surface of α-ZrP was initially examined by XRPD. **Figure 76** (A) shows the XRPD of α-ZrP along with the tetravalent metal modified ZrP (Sn/ZrP and Hf/ZrP). It can be seen that the XRPD patterns are identical to that of α-ZrP suggesting that the α-ZrP structure is intact and there has been no change within the interlayer structure of the nanoparticles or intercalation. The metal ion layer on the surface of the ZrP particles is amorphous, therefore no diffraction changes are expected in the XRPD.

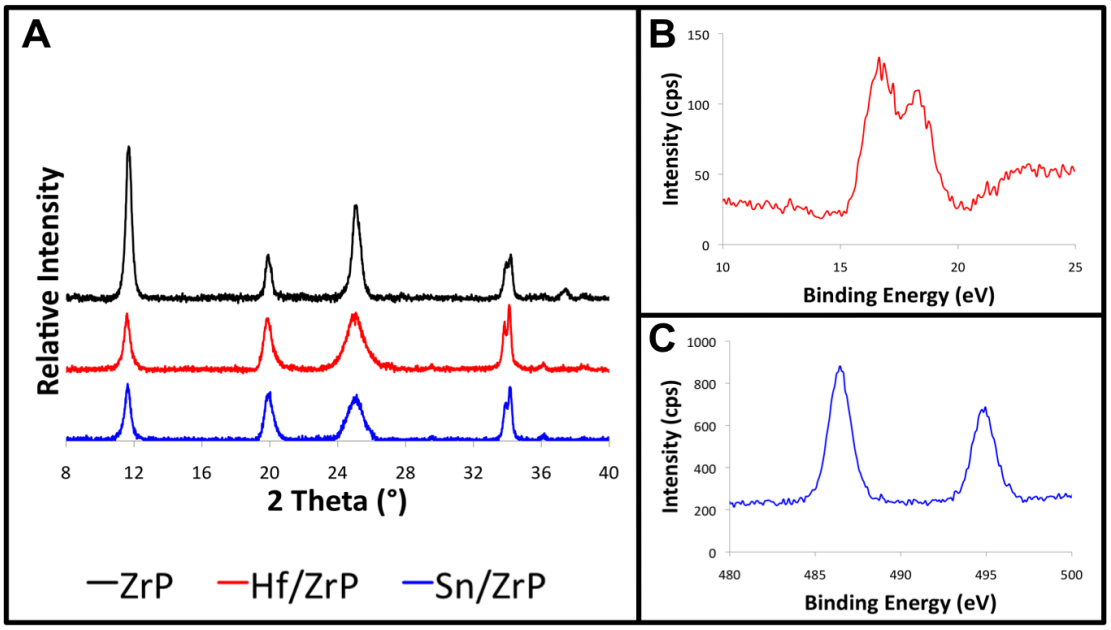

Figure 76. (A) XRPD of ZrP along with samples with metal ions deposited on the surface. (B-C) XPS spectra of Hf/ZrP,(B), and Sn/ZrP, (C) displaying the spectral region of the tetravalent metal ions.

To verify the presence of Sn and Hf on the surface of α-ZrP, XPS spectra were obtained for both materials. Observation of the spectra revealed the characteristic peaks for Zr, P, and O, in all cases, in addition to the peaks for Sn and Hf in the respective modified materials; confirming the presence of all expected elements. Both the 5/2 and 3/2 signals for the Sn(3d) electrons are observed at 486.8 and 493.8 eV, respectively, along with the 7/2 and 5/2 signals for the Hf(4f) electrons at 17.4 and 19.0 eV shown in **Figure 76** (B-C). The peaks observed for Sn and Hf indicate that the newly formed metal layer exist as an oxide on the surface of ZrP.[173, 174] In both cases fitting of the XPS peaks revealed that only one type of Sn or Hf exist within the material. As noted earlier, in the XPS spectra

of intercalated ZrP the binding energies of Zr and P are expected to decrease, relative to ZrP due to a loss of positive character of the atoms as a result of the ionic couples formed during intercalaition.[170] In the XPS spectra of the M(IV) modified samples a shift in the binding energies of Zr and P was not observed when compared to pristine α-ZrP , **Figure 77**. This suggests that the interaction of the surface phosphates with M(IV) ions is not significant enough to affect the overall charge of the Zr and P atoms within the ZrP nanoparticles. Although the surface and interlayer phosphates have the same reactivity, this suggests that the interaction of the surface phosphates with M(IV) ions is not significant enough to affect the overall charge of the Zr, P, and O atoms within the ZrP nanoparticles.

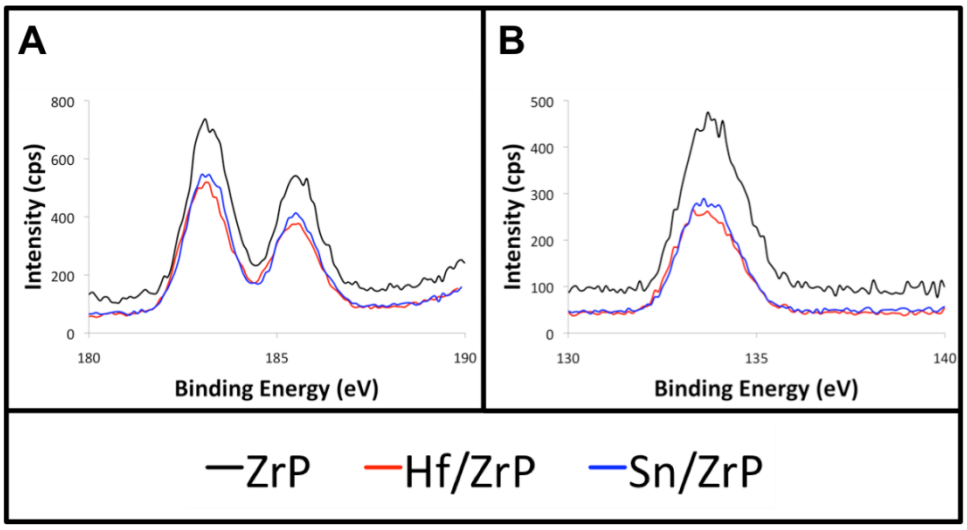

Figure 77. XPS spectra of ZrP and M(IV) ZrP displaying the spectral regions for (A) Zr, (B) P.

Even with the relatively thin particles the percentage of surface phosphates in comparison to interlayer phosphate groups is still too low and makes the observation of such a shift difficult to detect. Moreover, the fact that no shift in the XPS signals of the Zr and P atoms were observed supports the claim that the metal ions have not been intercalated within ZrP and are associated with and limited to the surface of the ZrP particles.

In the case of the O 1s XPS spectrum it has previously been reported that three distinct environments exist in ZrP corresponding to the oxygen atoms of zirconium hydroxide produced by hydrolysis, the ZrO_6 octahedra within the layers, and the hydroxy phosphate groups that exists within the interlayer and on the surface.[175] The three distinct environments can be seen in the ZrP starting material and appear at 530.9 eV, 531.6 eV, and 532.9 eV respectively in this case (**Figure 78**). Additionally, three distinct environments can also be observed in the M(IV) modified samples. Compared to ZrP, the intensity of the high energy signal corresponding to P-OH is diminished. This is reasonable as the surface phosphate groups have now been exchanged with metal ions and the P-OH signal is now limited to the interlayer of the nanoparticles. Additionally, it can be observed that the low energy signal increases in intensity. It is unlikely that further hydrolysis has occurred; this signal is corresponding to the oxygen atoms of the metal ion on the surface, which is thought to exist as a hydroxide species. Additionally, previous reports suggest that the low energy signal is influenced by water.[175] The ZrP uptakes a substantial amount of water upon modification with a tetravalent metal

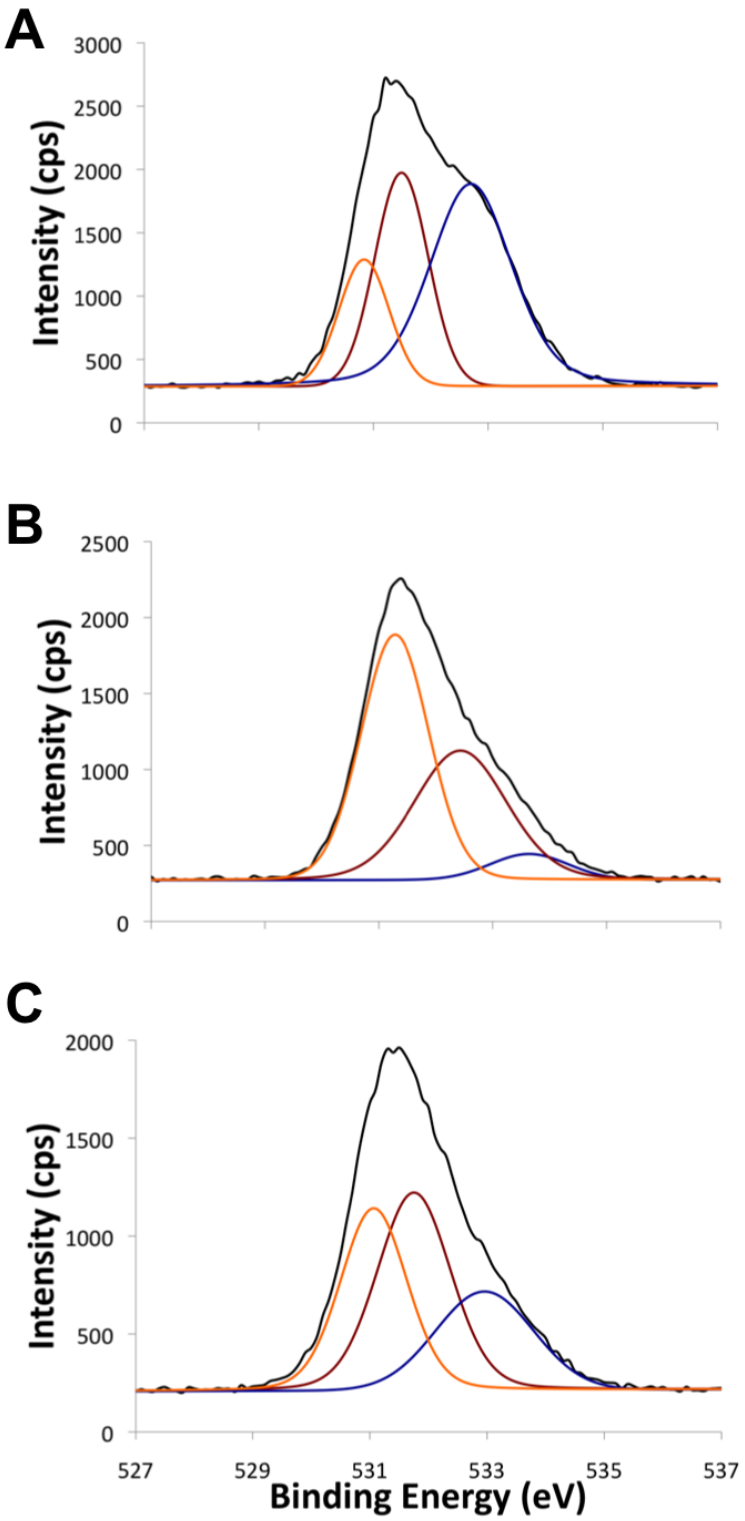

Figure 78. O 1s XPS spectra of (A) ZrP, (B) Sn/ZrP, and (C) Hf/ZrP.

resulting in the increase in the intensity of the low energy signal. Ultimately, the change of intensity in the O 1s spectra along with the identical P 2p and Zr 3d spectra supports the successful surface reaction of ZrP with the tetravalent metal ions.

To quantify the amount of M(IV) present in the samples electron microprobe analysis was utilized. The Zr:M(IV) ratios were varied in the synthesis in order to determine the amount of metal ion needed to fully cover the surface. If the metal is deposited on the surface by a pure ion exchange interaction then the reaction should stop once all protons have been exchanged from the surface and any additional metal ions should remain in solution. Microprobe analysis confirms in all cases that the metal ion has been successfully deposited on the nanoparticles, as determined by XPS. Moreover, the atomic concentration of Zr and M(IV) in the Sn/ZrP and Hf/ZrP synthesized at different molar ratios (M(IV):Zr = 1:1, 1:5, and 1:10) show an atomic abundance of ca. 11% for Sn or Hf relative to Zr in each case , **Figure 79**. In the case of Hf/ZrP all the Hf ions are deposited on the surface when the 10:1 (Zr: M(IV)) ratio is used, increasing the amount of Hf(IV) by using ratios 5:1 and 1:1 ratio resulted in identical uptakes of 0.11 moles of Hf ,relative to Zr, in both samples. This suggests that the surface is saturated when 0.11 moles of Hf are deposited and the material is unable to take up any more ions. In the case of Sn/ZrP a similar result can be observed in which 0.1 moles of Sn are deposited on the surface in all cases. The values of 0.10 moles and 0.11 moles obtained for Sn and Hf, respectively are within error of each other therefore it is very likely that equal amounts of metal ion are on the surface as it is expected that ions with the same charge

and similar sizes will behave in an identical fashion with the surface. Cs(I) is known to exchange with surface protons in a one to one fashion, utilizing this ion it was also found that 0.11 moles was the maximal uptake, **Table 7**.[176] This confirms that for this particular ZrP particle size 0.11 moles is indicative of complete surface coverage, in addition this

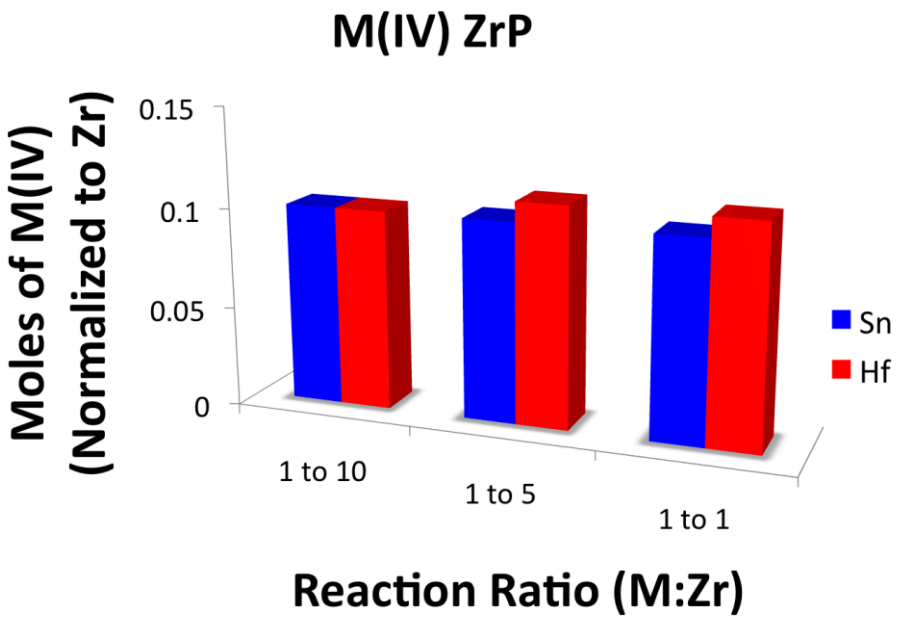

Figure 79. Graph displaying the atomic concentration of M(IV) in M(IV)/ZrP samples synthesized at different (M:Zr) ratios.

suggests that the ions will behave similarly with the surface protons regardless of the ion charge.

Table 7. Formula of the Cs modified ZrP as determined by microprobe.

Atomic Concentration P	Atomic Concentration Zr	Atomic Concentration Cs	Calculated Formula
14.05	7.66	0.82	$Zr(H_{0.89}PO_4)_2Cs_{0.11} \bullet H_2O$

Microprobe analysis indicated the homogeneity of the samples as well, **Figure 80**. All Zr:M(IV) ratios utilized were found to be largely homogeneous. In all cases it seems that M(IV) can be deposited on the surface of ZrP nanoplatelets to prepare a uniform surface and a homogeneous material. It is worth noting that both XPS and microprobe analysis showed exclusively Zr, P, O, Sn, and Hf in the samples. This data suggests that the M(IV) on the surface must exist as an oxide, hydroxide, or mixture of both to achieve charge balance of the M(IV) ion.

Once the presence of M(IV) on the surface was confirmed the metal ion layer was functionalized by coordination with phosphonic acid ligands. The phosphonic acid modified M(IV) ZrP was examined by XRPD, FTIR, and TGA to confirm the presence of the ligand. The X-ray diffraction patterns of the modified ZrP samples are identical to

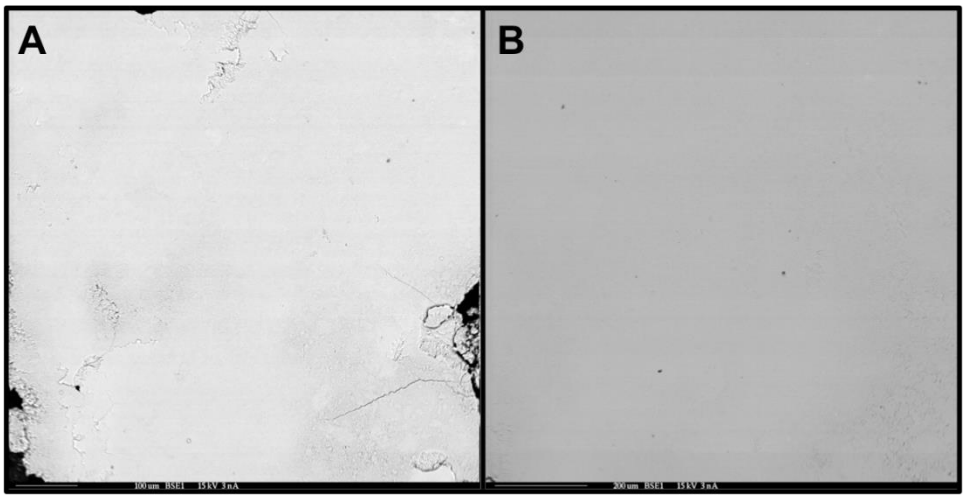

Figure 80. Electron microprobe images of (A) Sn/ZrP and (B) Hf/ZrP displaying the homogeneity of the samples.

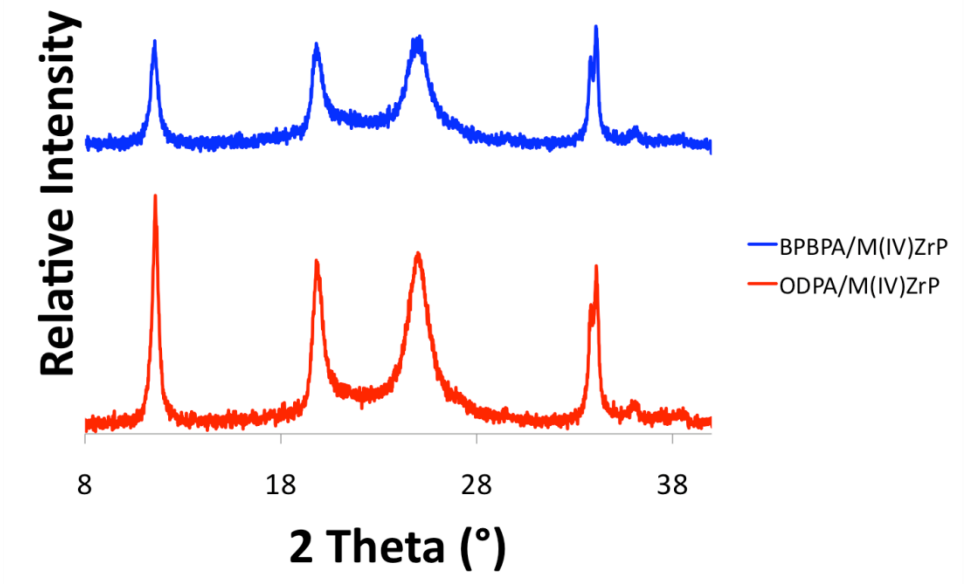

Figure 81. Powder X-ray diffraction of ligand modified samples.

α-ZrP and M(IV) modified ZrP confirming no unwanted interaction of the modifier with the interlayer region , **Figure 81**. Examination of the FTIR spectra in **Figure 82** shows the typical stretches for ZrP in relatively high intensities along with the stretches for the ligands. As in the prior case alkyl stretching and bending bands between 2850 cm^{-1} and 3000 cm^{-1} and 1350 cm^{-1} and 1470 cm^{-1} evidence successful modification with ODPA. In the case of BPBPA, stretches can be observed at 716 cm^{-1} and 815 cm^{-1} for the C-H bending and ring puckering of the phenyl rings. In all cases it can be seen that the ligands are successfully attached to the tetravalent metals on the ZrP surface as evidenced by the infrared stretches.

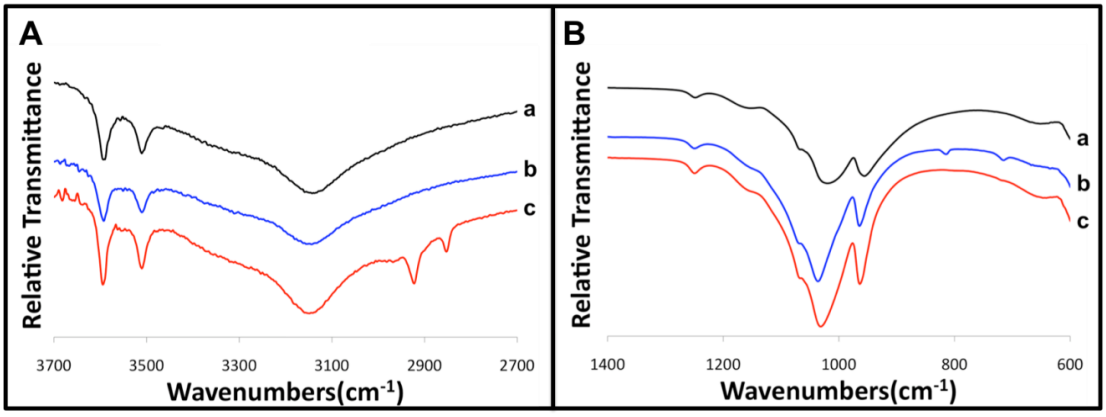

Figure 82. FTIR spectra of ZrP (a) and M(IV)/ZrP surface modified with (b) BPBPA and (c) ODPA focusing on the alkyl (A) and aromatic (B) regions.

TGA was used to determine the extent of modification within the samples, **Figure 83.** As in the prior case the weight losses fall within the expected range for organically

modified ZrP. According to calculations based upon TGA and microprobe the uptake of the modifier normalized to zirconium is 0.04 moles for ODPA and 0.02 moles for BPBPA. It is likely that the expected close packing of the C_{18} chains allows for a larger amount of the ODPA ligand to coordinate to the surface whereas the bulky biphenyl group may not allow such a packed structure.

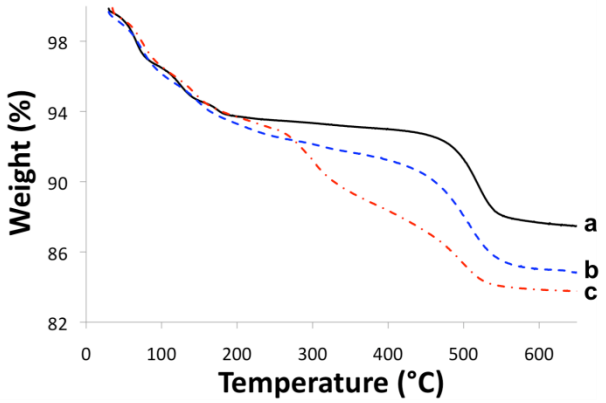

Figure 83. TGA thermogram of (a) ZrP, (b) BPBPA modified Hf/ZrP, and (c) ODPA modified Hf/ZrP.

In order to investigate how much time was required to fully functionalize the surface with the ligands time trials were conducted. The synthesized products were analyzed by TGA and the moles of modifier were compared to determine the optimal reaction time, **Table 8**. In the case of ODPA it appears that initially at the 1 hour point the surface is not covered completely. Between 3 and 12 hours the amount of moles remain constant suggesting that the surface is saturated and the maximum amount of ligand has been

bonded to the metal ion layer. However at the 24 hour point the uptake continues to increase, it is likely that this is a result of bilayers of ODPA forming on the surface in a tail to tail fashion.

Table 8. TGA data along with calculated formulas for ligand modified Hf/ZrP.

Time (hours)	TGA Total Weight Loss (%)	Calculated Formula	M(IV) to Ligand Ratio
1	15.22	$Zr(H_{0.89}PO_4)_2$ $Hf_{0.11}(ODPA)_{0.03}$• 1.1 H_2O	4
3	15.56	$Zr(H_{0.89}PO_4)_2$ $Hf_{0.11}(ODPA)_{0.04}$• 1.1 H_2O	3
6	15.98	$Zr(H_{0.89}PO_4)_2$ $Hf_{0.11}(ODPA)_{0.04}$• 1.1 H_2O	3
12	16.26	$Zr(H_{0.89}PO_4)_2$ $Hf_{0.11}(ODPA)_{0.04}$• 1.2 H_2O	3
24	17.32	$Zr(H_{0.89}PO_4)_2$ $Hf_{0.11}(ODPA)_{0.06}$• 1.2 H_2O	2
1	14.97	$Zr(H_{0.89}PO_4)_2$ $Hf_{0.11}(BPBPA)_{0.02}$• 1.3 H_2O	6
3	14.83	$Zr(H_{0.89}PO_4)_2$ $Hf_{0.11}(BPBPA)_{0.02}$• 1.2 H_2O	6
6	15.47	$Zr(H_{0.89}PO_4)_2$ $Hf_{0.11}(BPBPA)_{0.02}$• 1.4 H_2O	6
12	15.11	$Zr(H_{0.89}PO_4)_2$ $Hf_{0.11}(BPBPA)_{0.02}$• 1.3 H_2O	6
24	15.35	$Zr(H_{0.89}PO_4)_2$ $Hf_{0.11}(BPBPA)_{0.03}$• 1.3 H_2O	4

In the case of ODPA a similar result is found but in this case the uptake remains constant from 1 to 12 hours and at the 24 hour point the uptake increases. Additional information can be gained by determining the M(IV) to ligand ratio of the products. In the case of ODPA it was found that the M(IV) to ligand ratio of the products was ~ 3 to 1 in all cases except the 1 hour and 24 hour case. The surface phosphates of ZrP form a triangle, it is therefore expected that each proton has been replaced with a metal ion and the ligand sits in the center of the triangle and coordinates each of its oxygen atoms to a separate M(IV) ion, **Figure 84**. The results agree well with previous ^{17}O NMR studies that verify the tridentate bridging of phosphonic acids with tetravalent metals in hybrid compounds and in the case of surface modifications.[177, 178] In addition, it is crystalographically known that the tridentate bridging of phosphonic acids with tetravalent metals is the primary coordination mode in α type compounds and other hybrid materials.[15, 179-181] This suggests that one hour is not long enough for all the ligand to coordinate properly and as alluded to earlier bilayers of ODPA are likely forming in the 24 hour case. The 3 fold coordination is also found in the BPBPA samples. In this case a ratio of ~ 6 to 1 is observed suggesting that the bisphosphonic acid is crosslinking particles. Although the crosslinking occurs it is not permanent, the individual particles can be redispersed in solution, as results discussed subsequently will indicate. The 6 to 1 ratio is observed in all cases except the 24 hour case. At this point the ratio is nearly 4 to 1. The steric bulk of the BPBPA may result in the coordination to the metal ion layer taking a longer amount of time. Also the possibility of crosslinking an unreacted metal ion layer with the distal end of an already coordinated ligand would

also increase the time needed to fully react all surfaces. It is therefore concluded that around 24 hours is needed to obtain full coverage with the BPBPA ligand. Based on the TGA, IR, microprobe, and XPS results we conclude that it is possible to deposit M(IV) on the surface of ZrP and coordinate phosphonic acid ligands to the metal surfaces to functionalize ZrP nanoplatelets.

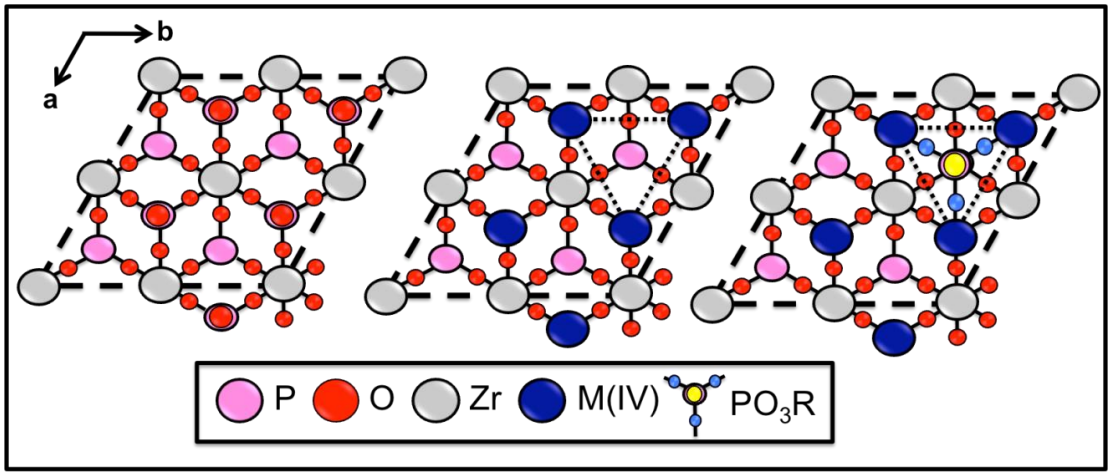

Figure 84. Representation of the surface structure of ZrP, M(IV)ZrP in which metal ions have replaced the surface protons, and phosphonic acid modified M(IV)ZrP .

Solid-state NMR experiments were conducted on the functionalized samples to gain further information on the environments of the M(IV), P, and C atoms in the compounds. ^{31}P experiments were initially conducted on Sn/ZrP and Hf/ZrP precursor samples; it was found that the spectra were not significantly different when compared to pristine ZrP, **Figure 85** (A). The dominant peak in the spectra appears at -19 ppm and can be

assigned to the P-OH groups of the interlayer, the slight shoulders at -17.8 and -21.2 ppm are assigned to phosphates that are in slightly different positions than the bulk due to partial hydrolysis and dehydration of the particles, which likely exist on the edges of the nanoparticles.[40, 139, 142, 182] Based on the thickness of the nanoparticles used they are estimated to have *ca.* 11 layers. The metal ions only interact with the surface phosphate groups of the 2 exposed layers; it should also be taken into account that each layer has a set of phosphate groups on each side. Given this approximation there are 22 sets of phosphates and only two accessible via the surface, in comparison to the bulk phosphates the ionic interaction of the tetravalent metals with the surface phosphates is weak and it is reasonable that a signal is not present in the spectra. Although covalent functionalization methods with identical particles lead to a signal in the ^{31}P spectra, this is not the case for the ionic interaction produced by this reaction. On the other hand, ^{119}Sn NMR displayed a broad resonance, which can be interpreted as two signals centered at -520 ppm and -561 ppm, **Figure 85** (B). In this case the Sn ion is expected to be interacting partially with phosphates and partially with oxides therefore the presence of two signals is reasonable. It can also be seen that both signals have similar intensity, which would also be true if this were the case. The chemical shift values also indicate that the Sn present is four coordinate as in the prior case.[172]

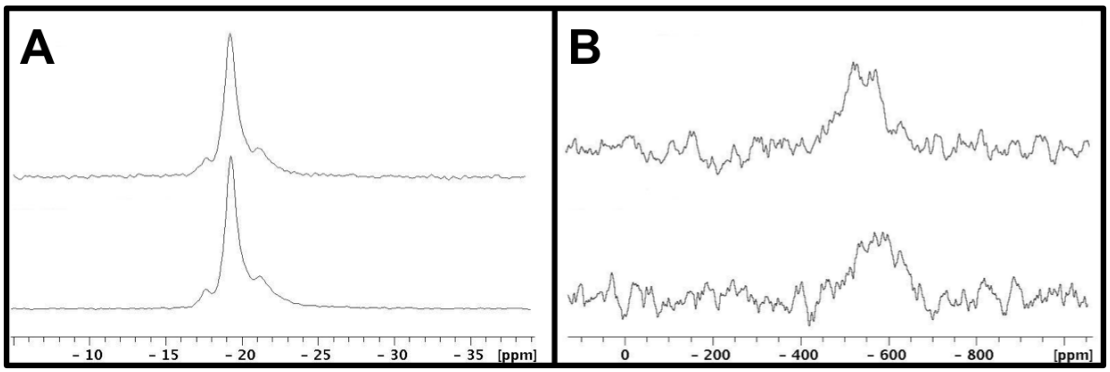

Figure 85. ^{31} P (A) and ^{119} Sn NMR (B) spectra of Sn/ZrP (top) and ODPA modified Sn/ZrP (bottom).

Addition of the ligand to the material did not significantly alter the NMR spectra, **Figure 85 A-B**. The ^{31}P spectra remained practically unchanged and the phosphonic acid that was coordinated to the metal ion layer is not observed. The phosphorus atoms in the phosphonic acid ligands make up ~2% of phosphorus in the compound due to the abundance of phosphate groups in ZrP, therefore it is unlikely to observe the functionalization by ^{31}P NMR. The ^{119}Sn spectrum of the functionalized material displays a very broad signal with a center at -565 ppm. This resonance is only shifted slightly in comparison to the peak observed in the non-functionalized material and is still well within the range of four coordinate Sn. In this case a single resonance seems to exist as opposed to two, however the broad signal is likely not indicative of a single Sn(IV) environment. After functionalization all the Sn(IV) ions should have interactions with phosphate, through the surface and ligand, and the Sn(IV) is still expected to be coordinated by an oxide or hydroxide to achieve charge balance. The broadness of the signals in the Sn case is also likely a result of chemical shift dispersion in amorphous

systems due to the large chemical shift range of Sn and is considered to be insignificant. The ^{13}C NMR spectrum displays signals at 29 ppm and 22 ppm, **Figure 86**. The resonances can be assigned to the alkyl chains of the ODPA and are similar to those of other C_{18} functionalized ZrP using both epoxides and silanes.'[146, 182]

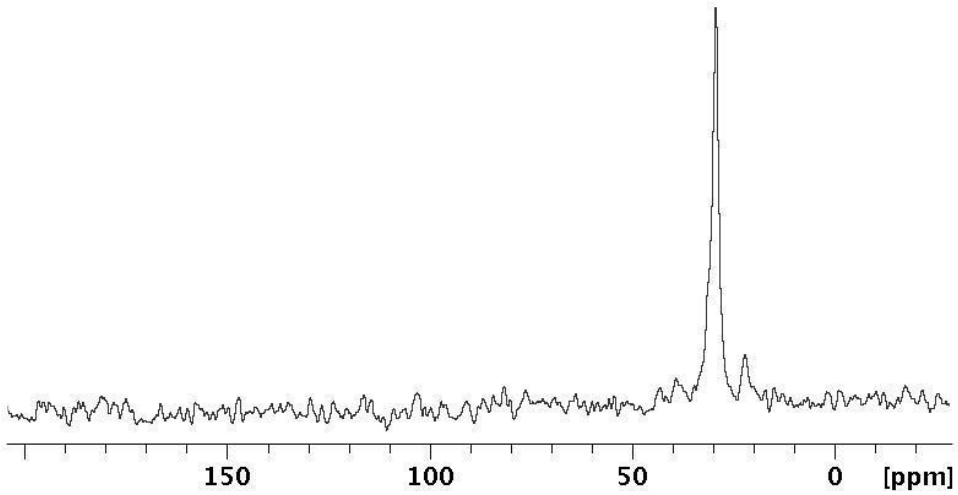

Figure 86. ^{13}C NMR spectrum of ODPA modified Sn/ZrP.

6.4 Surface Exchange of Metal Ions of Various Charges

Phosphonate compounds have been synthesized with metal ions of various valency.[10, 183-186] Current data suggests that the metal ion is deposited on the surface in an identical

fashion regardless of the charge, however the charge of the metal ion will likely dictate how a ligand would preferably bind to the metal ion layer and yield various structurally diverse assemblies of phosphonic acids on the ZrP surface. In addition, ligands other than phosphonic acids can be used depending on the metal ion layer deposited on the surface. The variation of ligands would also produce different bonding motifs on the surface. The interactions of other metal species with the surface of ZrP were investigated using the 5 to 1 (Zr to ion) ratio as it was shown to be excess in regards to the surface. **Figure 87** shows the atomic concentration of each ion normalized to Zr. It can be observed that in all cases the ion is deposited on the surface, however a monolayer is not formed in all cases.

As noted previously a monolayer exists as approximately 0.1 moles of ion on the surface. It can be noted that several of the ions are close to this configuration including Cs(I), Ni(II), Zn(II), Fe(III), and Cr(VI). All other ions display concentrations close to 0.2 moles suggesting that the ion simply agglomerated on the surface and did not interact with the surface phosphates purely by ion exchange. Agglomeration is likely as other divalent ions were able to achieve a monolayer. Additionally some ions that agglomerated have similar sizes and identical charges to others that formed monolayers. Therefore there is not an obvious trend as to why agglomeration occurs in some cases

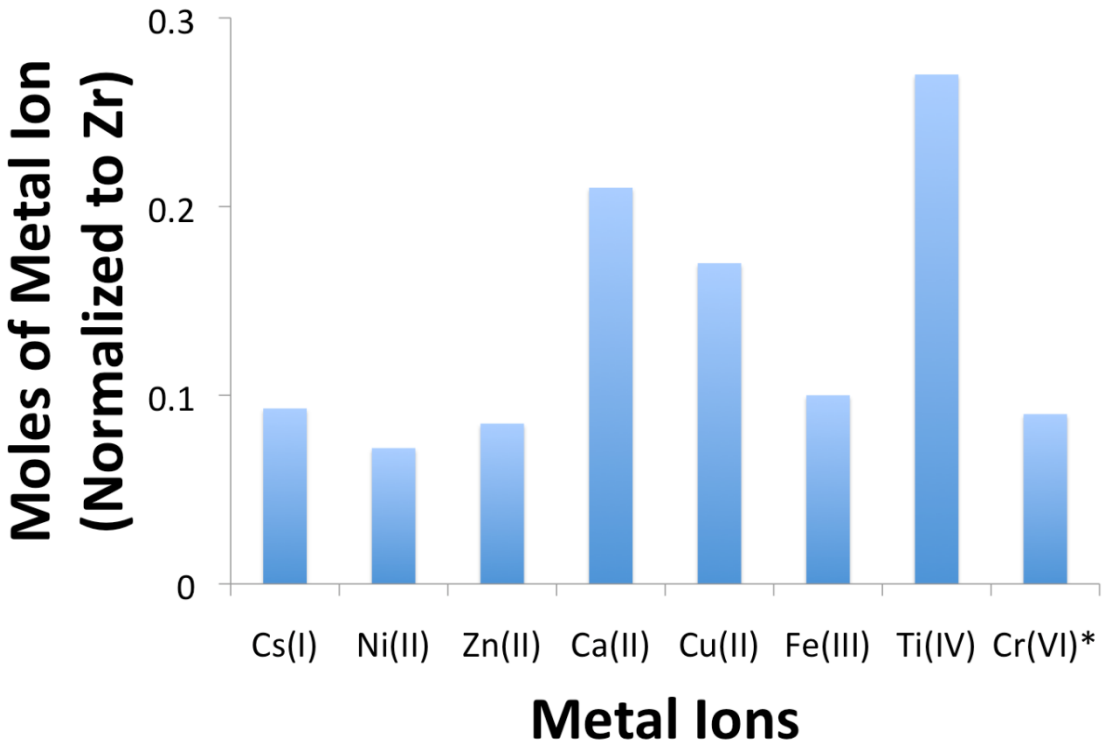

Figure 87. Atomic concentration of various ions on the surface of ZrP. *The Cr(VI) is CrO_3 and does not necessarily exists as an ion in solution.

and not others. In the case of Ti(IV) the value is artificially increased due to the lack of homogeneity within the sample. Different solvent systems may need to be investigated to produce a monolayer of the ions on the surface and a homogenous material. Additionally, CrO_3 was successfully deposited on the surface suggesting that metal oxides may also have an affinity for the surface. It is our current endeavor to continue analysis of these materials, to finalize the structure, and also systematically investigate how the use of different ions affects the structure of the phosphonic acid layer.

Additionally a variety of metal oxides may bond to the surface groups and possibly be used for catalysis.

6.5 Conclusion

In summary it has been shown that tetravalent metal ions can be deposited on the surface of ZrP nanoplatelets by ion exchange. Using the metal ion layer, it is possible to coordinate both phosphates and phosphonates to the surface of ZrP nanoplatelets. This ability adds an additional method of surface modifying ZrP to the others that our group has investigated such as silanes, epoxides and isocyanates.[74, 146, 182] With the abundance of phosphates and phosphonates that exist, this methodology makes it is possible to impart a wide variety of functionality to ZrP systems. It is also possible to impart phosphate and phosphonate functionality onto a number of compounds through synthetic reactions.[10, 81] This provides a vast number of compounds that could be used to functionalize the surface and exponentially increases the usefulness of this method. Among such are peptides, proteins, and biological molecules containing a free phosphate that can be used to functionalize the ZrP surface for biological applications.[81] Additionally it was demonstrated that metal ions of various charges and metal oxides could also be deposited on the ZrP surface. This functionality can then be used to drastically improve current applications of ZrP and possibly produce new uses for the synthesized materials.

CHAPTER VII

MULTIFUNCTIONAL NANOPARTICLES BASED ON ZIRCONIUM PHOSPHATE

7.1 Introduction

The intercalation chemistry of ZrP has been thoroughly investigated throughout the years and has led to the diverse applicability of ZrP.[2, 10] The previous chapters have demonstrated that the surface of ZrP can be functionalized with a number of different reactive groups and various methodologies. Multifunctional nanoparticles can be defined simply as nanoparticles that have more than one component that add functionality to the particle. Commonly the term is used to refer to particles with biomedical applications, however there is no apparent reason to limit the term to this category of materials. There are two predominant classes of multifunctional particles that can be synthesized; a functional nanoparticle can be further functionalized by a ligand to add additional character, or different types of functional nanoparticles can be combined with each other.[103] Among common ligands employed are polymers, peptides, proteins, receptors, and dyes. Additionally, the functional nanoparticles could be magnetic particles, quantum dots, or metal nanoparticles. In many cases multiple synthetic steps are needed to produce such materials and once produced they cannot be characterized very thoroughly. Multifunctional nanoparticles can certainly be applied to areas outside of biotechnology. ZrP based multifunctional nanoparticles in which the interlayer and surface chemistry are both exploited to produce particles with a controllable interlayer

and surface can be synthesized, **Figure 88**. In this section the characterization of these multifunctional materials will be addressed and some potential applications will be demonstrated in the following chapter.

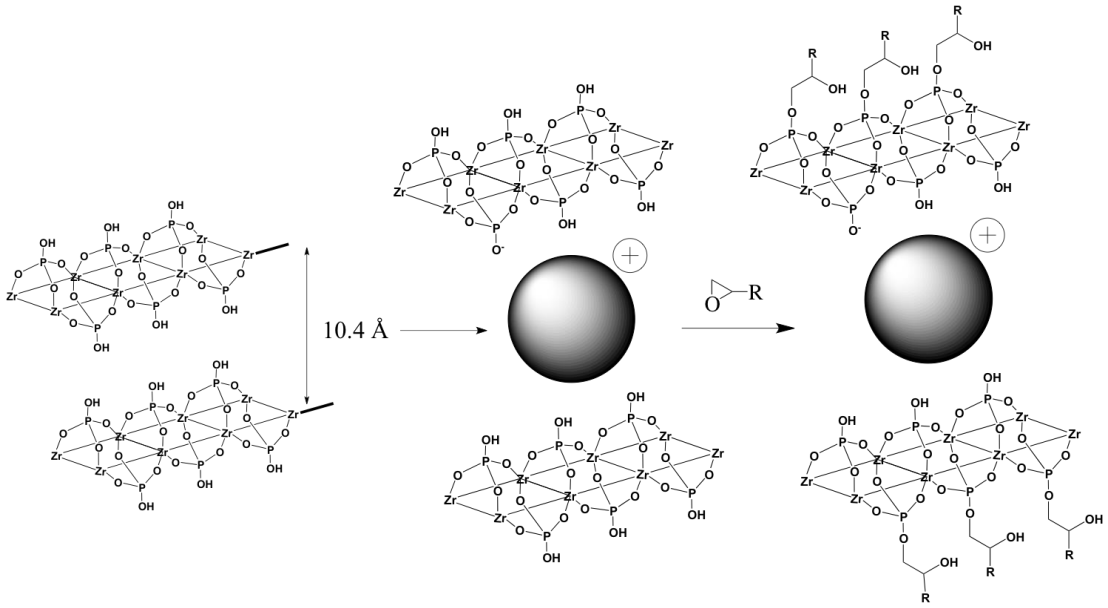

Figure 88. Proposed method for producing multifunctional ZrP particles by combining intercalation and surface modification.

7.2 Modification of Intercalated ZrP with 1,2-epoxyoctadecane

7.2.1 $Ru(bpy)_3^{2+}$*@ZrP*

Initially the XRPD of the modified sample was examined. It is well known that upon intercalation of a molecule within the interlayer of ZrP that the d-spacing

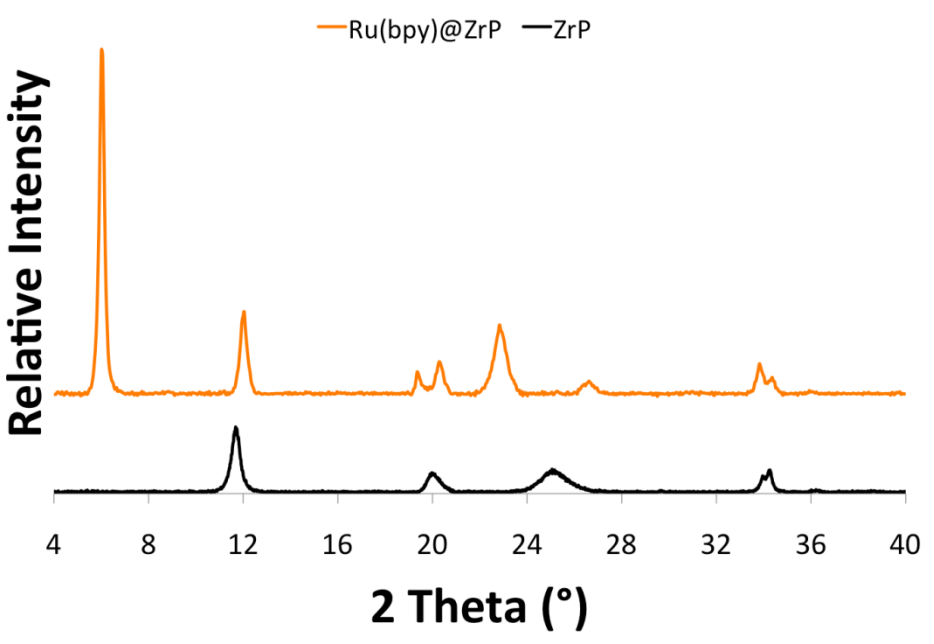

Figure 89. XRPD of the ZrP starting material and $Ru(bpy)_3^{2+}$@ZrP.

increases, shifting to lower 2-theta values. In the case of $Ru(bpy)_3^{2+}$@ZrP prepared by direct intercalation into θ-ZrP, this spacing is 15.2 Å.[28, 187] Examination of **Figure 89**

shows the successful intercalation of $Ru(bpy)_3^{2+}$ into ZrP and the corresponding interlayer spacing. As was the case with surface modification with pristine ZrP, it is expected that if only the surface is modified that the d-spacing of the modified material should not be different than the unmodified material. The X-ray pattern of the modified sample is identical to that of $Ru(bpy)_3^{2+}$@ZrP. This suggests that there were no interactions of the modifier with the interlayer region. Although such an interaction was found not to occur in the case of pristine ZrP, the intercalated case is slightly more complex. First of all, the interlayer spacing of the ZrP is much larger than in the pristine case. This gives more space and therefore increases the chances that the modifier could possibly interact with the interlayer in some fashion. Although the chances are increased it is not likely as the interlayer of ZrP is still very hydrophilic. The interaction of the hydrophobic modifier with the hydrophillic interlayer is unlikely therefore it is much more favorable for the modifier to remain in solution or interact exclusively with the surface of the nanoparticles. Additionally, the fact that the XRPD patterns are identical suggests that the $Ru(bpy)_3^{2+}$ is still encapsulated within the interlayer of ZrP and none of the molecule has leached out. As mentioned earlier, the hydrophilic interlayer stabilizes the $Ru(bpy)_3^{2+}$and it would not be favorable for it to leave this strong interaction and leach into a non-polar environment, which it does not interact well with.

The presence of the epoxide on the surface of ZrP can be probed using FTIR. The FTIR spectrum of $Ru(bpy)_3^{2+}$@ZrP displays the expected stretches for the phosphate groups of ZrP along with the aromatic stretches of the bipyridines of the intercalated complex . It

should be noted that the stretches for the interlayer water are no longer present due to the displacement of the water by the intercalated ion. In addition, as was the case with pristine ZrP, $Ru(bpy)_3^{2+}$@ZrP has no alkyl carbons in its structure. Therefore all alkyl stretching can be attributed to the interaction of epoxides with the surface of the nanoparticles. **Figure 90** shows the presence of alkyl chains in the compound, which are attributed to the epoxide. The C-H stretching appears in the expected region between 2850 cm^{-1} and 3000 cm^{-1}, however bending and other expected signals are too weak to observe due to the abundance of phosphates and $Ru(bpy)_3^{2+}$in the compound.

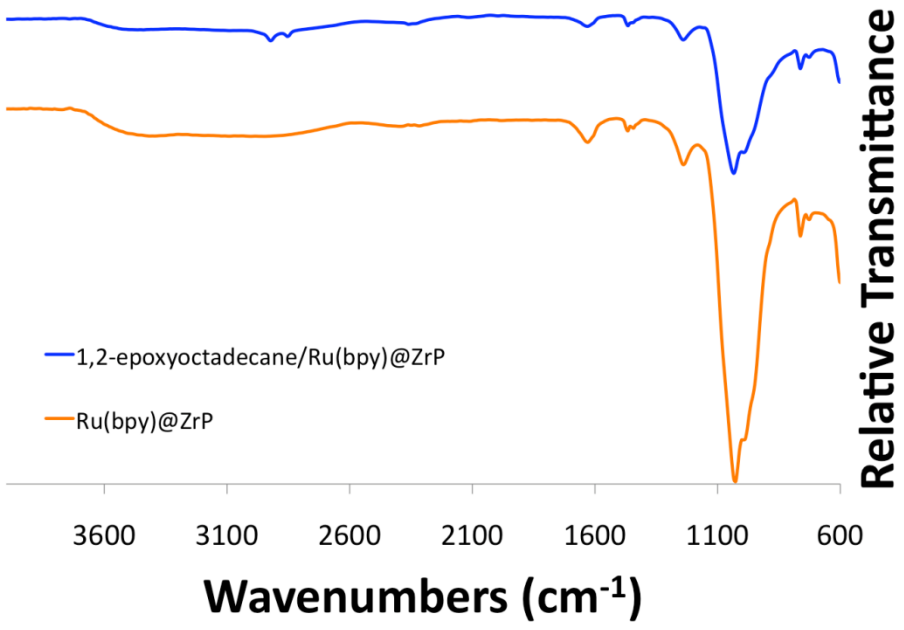

Figure 90. FTIR spectra of $Ru(bpy)_3^{2+}$@ZrP before and after modification.

TGA can be used to determine if any weight loss that can be attributed to the modifier is present in the thermal decomposition of the compound. In the TGA thermogram of $Ru(bpy)_3^{2+}$@ZrP there are three predominant weight losses. Initially, as with most ZrP based compounds, surface water is lost below 100°C. However, in the case of $Ru(bpy)_3^{2+}$@ZrP there are two weight loss events below 100°C, the first below 50°C which is expected to be surface water and solvent, and the latter from 75°C to 88°C, which is likely interlayer water. The decomposition of the $Ru(bpy)_3^{2+}$and the condensation of the phosphates occurs in a single step from 420°C to 425°C. The total weight loss attributed to the compound is ~ 28.85%, the compound is calculated to posses *ca.* 0.10 moles of $Ru(bpy)_3^{2+}$ relative to Zr. The TGA thermogram of the modified sample contains largely the same decomposition pattern except for the addition of a new weight loss event from 220°C to 303°C, **Figure 91**. The new weight loss process is attributed to the epoxide that is now attached to the surface of the $Ru(bpy)_3^{2+}$@ZrP nanoparticles. In addition to the epoxide weight loss it can be noted that the weight loss event corresponding to the decomposition of $Ru(bpy)_3^{2+}$ and the condensation of the phosphate begins at a slightly lower temperature range, suggesting a possible destabilization of the interlayer.

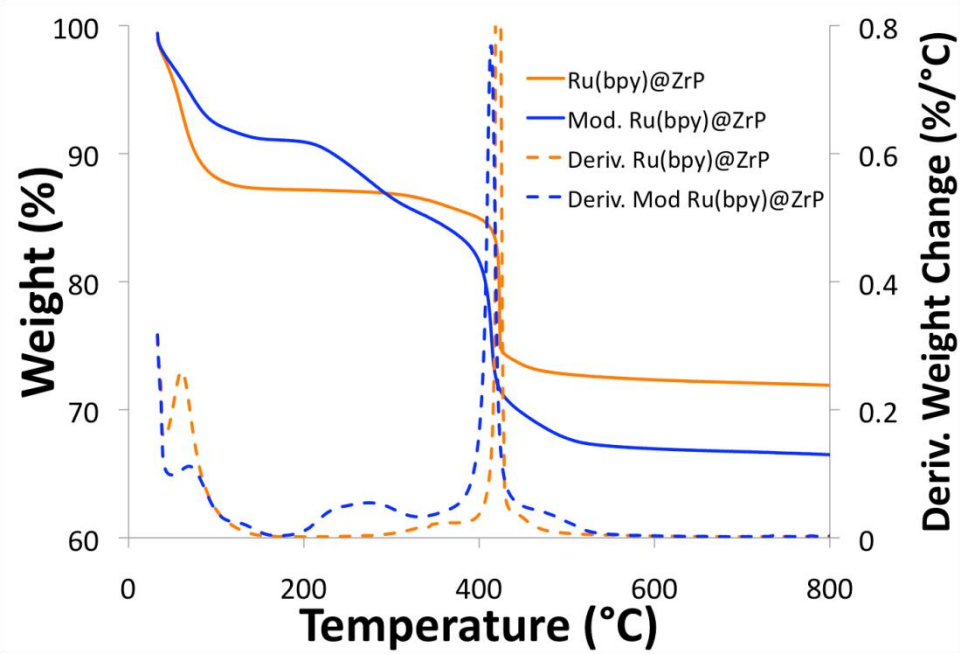

Figure 91. TGA of $Ru(bpy)_3^{2+}$@ZrP before and after modification.

7.2.2 $Fe(phen)_3^{2+}$@ZrP (Ferroin@ZrP)

It was previously demonstrated that it is possible to surface modify a pre-intercalated ZrP compound using epoxides. Although, $Fe(phen)_3^{2+}$ has an identical charge as $Ru(bpy)_3^{2+}$ the size is somewhat different. As a result of the size difference between the two molecules the maximal loading of each within the layers of ZrP differs. The size and thus the loading of the intercalated molecule within the interlayer is likely to have an effect on the surface modification.

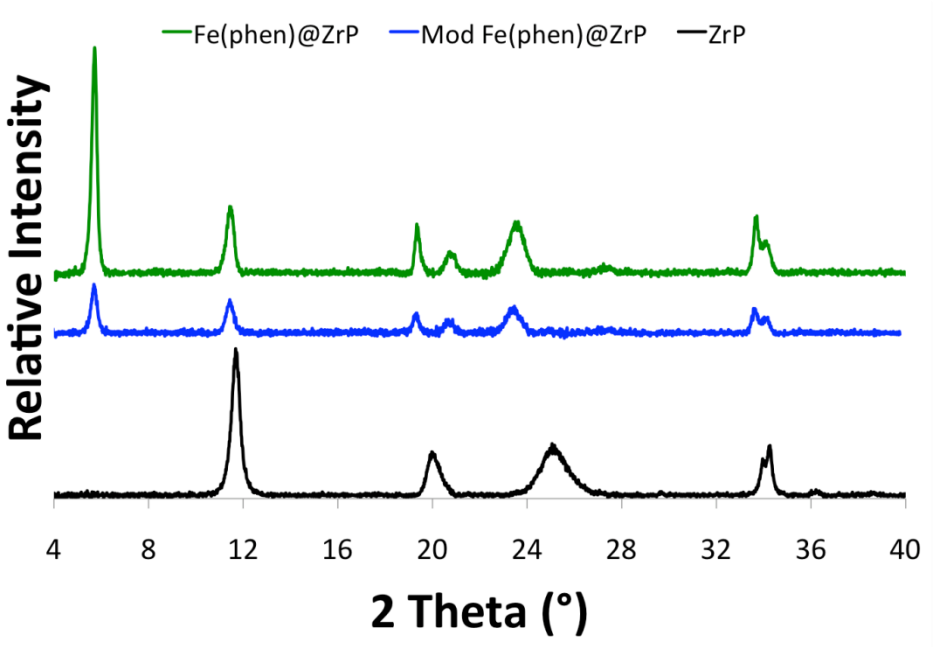

Figure 92. XRPD of $Fe(phen)_3^{2+}$@ZrP before and after modification along with the ZrP starting materials.

As in the prior case XRPD is used initially to verify the successful intercalation of the metal complex into ZrP and confirm that the interlayer remains unchanged upon surface modification. The d-spacing of the $Fe(phen)_3^{2+}$@ZrP is 15. 6 Å, spreading the layers slightly further apart than $Ru(bpy)_3^{2+}$@ZrP . It can be observed in **Figure 92** that the surface modification of $Fe(phen)_3^{2+}$@ZrP does not alter the X-ray pattern. In this case the interlayer is somewhat more hydrophobic than that of the $Ru(bpy)_3^{2+}$@ZrP as there are multiple phenanthrolines within the interlayer region. Ultimately it appears that this increase in hydrophobicity has no effect on the modification and no unwanted interlayer interactions are observed.

The FTIR spectra of the modified sample displays the alkyl stretching of the alkyl modifier as expected based on the prior case. As noted earlier no alkyl carbons exist in the $Fe(phen)_3^{2+}$@ZrP therefore all of this stretching can be attributed to the modification. The TGA thermogram of $Fe(phen)_3^{2+}$@ZrP also contains three main regions. Surface water and solvent alongside interlayer water are all lost below 100°C. The first weight loss process occurs from 320°C to 400°C. This weight loss likely corresponds to the initial decomposition of the phenanthroline within the interlayer; it can be observed that the process occurs in two overlapping events. It is likely that these are the phenanthroline molecules that are towards the exterior of the nanoparticle and therefore posses a lower level of stability. Immediately following the initial weight loss the condensation occurs from 490°C to 525°C and is mixed with further decomposition of the complex as in the $Ru(bpy)_3^{2+}$@ZrP case. The total weight loss of the compound is ~ 18.6% and the estimated loading is 0.17 moles of $Fe(phen)_3^{2+}$ relative to Zr. Addition of the epoxide to the surface of the nanoparticles leads to an additional weight loss process from 212°C to 275°C, **Figure 93**. As in the $Ru(bpy)_3^{2+}$@ZrP case a slight decrease in the starting temperature of the condensation is observed, however the initial weight loss attributed to the phenanthroline is stabilized due to the modification. In the surface modification reactions of pristine ZrP it was found that the addition of organic molecules to the surface had a somewhat stabilizing effect to the interlayer water. A similar phenomenon may exist in this case.

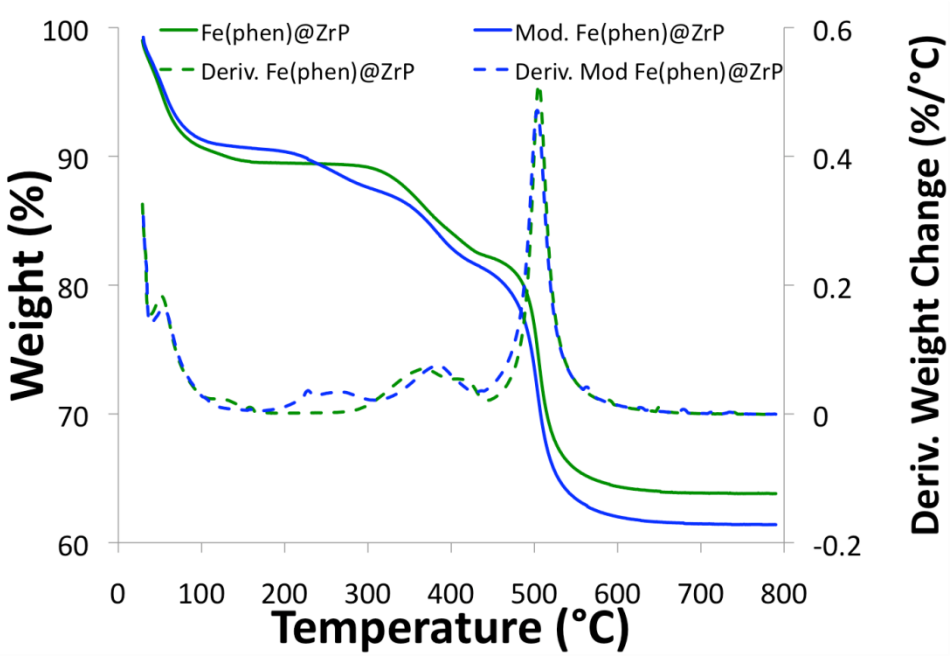

Figure 93. TGA of $Fe(phen)_3^{2+}$@ZrP before and after modification.

7.2.3 Rhodamine 6G@ZrP (Rho-6G@ZrP)

The two previous intercalated species proceeded by the ion-exchange mechanism, in which a cation displaced protons from the interlayer for the intercalation to occur. In both cases it appears that surface functionalization is possible and that none of the intercalated molecules is lost in the course of the reaction. A molecule that is intercalated through the acid base mechanism will now be investigated to see how the intercalation mechanism affects the stability of the interlayer upon modification.

XRPD of the intercalated sample reveals an interlayer spacing of 19.4 Å, verifying the successful intercalation of Rhodamine 6G into the interlayer of ZrP. The surface modified product displays an identical powder pattern indicating that leaching of the Rhodamine from the interlayer or unwanted interactions of the epoxide with the interlayer region did not occur, **Figure 94**.

The FTIR spectra of Rhodamine 6G@ZrP is comprised of stretches representative of ZrP and Rhodamine 6G, where Rhodamine 6G dominates the spectra due to the apparent high loading of the molecule within the interlayer. In addition Rhodamine 6G has alkyl, aryl, amino, and imine groups therefore the majority of the signals in the spectra can be attributed to Rhodamine 6G. Upon completion of the surface modification reaction the spectrum does not change significantly, **Figure 95**. Unlike the previous molecules used for intercalation, Rhodamine 6G possesses alkyl groups within its structure. As a result, the presence of alkyl stretches in the spectrum does not necessarily mean functionalization has occurred. Close examination of the spectrum of the modified sample shows that the alkyl stretching is considerably stronger in the modified sample than in the pure intercalation compound. Although the intensities in FTIR spectra are not necessarily comparable in all cases this can be used to suggest that the modifier did in fact interact with the surface of the Rhodamine 6G@ZrP nanoparticles.

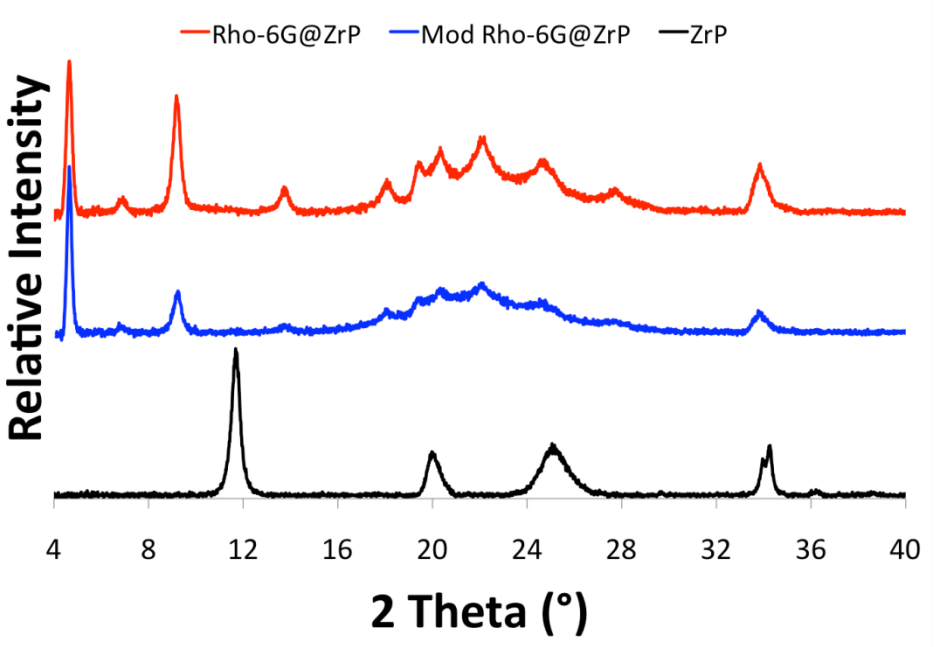

Figure 94. XRPD of Rho-6G@ZrP before and after modification along with the ZrP starting materials.

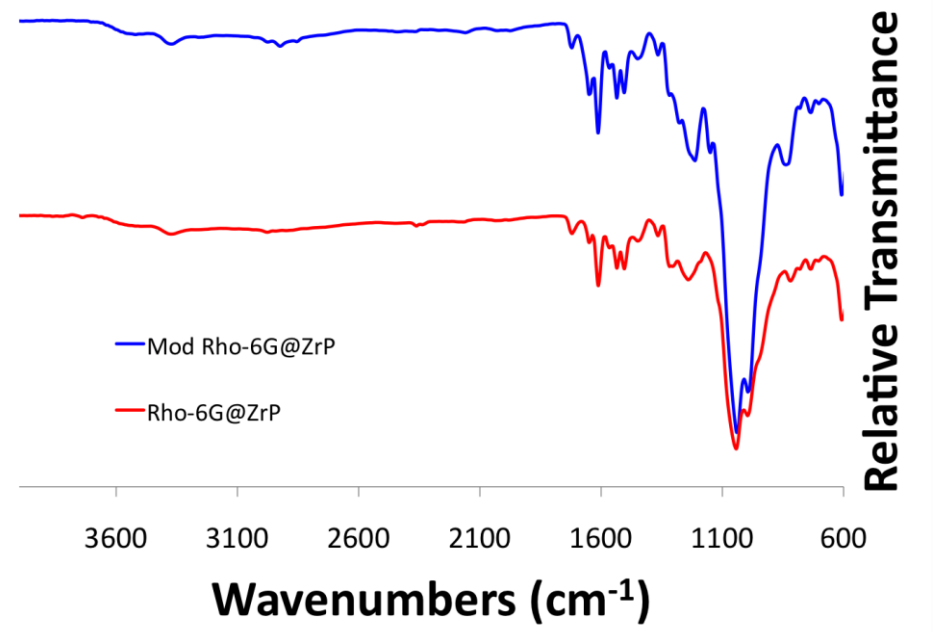

Figure 95. FTIR of Rho-6G@ZrP before and after modification.

To verify the attachment of the epoxide to the surface of the nanoparticles TGA was used. The TGA thermogram of Rhodamine 6G@ZrP displays a total weight loss of 50.26% and calculations reveal that this is representative of 0.45 moles of Rhodamine 6G relative to Zr in the compound. As is typical surface water and solvent and interlayer water is lost below 100°C. The decomposition of the Rhodamine 6G occurs in three distinct steps; the first from 305°C to 335°C, the second from 445°C to 515°C, and the last from 565°C to 620°C. The first step is the least intense of them all whereas the second is the most dominant. It is likely that the second step is the decomposition of the bulk of the Rhodamine 6G, while the last step is the condensation of the phosphates mixed with the residual Rhodamine 6G that is yet to decompose. The TGA thermogram of the modified Rhodamine 6G@ZrP follows the same pattern with the exception of a new weight loss event occurring from 175°C to 205°C indicative of the epoxide modifier, **Figure 96**. It is therefore confirmed by TGA that the surface of the particles was successfully modified.

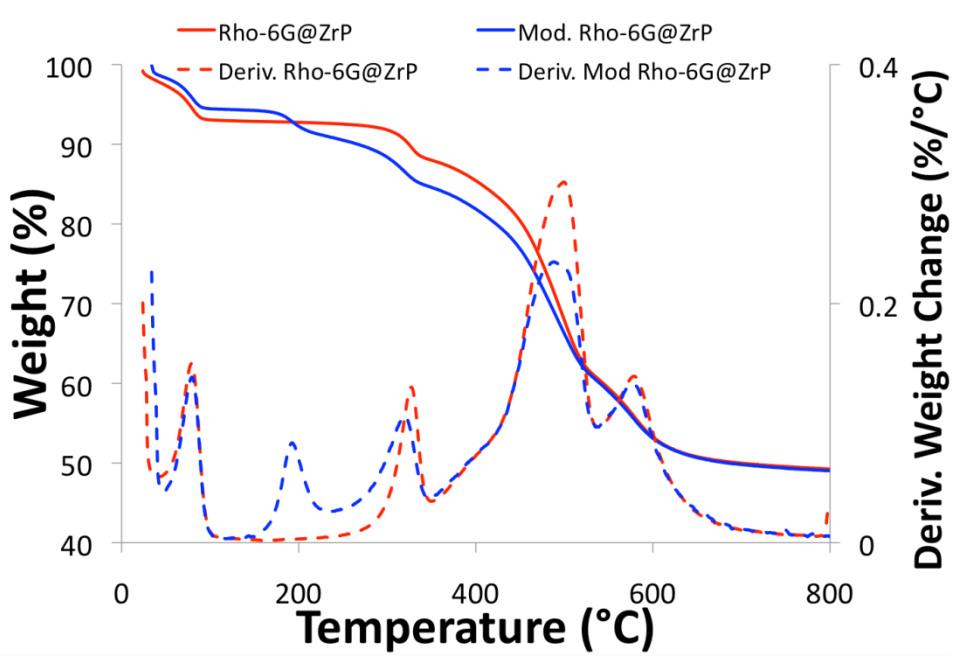

Figure 96. TGA of Rho-6G@ZrP before and after modification.

7.2.4 Room Temperature Surface Modification

It has been demonstrated that the surface of intercalated ZrP can be functionalized with epoxides through an identical reflux reaction as is used for pristine ZrP. However, in some cases, depending on the intercalated molecule, such a reflux could be harmful therefore a less harsh approach is needed to modify the surface of intercalated ZrP. It is known that the covalent attachment of epoxides to the surface of ZrP proceeds through the nucleophillic attack of the phosphate groups to a carbon of the epoxide ring.[68] This reaction should be able to proceed without heat, therefore a solution based self-assembly

technique will be investigated in which the epoxides are bonded to the surface by simply exposing ZrP to an epoxide solution.

This investigation was carried out with $Fe(phen)_3^{2+}$@ZrP. The FTIR and XRPD of the material are identical to the former case therefore TGA was used exclusively to determine if the amount of epoxide on the surface is comparable to that of the reflux method. **Figure 97** shows that the TGA thermogram of the modified sample prepared at room temperature is nearly identical to that of the reflux case. The total weight loss between the two samples only differs by 0.01%, suggesting that samples have the same thermal behavior and composition. To confirm this a formula was calculated for the room temperature prepared compound and it was found to contain 0.08 moles of modifier, relative to Zr. Based on this it can be concluded that the room temperature method is just as effective as the reflux case. Therefore ZrP intercalated with molecules that are not thermally stable can be functionalized without causing degradation of the compound.

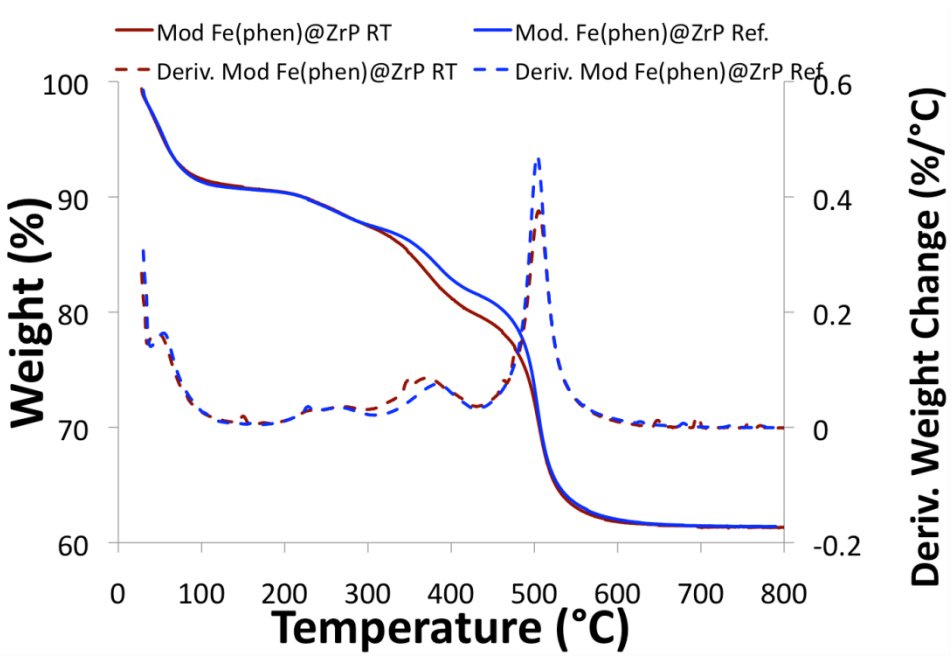

Figure 97. TGA of modified $Fe(phen)_3^{2+}$@ZrP using the reflux and room temperature method.

7.2.5 Comparison of Intercalated and Pristine Epoxide Modified ZrP

Previous experiments in which pristine ZrP was modified with 1,2-epoxyoctadecane showed the attachment of 0.14 moles of epoxide to the surface. In addition it was found that during these reactions the compound became slightly dehydrated as some of the interlayer water that was loosely held escaped the interlayer region. Experiments showed the dehydration could be greatly decreased by lowering the reflux temperature. In this case we seek to compare the extent of modification and the thermal stability of the modifier in the case of pristine ZrP and the intercalated samples. **Table 9** displays the calculated formulas for all the modified samples discussed. It can be observed that there

is some slight variation in the amount of modifier in the intercalated ZrP, however in all cases the surface is successfully modified. The data shows that intercalated samples with lower loadings tend to uptake more surface modifier than those with higher loadings. Additionally, there is not a significant difference between the uptake in the low loading samples and the pristine ZrP. It can also be noted that as is the case with the pristine ZrP the derivative of the epoxide weight loss occurs in two steps; this suggests that the bonding is identical in both cases.

Table 9. Calculated formulas for the multifunctional ZrP along with other thermal data.

Modified Sample (Modifier is 1,2-epoxyoctadecane)	Formula	Weight Loss Range (°C)	T at Derivative Maxima (°C)
ZrP	$Zr(H_{0.861}PO_4)_2(Mod)_{0.139}\cdot 0.6\ H_2O$	166-380	288/336
$Ru(bpy)_3^{2+}$@ZrP	$Zr(H_{0.91}PO_4)_2\,(Ru(bpy)_3)_{0.09}(Mod)_{0.13}\bullet\ 1.4\ H_2O$	188-326	262
$Fe(phen)_3^{2+}$@ZrP (Ref.)	$Zr(H_{0.84}PO_4)_2\,(Fe(phen)_3)_{0.16}(Mod)_{0.06}\bullet\ 1.4\ H_2O$	183-306	270
$Fe(phen)_3^{2+}$@ZrP (RT)	$Zr(H_{0.84}PO_4)_2\,(Fe(phen)_3)_{0.16}(Mod)_{0.07}\bullet\ 1.4\ H_2O$	190- 299	230/270
Rho-6GZrP	$Zr(H_{0.66}PO_4)_2\,(Rho\text{-}6G)_{0.44}(Mod)_{0.08}\bullet\ 1.4\ H_2O$	144- 230	193

Observation of the thermal decomposition of the epoxide on the surface in the samples shows slight fluctuations of the temperature range depending on the interlayer molecule.

The temperature range for the epoxide weight loss for modified $Ru(bpy)_3^{2+}$@ZrP was 188°C to 326°C. In the case of $Fe(phen)_3^{2+}$@ZrP it occurs from 183°C to 306°C, which falls within the same range as $Ru(bpy)_3^{2+}$@ZrP. In fact the weight loss occurs quicker in this case, finishing ~ 25° earlier. This data could possibly suggest that the increase in the loading level within the particle causes somewhat of a destabilization of the surface. The surface layer of ZrP has a layer of phosphates in the interlayer and on the surface. Electronically these phosphates are connected, it is plausible that if the interlayer phosphates are engaged in a considerable amount of ionic interaction due to intercalation, that the surface phosphates of that layer may have less electron density and therefore form weaker, less stable bonds. In comparison to the ion-exchange compounds investigated it can be noted that the decomposition temperature of the epoxide in modified Rhodamine 6G@ZrP is substantially lower, occurring from 144°C to 230°C. In fact, in this case the decomposition of the epoxide is completed before the decomposition even begins in the other cases. However, it cannot be said with certainty whether this occurrence is the result of the high loading of the Rhodamine 6G@ZrP, the acid-base intercalation mechanism, or a combination of both. In comparison to the pristine modified ZrP the weight loss ranges exhibited in the intercalated materials are similar for $Ru(bpy)_3^{2+}$@ZrP however as the loading of the intercalated molecule increases the stability shifts to lower temperatures.

7.3 Order of Synthesis in Multifunctional ZrP

The previous section has shown that intercalated ZrP can be successfully surface modified, however it is of interest whether the order of the synthesis affects the end product. If Θ-ZrP is used to intercalate a molecule the surface modification must come after the intercalation by default, however if α-ZrP is the starting material it may be possible to surface modify before intercalation in some cases. The following will be investigated using NH_4^+@ZrP as the ammonium ion can easily be intercalated into α-ZrP.

Initially ammonium was intercalated into ZrP followed by the surface modification reaction. The XRPD of the NH_4^+@ZrP displays a d-spacing of *ca.* 9 Å confirming that the intercalation was successful. In addition to this initial reflection a second broad reflection can be observed at a 2 theta value of *ca.* 11°, corresponding to an interlayer distance of *ca.* 8 Å. According to Hasegawa and Aoki additional signals are observed when the intercalated phase is not pure.[188] It is likely that the broad signal is a combination of two signals that are typically observed at with d values of 8.2 Å and 7.6 Å. This suggests that full loading of ammonium within the ZrP was not achieved in this case. TGA analysis of the intercalated material confirms that the loading level of the ammonium is below 100%. Ammonium typically intercalates within the interlayer in a 2 to 1 NH_4^+ to Zr ratio, however in this case it was found that only 1.25 moles of ammonium exist per mole of Zr.

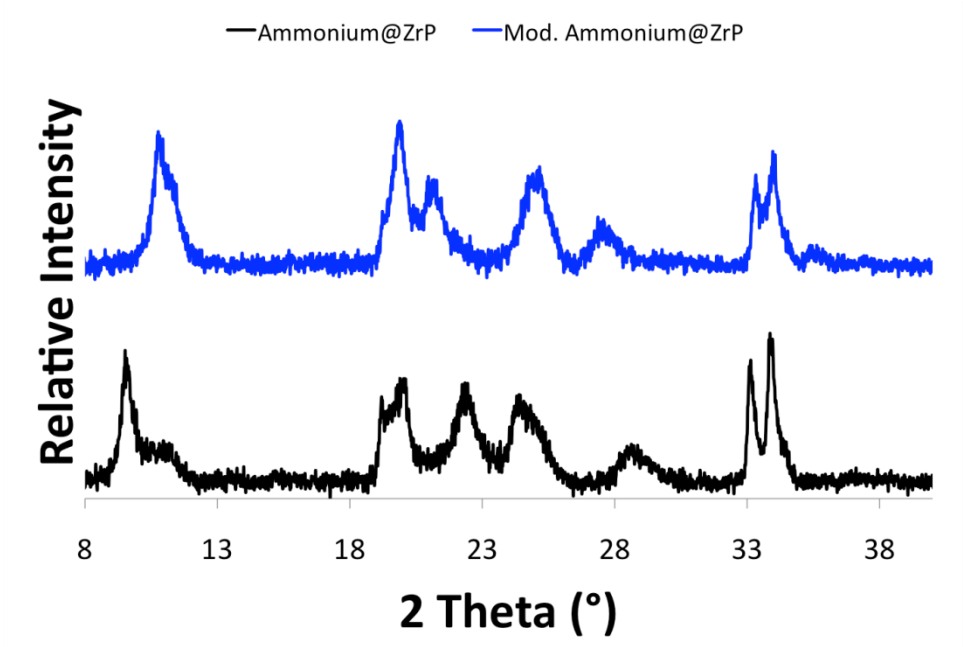

Figure 98. XRPD of NH_4^+@ZrP before and after modification with styrene oxide.

The intercalated sample was then functionalized with styrene oxide using the traditional reflux reaction. The XRPD displays a slightly different pattern than that of the pure intercalation compound, **Figure 98**. The peak corresponding to the fully ammonium exchanged phase is no longer present. Instead the dominant signal exists at *ca.* 10.7° 2 theta and corresponds to a partially intercalated phase of ZrP. It can therefore be concluded from the XRPD that in the case of NH_4^+@ZrP

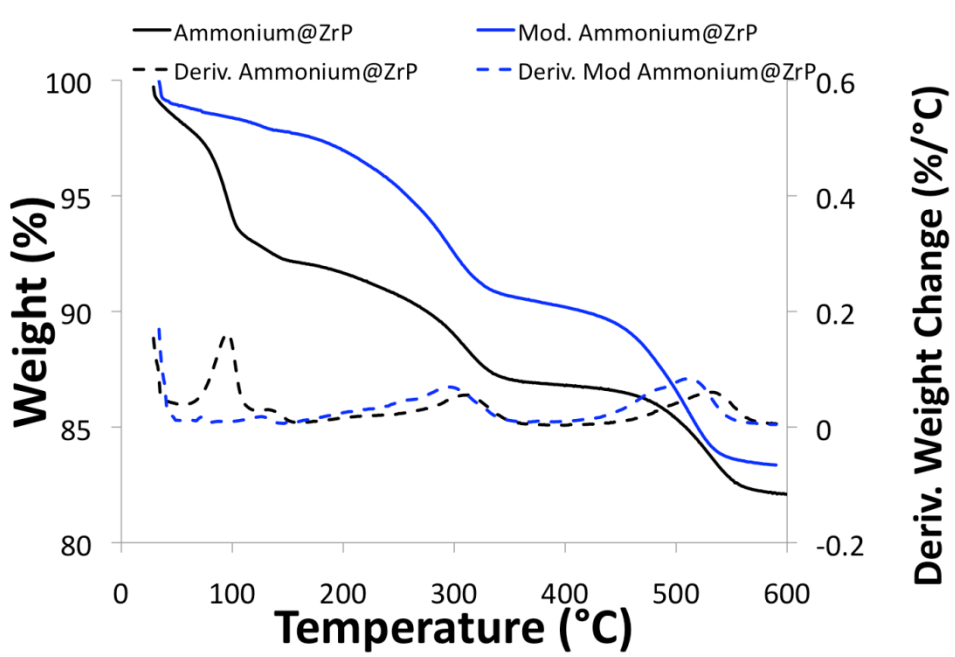

Figure 99. TGA of SO/ZrP NH_4^+@ZrP before and after modification with styrene oxide.

leaching of the intercalated molecule from the interlayer occurs during the surface modification reaction. TGA of the SO/ NH_4^+@ZrP further confirms that leaching of ammonium from the interlayer of the nanoparticles occurred, **Figure 99**. Initially it can be observed that the total weight loss of the modified sample is less than the NH_4^+@ZrP. As is typical the surface and intercalated water is lost below 100°C. A single weight loss occurs from 155°C to 364°C in which the epoxide is decomposed and the ammonium is released as NH_3. Finally the condensation of the phosphates to pyrophosphate can be observed from 465°C to 535°C. As the epoxide and the ammonium cannot be distinguished by TGA, the nitrogen content was determined by elemental analysis to determine the proper formula of the compound. It was found that 0.93 moles of

ammonium ion are in the SO/NH_4^+@ZrP. This amount is reasonable based on the decrease in interlayer spacing observed in the XRPD. It is interesting however that leaching occurs in the case of NH_4^+@ZrP. In most cases the leaching of ammonium from the interlayer is attributed to the re-exchange of protons into the interlayer. It is possible that upon the successful surface modification that the protons liberated from the surface phosphates were released into solution and exchanged with some of the ammonium within the layers, causing the decrease in ammonium. Also, the intercalation of ammonium within ZrP is highly ionic in nature, and is not a typical acid-base or ion exchange reaction as previous molecules we have investigated. Each ammonium is surrounded by the maximum number of negative charges and the water molecules positioning is based upon the location of the ammonium.[189] It is likely that upon heating the motion of water molecules and possible dehydration could have caused reorganization within the layer facilitating the production of the new phases. Although the surface modification is successful in this case the leaching makes the synthesis problematic. An attempt will now be made to prepare an identical compound by modifying the surface first then intercalating the ammonium.

In this case SO/ZrP was prepared by the reflux method as discussed in Chapter IV. The XRPD of the material displayed an interlayer spacing of 7.6 Å confirming no unwanted interaction of the epoxide with the interlayer. TGA confirms the partial dehydration of the interlayer water, as is typical and the uptake of the epoxide was determined to be 0.13 moles. Styrene oxide does not possess as much hydrophobic character as other long

chain alkyl epoxides therefore it can be dispersed in some polar solvents such as alcohols and even water in some cases. Ammonium ion was added drop wise to a suspension of surface modified nanoparticles in order to intercalate the ion. The XRPD of the SO/NH_4^+@ZrP confirms the successful intercalation of a pure ammonium intercalated compound, **Figure 100**.

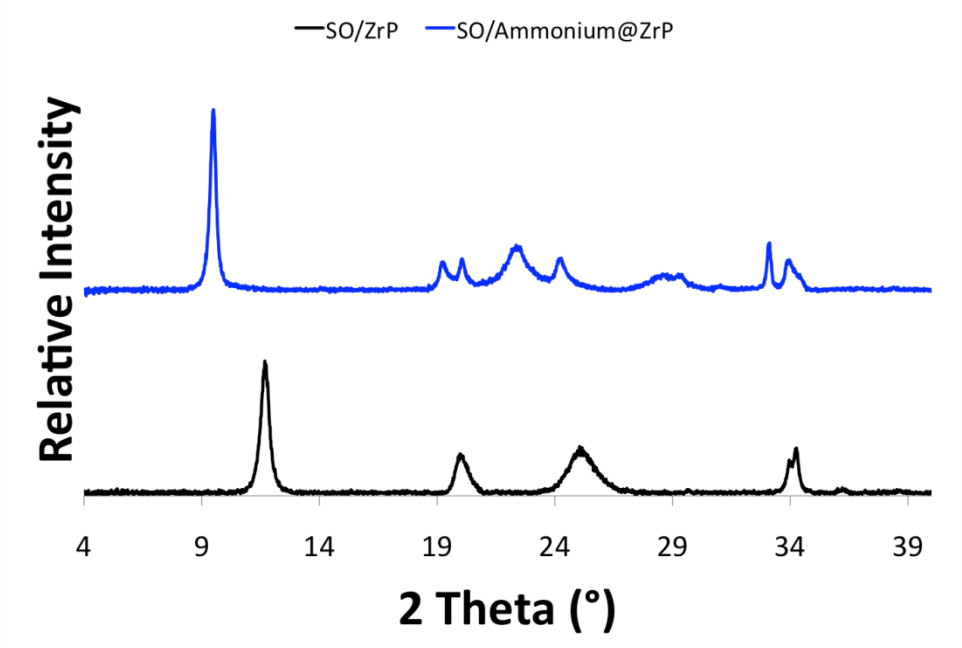

Figure 100. XRPD of SO/ZrP before and after intercalation with ammonium.

The diffraction pattern exhibits a d-spacing of 9.06 Å, this corresponds to a pure ammonium intercalated phase. The broad reflection indicative of the re-exchange of protons into the interlayer and leaching of ammonium is not observed in this case. This

suggests that the nanoparticles are fully loaded with ammonium ion in the 2 to 1 ratio as discussed earlier. TGA further confirms the successful incorporation of ammonium ion into the nanoparticles as the total weight loss observed is increased by 10%, **Figure 101**. In this case 1.84 moles of ammonium were found to exist within the compound, confirming the near full loading.

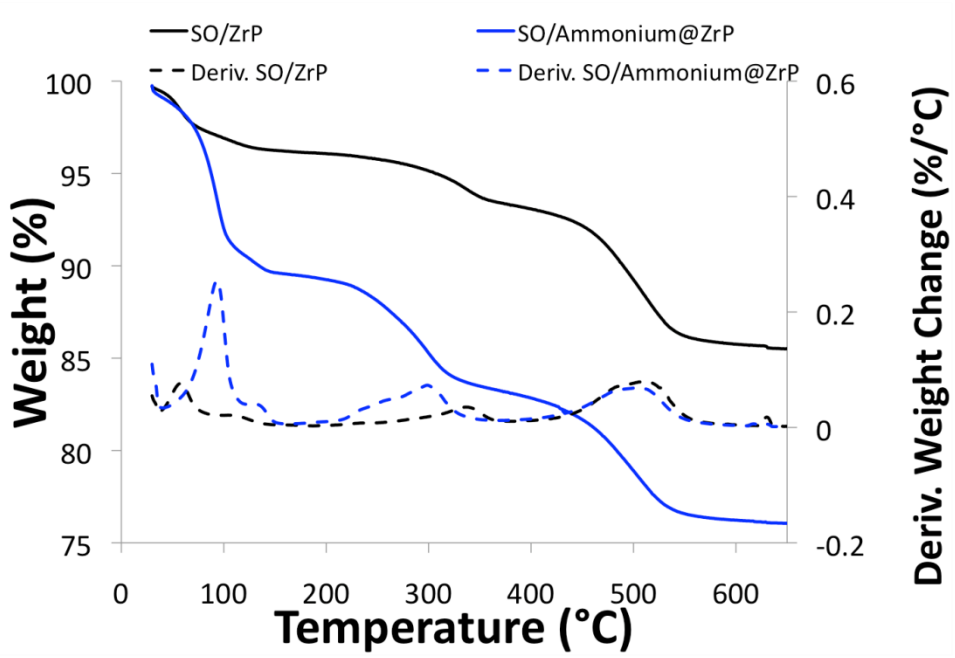

Figure 101. TGA of SO/ZrP before and after intercalation of ammonium.

It should be noted that although 2 moles of ammonium ion are expected per mole of Zr, this is the ratio that was observed in the single crystals of the compound. As discussed in chapter III, the less crystalline nanoparticles are often hydrolyzed as they are washed

upsetting the expected 2 to 1,P to Zr, ratio. Electron microprobe experiments have shown that there are 1.84 moles of P instead of 2; therefore we have full loading in this case and half loading in the prior case. Ultimately the results suggest that multifunctional ZrP can be synthesized by either intercalation or surface modification first. The determining factor should be based on the desired intercalation method to be used, the mechanism of the intercalation reaction, and the stability of the interlayer molecule.

7.4 M(IV) Modification of Intercalated ZrP

It has now been shown that the surface of intercalated ZrP can be functionalized by covalent attachment of modifying groups to the surface producing multifunctional nanoparticles. We now turn our attention to the ionic surface functionalization methods. It has previously been demonstrated that phosphonic acids can be used to functionalize a metal ion layer deposited on the surface of ZrP. We now aim to display the use of phosphonic acids with the M(IV) method to show that through the use of bisphosphonic acids, multiple functionalities can be added to a nanoparticle. In this case a polyethylene glycol bisphosphonic acid was synthesized. To add an additional functionality to the PEG bisphosphonic acid, the polymer was reacted with Fe_3O_4. The resulting polymer possesses both free phosphate groups and iron oxide nanoparticles. This polymer was then reacted with the Hf(IV)/Rhodamine 6G@ZrP in order to produce a multifunctional ZrP based nanoparticle with three functionalities, Rhodamine 6G (interlayer),

Polyethylene glycol (surface), and iron oxide (surface), **Figure 102**. The Rhodamine 6G adds fluorescent character to the particles while the PEG makes them more water-soluble and the iron oxide imparts magnetic properties to the particles.

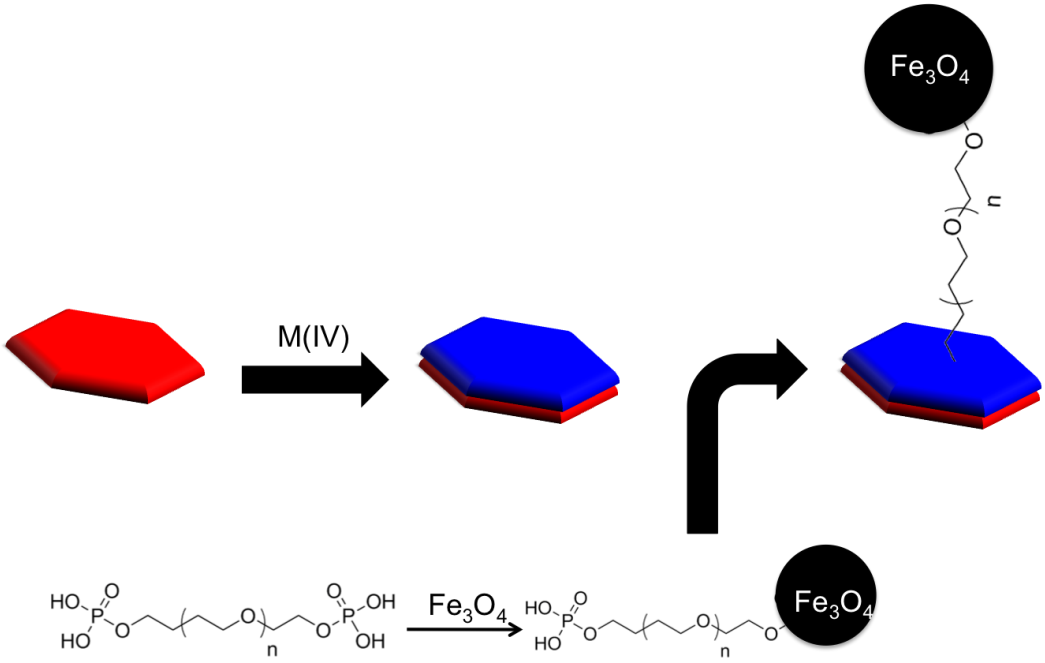

Figure 102. Schematic depicting the treatment of intercalated ZrP with a metal ion and subsequent functionalization with a multifunctional ligand to produce a particle with three functionalities.

Initially, Rhodamine 6G@ZrP was modified with Hf(IV) using the surface ion exchange reaction discussed in Chapter VI. As in all other cases the XRPD of the sample before and after modification are identical, **Figure 103**. This suggests that the metal ion

exclusively displaced the surface protons and did not have any unwanted interactions with the interlayer region. It should be noted however that in this case the interaction of

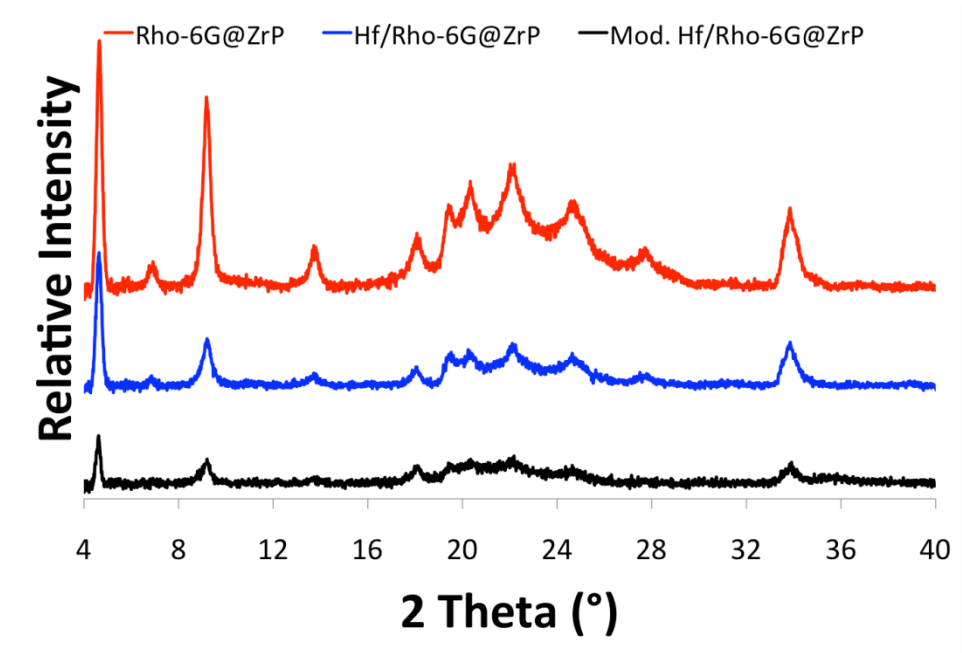

Figure 103. XRPD of Rho-6G@ZrP modified materials.

Hf(IV) with the interlayer was a strong possibility. The Rhodamine 6G is intercalated into the ZrP by the acid-base intercalation mechanism, addition of Hf(IV) to the reaction adds a cation, which can also form favorable interactions with the interlayer. It was possible for the Hf(IV) to exchange some of the Rhodamine 6G and cause leaching, however it appears that this is not the case. It is likely that the small amount of Hf(IV) added was not sufficient enough to cause this effect. Also the the acid base pairs in the

interlayer were likely more stable than the formation of the ion exchange intercalation species with Hf(IV). Addition of the ligand to the surface also does not alter the X-ray pattern. However, it can be observed that upon each successive surface reaction the intensity of the reflections decreases.

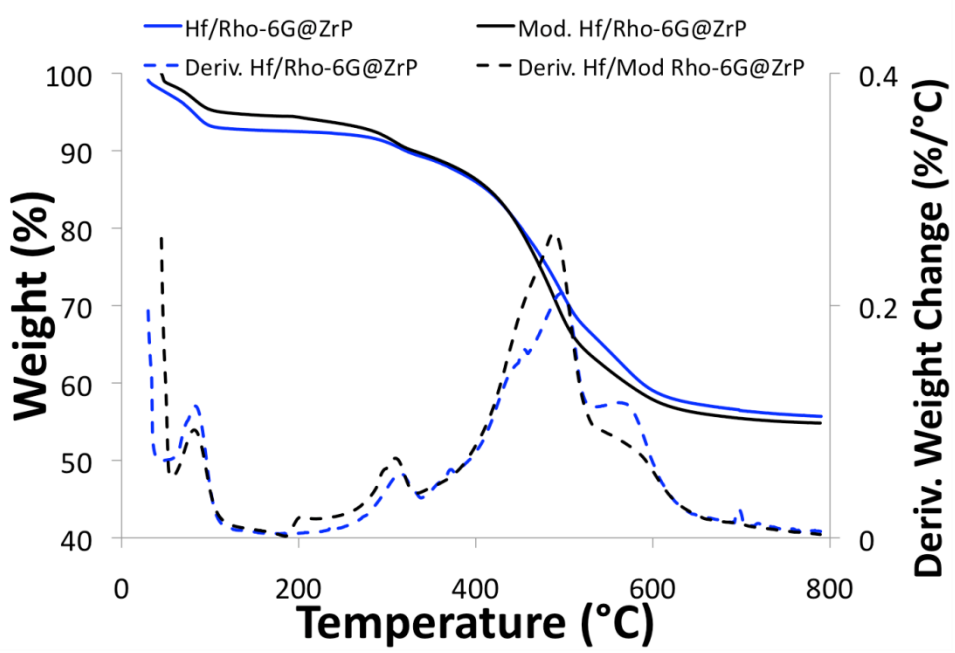

Figure 104. TGA of the Hf/Rho-6G@ZrP starting material and the compound modified with iron oxide PEG.

TGA of the Hf(IV)/ Rhodamine 6G@ZrP displays a reduction of the total percent weight loss when compared to the starting material. The addition of a layer of Hf(IV) adds mass to the compound that does not decompose when heated, therefore the reduction is expected. Examination of the TGA of the new multifunctional nanoparticle

reveals largely the same decomposition pattern as the starting material except for a new weight loss process occurring roughly from 180°C to 225°C, corresponding to the PEG attached to the surface, **Figure 104**.

It should be noted that the weight loss is not very substantial as the PEG used is a short chain and also the iron oxide was attached to the PEG adding additional inorganic weight to the compound. TEM images of the resulting material verify the presence of iron oxide on the particles, **Figure 105**. The 6 nm Fe_3O_4 particles can be observed as small dark spots in the images. It can be noted that there are not a large number of iron oxide particles present.

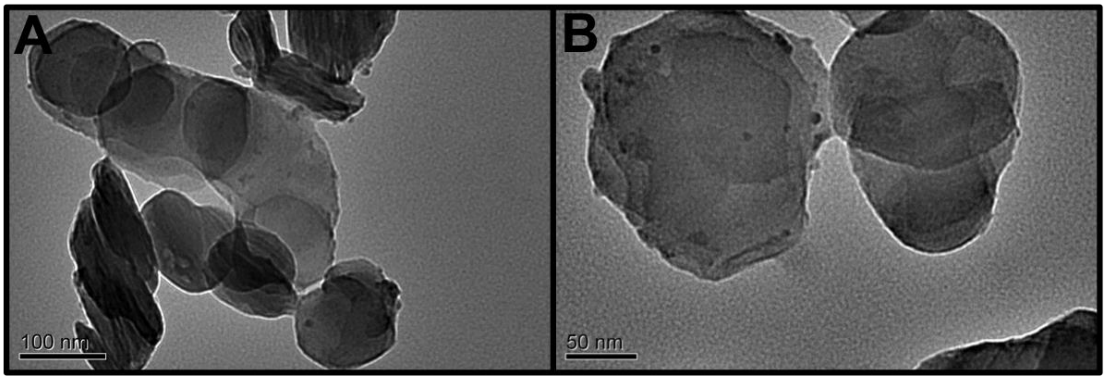

Figure 105. TEM images of the iron oxide PEG modified Hf/Rho-6G@ZrP.

This is likely due to the small amount of Fe_3O_4 coordinated to the phosphonic acid group of the PEG. The low uptake of polymer is also verified by TGA, as the new weight loss

event corresponding to modification is very small. It is likely that the low uptake is directly related to the successful synthesis of the ligand. If there is no free phosphate group at the distal end of the polymer, the ligand will not bond to the surface. The bisphosphonic acid could have coordinated two iron oxides and therefore not been able to bond to the surface effectively. The synthesis of the multifunctional ligand must be improved in order to selectively uptake a single iron oxide. In turn the coverage of the magnetic particles on the ZrP surface will be improved. Although the amount of magnetic particles is relatively small, the resulting ZrP particles are still magnetic. It has therefore been verified that M(IV) can be deposited on the surface of intercalated ZrP and the resulting structure can be functionalized with ligands to synthesize multifunctional ZrP. In addition, the use of bisphosphonic acids leads to the ability to add multiple functionalities to the ligand and therefore increase the number of functional components in the nanoparticles themselves.

7.5 Conclusion

It has been properly demonstrated that ZrP can be used to synthesize multifunctional nanoparticles in a simple manner by combining intercalation and surface modification. It is possible to control both the interior and exterior of the nanoparticles using this method, opening the opportunity to design nanoparticles for specific applications by careful selection of both the interlayer and surface groups. Additionally, it was shown that using bisphosphonic acids, further control of the surface functionality could be

gained by adding multifunctional ligands to the nanoparticle surface. In the case of the covalent attachment of modifiers on the surface of intercalated ZrP it was observed that the extent of functionalization is similar to that of the modified pristine ZrP. Although the amount of epoxide bonded is similar, the stability of the epoxide on the surface appears to be dependent on the intercalation mechanism and loading level of the intercalated molecule, suggesting that the interlayer has an effect on the stability of the surface.

CHAPTER VIII

DESIGNABLE ZIRCONIUM PHSOPHATE NANOPARTICLES FOR ENHANCED APPLICABILITY*

8.1 Introduction

It has been successfully demonstrated that surface chemistry can be used to add additional functionality to both pristine and intercalated ZrP. Surface modification can not only lead to enhancement of prior ZrP applications but also to new applications of the nanoparticles, which were previously not possible. Integral in the applicability is the control of both the interior and exterior of the nanoparticles, allowing the particles to be tailored for particular applications. In this chapter we will display particular applications of multifunctional ZrP nanoparticles and discuss how they are superior to the pure intercalation compounds. Initially one of the new applications of ZrP will be discussed followed by enhancements on some prior applications of the material.

---

* Part of this chapter is reprinted with permission from "Self-Assembled Monolayers Based Upon a Zirconium Phosphate Platform" by Díaz, A., Mosby, B.M., Bakhmutov ,V.I., Martí, A., Batteas, J. and Clearfield, A. *Chemistry of Materials,* **2013**, 25 (5), 723-728, copyright 2013 by American Chemical Society; "Surface Modification of Zirconium Phosphate Nanoplatelets for the Design of Polymer Fillers" by Mosby, B.M., Díaz, A., Bakhmutov ,V.I., and Clearfield, A. *ACS Applied Materials and Interfaces*, **2014**, 6 (1), 585-592, copyright 2013 by American Chemical Society; and "Designable Architectures on Nanoparticle Surfaces: Zirconium Phosphate Nanoplatelets as a Platform for Tetravalent Metal and Phosphonic Acid Assemblies" by Mosby, B.M., Goloby, M., Díaz, A., Bakhmutov ,V.I., and Clearfield, A., *Langmuir,* **2014**, 30 (9), 2513-2521, copyright 2014 by American Chemical Society.

8.2 Formation of Layer-by-Layer Assemblies on the ZrP Surface

Previously it has been demonstrated that metal ions can be deposited on the surface of ZrP and subsequently functionalized with phosphonic acid ligands. Coordination of a bisphosphonic acid to the surface would leave a free terminal phosphonic acid group that could be further functionalized. If the bisphosphonic acid is a long alkyl chain it is possible that it would fold over and therefore have both phosphonic acid groups bonding to the same metal ion layer. To avoid this a rigid bisphosphonic acid, biphenyl bisphosphonic acid, was utilized. Using this strategy, assemblies can be made on the ZrP surface in a layer-by-layer fashion, **Figure 106**. Previously synthesized BPBPA/Hf/ZrP was initially treated with a solution of Hf(IV) followed by reaction with BPBPA, this sequence was repeated until the desired number of layers was achieved. Previous results indicate that on the initial metal ion layer each ion interacts with a single surface phosphate group. As the coordination of the ligand to the metal ion layer is in a three to one fashion, it is expected that the terminal phosphate of the bisphosphonic acid will also bond to three distinct metal ions causing an identical amount of metal ion to be taken up by the ligand layer as the initial reaction of surface phosphates.

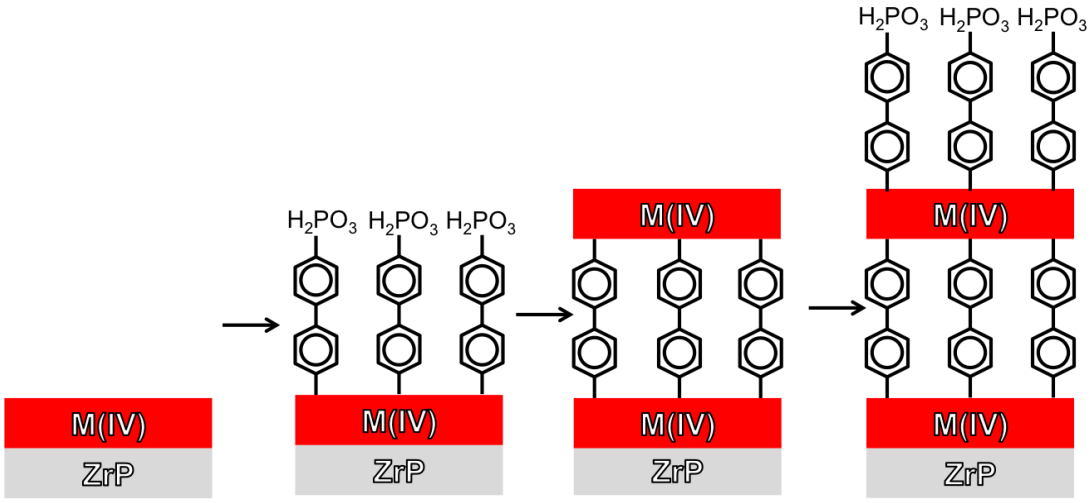

Figure 106. The formation of layer-by-layer assemblies on the ZrP surface by alternating treatment of M(IV) and bisphosphonic acids. Note the assemblies are formed on both sides of the ZrP, however only one is shown for clarity.

The multilayer compounds were initially examined by FTIR. As additional layers of BPBPA are deposited on the surface it can be seen that the intensity of the aromatic stretching increases, **Figure 107**. Initially the stretching is low as the percentage of modifier is low compared to the many layers of ZrP. As subsequent layers of BPBPA and Hf(IV) are deposited the contribution of organic in the compound is increased. The ZrP used is expected to have *ca.* 11 layers and in this case 4 layers of hafnium biphenyl phosphonate were added to the surface of ZrP. Considering that the hafnium biphenyl phosphonate layers exist on the top and bottom of the nanoparticles, the total number of layers is actually eight. As the ratio of biphenyl layers to ZrP layers increases, a corresponding increase in the aromatic stretching is observed.

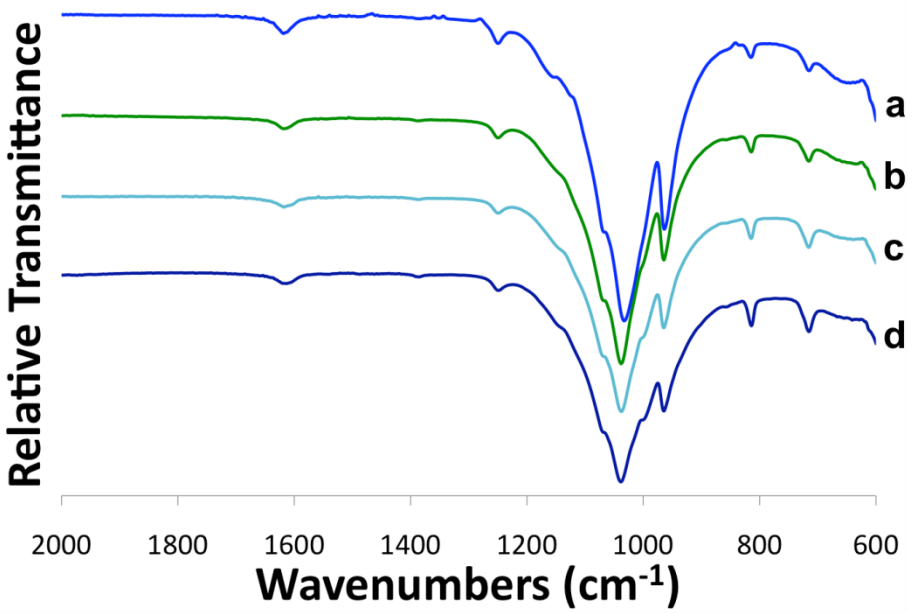

Figure 107. FTIR of layer-by-layer compounds with (a) 1, (b) 2, (c) 3, and (d) 4 layers of BPBPA in the structure. These samples represent generation 1,3,5, and 7 respectively.

In addition, XRPD patterns show a decrease in the intensity of the 002 peak relative to the starting material as more layers of Hf(IV) and ligand were added to the surface , **Figure 108**. As more Hf(IV) is added to the surface the diffraction of the X-rays at the crystalline ZrP core is reduced. The XRPD pattern does not exhibit any reflections at higher d-spacings corresponding to the hafnium biphenyl phosphonate. This suggests that the biphenyl layers are relatively amorphous in nature. This is reasonable as the reaction was carried out in a self-assembly fashion absent of heat. The pure M(IV) biphenylphosphonates are also relatively amorphous and to obtain a somewhat crystalline material and powder pattern the material must be refluxed at high temperatures for an extended period of time.[10]

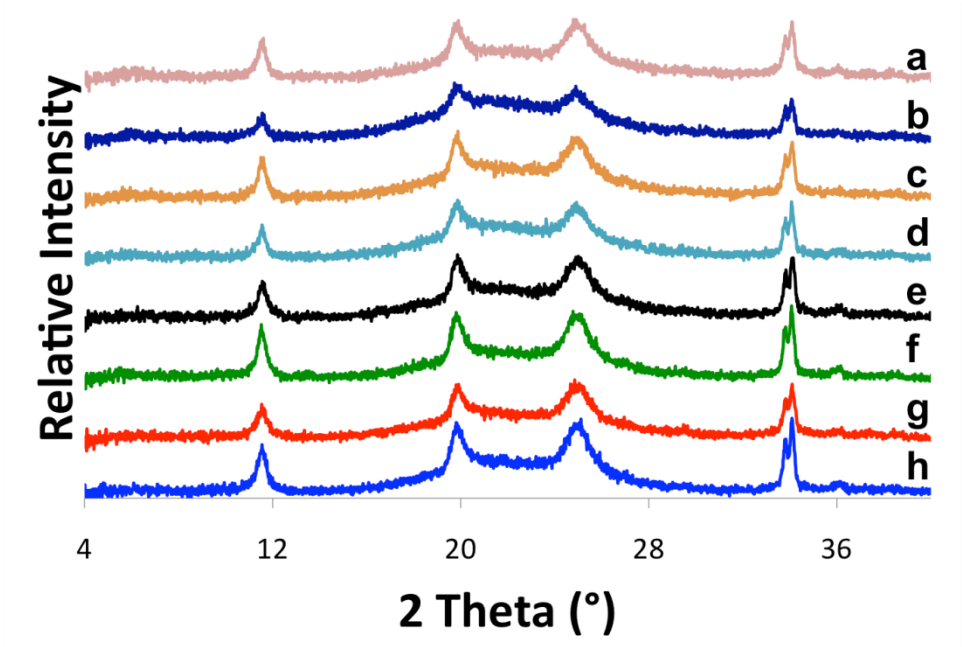

Figure 108. XRPD of layer-by-layer compounds of generation (a) 8, (b) 7, (c) 6, (d) 5, (e) 4, (f) 3, (g) 2, and (h) 1. Generation 1 is Hf/ZrP modified with BPBPA and each subsequent generation adds Hf(IV) or BPBPA alternately.

The weight losses observed in the TGA of the multilayer compounds is identical to that observed in BPBPA/HfZrP. It can however be noted that as the metal ion layer is added the derivative of the weight loss event corresponding to the ligand is greatly decreased due to the addition of inorganic mass. Upon the addition of an additional layer of phosphonic acid the intensity of the derivative peak increases once again. Formulas were determined for the multilayer compounds by combining the atomic concentrations determined by electron microprobe with thermal data gained with TGA, **Table 10**.

Table 10. Formulas of the layer-by-layer compounds as determined by TGA and microprobe.

Terminal Group	Generation	TGA Total Weight Loss (%)	Calculated Formula
BPBPA	1	15.45	$Zr(H_{0.9}PO_4)_2Hf_{0.1}(Mod)_{0.03}\cdot 1.2\ H_2O$
Hf (IV)	2	17.22	$Zr(H_{0.9}PO_4)_2Hf_{0.2}(Mod)_{0.03}\cdot 1.3\ H_2O$
BPBPA	3	17.68	$Zr(H_{0.9}PO_4)_2Hf_{0.2}(Mod)_{0.06}\cdot 1.3\ H_2O$
Hf (IV)	4	20.73	$Zr(H_{0.9}PO_4)_2Hf_{0.3}(Mod)_{0.06}\cdot 1.4\ H_2O$
BPBPA	5	19.97	$Zr(H_{0.9}PO_4)_2Hf_{0.3}(Mod)_{0.10}\cdot 1.4\ H_2O$
Hf (IV)	6	20.25	$Zr(H_{0.9}PO_4)_2Hf_{0.4}(Mod)_{0.10}\cdot 1.4\ H_2O$
BPBPA	7	21.38	$Zr(H_{0.9}PO_4)_2Hf_{0.4}(Mod)_{0.13}\cdot 1.3\ H_2O$
Hf (IV)	8	21.32	$Zr(H_{0.9}PO_4)_2Hf_{0.5}(Mod)_{0.13}\cdot 1.3\ H_2O$

It can be observed that upon addition of a metal ion layer, the ligand content stays constant and vice versa. This demonstrates that as additional layers are grown from the surface, the layers below are stable and do not degrade in any way. As stated earlier the initial Hf modified ZrP contains around 0.11 moles of Hf. Each addition of ligand to the surface resulted in the uptake of roughly 0.03 moles of the ligand and treatment with Hf(IV) to the ligand phosphonate terminated surface resulted in uptake of ~ 0.1 moles of Hf. The uptake of a consistent amount of ligand and metal suggests a specific ordering or regular unit attaching to the terminal surface structure.

The stability of the initial metal ion layer was investigated by treating BPBPA/Hf/ZrP with a different metal ion, Ca(II). In this case, as additional layers of Ca(II) and BPBPA were added to the surface the Hf content of the compound remained constant, as confirmed by microprobe, **Figure 109**. This demonstrates that the metal ions of the initial layer are not replaced by the new ions or detached from the surface when re-dispersed in solution. Similar results were obtained when using Sn(IV) as the initial metal layer. Not only can the metal ion be alternated in the multilayered structure but the phosphonic acid can be changed as well. Samples were prepared in which after the metal ion was added to the initial BPBPA layer, ODPA was used to functionalize the new metal ion layer. Infrared data show stretching for the aromatic rings and alkyl chains of both ligands confirming that multiple ligands can be used within the same structure, **Figure 110**. Using this model different bisphosphonic acids and metal ions can be

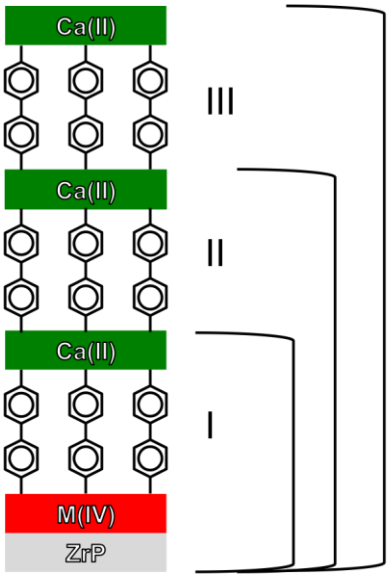

Generation	Zr	P	Hf	Ca
I	1	2.1	0.1	0.1
II	1	2.3	0.1	0.2
III	1	2.5	0.1	0.3
	Zr	P	Sn	Ca
I	1	1.9	0.1	0.1
II	1	2.0	0.1	0.2
III	1	2.2	0.1	0.3

Figure 109. Electron microprobe data of a mixed metal ion layer-by-layer system alongside a schematic of the structure.

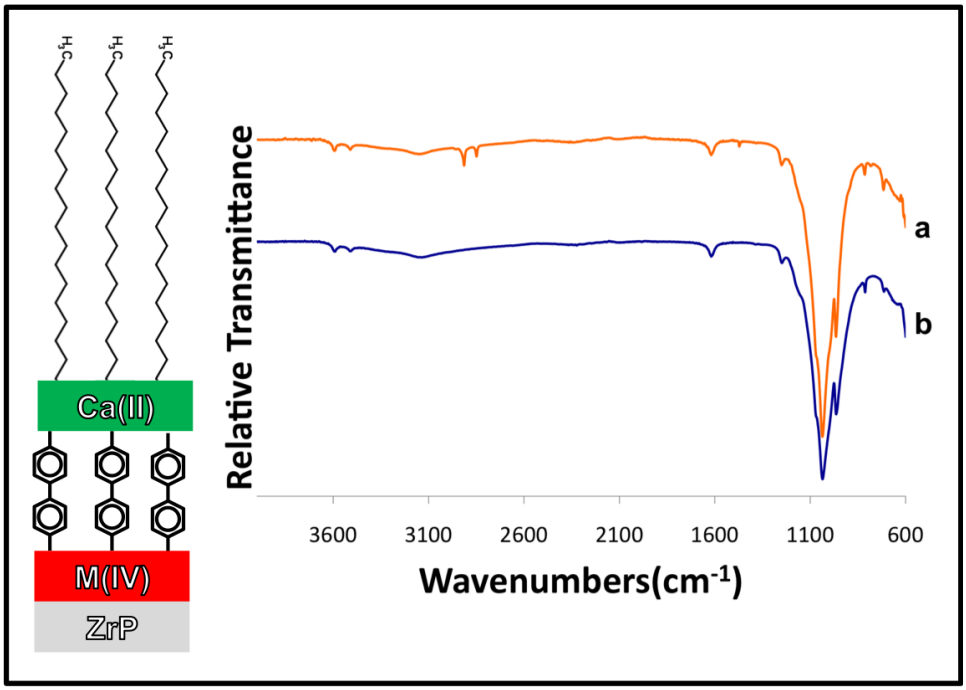

Figure 110. FTIR spectra of (a) a layer-by-layer system functionalized with two different ligands(see schematic) and (b) the base structure before functionalization with the second ligand.

alternated within the surface structure in order to build customizable systems from the surface. As a visual illustration and proof of concept, the relative wettability of the layer-by-layer materials was investigated by treating pellets of the nanoparticles with water droplets , **Figure 111**. It was found that the samples terminated with Hf(IV) or free phosphates were hydrophilic and absorbed the water drop whereas the ODPA terminated surface did not and produced a complete drop on the surface of the pellet. Compared to the other samples it is clear that the ODPA modified material is significantly more hydrophobic due to the fact that the water drop was not absorbed by the powdered nanoparticles contained in the pellet.

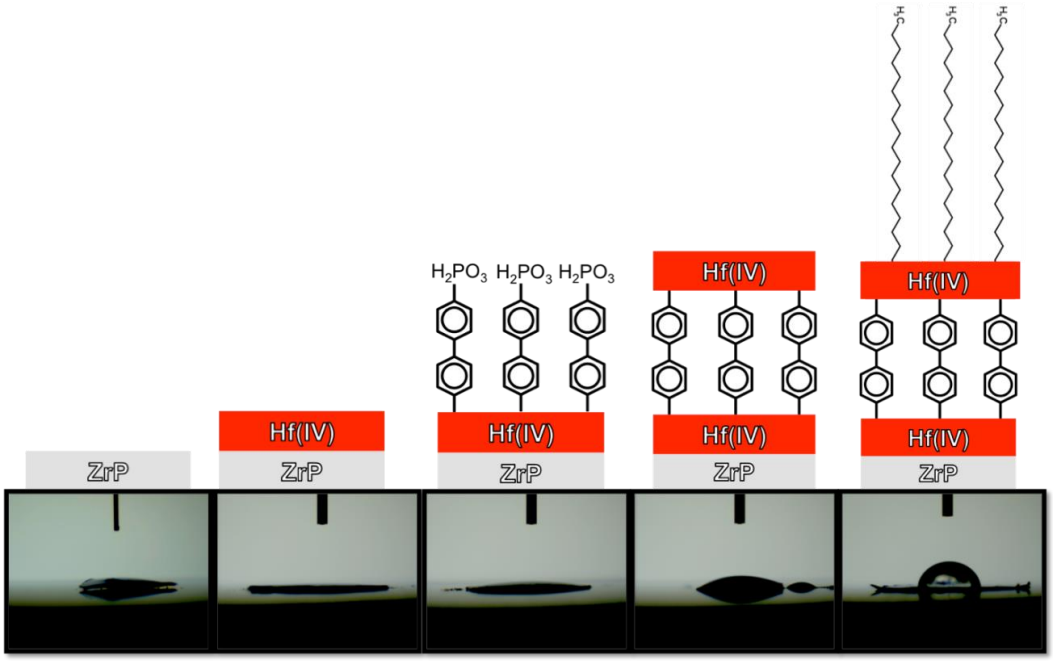

Figure 111. Schematic representation of layer-by-layer compounds along with images from the relative wettability experiments.

In addition, exfoliation of a layer-by-layer material and separation could lead to the ability to harvest a single layer of ZrP with the assembly on the surface. These materials could then be used for a number of applications such as polymer composites and electron transfer systems. Also, as displayed in the previous chapter, the surface chemistry can be combined with the interlayer chemistry to produce particles with a controlled interior and exterior, and therefore the ability to design nanoparticles for specific applications. [146, 182] In this case a molecule or ion could be encapsulated within the interlayer and then an assembly could be built on the surface to interact with the molecule within the layers or to give the particle specific properties.

8.3 Photoinduced Electron Transfer

In addition to the new opportunities and applications that the surface chemistry of ZrP leads to, it can also be used to improve current applications. Brunet and coworkers have shown efficient electron transfer reactions with photoactive species intercalated within the layers of ZrP.[190-192] Moreover, Colón and coworkers have also demonstrated that electron transfer reactions can take place between suspended nanoparticles of ZrP fully loaded with phototoactive electron donors and the electron acceptor in solution.[28, 42, 187] The electron donor $Ru(bpy)_3^{2+}$ was intercalated into ZrP in a number of these experiments. Due to the hydrophillicity of both ZrP and $Ru(bpy)_3^{2+}$ the prior work was limited to aqueous solutions. A large number of electron acceptors are extremely hydrophobic such as buckyballs and benzoquinines. In this case there is no way for the

nanoparticles to interact with such acceptors. Surface modification of $Ru(bpy)_3^{2+}$@ZrP with hydrophobic groups should impart hydrophobic character to the ZrP and thus allow interaction in non polar media with hydrophobic electron acceptors. $Ru(bpy)_3^{2+}$@ZrP was surface functionalized with octadecyltrichlorosilane (OTS) using the reflux procedure utilized for pristine α-ZrP. As stated in the previous chapter the surface modification reaction does not cause leaching of $Ru(bpy)_3^{2+}$ from the interlayer region. The principal photophysical properties of OTS/$Ru(bpy)_3^{2+}$ @ZrP were investigated to determine if the encapsulation within ZrP or the surface modification reaction caused changes. Initially the UV-visible spectra of OTS/$Ru(bpy)_3^{2+}$ @ZrP and $Ru(bpy)_3^{2+}$ @ZrP can be seen in **Figure 112** .The spectra of both compounds are identical confirming that the photophysical properties were unaltered. Additionally, the photoluminescent spectra in **Figure 113** verifies the retention of photophysical properties through the observation of emissions produced by the modified sample that are identical to those reported for $Ru(bpy)_3^{2+}$ @ZrP by Martí et al.[28, 187] The covalent attachment of OTS to the nanoparticle surface results in an extremely hydrophobic material that cannot be suspended in water and but disperses relatively easily in non-polar solvents.

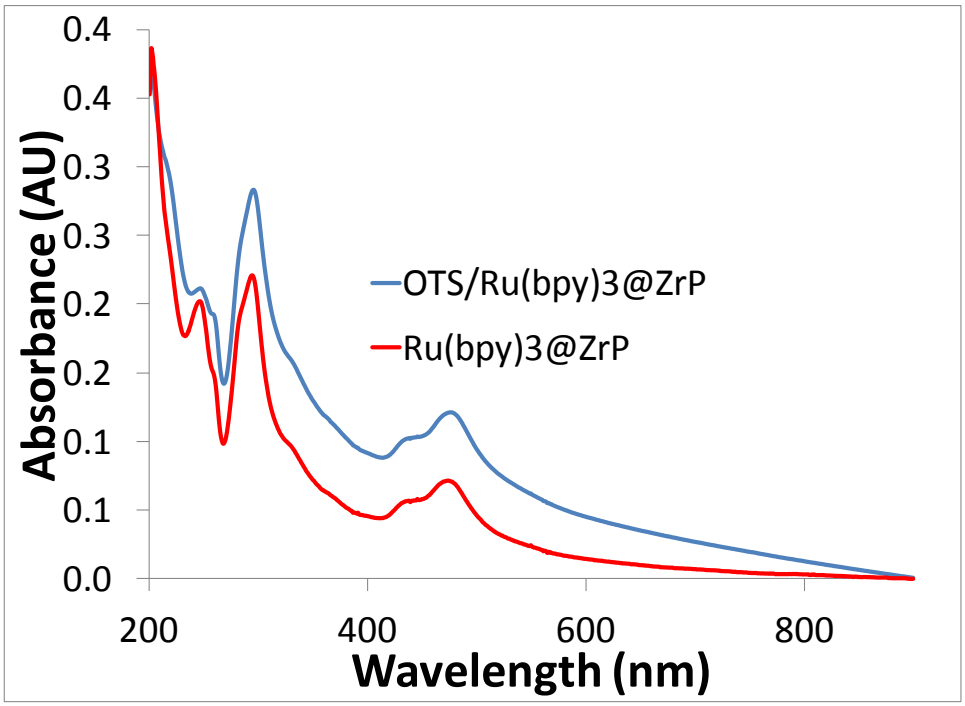

Figure 112. UV-vis spectra of OTS/Ru(bpy)$_3$@ZrP (blue line) and Ru(bpy)$_3$@ZrP (red line) in a 0.008% (w/v) ethanolic suspension.

Due to the hydrophobicity of the synthesized nanoparticles a photoinduced electron transfer reaction with an hydrophobic electron acceptor, 1,2-benzoquinone (BQ), could be performed.[193] **Figure 113** shows the photoluminescence spectra of surface modified Ru(bpy)$_3^{2+}$ @ZrP suspended in 1,2-dichlorobenzene (0.008% w/w) with different concentrations of BQ in the solution (from 0 to 728 μM). The steady-state photoluminescence spectra of the surface modified Ru(bpy)$_3^{2+}$ @ZrP suspended in 1,2-dichlorobenzene resembles the spectrum of Ru(bpy)$_3^{2+}$ in aqueous solution (λmax = 597 nm) and the non-surface modified material in water reported by Martí and Colón (λmax = 592 nm), with a λmax of 595 nm.[187]

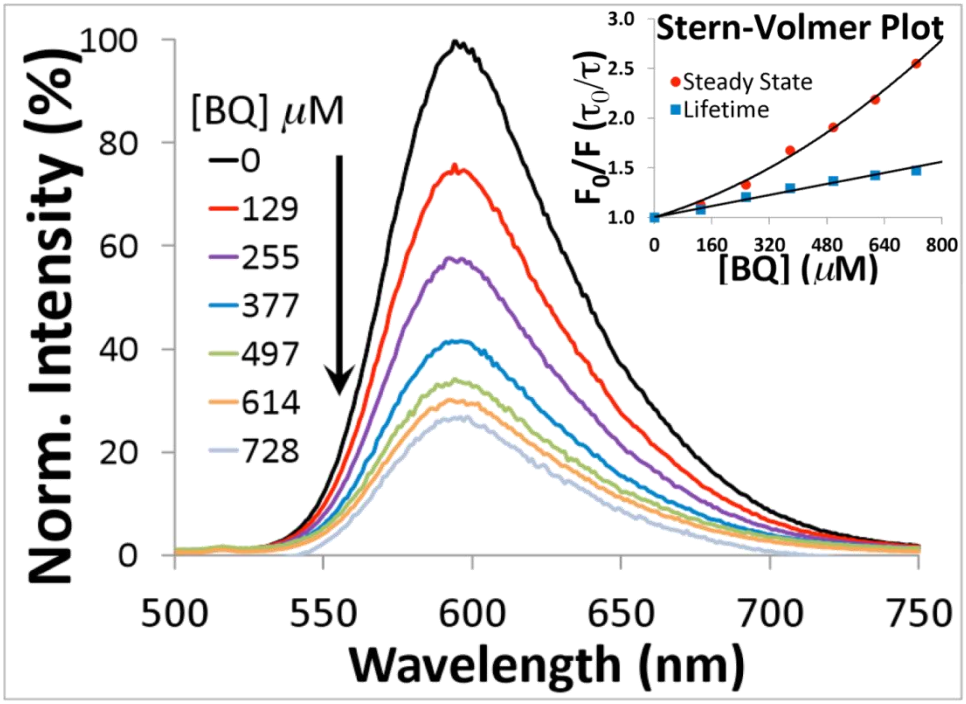

Figure 113. Photoluminescent spectra of OTS surface modified Ru(bpy)32+@ ZrP with different concentrations of BQ in 1,2-dichlorobenzene. Inset: Stern-Volmer plot for the quenching with BQ using steady-state fluorescence intensity (spheres) and fluorescence lifetime (squares). λex = 445 nm.

This result shows that the microenvironment of the intercalated $Ru(bpy)_3^{2+}$ is intact in the interlayer region and was not affected by the surface modification reaction. The inset in **Figure 113** also shows the Stern-Volmer plot for the quenching of the surface modified $Ru(bpy)_3^{2+}$ ZrP by BQ (inset), indicating a combined dynamic and static quenching mechanism, due to the lack of overlapping Stern-Volmer plots for the steady-state and photoluminescence lifetime experiments and the upward curvature of the fractional photoluminescence.[194] Based on the Stern-Volmer plots we obtained a static

quenching constant (KS) value of 8.82 x 10^2 M^{-1} and a dynamic quenching constant (KD) value of 6.99 x 10^2 M^{-1}.

8.4 Polymer Nanocomposites

As the surface of ZrP can be modified to have alkyl or aryl functionality, it is expected that the resulting materials can be designed for use as fillers in a variety of polymers to improve compatibility between the organic and inorganic components. ZrP has been used in the past for inorganic fillers in polymers, but most approaches involved exfoliation to disperse individual nanosheets throughout the polymer, intercalation of the monomer within the layers of ZrP followed by polymerization, synthesis of an organic derivative of ZrP to make the particles compatible with the polymer, or direct synthesis of ZrP inside ionic polymers by addition of phosphoric acid to a Zr (IV) exchanged polymer.[48, 55, 69, 78, 120, 195-197] Using surface modification a novel organic derivative can be synthesized in which α-ZrP can be dispersed within the polymer without delamination of the layers and without changing the interlayer functionality.

8.4.1 Effect of Particle Size on Composites

Initially 1,2-epoxyoctadecane/ZrP was used to make polymer nanocomposites with polystyrene. Polystyrene is highly hydrophobic and the C_{18} alkyl chain of 1,2-epoxyoctadecane was expected to impart hydrophobic character on the nanoparticles and

enable them to disperse well in the polymer. Using surface modification particles can now be dispersed within polymers without altering the interlayer or delaminating the particles. As the full particles will be intact within the polymer matrix it is of interest how the size of the particles will affect the properties of the composites. In this case we are mainly concerned with the thermal stability of the composites, however other properties such as the mechanical strength should also be investigated in the future. Identical composites were prepared using 12M reflux and 3MT ZrP surface modified with 1,2-epoxyoxtadecane in order to determine the impact the particle size on the composites.

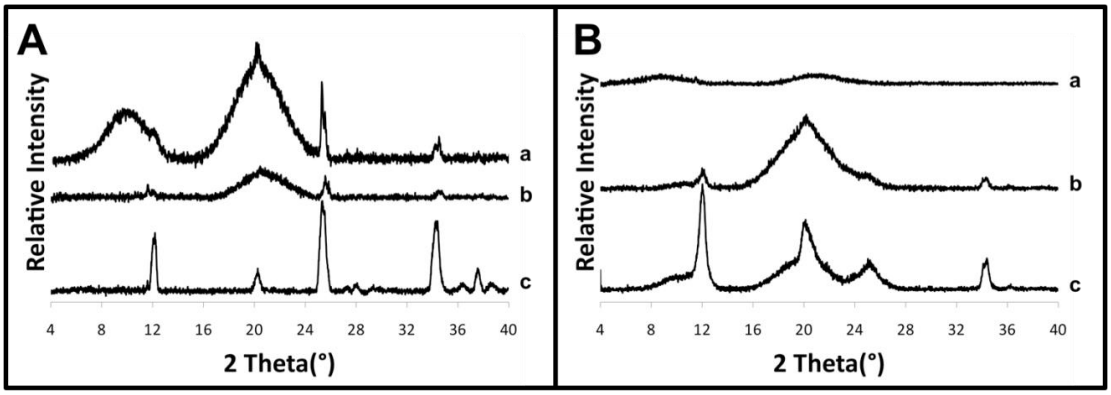

Figure 114. XRPD of 1,2-epoxyoctadecane/ZrP composites prepared with (A) 12M Reflux and (B) 3MT ZrP at loadings of (a) 1%, (b), 5%, and (c) 25%.

Initially the composite films were characterized by XRPD, **Figure 114**. The PS film is amorphous and yields no diffraction other than the halo observed as a result of the

sample holder (*ca.* 16°-25° 2 theta), therefore all peaks present in the powder pattern are a result of the SO/ZrP dispersed within the polymer matrix. XRPD patterns of the materials prepared with crystalline ZrP show intense reflections even at lower loading levels. The signal pertaining to the d-spacing of ZrP is observed in loadings above 5%, however it is difficult to resolve in lower loadings. The reflection at 2 theta of *ca.* 34° also appears in all of the samples while the reflection at *ca.* 20° is only observed in the 25% case. The diffraction patterns of the composite films prepared with 3MT ZrP are somewhat similar. In the case of the 1% loading no definite reflections can be observed other than at *ca.* 34°. In all other samples the reflections can be observed at *ca.* 12°, 20°, 25°, and 34° 2 theta. Although both samples share the same reflections, the reflections in the 3MT case are much broader and less well defined. This is due solely to the crystallinity of the nanoparticles used for the composite. All the films diffract the x-rays therefore it can be said that the ZrP nanoparticles are dispersed within the polymer matrix. Additionally, the particles must be intact and possess long range order in order to diffract x-rays so it is confirmed that the particles have not been delaminated.

TGA of the all samples prepared contained three main weight loss events, **Figure 115**. All weight loss occurring below 200°C was attributed to the residual toluene that was incorporated into the composite by strong interactions with the polystyrene. The second weight loss event is that of the polystyrene and the surface modifier of ZrP. Lastly, a small weight loss event can be observed above 500°C corresponding to the condensation of the phosphates in ZrP to pyrophosphates. It should be noted that the temperature

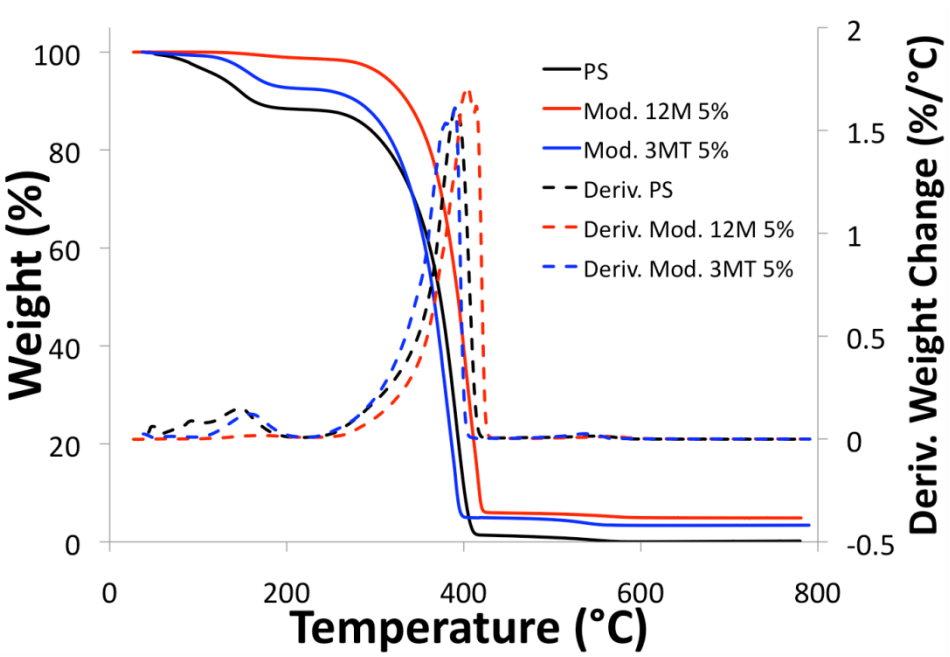

Figure 115. TGA of PS-1,2-epoxyoctadecane composites made with different ZrP and the PS film.

range of the three processes listed fluctuate based on the loading of the nanofillers within the polymer. In order to determine the stabilization effects of the fillers the maximum of the derivative signal pertaining to the decomposition of the polystyrene was used. In the case of the 1% loading it was found that the composite is actually destabilized when compared to the PS film itself. The thermal stability of the 5% loading is slightly higher than PS but the 25% composite has a nearly identical thermal stability as PS. Initially these results reveal that the optimal loading for these fillers is probably somewhere around the range of 5%. The extremely low loadings seem to add no stability ,however they manage to cause slight destabilization. It is possible that although the loading is somewhat low, there may be enough nanoparticles present to disrupt some of the

polymer-polymer interactions resulting in a destabilization. The particles are relatively large and at such a high loading level they are certainly disrupting the stabilizing interactions of the polymer. A similar trend can be observed for the samples prepared with 3MT ZrP. The 1% loading level is destabilized compared to the PS film whereas both the 5% and 25% loadings have nearly identical thermal stabilities as the original PS material. It is interesting to note that although the 1% loading is destabilized in the 3MT case it is more stable than the 12M ref case by about 10°C. This seems to suggest that the smaller particles interfere with the polymer matrix to a lesser extent than the large particles; this is reasonable based upon the thickness of the particles discussed in Chapter III. The loss of thermal stability observed in some cases is not desirable for the composites and is likely due to the lack of a strong interaction between the surface group and the polymer matrix. The surface group therefore must be tailored to maximize the interaction with the polymer.

8.4.2 Effect of Surface Group on Composites

It was previously shown that ZrP of different sizes could be used to successfully synthesize polymer nanocomposites. Ultimately it was found that the smaller particle size may be less of a hindrance to the polymer-polymer interactions, however it is necessary for the surface group to have a strong interaction with the polymer in order to avoid destabilization of the composite. In this case composites will be made with a

constant particle size (3M ZrP) and loading level (1%) while altering the surface group to evaluate which group interacts more strongly with the PS.

Table 11. Thermal data on 1% wt. composites prepared with ZrP modified with different epoxides.

Ligand	Derivative Maxima (°C)
none (PS)	391
cyclohexene oxide	345
styrene oxide	393
1,2-epoxy-9-decene	383
1,2-epoxydodecane	353
1,2-epoxyoctadecane	367

Table 11 displays the maximum of the derivative peak corresponding to the decomposition of the polymer. It can be noted that in all cases in which an alkyl modifier was used the composite is destabilized, as was the case in the initial investigation. The modifiers that have pi bonds or aryl functionality are substantially more stable. The 1,2-epoxy-9-decene displays a maximum at 383°C, this is less than a 10° difference than PS and more than a 30°C increase when compared to the C_{12} epoxide. It can therefore be supposed that the stability comes from the alkene functionality at the distal end of the

alkyl chain. It is likely that pi-pi interactions can be formed between the surface ligand and the polymer causing the stabilizing effect. Styrene oxide displays the highest stability; even at the 1% loading level it is more stable than PS. The styrene oxide should form the strongest possible interaction with the polymer out of all the groups, as they possess the same styrene functionality. In this case there are several pi bonds per modifier that can interact strongly with the polymer. Based on the results it is confirmed that the surface ligand does play a part in the stabilization of the composite. The ligand then should be selected based upon its interaction with the polymer matrix.

8.4.3 SO/ZrP Composites

It was previously demonstrated that styrene oxide formed the strongest interaction with polystyrene within the polymer composites. A series of composites will now be prepared using SO/ZrP at various loading levels. TGA reveals the same general trend as in other cases, **Figure 116**. Loading percentages 1% and 5% have nearly identical stabilities as the PS film while the 10% loading appears to be destabilized by about 20°C. Differing from the other cases is the fact that at the high loading of 25% the composite is stabilized rather than destabilized. Previously with the 1,2-epoxyoctadecane it was observed that a high loading produced thermal destabilization, however in that case the surface group did not have strong interactions with the ligand. It is likely that with styrene oxide increasing the loading of the nanofillers increases the amount of strong interactions between the surface and the polymer, resulting in the noted stabilization.

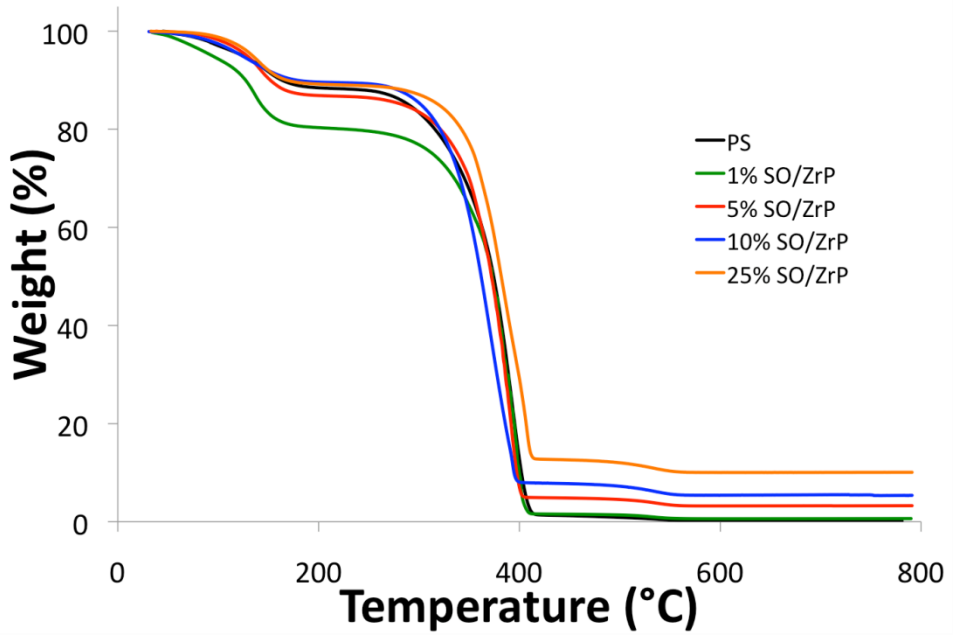

Figure 116. TGA of PS film and SO/ZrP of various loadings.

Although the 25% case is the most stable, such a high loading is typically not ideal for the formation of nanocomposites. It should be noted however that in this case the maximal loading of the nanofillers within the composite seems to be higher than other methods of synthesizing composites from ZrP. High percentages of the fillers can be dispersed neatly in the polymer due to the interactions of the surface with the polymer. In other cases the filler may not have such an interaction therefore a saturation point occurs where the concentration becomes too high for the fillers to be distributed throughout the polymer somewhat regularly.

8.4.4 Intercalation as a Method to Add Functionality to Composites

It has now been verified that surface modified ZrP can be used as a filler in a polymer matrix and that surface groups with strong interactions with the polymer produce more stable composites. The fact that the particles remain intact and the interlayer of ZrP remains unaltered allows for the unique opportunity to add specific functionality to the composite by intercalation into ZrP before it is dispersed in the polymer. The following is demonstrated with polystyrene and SO/ZrP loaded with ammonium ions (SO/ NH_4^+@ZrP) as a potential fire resistant polymer nanocomposite.

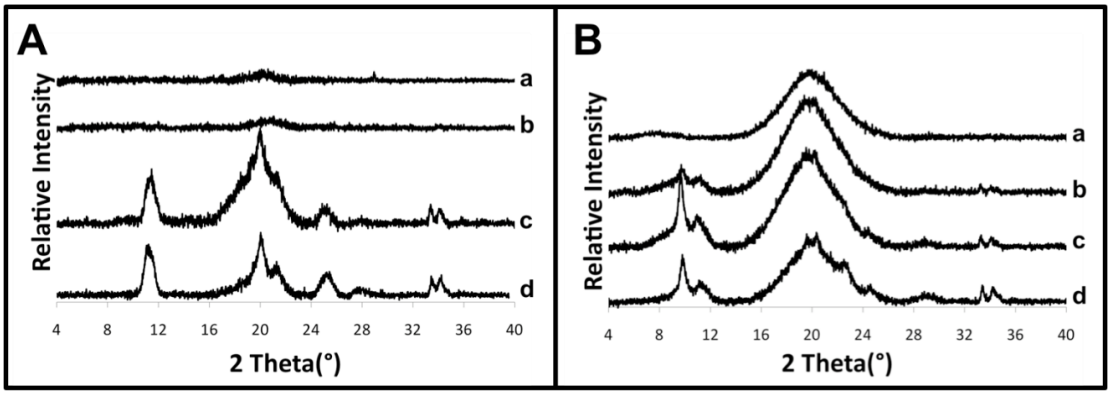

Figure 117. XRPD of (A) half loaded and (B) full loaded SO/NH_4^+@ZrP at loadings of (a) 1%, (b) 5%, (c) 10%, and (d) 25%.

Two phases are possible when intercalating ammonium ions into ZrP, the fully loaded phase in which there are 2 moles of ammonium ion per Zr, and the half loaded phase which has a 1:1 ratio of Zr:NH_4^+.[188, 189] Composites were successfully prepared for both phases and the effect of the encapsulated molecule on the thermal stability of the nanocomposites was investigated. Initially the composite films were analyzed by XRPD. It can be observed in **Figure 117** that as the percentage loading of SO/NH_4^+@ZrP increases the diffraction of the films increases. In all cases diffraction was observed from the film that was indicative of the corresponding ammonium intercalated ZrP phase, this verifies that the particles remain intact and are not delaminated. For the half loaded phase the initial reflection occurs at a 2 theta value of *ca.* 11.3°, however this broad signal is only present in the 10% and 25% loading levels. Loadings of 5% and below display no diffraction in the half loaded case. Additional signals can be observed at 2 theta values of 19°, 20°, 25°, and 34°. The fully loaded phase shows a d-spacing of 9.03 Å, which is a result of the pure phase of the ammonium ion intercalated into the nanoplatelets. This peak is followed by a broad peak centered at a 2-theta value of *ca.* 11°. This peak is likely a combination of two peaks with d values of 8.2 Å and 7.6 Å which were reported by Hasegawa and Aoki as the initial indication of the re-exchange of protons into NH_4^+@ZrP.[188] The intercalation of ammonium ion within ZrP is highly ionic in nature, each ammonium is surrounded by the maximum number of negative charges and the water molecules positioning is based upon the location of the ammonium.[189] It is likely that upon heating the motion of water molecules could have caused reorganization within the layer facilitating the production of the new phases.

Other diffraction peaks of the SO/NH_4^+@ZrP starting material are also observed at 2 theta values between 20° and 25°, and at *ca.* 34°. In both cases it can be observed that the reflections of the composites are largely identical to that of the nanoparticles used. Ultimately the signals observed are slightly shifted when compared to the SO/ NH_4^+@ZrP particles themselves. The apparent shift is likely due to instrumental effects as one sample was analyzed in powder form and the other as a film.

Both the transparency and thermal stability of the nanocomposites was then investigated as seen in **Figure 118**. All composites appear to be transparent, however UV-visible spectroscopy was utilized to investigate the level of transparency. The half loaded particles were found to be less transparent than PS in all cases, with the 5% composite coming the closest to PS. The composites prepared with the fully loaded NH_4^+@ZrP displayed much different behavior than those prepared with the half loaded material. Composites with nanoparticle loadings of 5% and below were shown to retain the transparency of the original PS film whereas a decrease in transparency was observed for loadings of 10% and above. The decreased transparency and red shift observed in the onset of the spectra can be attributed to aggregation of nanoparticles within the polymer.[198, 199] Overall, the nanoparticles are dispersed somewhat uniformly in the polymer but some aggregation is likely to occur at higher loading levels. In the case of the half loaded particles it appears that this aggregation may be present in all cases.

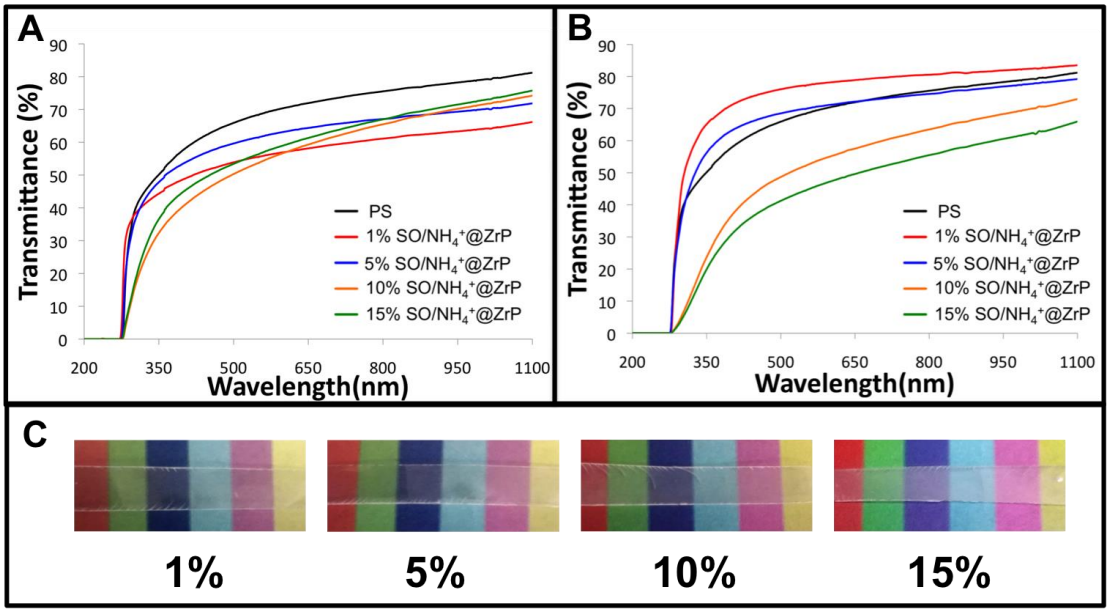

Figure 118. UV-visible spectra of (A) half loaded and (B) full loaded NH_4^+@ZrP along with images of the fully loaded composites (C).

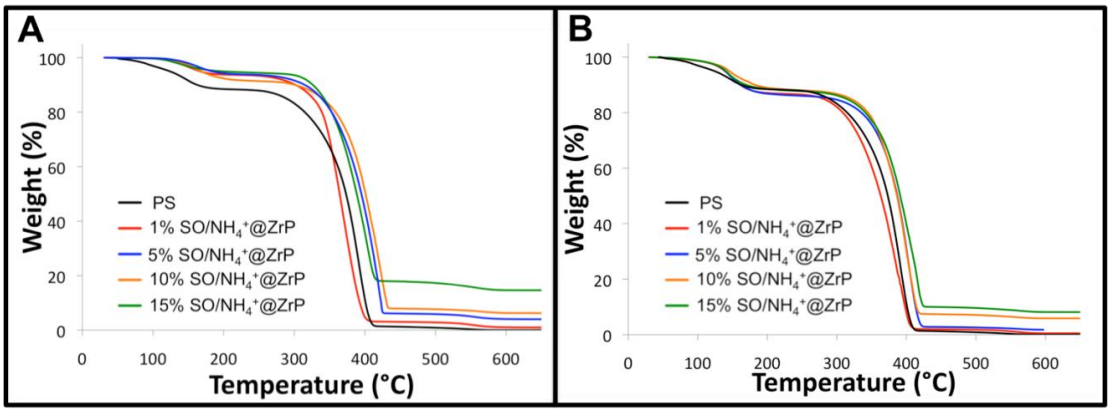

Figure 119. TGA of (A) half loaded and (B) full loaded NH_4^+@ZrP.

TGA was utilized to study the thermal stability of the nanocomposites and the influence of the intercalated guest into the nanofillers on the thermal stability, **Figure 119**. The

derivative of the thermograms reveals three weight loss events. The first event ranging roughly from 110 °C to 170 °C can be attributed to the toluene that is incorporated in the film due to strong interactions with the polystyrene and the water in the interlayer of ZrP. The second decomposition is that of the polymer and occurs anywhere between 360 °C and 411 °C for polystyrene but fluctuates depending on the loading of the ZrP. Lastly, from 500 °C to 550 °C the condensation of ZrP to zirconium pyrophosphate can be observed verifying that the particles were not delaminated and that the full particle was dispersed in the composite. The thermal data of all composites is shown for comparison in **Table 12** using the maxima of the derivative and in **Table 13** using the maximum ΔT. In all cases it is observed that the intercalated composites are more stable than PS and the SO/ZrP composites, not only is the thermal decomposition delayed but the temperature at which the decomposition ends is increased due to the presence of the nanofillers. This suggests that the presence of NH_4^+ in the composite adds thermal stability. The results demonstrate that it is possible to add functionality into composites through intercalation of a surface modified nanoparticle without hindering the thermal stability of the composite, in this case the stability was improved upon. Utilizing this approach numerous combinations of surface groups and intercalated molecules can be utilized to make nanocomposites for particular applications.

Table 12. Maxima of derivative corresponding to polymer degradation in the composites.

	Maxima of Derivative (°C) at various loadings				
Sample	1%	5%	10%	15%	25%
SO/ZrP	393	390	371	--	406
SO/ NH_4^+@ZrP (half)	379	414	415	--	401
SO/ NH_4^+@ZrP (full)	387	400	401	416	401

Table 13. Maximum temperature change observed in the synthesized composites relative to PS.

	ΔT Max (°C) at various loadings				
Sample	1%	5%	10%	15%	25%
SO/ZrP	1	2.3	6.6	--	16.6
SO/ NH_4^+@ZrP (half)	8.9	24.9	34.4	--	29.8
SO/ NH_4^+@ZrP (full)	4.8	24.7	19.6	30.8	17.3

8.5 Conclusion

Multiple examples of systems made using the surface modification of ZrP have been demonstrated. Surface chemistry allows some new applicability of ZrP, but it can also be used to improve all current applications. The variety of different ligands and functional groups that can interact with the surface make this a desirable technique. Also, the ability to select and alter the interlayer and surface group allows particles to be designed for a wide variety of applications.

CHAPTER IX

SUMMARY AND FUTURE WORK

9.1 Summary

The previous chapters have demonstrated that ZrP can be surface functionalized by covalent attachment of molecules directly to the surface. This functionalization is possible with nano-sized ZrP of various sizes. Additionally, the functionalization is possible in the micron sized and even single crystal particles, however successful functionalization is difficult to detect in the cases. Covalent attachment of epoxides to the surface was found to be successful using a typical reflux reaction but when a microwave synthetic method was used covalent attachment was not verified. The polymerization of epoxides on the exterior of ZrP was also presented for the first time. In regards to silanes it was also found that P-O-Si linkages were formed between the reactive molecule and the surface, however in this case the direct linkages between the silane and surface are not the predominant bonding. Siloxane bond formation between the silanes produces most of the coverage whereas there are only a few sites in which the phosphorus atoms are bonded to the silane through the oxygen bridge.

Additionally, it was demonstrated that functionalization of the surface could be achieved and through an ion exchange and self-assembly based procedure. Metal ions of various valency were shown to exclusively replace the surface protons of ZrP and deposit a

monolayer of ions on the surface. This monolayer was subsequently functionalized with phosphonic acids. The phosphates of the phosphonic acid were found to bridge between three surface metal ions.

The discussed surface modification techniques were then combined with the prior intercalation chemistry of ZrP in order to produce multifunctional nanoparticles. In this case the functionality of the interior was imparted through intercalation and the composition of the exterior of the particles was imparted through surface functionalization with the desired ligand. It was found that regardless of the intercalation mechanism that the particles could be successfully modified. It was also found that particles with a larger loading level tended to have a smaller uptake of modifier on the surface. Additionally, there was found to be a correlation between the stability of the modifier on the surface and the loading of the interlayer. In most cases no leaching of the interlayer molecule occurs during the surface modification reaction, however in the acid-base intercalation systems the pH should be monitored to avoid leaching. It was also demonstrated that in the synthesis of multifunctional ZrP particles that the order of the surface modification and intercalation can be varied depending on the compounds used.

Lastly, the applicability of both surface modified and multifunctional ZrP was demonstrated. The surface ion exchange and ligand functionalization reactions allow for the formation of layer-by-layer assemblies from the nanoparticle surface. Within these

assemblies both the ligands and metal ions can be altered to design customizable architectures on the surface. The possibility of conducting photo-induced electron transfer reactions in non-polar media was demonstrated using multifunctional ZrP consisting of hydrophobic groups on the surface and a photoactive molecule within the interlayer. Polymer nanocomposites with fire retardant functionality were designed through intercalation of ammonium ions into ZrP surface modified with styrene groups. The resulting materials possessed an increased thermal stability and the particles were found to be well dispersed within the polymer matrix.

9.2 Future Work

In regards to the work presented for ZrP in this dissertation there are some areas that could be addressed immediately in the future. Preliminary experiments have been conducted with a number of phosphate and phosphonate ligands other than the ODPA and BPBPA presented herein. For example, an azido phosphonic acid and alkyne phosphate compound were synthesized and deposited on the surface for click conjugation reactions. Additionally, epoxide functionality can be added to many ligands like 1,10-phenanthroline. In this case metallic complexes can be covalently attached to the surface for a number of applications including catalysis. Much investigation has gone into the prospect of using nanomaterials as drug delivery vehicles the past few decades; more recently inorganic layered materials have found to be useful in this area, leading to investigations with ZrP. It was found that several molecules with biological activity

could be intercalated into ZrP including insulin, cisplatin, and doxorubicin. ZrP is ideal as a drug delivery vehicle due to its tunable particle size, the ability to load high levels of compounds within the interlayer, and non-toxicity. Several successful studies have shown that using ZrP as a carrier for drugs drastically increases the IC_{50} of the drugs and is more effective than when the drug is used by itself. To further improve the system we propose that surface chemistry can be used on the drug loaded ZrP in order to target the particles exclusively to cancerous cells while avoiding healthy tissues, increasing the retention time of the drugs within the body, and altering the solubility. Samples have been synthesized in which polyethylene glycol has been successfully bonded to the surface of ZrP. Although cellular work has not been completed on these type samples it is part of future work. The polymer can be attached either by the synthesis of a polyethylene glycol phosphonic acid or epoxide.

An additional area of interest is the use of fluorescent and magnetic materials for biological imaging applications. In this case the particles are inserted to the area of interest and the fluorescence is used to image the area. Additionally the magnetic functionality allows control of the particles and the imager to move them to the desired location. This type of material was displayed in the dissertation however the particles have not been tested within the body as of yet.

Lastly, it has been well demonstrated that intercalated ZrP can be used to make composites. In addition photoinduced electron transfer reactions have been

demonstrated. The two concepts can be combined in which case the polymer can be the electron acceptor. The resulting materials can be used for fuel cells or batteries.

Other future work mainly deals with expanding the presented results to additional tetravalent metal phosphates and inorganic layered materials. First of all, tetravalent metal phosphates exist with a variety of ions including Ti(IV), Hf(IV), and Sn(IV) among others. All the structures are identical, with the bond distances fluctuating only because the size of the metal ion used. Although the structures are the same the stability of the various compounds is somewhat different. In all cases it is expected that the surface reactions presented should be possible with these systems as well. Changing the metal ion of the phosphate may be an additional way to control the character of the resulting nanoparticle. In addition to the α type structures, tetravalent metal phosphates exist in other forms as well with the γ being one of the predominate phases. The surface structure of γ-ZrP differs from that of α because the surface phosphates each possess two hydroxyl groups. Similar functionalization reactions should be possible for the γ phase as those presented in this dissertation. The uptake of the modifier is expected to be greater for the γ-ZrP. The metal ion functionalization of γ-ZrP should yield interesting and diverse structures due to the dual hydroxyl group of the phosphates.

As metal phosphates are cation exchangers there are a number of other layered materials that can exchange anions or other species. The same surface functionalization can be applied to these materials, and when coupled with intercalation can lead to

multifunctional particles that are unique and not possible with other systems. The investigation of this chemistry with systems such as layered double hydroxides and clays should be carried out.

REFERENCES

1. Solin, S. A., Clays and Clay Intercalation Compounds:Properties and Physical Phenomena. *Annual Review of Materials Science* **1997,** 27, 89-115.

2. Clearfield, A.; Costantino, U., *Layered Metal Phosphates and their Intercalation Chemistry*. Pergamon: New York, 1996; Vol. 7, p 107-149.

3. Gao, M.-R.; Xu, Y.-F.; Jiang, J.; Yu, S.-H., Nanostructured Metal Chalcogenides: Synthesis, Modification, and Applications in Energy Conversion and Storage Devices. *Chemical Society Reviews* **2013,** 42, 2986-3017.

4. Aldakov, D.; Lefrancois, A.; Reiss, P., Ternary and Quaternary Metal Chalcogenide Nanocrystals: Synthesis, Properties and Applications. *Journal of Materials Chemistry C* **2013,** 1, 3756-3776.

5. Viciu, L.; Caruntu, G.; Royant, N.; Koenig, J.; Zhou, W. L.; Kodenkandath, T. A.; Wiley, J. B., Formation of Metal Anion Arrays within Layered Perovskite Hosts. Preparation of a Series of New Metastable Transition-Metal Oxyhalides, (MCl)$LaNb_2O_7$ (M = Cr, Mn, Fe, Co). *Inorganic Chemistry* **2002,** 41, 3385-3388.

6. Halbert, T. R.; Johnston, D. C.; McCandlish, L. E.; Thompson, A. H.; Scanlon, J. C.; Dumesic, J. A., Intercalation of Organometallic Compounds into Layered Transition Metal Oxyhalides. *Physica B+C* **1980,** 99, 128-132.

7. Hong, Z.; Wei, M., Layered Titanate Nanostructures and their Derivatives as Negative Electrode Materials for Lithium-ion Batteries. *Journal of Materials Chemistry A* **2013,** 1, 4403-4414.

8. Zümreoglu-Karan, B.; Ay, A., Layered Double Hydroxides-Multifunctional Nanomaterials. *Chem. Pap.* **2012,** 66, 1-10.

9. Wang, Q.; O'Hare, D., Recent Advances in the Synthesis and Application of Layered Double Hydroxide (LDH) Nanosheets. *Chemical Reviews* **2012,** 112, 4124-4155.

10. Clearfield, A.; Demadis, K. D., *Metal Phosphonate Chemistry From Synthesis to Applications*. 1st ed.; RSC Publishing: Cambridge, 2012.

11. Alberti, G.; Costantino, U., Layered Solids and Their Intercalation Chemistry. In *Solid-state Supramolecular Chemistry: Two- and Three-dimensional Inorganic Networks*, First ed.; Alberti, G.; Bein, T., Eds. Elsevier: New York, 1996; Vol. 7, pp 1-23.

12. Solin, S. A., Novel Properties of Intercalated Layered Solids: from Graphite to Sheet Silicates. *Journal of Molecular Catalysis* **1984,** 27, 293-303.

13. Poojary, D. M.; Shpeizer, B.; Clearfield, A., X-Ray Powder Structure and Rietveld Refinement of γ-Zirconium Phosphate, $Zr(PO_4)(H_2PO_4)\bullet 2H_2O$. *Journal of the Chemical Society, Dalton Transactions* **1995**, 111-113.

14. Clearfield, A.; Stynes, J. A., The Preparation of Crystalline Zirconium Phosphate and Some Observations on its Ion Exchange Behaviour. *Journal of Inorganic and Nuclear Chemistry* **1964,** 26, 117-129.

15. Troup, J. M.; Clearfield, A., Mechanism of Ion Exchange in Zirconium Phosphates. 20. Refinement of the Crystal Structure of α-Zirconium Phosphate. *Inorganic Chemistry* **1977,** 16, 3311-3314.

16. Bringley, J. F.; Liebert, N. B., Controlled Chemical and Drug Delivery via the Internal and External Surfaces of Layered Compounds. *Journal of Dispersion Science and Technology* **2003,** 24, 589-605.

17. Alberti, G.; Costantino, U., Recent Progress in the Intercalation Chemistry of Layered α-Zirconium Phosphate and its Derivatives, and Future Perspectives for their use in Catalysis. *Journal of Molecular Catalysis* **1984,** 27, 235-250.

18. Clearfield, A.; Duax, W. L.; Medina, A. S.; Smith, G. D.; Thomas, J. R., Mechanism of Ion Exchange in Crystalline Zirconium Phosphates. I. Sodium Ion Exchange of α-Zirconium Phosphate. *Journal of Physical Chemistry* **1969,** 73, 3424-3430.

19. Clearfield, A.; Medina, A. S., Mechanism of Ion Exchange in Crystalline Zirconium Phosphates. V. Thermodynamic Treatment of the Hydrogen ion-Sodium ion Exchange of α-Zirconium Phosphate. *Journal of Physical Chemistry* **1971,** 75, 3750-3756.

20. Alberti, G.; Casciola, M.; Costantino, U.; Vivani, R., Layered and Pillared Metal(IV) Phosphates and Phosphonates. *Advanced Materials* **1996,** 8, 291-303.

21. Kullberg, L.; Clearfield, A., Mechanism of Ion Exchange in Zirconium Phosphates. 32. Thermodynamics of Alkali Metal Ion Exchange on Crystalline α-Zirconium Phosphate. *Journal of Physical Chemistry* **1981,** 85, 1585-1589.

22. Clearfield, A.; Djurić, Z., On the Mechanism of Ion Exchange in Zirconium Phosphates—XXV. Exchange of Surface Protons with Ammonium ion. *Journal of Inorganic and Nuclear Chemistry* **1979,** 41, 903-904.

23. Alberti, G.; Bertrami, R.; Costantino, U.; Gupta, J. P., Crystalline Insoluble Acid Salts of Tetravalent Metals—XXVI: Ammonium and Ammonia Uptake on Different Ionic Forms of Crystalline Zirconium Phosphate. *Journal of Inorganic and Nuclear Chemistry* **1977,** 39, 1057-1060.

24. Alberti, G.; Casciola, M.; Costantino, U.; Levi, G.; Ricciardi, G., On the Mechanism of Diffusion and Ionic Transport in Crystalline Insoluble Acid Salts of Tetravalent Metals-I Electrical Conductance of Zirconium bis (monohydrogen ortho-phosphate) monohydrate with a Layered Structure. *Journal of Inorganic and Nuclear Chemistry* **1978,** 40, 533-537.

25. Clearfield, A., Inorganic Ion Exchangers with Layered Structures. *Annual Review of Materials Science* **1984,** 14, 205-229.

26. Alberti, G.; Bernasconi, M. G.; Casciola, M.; Costantino, U., Ion Exchange of Some Divalent and Trivalent Cations on the Surface of Zirconium Acid Phosphate Micro-crystals. *Journal of Chromatography A* **1978,** 160, 109-115.

27. Kijima, T., Direct Preparation of θ-Zirconium Phosphate. *Bulletin of the Chemical Society of Japan* **1982,** 55, 3031-3032.

28. Martí, A. A.; Colón, J. L., Direct Ion Exchange of Tris(2,2‘-bipyridine)ruthenium(II) into an α-Zirconium Phosphate Framework. *Inorganic Chemistry* **2003,** *42*, 2830-2832.

29. Sun, L.; O'Reilly, J. Y.; Kong, D.; Su, J. Y.; Boo, W. J.; Sue, H. J.; Clearfield, A., The Effect of Guest Molecular Architecture and Host Crystallinity Upon the

Mechanism of the Intercalation Reaction. *Journal of Colloid and Interface Science* **2009,** 333, 503-509.

30. Alberti, G.; Costantino, U.; Gill, J. S., Crystalline Insoluble Acid Salts of Tetravalent Metals-XXIII: Preparation and Main Ion Exchange Properties of Highly Hydrated Zirconium bis monohydrogen orthophosphates. *Journal of Inorganic and Nuclear Chemistry* **1976,** 38, 1733-1738.

31. Costantino, U., Intercalation of Alkanols and Glycols into Zirconium(IV) hydrogenphosphate monohydrate. *Journal of the Chemical Society, Dalton Transactions* **1979**, 402-405.

32. Amphlett, C. B.; McDonald, L. A., Ion-sieve Properties of Zirconium Phosphate. *Proceedings of the Chemical Society* **1962**, 276.

33. Michel, E.; Weiss, A., *Z. Naturforsch.* **1965,** 20 B, 1307-1308.

34. Clearfield, A.; Smith, G. D., The Crystallography and Structure of α-Zirconium bis(monohydrogen orthophosphate) monohydrate. *Inorganic Chemistry* **1969,** 8, 431-436.

35. Yamanaka, S., Synthesis and Characterization of the Organic Derivatives of Zirconium Phosphate. *Inorganic Chemistry* **1976,** 15, 2811-2817.

36. Behrendt, D.; Beneke, K.; Lagaly, G., Intercalation Compounds of Zirconium Phosphate. *Angew. Chem., Int. Ed. Engl.* **1976,** 15, 544-545.

37. Hasegawa, Y.; Akimoto, T.; Kojima, D., Intercalation of Pyridine and Quinoline into α-Zirconium Phosphate. *J Incl Phenom Macrocycl Chem* **1994,** 20, 1-12.

38. Clearfield, A.; Tindwa, R. M., On the Mechanism of Ion Exchange in Zirconium Phosphates-XXI Intercalation of Amines by α-Zirconium Phosphate. *Journal of Inorganic and Nuclear Chemistry* **1979,** 41, 871-878.

39. MacLachlan, D. J.; Morgan, K. R., Phosphorus-31 Solid-State NMR Studies of the Structure of Amine-intercalated α-Zirconium Phosphate. 2. Titration of α-Zirconium with n-propylamine and n-butylamine. *Journal of Physical Chemistry* **1992,** 96, 3458-3464.

40. MacLachlan, D. J.; Morgan, K. R., Phosphorus-31 Solid-State NMR Studies of the Structure of Amine-intercalated α-Zirconium Phosphate: Reaction of α-Zirconium Phosphate with Excess Amine. *Journal of Physical Chemistry* **1990,** 94, 7656-7661.

41. Jacobson, A. J.; Johnson, J. W.; Brody, J. F.; Scanlon, J. C.; Lewandowski, J. T., Redox Intercalation Reactions of Vanadium Oxide Phosphate dihydrate ($VOPO_4.2H_2O$) with Mono- and Divalent Cations. *Inorganic Chemistry* **1985,** 24, 1782-1787.

42. Santiago, M. E. B.; Declet-Flores, C.; Díaz, A.; Vélez, M. M.; Bosques, M. Z.; Sanakis, Y.; Colón, J. L., Layered Inorganic Materials as Redox Agents:Ferrocenium-Intercalated Zirconium Phosphate. *Langmuir* **2007,** 23, 7810-7817.

43. Costantino, U.; Marmottini, F., Intercalation of Insulating Polymers into Layered Zirconium Phosphates. *Materials Chemistry and Physics* **1993,** 35, 193-198.

44. Hasegawa, Y.; Kontani, S.; Tomita, I., Direct and Stepwise Intercalation of Alkylalcohols intoα-Zirconium Phosphate. *J Incl Phenom Macrocycl Chem* **1993,** 16, 329-337.

45. Melánová, K.; Beneš, L.; Zima, V.; Svoboda, J.; Trchová, M.; Dybal, J., Intercalation of 1,2-Alkanediols into α-Zirconium Hydrogenphosphate. *Journal of Inclusion Phenomena and Macrocyclic Chemistry* **2007,** 58, 95-101.

46. Ma, R.; Sasaki, T., Nanosheets of Oxides and Hydroxides: Ultimate 2D Charge-Bearing Functional Crystallites. *Advanced Materials* **2010,** 22, 5082-5104.

47. Nicolosi, V.; Chhowalla, M.; Kanatzidis, M. G.; Strano, M. S.; Coleman, J. N., Liquid Exfoliation of Layered Materials. *Science* **2013,** 340.

48. Sun, L.; Boo, W. J.; Sun, D.; Clearfield, A.; Sue, H.-J., Preparation of Exfoliated Epoxy/α-Zirconium Phosphate Nanocomposites Containing High Aspect Ratio Nanoplatelets. *Chemistry of Materials* **2007,** 19, 1749-1754.

49. Kaschak, D. M.; Johnson, S. A.; Hooks, D. E.; Kim, H.-N.; Ward, M. D.; Mallouk, T. E., Chemistry on the Edge: A Microscopic Analysis of the Intercalation, Exfoliation, Edge Functionalization, and Monolayer Surface Tiling Reactions of α-Zirconium Phosphate. *Journal of the American Chemical Society* **1998,** 120, 10887-10894.

50. Alberti, G.; Casciola, M.; Costantino, U., Inorganic Ion-exchange Pellicles Obtained by Delamination of α-Zirconium Phosphate Crystals. *Journal of Colloid and Interface Science* **1985,** 107, 256-263.

51. Alberti, G.; Marmottini, F., Preparation of Layered α-Zirconium Phosphate with a Controlled Degree of Hydrolysis via Delamination Procedure. *Journal of Colloid and Interface Science* **1993,** 157, 513-515.

52. Kim, H.-N.; Keller, S. W.; Mallouk, T. E.; Schmitt, J.; Decher, G., Characterization of Zirconium Phosphate/Polycation Thin Films Grown by Sequential Adsorption Reactions. *Chemistry of Materials* **1997,** 9, 1414-1421.

53. Bhambhani, A.; Kumar, C. V., Tuning the Properties of Hb Intercalated in the Galleries of α-ZrP with Ionic Strength: Improved Structure Retention and Enhanced Activity. *Chemistry of Materials* **2006,** 18, 740-747.

54. Kumar, C. V.; Chaudhari, A., Proteins Immobilized at the Galleries of Layered α-Zirconium Phosphate: Structure and Activity Studies. *Journal of the American Chemical Society* **2000,** 122, 830-837.

55. Sue, H. J.; Gam, K. T.; Bestaoui, N.; Spurr, N.; Clearfield, A., Epoxy Nanocomposites Based on the Synthetic α-Zirconium Phosphate Layer Structure. *Chemistry of Materials* **2003,** 16, 242-249.

56. Alberti, G.; Costantino, U.; Allulli, S.; Tomassini, N., Crystalline $Zr(R\text{-}PO_3)_2$ and $Zr(R\text{-}OPO_3)_2$ Compounds (R = organic radical): A New Class of Materials Having Layered Structure of the Zirconium Phosphate Type. *Journal of Inorganic and Nuclear Chemistry* **1978,** 40, 1113-1117.

57. Poojary, M. D.; Hu, H. L.; Campbell, F. L.; Clearfield, A., Determination of Crystal Structures from Limited Powder Data Sets: Crystal Structure of Zirconium Phenylphosphonate. *Acta Crystallographica Section B: Structural Science* **1993,** 49, 996-1001.

58. Alberti, G.; Costantino, U., Synthesis and Preliminary Characterization of Ion Exchange and Intercalation Behaviour of Zirconium Phosphate Phosphite with Layered Structure of α Type. *Gazzetta Chimica Italiana* **1983,** 113, 547.

59. Alberti, G.; Costantino, U.; Környei, J.; Giovagnotti, M. L. L., Derivatives of α-Zirconium Phosphate with Two Different Functional Groups. *Reactive Polymers, Ion Exchangers, Sorbents* **1985,** 4, 1-10.

60. Alberti, G.; Costantino, U.; Perego, G., Structural Investigation on Layered α-Zirconium Phosphite and Zirconium Phosphate-Phosphites from X-ray Powder Data. *Journal of Solid State Chemistry* **1986,** 63, 455-460.

61. Wang, J. D.; Clearfield, A.; Guang-Zhi, P., Preparation of Layered Zirconium Phosphonate/Phosphate, Zirconium Phosphonate/Phosphite and Related Compounds. *Materials Chemistry and Physics* **1993,** 35, 208-216.

62. Dines, M. B.; Griffith, P. C., Surface Texture and Crystallinity Behavior of Zirconium bis(methylphosphonate). *Journal of Physical Chemistry* **1982,** 86, 571-576.

63. DiGiacomo, P. M.; Dines, M. B., Lamellar Zirconium Phosphonates Containing Pendant Sulphonic acid Groups. *Polyhedron* **1982,** 1, 61-68.

64. Clearfield, A.; Wang, Z., Organically Pillared Microporous Zirconium Phosphonates. *Journal of the Chemical Society, Dalton Transactions* **2002**, 2937-2947.

65. Clearfield, A., Unconventional Metal Organic Frameworks: Porous Cross-linked Phosphonates. *Dalton Transactions* **2008**, 6089-6102.

66. Burns, J. D.; Shehee, T. C.; Clearfield, A.; Hobbs, D. T., Separation of Americium from Curium by Oxidation and Ion Exchange. *Analytical Chemistry* **2012,** 84, 6930-6932.

67. Ortiz-Avila, C. Y.; Clearfield, A., Polyether Derivatives of Zirconium Phosphate. *Inorganic Chemistry* **1985,** 24, 1773-1778.

68. Casciola, M.; Capitani, D.; Donnadio, A.; Munari, G.; Pica, M., Organically Modified Zirconium Phosphate by Reaction with 1,2-Epoxydodecane as Host Material for Polymer Intercalation: Synthesis and Physicochemical Characterization. *Inorganic Chemistry* **2010,** 49, 3329-3336.

69. Pica, M.; Donnadio, A.; Troni, E.; Capitani, D.; Casciola, M., Looking for New Hybrid Polymer Fillers: Synthesis of Nanosized α-Type Zr(IV) Organophosphonates through an Unconventional Topotactic Anion Exchange Reaction. *Inorganic Chemistry* **2013,** 52, 7680-7687.

70. Roziere, J.; Jones, D. J.; Cassagneau, T., Crosslinked Layered Materials Formed by Intercalation of Octameric Siloxanes in Metal(IV) Hydrogen Phosphates. *Journal of Materials Chemistry* **1991,** 1, 1081-1082.

71. Katz, H. E.; Schilling, M. L.; Chidsey, C. E. D.; Putvinski, T. M.; Hutton, R. S., Quaterthiophenediphosphonic acid (QDP): a Rigid, Electron-rich Building Block for Zirconium-based Multilayers. *Chemistry of Materials* **1991,** 3, 699-703.

72. Sylvester, P.; Cahill, R.; Clearfield, A., Pillaring of Layered Tetravalent Metal Phosphates and Oxides Using (3-Aminopropyl)trimethoxysilane. *Chemistry of Materials* **1994,** 6, 1890-1898.

73. Takei, T.; Kumada, N.; Kinomura, N.; Nakayama, H.; Tsuhako, M., Preparation of Silylated α-Zirconium Phosphate and its Thermal Behavior. *Materials Research Bulletin* **2008,** 43, 111-119.

74. Mejia, A. F.; Diaz, A.; Pullela, S.; Chang, Y.-W.; Simonetty, M.; Carpenter, C.; Batteas, J. D.; Mannan, M. S.; Clearfield, A.; Cheng, Z., Pickering Emulsions Stabilized by Amphiphilic Nano-sheets. *Soft Matter* **2012,** 8, 10245-10253.

75. Kumar, C. V.; Asuncion, E. H.; Rosenthal, G., Formation of Static Anthracene Excimers at Hydrophobic Phosphate Surfaces. *Microporous Materials* **1993,** 1, 123-129.

76. Kumar, C. V.; Chaudhari, A.; Rosenthal, G. L., Enhanced Energy Transfer between Aromatic Chromophores Bound to Hydrophobically Modified Layered Zirconium Phosphate Suspensions. *Journal of the American Chemical Society* **1994,** 116, 403-404.

77. Kumar, C. V.; Asuncion, E. H.; Rosenthall, G., Static Pyrene Excimer Formation at Hydrophobic Zirconium Phosphate Surfaces: The Salt Effect. *Microporous Materials* **1993,** 1, 299-308.

78. Boo, W. J.; Sun, L.; Liu, J.; Clearfield, A.; Sue, H.-J., Effective Intercalation and Exfoliation of Nanoplatelets in Epoxy via Creation of Porous Pathways. *Journal of Physical Chemistry C* **2007,** 111, 10377-10381.

79. Zhang, R.; Hu, Y., Solvothermal Synthesis of Organically Modified α-Zirconium Phosphate-based Polystyrene Nanocomposites and Thermal Stability. *Journal of Applied Polymer Science* **2011,** 122, 593-598.

80. Cao, G.; Hong, H. G.; Mallouk, T. E., Layered Metal Phosphates and Phosphonates: from Crystals to Monolayers. *Accounts of Chemical Research* **1992,** 25, 420-427.

81. Queffélec, C.; Petit, M.; Janvier, P.; Knight, D. A.; Bujoli, B., Surface Modification Using Phosphonic Acids and Esters. *Chemical Reviews* **2012,** 112, 3777-3807.

82. Byrd, H.; Pike, J. K.; Talham, D. R., Inorganic Monolayers Formed at an Organic Template: a Langmuir-Blodgett Route to Monolayer and Multilayer Films of Zirconium Octadecylphosphonate. *Chemistry of Materials* **1993,** 5, 709-715.

83. Talham, D. R.; Seip, C. T.; Whipps, S.; Fanucci, G. E.; Petruska, M. A.; Byrd, H., Incorporating Inorganic Extended Lattice Structures into Langmuir—Blodgett Films: Comparing Metal Phosphonate LB Films to Their Solid-State Analogs. *Comments on Inorganic Chemistry* **1997,** 19, 133-151.

84. Lee, H.; Kepley, L. J.; Hong, H. G.; Akhter, S.; Mallouk, T. E., Adsorption of Ordered Zirconium Phosphonate Multilayer Films on Silicon and Gold Surfaces. *Journal of Physical Chemistry* **1988,** 92, 2597-2601.

85. Lee, H.; Kepley, L. J.; Hong, H. G.; Mallouk, T. E., Inorganic Analogs of Langmuir-Blodgett Films: Adsorption of Ordered Zirconium 1,10-decanebisphosphonate Multilayers on Silicon Surfaces. *Journal of the American Chemical Society* **1988,** 110, 618-620.

86. Putvinski, T. M.; Schilling, M. L.; Katz, H. E.; Chidsey, C. E. D.; Mujsce, A. M.; Emerson, A. B., Self-assembly of Organic Multilayers with Polar Order using Zirconium Phosphate Bonding between Layers. *Langmuir* **1990,** 6, 1567-1571.

87. Katz, H. E.; Scheller, G.; Putvinski, T. M.; Schilling, M. L.; Wilson, W. L.; Chidsey, C. E. D., Polar Orientation of Dyes in Robust Multilayers by Zirconium Phosphate-Phosphonate Interlayers. *Science* **1991,** 254, 1485-1487.

88. Byrd, H.; Whipps, S.; Pike, J. K.; Ma, J.; Nagler, S. E.; Talham, D. R., Role of the Template Layer in Organizing Self-assembled Films: Zirconium Phosphonate Monolayers and Multilayers at a Langmuir-Blodgett Template. *Journal of the American Chemical Society* **1994,** 116, 295-301.

89. Seip, C. T.; Talham, D. R., Organic/Inorganic Langmuir-Blodgett Films Based on Known Layered Solids: Characterization and Reaction of Cobalt octadecylphosphonate. *Materials Research Bulletin* **1999,** 34, 437-445.

90. Petruska, M. A.; Talham, D. R., Organic/Inorganic Langmuir−Blodgett Films Based on Metal Phosphonates. 3. An Azobenzene-Derivatized Phosphonic Acid Forms Continuous Lattice Layers with Divalent, Trivalent, and Tetravalent Metal Ions1. *Chemistry of Materials* **1998,** 10, 3672-3682.

91. Fang, M.; Kaschak, D. M.; Sutorik, A. C.; Mallouk, T. E., A "Mix and Match" Ionic−Covalent Strategy for Self-Assembly of Inorganic Multilayer Films. *Journal of the American Chemical Society* **1997,** 119, 12184-12191.

92. Petruska, M. A.; Fanucci, G. E.; Talham, D. R., Organic/Inorganic Langmuir−Blodgett Films Based on Metal Phosphonates: Preparation and

Characterization of Phenoxy- and Biphenoxy-Substituted Zirconium Phosphonate Films. *Chemistry of Materials* **1998,** 10, 177-189.

93. Akhter, S.; Lee, H.; Hong, H.-G.; Mallouk, T. E.; White, J. M., Structural Characterization of Multilayer Metal Phosphonate Film on Silicon using Angular-Dependent X-ray Photoelectron Spectroscopy. *Journal of Vacuum Science and Technology A* **1989,** 7, 1608-1613.

94. Petruska, M. A.; Fanucci, G. E.; Talham, D. R., Organic/Inorganic Langmuir–Blodgett Films based on Metal Phosphonates 2: Zirconium Phosphonate-based Alternating Layer Films. *Thin Solid Films* **1998,** 327–329, 131-135.

95. Netzer, L.; Sagiv, J., A New Approach to Construction of Artificial Monolayer Assemblies. *Journal of the American Chemical Society* **1983,** 105, 674-676.

96. Ulman, A., Formation and Structure of Self-Assembled Monolayers. *Chemical Reviews* **1996,** 96, 1533-1554.

97. Love, J. C.; Estroff, L. A.; Kriebel, J. K.; Nuzzo, R. G.; Whitesides, G. M., Self-Assembled Monolayers of Thiolates on Metals as a Form of Nanotechnology. *Chemical Reviews* **2005,** 105, 1103-1170.

98. Flink, S.; van Veggel, F. C. J. M.; Reinhoudt, D. N., Sensor Functionalities in Self-Assembled Monolayers. *Advanced Materials* **2000,** 12, 1315-1328.

99. Kumar, A.; Biebuyck, H. A.; Whitesides, G. M., Patterning Self-Assembled Monolayers: Applications in Materials Science. *Langmuir* **1994,** 10, 1498-1511.

100. Kango, S.; Kalia, S.; Celli, A.; Njuguna, J.; Habibi, Y.; Kumar, R., Surface Modification of Inorganic Nanoparticles for Development of Organic-Inorganic Nanocomposites-A review. *Progress in Polymer Science* **2013,** 38, 1232-1261.

101. Storm, G.; Belliot, S. O.; Daemen, T.; Lasic, D. D., Surface Modification of Nanoparticles to Oppose Uptake by the Mononuclear Phagocyte System. *Advanced Drug Delivery Reviews* **1995,** 17, 31-48.

102. Sperling, R. A.; Parak, W. J., Surface Modification, Functionalization and Bioconjugation of Colloidal Inorganic Nanoparticles. *Philosophical Transactions of the Royal Society of London, Series A* **2010,** 368, 1333-1383.

103. Gao, J.; Gu, H.; Xu, B., Multifunctional Magnetic Nanoparticles: Design, Synthesis, and Biomedical Applications. *Accounts of Chemical Research* **2009,** 42, 1097-1107.

104. Gu, H.; Yang, Z.; Gao, J.; Chang, C. K.; Xu, B., Heterodimers of Nanoparticles: Formation at a Liquid-Liquid Interface and Particle-Specific Surface Modification by Functional Molecules. *Journal of the American Chemical Society* **2004,** 127, 34-35.

105. Kim, H.; Achermann, M.; Balet, L. P.; Hollingsworth, J. A.; Klimov, V. I., Synthesis and Characterization of Co/CdSe Core/Shell Nanocomposites: Bifunctional Magnetic-Optical Nanocrystals. *Journal of the American Chemical Society* **2004,** 127, 544-546.

106. Gu, H.; Zheng, R.; Liu, H.; Zhang, X.; Xu, B., Direct Synthesis of a Bimodal Nanosponge Based on FePt and ZnS. *Small* **2005,** 1, 402-406.

107. Gu, H.; Zheng, R.; Zhang, X.; Xu, B., Facile One-Pot Synthesis of Bifunctional Heterodimers of Nanoparticles:A Conjugate of Quantum Dot and Magnetic Nanoparticles. *Journal of the American Chemical Society* **2004,** 126, 5664-5665.

108. Selvan, S. T.; Tan, T. T. Y.; Yi, D. K.; Jana, N. R., Functional and Multifunctional Nanoparticles for Bioimaging and Biosensing. *Langmuir* **2009,** 26, 11631-11641.

109. Liong, M.; Angelos, S.; Choi, E.; Patel, K.; Stoddart, J. F.; Zink, J. I., Mesostructured Multifunctional Nanoparticles for Imaging and Drug Delivery. *Journal of Materials Chemistry* **2009,** 19, 6251-6257.

110. Pellegrino, T.; Kudera, S.; Liedl, T.; Muñoz Javier, A.; Manna, L.; Parak, W. J., On the Development of Colloidal Nanoparticles towards Multifunctional Structures and their Possible Use for Biological Applications. *Small* **2005,** 1, 48-63.

111. Liong, M.; Lu, J.; Kovochich, M.; Xia, T.; Ruehm, S. G.; Nel, A. E.; Tamanoi, F.; Zink, J. I., Multifunctional Inorganic Nanoparticles for Imaging, Targeting, and Drug Delivery. *ACS Nano* **2008,** 2, 889-896.

112. Lin, Y.-S.; Wu, S.-H.; Hung, Y.; Chou, Y.-H.; Chang, C.; Lin, M.-L.; Tsai, C.-P.; Mou, C.-Y., Multifunctional Composite Nanoparticles:, A Magnetic, Luminescent, and Mesoporous.*Chemistry of Materials* **2006,** 18, 5170-5172.

113. Jin, Y.; Jia, C.; Huang, S.-W.; O'Donnell, M.; Gao, X., Multifunctional Nanoparticles as Coupled Contrast Agents. *Nat Commun* **2010,** 1, 41.

114. Kim, J.; Kim, H. S.; Lee, N.; Kim, T.; Kim, H.; Yu, T.; Song, I. C.; Moon, W. K.; Hyeon, T., Multifunctional Uniform Nanoparticles Composed of a Magnetite

Nanocrystal Core and a Mesoporous Silica Shell for Magnetic Resonance and Fluorescence Imaging and for Drug Delivery. *Angewandte Chemie International Edition* **2008,** 47, 8438-8441.

115. Jones, R. L.; Pearsall, N. C.; Batteas, J. D., Disorder in Alkylsilane Monolayers Assembled on Surfaces with Nanoscopic Curvature. *Journal of Physical Chemistry C* **2009,** 113, 4507-4514.

116. Ramachandran, R.; Paul, W.; Sharma, C. P., Synthesis and Characterization of PEGylated Calcium Phosphate Nanoparticles for Oral Insulin Delivery. *Journal of Biomedical Materials Research Part B: Applied Biomaterials* **2009,** 88B, 41-48.

117. Dumont, M. F.; Baligand, C.; Li, Y.; Knowles, E. S.; Meisel, M. W.; Walter, G. A.; Talham, D. R., DNA Surface Modified Gadolinium Phosphate Nanoparticles as MRI Contrast Agents. *Bioconjugate Chemistry* **2012,** 23, 951-957.

118. Costantino, U.; Marmottini, F.; Curini, M.; Rosati, O., Metal Exchanged Layered Zirconium Hydrogen Phosphate as Base Catalyst of the Michael Reaction. *Catalysis Letters* **1993,** 22, 333-336.

119. Wu, H.; Liu, C.; Chen, J.; Yang, Y.; Chen, Y., Preparation and Characterization of Chitosan/α-Zirconium Phosphate Nanocomposite Films. *Polymer International* **2010,** 59, 923-930.

120. Sun, L.; Liu, J.; Kirumakki, S. R.; Schwerdtfeger, E. D.; Howell, R. J.; Al-Bahily, K.; Miller, S. A.; Clearfield, A.; Sue, H.-J., Polypropylene Nanocomposites Based on Designed Synthetic Nanoplatelets. *Chemistry of Materials* **2009,** 21, 1154-1161.

121. Díaz, A.; David, A.; Pérez, R.; González, M. L.; Báez, A.; Wark, S. E.; Zhang, P.; Clearfield, A.; Colón, J. L., Nanoencapsulation of Insulin into Zirconium Phosphate for Oral Delivery Applications. *Biomacromolecules* **2010,** 11, 2465-2470.

122. Diaz, A.; Saxena, V.; Gonzalez, J.; David, A.; Casanas, B.; Carpenter, C.; Batteas, J. D.; Colon, J. L.; Clearfield, A.; Delwar Hussain, M., Zirconium Phosphate Nano-platelets: a Novel Platform for Drug Delivery in Cancer Therapy. *Chemical Communications* **2012,** 48, 1754-1756.

123. Saxena, V.; Diaz, A.; Clearfield, A.; Batteas, J. D.; Hussain, M. D., Zirconium Phosphate Nanoplatelets: a Biocompatible Nanomaterial for Drug Delivery to Cancer. *Nanoscale* **2013,** 5, 2328-2336.

124. Tian, Y.; Yu, B.; Li, X.; Li, K., Facile Solvothermal Synthesis of Monodisperse Fe_3O_4 Nanocrystals with Precise Size Control of One Nanometre as Potential MRI Contrast Agents. *Journal of Materials Chemistry* **2011,** 21, 2476-2481.

125. Lee, L. V.; Mitchell, M. L.; Huang, S.-J.; Fokin, V. V.; Sharpless, K. B.; Wong, C.-H., A Potent and Highly Selective Inhibitor of Human α-1,3-Fucosyltransferase via Click Chemistry. *Journal of the American Chemical Society* **2003,** 125, 9588-9589.

126. Tucker-Schwartz, A. K.; Garrell, R. L., Simple Preparation and Application of TEMPO-Coated Fe_3O_4 Superparamagnetic Nanoparticles for Selective Oxidation of Alcohols. *Chemistry A European Journal* **2010,** 16, 12718-12726.

127. Wang, Z.; Heising, J. M.; Clearfield, A., Sulfonated Microporous Organic-Inorganic Hybrids as Strong Bronsted Acids1. *Journal of the American Chemical Society* **2003,** 125, 10375-10383.

128. Krishnan, S.; Kuhn, D. G.; Hamilton, G. A., Direct Oxidation in High Yield of Some Polycyclic Aromatic Compounds to Arene Oxides Using Hypochlorite and Phase Transfer Catalysts. *Journal of the American Chemical Society* **1977,** 99, 8121-8123.

129. Shen, Y.; Sullivan, B. P., A Versatile Preparative Route to 5-Substituted-1,10-Phenanthroline Ligands via 1,10-Phenanthroline 5,6-Epoxide. *Inorganic Chemistry* **1995,** 34, 6235-6236.

130. Carter, R. O.; Parsons, J. L.; Holubka, J. W., Synthesis and Characterization of Epoxy Phosphate Steel Surface Modifiers. *Industrial & Engineering Chemistry Research* **1987,** 26, 1518-1523.

131. Stiddard, M. H. B., 910. 2,2'-Bipyridyl Derivatives of Group VI Carbonyls. *Journal of the Chemical Society* **1962**, 4712-4715.

132. Martí, Angel A.; Mezei, G.; Maldonado, L.; Paralitici, G.; Raptis, Raphael G.; Colón, Jorge L., Structural and Photophysical Characterisation of fac-[Tricarbonyl(chloro)(5,6-epoxy-1,10-phenanthroline)rhenium(I)]. *European Journal of Inorganic Chemistry* **2005,** 2005, 118-124.

133. Clearfield, A.; Berman, J. R., On the Mechanism of Ion Exchange in Zirconium Phosphates,XXXIV. Determination of the Surface Areas of α-$Zr(HPO_4)_2$•H2O by Surface Exchange. *Journal of Inorganic and Nuclear Chemistry* **1981,** 43, 2141-2142.

134. Horsley, S. E.; Nowell, D. V.; Stewart, D. T., The Infrared and Raman Spectra of α-Zirconium Phosphate. *Spectrochimica Acta* **1974,** 30A, 535-541.

135. Clearfield, A.; Pack, S. P., Factors Determining Ion Exchange Selectivity- I High Temperature Phases Formed by α-Zirconium Phosphate and its Sodium and Potassium Exchanged Forms. *Journal of Inorganic and Nuclear Chemistry* **1975,** 37, 1283-1290.

136. Horsley, S. E.; Nowell, D. V., The Preparation and Characterisation of Crystalline α-Zirconium Phosphate. *Journal of Applied Chemistry and Biotechnology* **1973,** 23, 215-224.

137. La Ginestra, A.; Patrono, P., Acidic Properties of Ge, Ti, Zr and Sn Phosphates and Arsenates. *Materials Chemistry and Physics* **1987,** 17, 161-179.

138. Clearfield, A.; Costantino, U., Layered Metal Phosphates and Their Intercalation Chemistry. In *Solid-state Supramolecular Chemistry: Two- and Three-dimensional Inorganic Networks*, 1st ed.; Alberti, G.; Bein, T., Eds. Pergamon Press: Oxford, 1996; Vol. 7, pp 111-112.

139. Clayden, N. J., Solid-State Nuclear Magnetic Resonance Spectroscopic Study of γ-Zirconium Phosphate. *Journal of the Chemical Society, Dalton Transactions* **1987**, 1877-1881.

140. Segawa, K.-i.; Nakajima, Y.; Nakata, S.-i.; Asaoka, S.; Takahashi, H., 31P-MASNMR Spectroscopic Studies with Zirconium Phosphate Catalysts. *Journal of Catalysis* **1986,** 101, 81-89.

141. Rodriguez-Castellon, E.; Olivera-Pastor, P.; Maireles-Torres, P.; Jimenez-Lopez, A.; Sanz, J.; Fierro, J. L. G., MAS-NMR Study of Pillared α-Tin and α-Zirconium Phosphates with Aluminum Oligomers. *Journal of Physical Chemistry* **1995,** 99, 1491-1497.

142. Capitani, D.; Casciola, M.; Donnadio, A.; Vivani, R., High Yield Precipitation of Crystalline α-Zirconium Phosphate from Oxalic Acid Solutions. *Inorganic Chemistry* **2010,** 49, 9409-9415.

143. Tahara, S.; Takakura, Y.; Sugahara, Y., Preparation of α-Zirconium Phosphate from Fluorozirconate and Phosphoric Acid by Liquid-phase Deposition. *Chemistry Letters* **2012,** 41, 555-557.

144. Clearfield, A.; Oskarsson, A.; Oskarsson, C., On the Mechanism of Ion Exchange in Crystalline Zirconium Phosphates. VI. The Effect of Crystallinity of the Exchanger on Na+/H+ Exchange. *Ion Exch Membr* **1972,** 1, 91-107.

145. Saxena, V.; Diaz, A.; Clearfield, A.; Batteas, J. D.; Hussain, M. D., Zirconium Phosphate Nanoplatelets: A Biocompatible Nanomaterial for Drug Delivery to Cancer. *Nanoscale* **2013,** 5, 2328-2336.

146. Díaz, A.; Mosby, B. M.; Bakhmutov, V. I.; Martí, A. A.; Batteas, J. D.; Clearfield, A., Self-Assembled Monolayers Based Upon a Zirconium Phosphate Platform. *Chemistry of Materials* **2013,** 25, 723-728.

147. Levitt, B. W., New Organic Ester Derivatives of γ-Zirconium Phosphate Sheet Polymer. *Colloid & Polymer Science* **1981,** 259, 402-403.

148. Li, L.; Liu, X.; Ge, Y.; Li, L.; Klinowski, J., Intercalation and Pillaring of Zirconium bis(monohydrogenphosphate) with 3-[(triethoxy)silyl]-1-propylamine. *Journal of Physical Chemistry* **1991,** 95, 5910-5914.

149. Slade, R. C. T.; Forano, C. R. M.; Peraio, A.; Alberti, G., A ^{1}H NMR Relaxation Time Study of Dynamic Processes in Zirconium Phosphates of Differing Crystallinities and in Related Compounds. *Solid State Ionics* **1993,** 61, 23-31.

150. Bakhmutov, V. I., *Solid state NMR in Materials Science: Principles and Applications*. CRC Press: 2011.

151. Nakayama, H., Intercalation of Organic Molecules into Layared Phosphates Correlation Between Structure and Function. *Phosphorus Res. Bull.* **2009,** 23, 1-9.

152. Alberti, G.; Cavalaglio, S.; Marmottini, F.; Matusek, K.; Megyeri, J.; Szirtes, L., Preparation of a Composite γ-Zirconium Phosphate-Silica with Large Specific Surface and its First Characterisation as Acid Catalyst. *Appl. Catal. A-Gen* **2001,** 218, 219-228.

153. Sylvester, P.; Cahill, R.; Clearfield, A., Pillaring of Layered Tetravalent Metal Phosphates and Oxides Using (3-Aminopropyl)Trimethoxysilane. *Chem. Mater.* **1994,** 6, 1890-1898.

154. Clearfield, A.; Landis, A. L.; Medina, A. S.; Troup, J. M., More on Crystalline Zirconium Phosphates. *Journal of Inorganic and Nuclear Chemistry* **1973,** 35, 1099-1108.

155. Krogh Andersen, A. M.; Norby, P.; Hanson, J. C.; Vogt, T., Preparation and Characterization of a New 3-Dimensional Zirconium Hydrogen Phosphate,τ- $Zr(HPO_4)_2$. Determination of the Complete Crystal Structure Combining Synchrotron X-ray Single-Crystal Diffraction and Neutron Powder Diffraction. *Inorganic Chemistry* **1998,** 37, 876-881.

156. Sambasivan, S.; Hsieh, S.; Fischer, D. A.; Hsu, S. M. In *Effect of Self-assembled Monolayer Film Order on Nanofriction*, 2006; AVS: 2006; pp 1484-1488.

157. Xiao, X.; Hu, J.; Charych, D. H.; Salmeron, M., Chain Length Dependence of the Frictional Properties of Alkylsilane Molecules Self-Assembled on Mica Studied by Atomic Force Microscopy. *Langmuir* **1996,** 12, 235-237.

158. Radhakrishnan, B.; Ranjan, R.; Brittain, W. J., Surface Initiated Polymerizations from Silica Nanoparticles. *Soft Matter* **2006,** 2, 386-396.

159. Sakellariou, G.; Priftis, D.; Baskaran, D., S urface-initiated Polymerization from Carbon Nanotubes: Strategies and Perspectives. *Chemical Society Reviews* **2013,** 42, 677-704.

160. Advincula, R. C., Surface Initiated Polymerization from Nanoparticle Surfaces. *Journal of Dispersion Science and Technology* **2003,** 24, 343-361.

161. Yahiaoui, A.; Belbachir, M.; Hachemaoui, A., Cationic Polymerization of 1,2-Epoxypropane by an Acid Exchanged Montmorillonite Clay in the Presence of Ethylene Glycol. *International Journal of Molecular Sciences* **2003,** 4, 572-585.

162. Yahiaoui, A.; Belbachir, M.; Hachemaoui, A., An Acid Exchanged Montmorillonite Clay-Catalyzed Synthesis of Polyepichlorhydrin. *International Journal of Molecular Sciences* **2003,** 4, 548-561.

163. Yahiaoui, A.; Belbachir, M.; Soutif, J. C.; Fontaine, L., Synthesis and Structural Analyses of poly (1, 2-cyclohexene oxide) Over Solid Acid Catalyst. *Materials Letters* **2005,** 59, 759-767.

164. Biedron, T.; Szymanski, R.; Kubisa, P.; Penczek, S., Kinetics of Polymerization by Activated Monomer Mechanism. *Makromolekulare Chemie. Macromolecular Symposia* **1990,** 32, 155-168.

165. Lagarde, F.; Reibel, L.; Franta, E., Cationic Polymerization of 1,2-epoxy-3-nitropropane in the Presence of ethylene glycol, 1. Lower Oligodiols Obtained According to the Activated Monomer Mechanism. *Die Makromolekulare Chemie* **1992,** 193, 1087-1097.

166. Kubisa, P., Hyperbranched Polyethers by Ring-opening Polymerization: Contribution of Activated Monomer Mechanism. *Journal of Polymer Science Part A: Polymer Chemistry* **2003,** 41, 457-468.

167. Tokar, R.; Kubisa, P.; Penczek, S.; Dworak, A., C Cationic Polymerization of Glycidol: Coexistence of the Activated Monomer and Active Chain End Mechanism. *Macromolecules* **1994,** 27, 320-322.

168. Dworak, A.; Walach, W.; Trzebicka, B., Cationic Polymerization of Glycidol. Polymer Structure and Polymerization Mechanism. *Macromolecular Chemistry and Physics* **1995,** 196, 1963-1970.

169. Bednarek, M.; Biedroń, T.; Kahłużyński, K.; Kubisa, P.; Pretula, J.; Penczek, S., Ring-opening Polymerization Processes Involving Activated Monomer Mechanism. Cationic Polymerization of Cyclic Ethers Containing Hydroxyl Groups. *Macromolecular Symposia* **2000,** 157, 1-12.

170. Arfelli, M.; Mattogno, G.; Ferragina, C.; Massucci, M. A., XPS Characterization of γ-Zirconium Phosphate and of some of its Intercalation Compounds. A Comparison

with the α-Zirconium Phosphate Analogues. *Journal of Inclusion Phenomena and Macrocyclic Chemistry* **1991,** 11, 15-27.

171. Clearfield, A.; Pack, S. P., Factors Determining Ion Exchange Selectivity - I High Temperature Phases Formed by α-Zirconium Phosphate and its Sodium and Potassium Exchanged Forms. *J. Inorg. Nucl. Chem.* **1975,** 37, 1283-1290.

172. Kirumakki, S.; Huang, J.; Subbiah, A.; Yao, J.; Rowland, A.; Smith, B.; Mukherjee, A.; Samarajeewa, S.; Clearfield, A., Tin(IV) Phosphonates: Porous Nanoparticles and Pillared Materials. *Journal of Materials Chemistry* **2009,** 19, 2593-2603.

173. Nayral, C.; Viala, E.; Fau, P.; Senocq, F.; Jumas, J.-C.; Maisonnat, A.; Chaudret, B., Synthesis of Tin and Tin Oxide Nanoparticles of Low Size Dispersity for Application in Gas Sensing. *Chemistry A European Journal* **2000,** 6, 4082-4090.

174. Morant, C.; Galán, L.; Sanz, J. M., An XPS Study of the Initial Stages of Oxidation of Hafnium. *Surface and Interface Analysis* **1990,** 16, 304-308.

175. Alberti, G.; Costantino, U.; Marletta, G.; Puglisi, O.; Pignataro, S., ESCA Investigations of Amorphous and Crystalline Zirconium Acid Phosphates. *Journal of Inorganic and Nuclear Chemistry* **1981,** 43, 3329-3334.

176. Alberti, G.; Casciola, M.; Costantino, U.; Levi, G.; Ricciardi, G., On the Mechanism of Diffusion and Ionic Transport in Crystalline Insoluble Acid Salts of Tetravalent Metals, Electrical Conductance of Zirconium bis (monohydrogen ortho-phosphate) monohydrate with a Layered Structure. *Journal of Inorganic and Nuclear Chemistry* **1978,** 40, 533-537.

177. Brodard-Severac, F.; Guerrero, G.; Maquet, J.; Florian, P.; Gervais, C.; Mutin, P. H., High-Field ^{17}O MAS NMR Investigation of Phosphonic Acid Monolayers on Titania. *Chemistry of Materials* **2008,** 20, 5191-5196.

178. Lafond, V.; Gervais, C.; Maquet, J.; Prochnow, D.; Babonneau, F.; Mutin, P. H., ^{17}O MAS NMR Study of the Bonding Mode of Phosphonate Coupling Molecules in a Titanium Oxo-Alkoxo-Phosphonate and in Titania-Based Hybrid Materials. *Chemistry of Materials* **2003,** 15, 4098-4103.

179. Mehring, M.; Guerrero, G.; Dahan, F. o.; Mutin, P. H.; Vioux, A., Syntheses, Characterizations, and Single-Crystal X-ray Structures of Soluble Titanium Alkoxide Phosphonates. *Inorganic Chemistry* **2000,** 39, 3325-3332.

180. Chakraborty, D.; Chandrasekhar, V.; Bhattacharjee, M.; Krätzner, R.; Roesky, H. W.; Noltemeyer, M.; Schmidt, H.-G., Metal Alkoxides as Versatile Precursors for Group 4 Phosphonates: Synthesis and X-ray Structure of a Novel Organosoluble Zirconium Phosphonate. *Inorganic Chemistry* **1999,** 39, 23-26.

181. Serre, C.; Ferey, G., Synthesis and Structure Determination from Powder Data of the First Organically Templated Tin(IV) Phosphate : MIL-76 or $Sn_3IVO_2(H2O)(HPO_4)_4.\{H_2N\text{-}C_2H_4\text{-}NH_2\}2.5.\{H_2O\}_2$. *Chemical Communications* **2003**, 1818-1819.

182. Mosby, B.; Díaz, A.; Bakhmutov, V. I.; Clearfield, A., Surface Functionalization of Zirconium Phosphate Nanoplatelets for the Design of Polymer Fillers. *ACS Applied Materials & Interfaces* **2013,** 6, 585-592.

183. Rao, K. P.; Vidyasagar, K., Syntheses, Structure and Intercalation Properties of Low-Dimensional Phenylphosphonates, $A(HO_3PC_6H_5)(H_2O_3PC_6H_5)$ (A = Alkali Metal, NH_4 and Tl).*European Journal of Inorganic Chemistry* **2005,** 2005, 4936-4943.

184. Cao, G.; Lee, H.; Lynch, V. M.; Mallouk, T. E., Synthesis and Structural Characterization of a Homologous Series of Divalent-metal Phosphonates, $MII(O_3PR)•H2O$ and $MII(HO_3PR)_2$. *Inorganic Chemistry* **1988,** 27, 2781-2785.

185. Cao, G.; Lynch, V. M.; Swinnea, J. S.; Mallouk, T. E., Synthesis and Structural Characterization of Layered Calcium and Lanthanide Phosphonate Salts. *Inorganic Chemistry* **1990,** 29, 2112-2117.

186. Mal, N. K.; Fujiwara, M.; Matsukata, M., Synthesis of Organic-Inorganic Hybrid Mesoporous Tin Oxophosphate in the Presence of Anionic Surfactant. *Chemical Communications* **2005**, 5199-5201.

187. Martí, A. A.; Colón, J. L., Photophysical Characterization of the Interactions among Tris(2,2′-bipyridyl)ruthenium(II) Complexes Ion-Exchanged within Zirconium Phosphate. *Inorganic Chemistry* **2010,** 49, 7298-7303.

188. Hasegawa, Y.; Aoki, H., The Ion-exchange Behavior of the Ammonium Ion on Crystalline Zirconium Phosphate. *Bulletin of the Chemical Society of Japan* **1973,** 46, 836-838.

189. Clearfield, A.; Troup, J. M., Mechanism of Ion Exchange in Crystalline Zirconium Phosphates. VII. Crystal Structure of α-Zirconium bis(ammonium orthophosphate) monohydrate. *Journal of Physical Chemistry* **1973,** 77, 243-247.

190. Teruel, L.; Alonso, M.; Quintana, M. C.; Salvador, A.; Juanes, O.; Rodriguez-Ubis, J. C.; Brunet, E.; Garcia, H., Photovoltaic Activity of Layered Zirconium Phosphates Containing Covalently Grafted Ruthenium tris(bipyridyl) and Diquat phosphonates as Electron Donor/Acceptor Sites. *Physical Chemistry Chemical Physics* **2009,** 11, 2922-2927.

191. Brunet, E.; Alonso, M.; Quintana, M. C.; Atienzar, P.; Juanes, O.; Rodriguez-Ubis, J. C.; Garcia, H., Laser Flash-Photolysis Study of Organic−Inorganic Materials Derived from Zirconium Phosphates/Phosphonates of $Ru(bpy)_3$ and C_{60} as Electron Donor−Acceptor Pairs. *J.Phys. Chem. C* **2008,** 112, 5699-5702.

192. Atienzar, P.; de Victoria-Rodriguez, M.; Juanes, O.; Rodriguez-Ubis, J. C.; Brunet, E.; Garcia, H., Layered γ-Zirconium Phosphate as Novel Semiconductor for Dye Sensitized Solar Cells: Improvement of Photovoltaic Efficiency by Intercalation of a Ruthenium Complex-viologen Dyad. *Energ. Environ. Sci.* **2011,** 4, 4718-4726.

193. Kim, H. B.; Kitamura, N.; Kawanishi, Y.; Tazuke, S., Photoinduced Electron Transfer Reactions of Ruthenium(II) Complexes. 2. Oxidative Quenching of Excited tris(2,2'-bipyridine)ruthenium(2+) by Neutral Organic Electron Acceptors. *Journal of Physical Chemistry* **1989,** 93, 5757-5764.

194. Lakowicz, J. R., Chapter 8: Quenching of Fluorescence. In *Principles of Fluorescence Spectroscopy*, Springer: 2009.

195. Casciola, M.; Alberti, G.; Donnadio, A.; Pica, M.; Marmottini, F.; Bottino, A.; Piaggio, P., Gels of Zirconium Phosphate in Organic Solvents and Their Use for the

Preparation of Polymeric Nanocomposites. *Journal of Materials Chemistry* **2005,** 15, 4262-4267.

196. Casciola, M.; Capitani, D.; Comite, A.; Donnadio, A.; Frittella, V.; Pica, M.; Sganappa, M.; Varzi, A., Nafion–Zirconium Phosphate Nanocomposite Membranes with High Filler Loadings: Conductivity and Mechanical Properties. *Fuel Cells* **2008,** 8, 217-224.

197. Casciola, M.; Bagnasco, G.; Donnadio, A.; Micoli, L.; Pica, M.; Sganappa, M.; Turco, M., Conductivity and Methanol Permeability of Nafion–Zirconium Phosphate Composite Membranes Containing High Aspect Ratio Filler Particles. *Fuel Cells* **2009,** 9, 394-400.

198. Xiong, H.-M.; Zhao, X.; Chen, J.-S., New Polymer-Inorganic Nanocomposites:PEO-ZnO and PEO-ZnO-$LiClO_4$ Films. *Journal of Physical Chemistry B* **2001,** 105, 10169-10174.

199. Singhal, A.; Dubey, K. A.; Bhardwaj, Y. K.; Jain, D.; Choudhury, S.; Tyagi, A. K., UV-shielding Transparent PMMA/In_2O_3 Nanocomposite Films Based on In_2O_3 Nanoparticles.*RSC Advances* **2013,** 3, 20913-20921.